

TABLE DES MATIÈRES

RÉSUMÉ.....	ii
TABLE DES MATIÈRES	iv
LISTE DES TABLEAUX	viii
LISTE DES FIGURES	x
LISTE DES ANNEXES.....	xvii
DÉDICACE	xix
REMERCIEMENTS.....	xx
Introduction	1
Références	11
CHAPITRE 1	16
Caractérisation et modélisation hydrogéologique des aquifères	16
1.1 Généralités en hydrogéologie.....	16
1.2 Les différentes approches pour modéliser un aquifère	18
1.3 Réalisation d'un essai hydraulique	20
1.4 Interprétation des essais de pompage.....	22
1.5 Effets de la structure physique du réservoir sur les écoulements	28
1.6 Équation de diffusivité	29
1.7 Solutions analytiques de l'équation de diffusivité.....	30
1.7.1 Modèles d'interprétation des essais de pompage conventionnels	30
1.7.2 Modèles non-conventionnels d'interprétation des essais de pompage.....	36

1.7.3	Discussions sur les modèles analytiques.....	51
1.8	Revue des logiciels intégrant l'analyse du signal ds/dlogt et/ou l'analyse de la dimension d'écoulement	51
1.9	Référence	55
CHAPITRE 2.....		62
Using flow dimension sequences to interpret non-uniform aquifers with constant-rate pumping-tests: a review		63
2.1	Abstract.....	64
2.2	Introduction	65
2.3	Background.....	71
2.3.1	Data processing and denoising of the derivative signal.....	71
2.3.2	Background of the flow dimension sequential analysis.....	74
2.4	Review of flow dimensions with known conceptual models	85
2.4.1	The linear flow regime: $n = 1$	94
2.4.2	Multi-linear combinations.....	101
2.4.3	The radial flow regime: $n = 2$	103
2.4.4	Multi-radial combinations.....	105
2.4.5	Linear – radial combinations	111
2.4.6	The “bilinear” flow regime: $n = 1.5$	112
2.4.7	The sphercial flow regime	119
2.4.8	Radial – spherical combinations.....	120
2.4.9	Linear – spherical combinations.....	126
2.4.10	Fractional flow regimes: non-integer n	127
2.4.11	Boundary flow regimes	129
2.5	Discussion.....	130
2.5.1	The hydraulic significance of multi-stage sequences.....	130
2.5.2	Influence of hydraulic domains with non-equal flow and topological dimensions	134

2.5.3	Limitations.....	135
2.5.4	Summary of the proposed methodology.....	139
2.6	Conclusion.....	141
2.7	Acknowledgments.....	142
2.8	References.....	143
CHAPITRE 3.....		155
Insights on pumping well interpretation from flow dimension analysis: the learnings		
of a multi-context field database.....		
156		
3.1	Abstract.....	157
3.2	Introduction.....	158
3.3	Theory and practice.....	165
3.3.1	Conventional analysis.....	165
3.3.2	The Generalized Radial Flow model.....	168
3.4	Data and method.....	175
3.4.1	Compilation of a pumping-well test database.....	175
3.4.2	Data pre-processing.....	176
3.4.3	Geological contexts.....	183
3.4.4	Comparison of hydraulic property values estimated from various models.....	186
3.5	Results and discussion.....	192
3.5.1	Flow dimension <i>versus</i> Theis analysis: case studies.....	192
3.5.2	The occurrences of flow dimension in natural aquifers.....	198
3.6	Discussion.....	222
3.7	Conclusion.....	229
3.8	Acknowledgments.....	233
3.9	References.....	234
CHAPITRE 4.....		244

Drawdown log-derivative analysis for interpreting constant-rate pumping-tests in inclined substratum aquifers.....	245
4.1	Abstract..... 246
4.2	Nomenclature..... 246
4.3	Introduction 248
4.4	The Theory of Flow Dimension..... 251
4.5	Materials and Methods 256
4.6	Numerical Results and Interpretations..... 260
4.6.1	Base Case Analysis and Hydrodynamic Interpretations..... 260
4.6.2	<i>ds/dlogt</i> plots and sensitivity analysis: Establishing empirical formulas for assessing the hydraulic properties of the aquifer..... 268
4.6.3	Estimation of Hydraulic Properties 279
4.7	Field Examples..... 287
4.8	Discussion..... 292
4.9	Conclusion 297
4.10	Acknowledgments 299
4.11	References..... 300
CHAPITRE 5.....	304
Discussions, recommandations et conclusions	304
5.1	La dimension d'écoulement dans la nature 304
5.2	Analyse séquentielle de la dimension d'écoulement : potentiel diagnostique et limites 310
5.3	Méthodologie et recommandations pour l'amélioration de l'interprétation des essais de pompage..... 316
5.4	Conclusion 324
5.5	Pistes de recherche 328

LISTE DE RÉFÉRENCES	343
ANNEXES	362

LISTE DES TABLEAUX

CHAPITRE 2

Table 2-1: Summary of drawdown log-derivative signatures and their associated conceptual models.	87
---	----

CHAPITRE 3

Table 3-1: Long-term pumping tests included in the pooled database: location of wells and observed lithology.	186
--	-----

Table 3-2: Hydraulic conductivity modeled and estimated from the Theis, Cooper-Jacob and radial derivative analysis for 4 conceptual models generating a radial-linear, a bilinear-radial, a radial and a spherical-radial flow regime. The grey lines represent the relative errors of the overlying K values. The derivative signals of the 4 conceptual models are shown in Figure 3 (linear- A_1 , bilinear- A_2 radial- A_3 and spherical- A_4). The simplified diagrams represent, from left to right, the semi-log plot of s vs t of the radial-linear, the bilinear-radial, the radial and the spherical-radial flow dimensions.	189
--	-----

Table 3-3: Hydraulic conductivity values estimated from the Theis and Cooper-Jacob methods and the radial derivative analysis and for the n -sequence $n=1.5 - 2$.	191
---	-----

Table 3-4: Summary of studies analyzing the frequency of occurrence of the flow dimension n	201
--	-----

Table 3-5: Summary of hydrodynamic interpretations of n and their graphical representations.	205
---	-----

Table 3-6: Summary of the pumping tests that show a spherical or a hyper-spherical flow dimension (highlighted in bold in the n -sequence column) with their intercepted aquifer thickness, their screen thickness and the ratio between both thickness and our interpretation of the spherical flow dimension. In the "location" column, the abbreviations	
---	--

CHCN, SLSJ and Qc designate, respectively, Charlevoix-Haute-Côte-Nord, Saguenay-Lac-Saint-Jean and Quebec. In the “*n*-sequence” column, the abbreviations MG, G and VG represent the appreciation of the quality of the *ds/dlogt* signal and signify, respectively, mediocre-good, good and very good. The letter (U) indicates either an undefinable slope of the *ds/dlogt* signal or a slope that has not been considered as a flow dimension, but rather as a transition or a boundary effect.228

CHAPITRE 4

Table 4-1: Synthesis of the Y-intercept of the radials and the spherical flow dimension m_{2-BC} , m_{2-AC} and m_3 and the parameters of the conceptual model such as K , S_s , Q , d , l_w and α282

Table 4-2: Comparative summary of the accuracy of the hydraulic properties estimated by means of the Theis model, the Cooper-Jacob model and the equations developed in this study.284

LISTE DES FIGURES

CHAPITRE 1

- Figure 1.1 : Porosité rencontrée dans deux grands types de réservoirs : le milieu poreux (sable, grès, craie *etc.*), où l'on considère la porosité primaire, et le milieu fissuré (roche calcaire fissurée ou karstifiée, roche cristalline, *etc.*), où l'on peut considérer à la fois, la porosité primaire (au sein de la matrice) et la porosité secondaire (dans les fissures). (<http://www.geologues-prospecteurs.fr>)..... 17
- Figure 1.2 : Lignes izopièzes dans un aquifère calcaire faillé et plissé après un pompage de 24 heures ($Q = 3.29 \text{ L}\cdot\text{min}^{-1}$). (Smith et Vaughan 1985).24
- Figure 1.3 : Influence des systèmes de coordonnées sur la forme des courbes représentées du rabattement en fonction du temps lors d'un essai de pompage, a) exemple du « Kangaroo plot » (Mattar 2004).....25
- Figure 1.4 : Graphique diagnostique du rabattement (essai de pompage à débit constant) et de la dérivée logarithmique du rabattement en échelle log-log. Ce graphique met en avant le potentiel diagnostique de la dérivée logarithmique du rabattement. (Beauheim et al. 2004).27
- Figure 1.5 : Schéma conceptuel d'un aquifère captif pompé selon la solution analytique de Theis (1935). h_0 représente la charge hydraulique initiale de l'aquifère, $h(r,t)$ représente le profil de charge hydraulique induit par le pompage, T est la transmissivité de l'aquifère, S est l'emmagasinement de l'aquifère et r est la distance radiale. (tiré de <http://www.aqtesolv.com/>)33
- Figure 1.6 : Séquences diagnostiques de la dérivée logarithmique du rabattement pour une faille verticale, non-connectée au puits de pompage (Rafini et Larocque 2009, 2012).42
- Figure 1.7 : Interprétation de la dimension d'écoulement en termes de géométrie de flux selon Doe, (1991), tiré de (Doe 1991).45
- Figure 1.8 : Simulation numérique de l'influence de conditions hydrauliques aux frontières sur la dimension d'écoulement. (Rafini 2008).49

Figure 1.9 : Schémas conceptuels des relations entre les caractéristiques d'écoulement et la dimension d'écoulement. Tiré de Dershowitz et al., (1998). 50

Figure 1.10 : Illustration de la relation entre l'aire d'écoulement (qui varie en fonction de la distance au puits r) et la dimension d'écoulement n , selon l'interprétation proposée par Doe, (1991). Tiré de Dershowitz et al., (1998). 50

CHAPITRE 2

Figure 2.1. Example of real drawdown data displaying two successive radial and non-radial flow regimes. 75

Figure 2.2. Summary of published theoretical flow regimes and their associated flow dimensions, n (modified from (Ehlig-Economides et al., 1994)). 82

Figure 2.3. Conceptual flow models associated with faulted rock aquifers with a linear flow regime within a) an infinite conductive fault and b) a finite conductive fault. ... 100

Figure 2.4. Field example of a linear flow regime in a fractured rock aquifer a) and in a fluvio-glacial deposit b). 101

Figure 2.5. a) Conceptual model of a distributary channel in a deltaic environment, b) T-shaped channel in a perpendicular arrangement modelled by Mijinyawa and Gringarten (2008) to reproduce the flow behavior of a distributary channel system c) Two successive channels with a non-equal diameter to reproduce the flow behavior of a distributary channel system. 102

Figure 2.6. Example of a n -sequence 1 – 1 in a crystalline fractured rock aquifer. 103

Figure 2.7. Examples of fractured rock conceptual models that induce a radial flow regime ($n = 2$). 105

Figure 2.8. Evolution of the “bilinear” $n = 1.5$ conceptual flow model. 114

Figure 2.9. Examples of a leaky vertical faults. a) Diagnostic plots and interpretations of a constant-rate pumping test given by Tiab (2005) (Example 2), b) Diagnostic plots and interpretations of a constant-rate pumping test (6.5 days) conducted in the P-8 well located in a Chasy carbonate rock aquifer of Sainte-Anne-des-Plaines (Quebec, Canada). 115

Figure 2.10. a) bilinear flow model for a vertical finite conductivity fault (Cinco-Ley and Samaniego-V., 1981b; Rafini and Larocque, 2009); b) bilinear flow model for a vertical

finite conductivity fault with a transient interporosity transfer (TIT) between the fault and the matrix (Valdes-Perez et al., 2011); c) trilinear flow model of a leaky vertical finite conductivity fault and a linear flow induced by an external drainage (Lee and Brockenbrough, 1986)..... 119

Figure 2.11. Conceptual flow model of a confined aquifer with short-screen length, partial completion or partial completion borehole. 121

Figure 2.12. Examples of locally leaky aquifers; spherical flow regime..... 122

Figure 2.13. Conceptual flow model of a confined aquifer with a well located a) close to; and b) further away - from a pinch-out boundary (modified from Horne and Temeng (1982) and Mijinyawa and Gringarten (2008))..... 124

Figure 2.14. Conceptual flow model of a confined aquifer with inclined substratum; a) early compensated radial flow regime ($n = 2$); b) predominant radial flow regime ($n = 2$); c) late infinite acting spherical regime ($n = 3$). 125

Figure 2.15. Diagnostic plots and interpretations of a constant-rate pumping test conducted in a thick alluvial deposit: example of a signal of a partially penetrated well ($n = 3$). 126

Figure 2.16. Diagnostic plots and interpretations of a constant-rate pumping test conducted in fluvio-glacial deposits (eskers) (Val d'Or, Quebec, Canada): example of a fractional flow dimension.. 129

CHAPITRE 3

Figure 3.1: Conceptual Theis model (1935) representing its main assumptions. The thick arrows represent the flow induced by the pumping test. In these IARF conditions, the cross-flow area $A(r)$ extends radially in the form of cylinders and the pressure front pulse expands radially in the form of concentric circles having a radius $r(t)$. This flow behavior is called the cylindrical-radial flow regime..... 166

Figure 3.2: Diagnostic plots of two pumping tests performed in two wells in alluvial deposits showing A) the effects of pumping rate adjustments and B) the effect of a temporary interruption of the pump on the s and $ds/d\log t$ signals. The diamond shapes represent the drawdown log-derivative signal and the "x" shapes represent the drawdown signal. The grey lines, derived from the algorithm of Bourdet et al. (1989), represent seven data smoothings for L ranging between 0.2 and 0.8. The R^2 value represents the coefficient of determination between the derivative data and the regression line..... 178

Figure 3.3: Derivative signals of 4 conceptual models (one for each column) modeled numerically using HydroGeoSphere (Therrien et al. 2010). Respectively, the first, second, third and fourth column represent a radial-linear, bilinear-radial, radial and spherical-radial n -sequence. Respectively, the first, second, third and fourth line represent a semi-log plot of the s with a constant-rate pumping test (CP_i), the derivative signal with a constant-rate pumping test (A_i), the derivative signal with 3 increased adjustments of the pumping rate (B_i) and a derivative signal disrupted by a pump shut-down (C_i)..... 180

Figure 3.4: A) 3 derivative signals associated with 3 different behaviours of the pumping rate of a same cylindrical-radial flow model modeled numerically using HydroGeoSphere (Therrien et al. 2010). The flow model is composed of an isotropic constant thickness aquifer bounded by constant head boundaries pumped by a vertical well located in the center. The solid lines with dots represent the drawdown log-derivative responses of the cylindrical-radial flow model induced by a particular pumping condition represented by dashed lines with triangles. $Q(A)$ and $ds/dlogt(A)$ are the curves of a constant rate pumping test and the associated derivative response, $Q(B)$ and $ds/dlogt(B)$ are the curves of an increasing power law pumping rate and the associated derivative response, and $Q(C)$ and $ds/dlogt(C)$ are the curves of a decreasing power law pumping rate and the associated derivative response. 183

Figure 3.5: Diagnostic plots and flow regime interpretations in fractured rock aquifers. A: constant-rate pumping test (6.5 days) conducted in the P-8 well located in a Chasy carbonate rock aquifer of Sainte-Anne-des-Plaines (Charlevoix, Quebec, Canada). B: constant-rate pumping test (6.5 days) conducted in the SE6 well located in the aquifer of Saint-Eustache composed of the Beauharnois rock unit (Mirabel, Quebec, Canada). The diamond shapes represent the drawdown log-derivative signal and the “x” shapes represent the drawdown signal. The R^2 value represents the coefficient of determination between the derivative data and the regression line..... 190

Figure 3.6: Diagnostic plots and interpretations of a constant-rate pumping test conducted in the PP-1 well located in the fluvio-glacial deposits of the Senneterre esker (Mirabel, Quebec, Canada). In the upper part of figures a) and b): Semi-log plot of the drawdown s ; in the lower part: log-log plot of the drawdown-log derivative $ds/dlogt$. A) Example of a conventional interpretation assuming radial flow regimes, B) Demonstration of a more accurate interpretation of the pumping test using a $ds/dlogt$ log-log plot. The grey lines, derived from the algorithm of Bourdet et al. (1989), represent seven data smoothings for L ranging between 0.2 and 0.8. The R^2 value represents the coefficient of determination between the derivative data and the regression line..... 194

Figure 3.7: Diagnostic plots and interpretations of a constant-rate pumping test (6.5 days) conducted in the P-8 well located in a Chasy carbonate rock aquifer of Sainte-Anne-des-Plaines (Charlevoix, Quebec, Canada). In the upper part of Figures A), B) and C): Semi-log plot of the drawdown s ; in the lower part of the same figures: log-log plot of the drawdown-log derivative $ds/dlogt$. a) Hydrodynamic analysis assuming one radial flow regime, b) Hydrodynamic analysis assuming a sequence of two radial flow regimes,

c) Hydrodynamic analysis assuming a sequence of a fractional and a radial flow regime. The grey lines, derived from the algorithm of Bourdet et al. (1989), represent seven data smoothings for L ranging between 0.2 and 0.8. The R^2 value represents the coefficient of determination between the derivative data and the regression line..... 197

Figure 3.8: Statistical analysis of the flow dimension occurrence during 69 constant-rate pumping tests (including respectively 19, 22 and 28 pumping tests in fractured rocks, deposits and carbonate rocks), located in Canada, France and Tunisia. The database contains 121 distinct flow dimension values. The “N” in the graph titles represents the number of observed flow dimensions. The flow dimension is manually estimated from a sequential analysis. The large bars are read on the left y-axis, the thin-dark bars are read on the right y-axis.....204

Figure 3.9: Proportional distribution of the 1, 2, 3 and 4 n sequences in the 69 pumping tests conducted for this study.208

Figure 3.10: Statistical analysis of the flow dimension occurrence in 69 constant-rate pumping tests performed A) in altered crystalline rock aquifers, B) in faulted crystalline rock aquifers, C) in carbonate rock aquifers and D) in alluvial deposits. The flow dimension was manually estimated based on a sequential analysis. The large dark bars that represent the flow dimension occurrence are read on the left y-axis. The thin clear bars that represent the mean logarithmic duration of n are read on the right y-axis. The “N” in the graph titles represents the number of observed flow dimensions.215

Figure 3.11: Example of a diagnostic plot with a flow dimension value greater than 3 ($n = 3.5$). The diamond shapes represent the drawdown log-derivative signal and the “x” shapes represent the drawdown signal. The well test was performed in a weathered crystalline rock located in France. The fit is performed using the SIREN code. The quality of the manual fit is evaluated using the determination coefficient R^2 between the regression line and the derivative data. The $n = 3.5$ is assumed to be induced by a partially penetrating/completed/screened well which is influenced by leakage.215

CHAPITRE 4

Figure 4.1: Example of the behavior of the cross-flow area in a 3D cylindrical-radial flow dimension conceptual model (A Theissian flow occurs before reaching the hydraulic boundaries).....257

Figure 4.2: Conceptual model of an aquifer having an inclined substratum. The arrows represent the geometrical parameters that were varied in the sensitivity analysis, such as the distance from the pumping well to the corner d , the length of the well L_w , the inclination of the substratum α259

- Figure 4.3: Examples of cross-flow area shapes throughout the aquifer in a X-cross section (A), a Y-cross section (B) and a plan view (C) for an aquifer having a 65° inclined substratum. The pumping well is located at $x = 10$ m and reaches the inclined substratum. (D) 3D conceptual model of a cross-flow area produced by a well located in an IS aquifer.261
- Figure 4.4: A) Semi-logarithmic plot of the drawdown signal (s) as a function of time (t), B) log-log plot of the drawdown log-derivative signal ($ds/d\log t$) as a function of time (t) of an aquifer with a sharply inclined substratum (65°).263
- Figure 4.5: Conceptual models of the diffusion of the cross-flow area before and after reaching the corner in $x = 0$. The notations with A_c ($A''c$, $A''c-loss$ and $A'c$) represent the different portions of surfaces of the truncated cylinder as visualized on the figure; the notation A_s represents the surface of the truncated hemisphere. The single apostrophe (for $A'c$ and $A's$) indicates the surface in the east direction, whereas the double apostrophe (for $A''c$ and $A''c-loss$) indicates the surfaces in the west direction (direction of the corner).267
- Figure 4.6: A) Log-log plot of the drawdown log-derivative signal versus time in a sensitivity analysis of the hydraulic conductivity K . B) depicts the Y-intercept of the radial flow dimension m^2-AC and the Y-intercept of the spherical flow dimension m^3 versus K270
- Figure 4.7: A) Log-log plot of the drawdown log-derivative signal versus time in a sensitivity analysis of the specific storage S_s . B) depicts the Y-intercept of the spherical flow dimension m^3 versus the specific storage S_s271
- Figure 4.8: A) shows the log-log plot of the drawdown log-derivative signal of an aquifer having a 65° inclined substratum versus time in a sensitivity analysis of the distance from the well to the corner d . B) depicts the time of the end of the early radial flow dimension (first plateau in $A1$) versus d . This first plateau represents the cylindrical-radial flow diffusion of the pressure front pulse before it reaches any flow boundary (compensated radial flow dimension). C) depicts the Y-intercept of the first plateau m^2-BC versus the length of the well L_w273
- Figure 4.9: A) shows the log-log plot of the drawdown log-derivative signal versus time in an aquifer having a 65° inclined substratum in a sensitivity analysis of the length of the well L_w . B) depicts the Y-intercept of the predominant radial flow dimension m^2-AC versus L_w274
- Figure 4.10: A) shows the log-log plot of the drawdown log-derivative signal of four conceptual models having, respectively, $\alpha = 5, 10, 20$ and 50° of inclination of the substratum, from dark to light-gray. B) depicts the Y-intercept of the spherical flow dimension m^3 versus α276

- Figure 4.11: A) Log-log plot of the drawdown log-derivative signal *versus* time in an IS aquifer having $\alpha = 65^\circ$. B) Same flow model as A) with $\alpha = 5^\circ$. Respectively, the black, the light grey, the grey and the dark grey curves are respectively associated with case 1 (isotropy of K), case 2 (anisotropy of K with highest K in the Z-direction), case 3 (anisotropy of K with highest K in the Y-direction) and case 4 (anisotropy of K with highest K in the X-direction). C), D), E), F) represent a plan and a transversal view of the equipotential surfaces of the pressure front pulse as it diffuses through aquifers of cases 1, 2, 3 and 4.278
- Figure 4.12: Log-log plot of the drawdown log-derivative signal *versus* time in a Theis-like conceptual model and an inclined substratum conceptual model when the well is located in the corner A) or in the center B) of the model.283
- Figure 4.13: Log-log plot of the drawdown *versus* time A) Theis model, semi-log plot of the drawdown *versus* time B) Cooper-Jacob model and log-log plot of the drawdown log-derivative signal C) Conceptual model developed in this study with substratum having an inclination of 50° , $K = 1 \times 10^{-5}$ m/s, $S_s = 1 \times 10^{-4}$ m⁻¹, $l_w = 2$ m.286
- Figure 4.14: North-south (A-A') and east-west (B-B') stratigraphic sections of the Longue-Rive region illustrating the inclined substratum aquifer conceptual model.290
- Figure 4.15: Log-log plot of the drawdown data *versus* time (cross data) and the drawdown log-derivative data *versus* time (black diamond data) of two constant-rate pumping tests, one performed in A) Longue-Rive (Haute-Côte-Nord region) and the other in B) Mirabel (St. Lawrence Lowlands of south-western Quebec). The P-1 well (Longue-Rive) is installed in glacial sands in a confined sand aquifer that fills a glacial valley. It produces the signal of an aquifer having an inclined substratum A). The Philipon well is installed in thick sandstone (generally exceeding 500 m). It produces the signal of a partially penetrated aquifer B).292

LISTE DES ANNEXES

ANNEXE 1 (Tableau 7 ; chapitre 3) : Table 3.7: Principal data (locations, well names, confinement conditions, simplified lithologies and pumping test durations) and n -sequences of the pumping tests in the database. In the fifth column, the letters in brackets refer to an evaluation of the quality of the signal: VG = very good, G = good, MG = mediocre-good, M = mediocre and U = either an undefinable slope of the $ds/dlogt$ signal or a slope that has not been considered as a flow dimension, but rather as a transition or a boundary effect.....361

" Si le problème a une solution, il ne sert à rien de s'inquiéter. Mais s'il n'en a pas, alors s'inquiéter ne change rien. " *Proverbe tibétain*

" To give a reason for anything is to breed a doubt of it. " *William Hazlitt (1826)*

" Tout dans la vie n'est qu'énergies et vibrations. " *Albert Einstein*

DÉDICACE

À mon papy,

À ma famille,

À tous ces enfants qui se battent pour apprendre,

À toutes ces femmes qui se battent pour leur liberté physique et intellectuelle,

À toutes celles et tous ceux qui changent le monde à leur manière.

REMERCIEMENTS

Comme le disait justement le philosophe Alain, « le secret de l'action, c'est de commencer », alors, allons-y... Si je commence à rédiger cette page de remerciement, c'est qu'une autre page, celle de ma vie de doctorante, est en train de se tourner. Ces années comme thésarde ont été tellement riches, tant sur le plan scientifique qu'humain que le temps s'est écoulé trop vite. Tout au long de cette thèse, il y a eu tellement de rencontres inattendues, inspirantes et enrichissantes, que ces quelques pages ne pourraient contenir ne serait-ce qu'un angström de toutes les personnes que je tiens à remercier. J'irai donc seulement à la quintessence de l'essence et me limiter à l'essentiel.

Je remercie tout d'abord mes directeur et co-directeur Dr. Romain Chesnaux et Dr. Silvain Rafini, sans qui, toute cette aventure n'aurait pas eu lieu. Et qu'elle aventure ! Je les remercie sincèrement pour tous ces moments tant scientifiques, énigmatiques que poétiques. Je les remercie de m'avoir soutenue et encouragée tout au long de cette thèse. Je les remercie pour tous ces commentaires, conseils et suggestions qui m'ont permis d'affiner, approfondir et murir mon travail, mes projets et mes présentations. Je les remercie de leur confiance et de leur sincérité. Je les remercie pour ces petits conciliabules improvisés : des moments simples autour d'une bonne bière et d'un baby-foot à méditer sur le sens physique de la dimension d'écoulement et le potentiel diagnostique de la dérivée logarithmique du rabattement.... Si je devais illustrer ces dernières années avec un seul souvenir, je choisirais celui où, bras dessus, bras dessous, nous avons traversé courageusement une rivière de l'ouest Canadien. Celle-ci, qui était au premier abord qu'un petit cours d'eau, était devenue submergée par les averses diluviennes du mois de septembre et déversait ses flots tumultueux dans le fracas des vagues déchainées du Pacifique en ébullition. Bref, une petite image métaphorique de trois petits chercheurs, faisant face à l'immensité et se soutenant afin de braver les tumultes de la vie scientifique, dans un fracas de publications et un bouillonnement de connaissances. Enfin, bref, une belle aventure... parmi tant d'autres! Je ne pourrais jamais oublier toutes ces aventures qui ont su pimenter, agrémenter et participer au bon déroulement de cette thèse... Que ce soit lors des présentations aux congrès internationaux d'hydrogéologie à Marakech, Rome, Montpellier et Vancouver, ou à dévaler les versants montagneux de la Colombie-Britannique à la recherche de morilles, ou à pêcher les capelans sur la glace, ou encore à explorer les forêts et les fjords du Québec à la recherche de trésors cachés et de champignons, ou enfin à naviguer sur les rivières en se faisant surprendre par les ours et les aurores boréales. Bref, je remercie sincèrement Romain de m'avoir inscrite à l'école de la vie et de m'avoir fait découvrir toutes ces merveilles de la forêt boréale, telles que le chaga, le thé du labrador, les matsutakés et les mouches noires !

Je remercie également les relecteurs des articles de cette thèse, notamment Dr. Thomas Doe pour ses nombreux conseils sur la dimension d'écoulement, Dr. John A. Barker pour ses explications sur les développements analytiques en lien avec la dimension d'écoulement, ainsi que Randall M. Roberts, Dr. Robert Chapuis et Dr. Jean-Raynald de Dreuzy pour leurs suggestions et commentaires. Je remercie tout particulièrement Dr. Pierre Cousineau, Dr. Benoît Dewandel et Dr. Alain Rouleau d'avoir accepté d'examiner ma thèse.

Je remercie Josée Kaufmann d'avoir relu et corrigé l'anglais de tous mes articles et surtout je la remercie pour tous ses bons conseils pratiques et culinaires.

Je remercie également les supports financiers du « conseil de recherches en sciences naturelles et en génie » (CRSNG – financement fédéral) du Canada dans le cadre de la « subvention de découverte » ainsi que les « fonds de recherche du Québec – Nature et Technologies » (FRQNT – financement provincial) dans le cadre la subvention individuelle des « nouveaux chercheurs » reçues par Dr. Romain Chenaux. Je remercie également le support financier du ministère du Développement durable, de l'Environnement et de la Lutte contre les changements climatiques (MDDELCC) et des municipalités de Charlevoix-Haute-Côte-Nord (Québec) dans le cadre du projet d'acquisition de connaissance sur les eaux souterraines (PACES-CHCN). Enfin, je remercie l'UQAC pour les bourses d'excellence qui m'ont été octroyées : la bourse du programme de soutien au développement de la recherche et création (PSDRc, volet F, soutien à la publication et à la diffusion des travaux de recherche et création pour la diffusion de travaux), la bourse de l'implication du fond de développement de l'UQAC (édition 2015-2016), la bourse de la fondation de l'UQAC (édition 2015-2016), la bourse du programme de soutien au développement de la recherche et création (PSDRc, volet F, soutien à la publication et à la diffusion des travaux de recherche et création pour la publication scientifique), la bourse d'excellence du groupe CEGER-Mecfor, Cegerco, Cegertec WorleyParsons (édition 2014-2015).

Je remercie également tous les amis et collègues du groupe de recherche R2Eau (Risque Ressource Eau) et des projets PACES (projets d'acquisition de connaissances sur les eaux souterraines). Je remercie spécialement Alain Rouleau pour ces conseils avisés sur mon devis de recherche et lors des présentations du R2Eau. Je le remercie également pour son éternelle sympathie, sa prévenante sollicitude et son immuable intégrité. Je remercie Ali Saeidi pour ses supers cours de géotechnique et sa gentillesse. Je remercie Mélanie Lambert pour son soutien technique avec ArcGIS. Je remercie entre autres, Marie-Line Tremblay, Denis Germaneau et Julien Walter d'avoir établi cette mine d'or qu'est la base de données PACES. Je remercie David Noël pour ses conseils techniques de terrain. Je remercie Maryse Doucet pour ces laboratoires à la fois studieux et décontractés.

Je remercie Yvon Robert pour toutes ces soirées de lutherie ainsi que ces beaux moments à la fois artistiques et épicuriens. Je remercie le « old » Dan pour ses conseils éclairés sur les règles de bonnes conduites face à un grizzly. Je remercie Éric Renald pour ces moments de divergence artistique à l'UQAC. Je remercie Maryline Huet et Amira Fortin d'avoir été de si bonnes colocs. Je remercie Jabril Abdelaziz pour ces moments de calme et de découvertes musicales. Je remercie Sandra Richard d'avoir joué le rôle de prédécesseur et de m'avoir fait bénéficier de son expérience de thésarde. Je remercie également les amis grimpeurs pour toutes ces belles sorties en escalade roche et de glace, les amis skieurs pour ces descentes magiques dans les sous-bois du Valinouët et du mont Édouard, les amis yogis pour ces soirées relaxantes et inspirantes, les amis danseurs pour ces soirées swing enflammées et enfin les amis géologues pour ces bonnes vieilles soirées « vins et fromages ».

Enfin et surtout, je remercie ma famille que j'aime très fort, d'avoir été si proche malgré la distance et d'avoir été présente à chaque instant.

INTRODUCTION

L'intensification de l'exploitation des aquifères induit un stress de plus en plus important sur les ressources en eau. En effet, l'accroissement de la population et l'augmentation de ses besoins en eau ainsi que l'intensification de l'agriculture et le développement industriel exercent une pression toujours plus grande sur les eaux souterraines. Ces enjeux conduisent la gestion des eaux souterraines au cœur de l'actualité : la consommation en eau, qui a plus que doublé depuis les 50 dernières années, est responsable d'importantes sécheresses à travers le monde (Wada et al. 2013). De plus, les changements climatiques peuvent vulnérabiliser les ressources en eau souterraine en impactant la recharge des aquifères (Vorosmarty et al. 2000, Eckhardt et Ulbrich 2003, Döll 2009, Taylor et al. 2013).

De l'alimentation en eau à l'exploitation pétrolière, en passant par l'enfouissement de déchets ménagers et radioactifs, les études géotechniques, la production d'énergie géothermique ou la séquestration de carbone, les essais de pompage constituent un outil essentiel pour la caractérisation du souterrain. Les essais de pompage sont particulièrement utilisés par les praticiens de hydrogéologie et de l'exploitation pétrolière afin d'estimer les propriétés hydrauliques des aquifères : à savoir la conductivité hydraulique K et l'emmagasinement spécifique S_s . La conductivité hydraulique est un paramètre clé dans la délimitation des périmètres de protection (Bear et Jacobs 1965, Wyssling 1979, Todd 1980, Grubb 1993, Karanta 2002, Paradis et al. 2007), la prédiction du transport de contaminant (Carrera 1993, Eggleston et Rojstaczer 1998) et l'estimation de la recharge des aquifères (Scanlon et al. 2002, Huet 2015). L'inadéquation entre la simplicité des modèles analytiques

et numériques, et la complexité des aquifères (tels que les aquifères fracturés, faillés, hétérogènes en termes de conductivité hydraulique et/ou de connectivité de fractures, karstiques, à géométrie variable) rend souvent l'interprétation des essais de pompage une tâche difficile et délicate induisant des erreurs et imprécisions dans l'estimation des propriétés hydrauliques.

L'interprétation des essais de pompage a connu un grand progrès en 1935 avec les travaux pionniers de Theis (1935) qui proposa la première solution transitoire à l'équation de diffusivité en se basant sur une analogie entre les conditions hydrologiques dans un aquifère et les conditions thermiques. Il a observé que l'influence du pompage, aussi appelée *cône de rabattement* ou *front de pression*, se propage radialement autour du puits pompé. Il proposa une méthode basée sur le calage d'une courbe théorique (*type-curve matching/fitting method*) avec les données de rabattement s représentées en fonction du temps t sur un diagramme log-log. Le modèle de Theis stipule que l'essai de pompage est à débit constant et qu'il est réalisé dans un puits captant totalement un aquifère captif, homogène, isotrope et d'étendue latérale infinie (*infinite-acting radial flow (IARF)*). Ce modèle conceptuel permet la mise en place d'un régime d'écoulement cylindrique-radial. La solution analytique de Theis a donné naissance à une multitude de modèles analytiques et de solutions en régime transitoire qui se sont basés sur la théorie et qui l'ont légèrement modifiée selon les hypothèses considérées. Par exemple, Cooper et Jacob (1946) ont proposé un cas particulier en simplifiant la solution de Theis pour des grandes valeurs de temps t suffisamment grandes et/ou de faibles valeurs de rayon r (distance par rapport au puits pompé), Hantush (1956) et a présenté une solution pour une nappe semi-captive, Neuman (1972) a présenté une solution pour une nappe libre, Warren et Root (1963) ont proposé un modèle à double porosité, etc. Des synthèses des solutions analytiques sont

notamment proposées par Kruseman et de Ridder (1994) et Chapuis (2007). Des solutions analytiques ont également été développées pour des aquifères intégrant quelques hétérogénéités à géométries simples telles des failles verticales à conductivité hydraulique infinie (Gringarten et al. 1974) ou finie (Cinco-Ley et al. 1978, Cinco-Ley et Samaniego-V. 1981b). Les méthodes d'analyse ont également été légèrement améliorées grâce à l'approche de lignes droites (*straight-line analysis*) sur un diagramme semi-logarithmique du rabattement s en fonction du temps t telle que proposée par Cooper et Jacob (1946) dans l'hypothèse que les conditions asymptotiques de l'équation de Theis sont atteintes aux temps longs. Cette approche se limite cependant au régime radial qui se manifeste par une ligne droite sur un diagramme semi-logarithmique de s en fonction de t .

L'interprétation des essais de pompage connût une nouvelle révolution avec l'analyse de la dérivée logarithmique du rabattement $ds/dlogt$ (nommé *pressure derivative signal* dans les revues pétrolières et *drawdown log-derivative signal* dans les revues hydrogéologiques). Proposé initialement par l'hydrogéologue Ven Te Chow (1952), ce n'est qu'en 1989 que le signal de la dérivée logarithmique du rabattement connaît un essor au sein de l'industrie pétrolière grâce aux travaux de Bourdet et al. (1989). Le signal de la dérivée logarithmique du rabattement (dérivée-log) $ds/dlogt$ est beaucoup plus sensible aux petites variations de rabattement que le signal simple du rabattement s , ce qui permet de poser un diagnostic plus fin puisque la détection des phénomènes influençant le rabattement est rendue plus subtile (Bourdet et al. 1989). Affichée sur un diagramme log-log, la série temporelle de $ds/dlogt$ en fonction de t met en avant des pentes caractéristiques qui reflètent les régimes d'écoulement ressentis par le pompage. Le signal de la dérivée-log permet ainsi de réduire la non-unicité des signatures hydrauliques, d'émettre un diagnostic plus juste (par rapport aux méthodes conventionnelles) vis-à-vis de l'expression hydraulique de l'aquifère, de

réduire la non-unicité du calage des courbes théoriques et ainsi d'améliorer la qualité de l'interprétation de l'essai de pompage (Bourdet et al. 1989, Mattar 1997, Renard et al. 2009). Il convient de noter que le terme « régime d'écoulement » réfère au comportement de la pression sous l'effet d'un pompage et non aux conditions laminaires et turbulentes, telles que définies par le nombre de Reynolds.

Dans les années 1990, Djebbar Tiab introduit une technique d'interprétation des essais de pompage basée sur l'analyse des diagrammes log-log du signal de $ds/d\log t$ en fonction de t sans utiliser le calage des courbes théoriques issues des modèles analytiques (Tiab 1993a, 1993b, 1993c, 1993d, 1994) (*without type-curve matching*). Cette technique, qui est basée sur des équations analytiques utilisant des points d'intersection et des pentes de la dérivée-log du rabattement est plus précise pour estimer les propriétés hydrauliques des aquifères qu'une analyse basée sur le calage de courbes théoriques des modèles analytiques (Horne 1990). De plus, cette approche, nommée technique TDS (*Tiab's Direct Synthesis technique*), ouvre l'interprétation des essais de pompage à une nouvelle philosophie : décomposer le signal hydraulique de la dérivée-log du rabattement en pentes afin d'identifier une séquence de régimes d'écoulement et d'interpréter indépendamment chaque régime d'écoulement. Analyser un signal hydraulique en observant les régimes d'écoulement au lieu de les supposer (tel que nous le faisons lorsque nous calons une courbe théorique de s en fonction de t sur des données de terrain), constitue une réelle amélioration qui permet à la fois de mieux choisir le modèle pour l'interprétation du pompage et d'investiguer le comportement hydraulique de l'aquifère au fur et à mesure que le front de pression se propage à travers celui-ci. Jusqu'à présent, l'essai de pompage permettait seulement d'estimer les propriétés hydrauliques de l'aquifère et d'identifier ses frontières. L'*approche séquentielle des régimes d'écoulement* amène l'idée que des données de rabattement

mesurées au puits permettent de retranscrire des hétérogénéités et des conditions hydrodynamiques dans le milieu aquifère autour du puits.

C'est face à la difficulté d'interpréter des essais de pompage en milieux de type rocheux fracturés, générant dans la majorité des cas des comportements hydrauliques complexes et hétérogènes, que Barker (1988) introduisit le modèle GRF (*Generalized Radial Flow*). Ce modèle a pour objectif d'offrir des solutions qui peuvent décrire le comportement du rabattement à la fois pendant un régime radial (tel que le régime cylindrique-radial du modèle de Theis et ses dérivées) et lors de régimes non-radiaux. Ce modèle généralise le paramètre de la dimension d'écoulement à des valeurs non-entières. Le paramètre n se définit de façon empirique, à partir de la pente v du signal de la dérivée-log du rabattement en fonction du temps (Équation (1)). Le paramètre n est donc défini par la dérivée seconde de la courbe de rabattement s vs. t .

$$n = 2 \cdot (1 - v) \quad (1)$$

Barker définit la dimension d'écoulement n comme étant un paramètre reflétant l'évolution de la géométrie de la surface hydraulique traversée par les écoulements (ou surface équipotentielle du front de pression) $A(r)$ au fur et à mesure que le front de pression se diffuse dans le milieu et parcourt une distance r . En d'autres termes, en se propageant à travers l'aquifère l'onde de pression induite par le pompage est influencée par les propriétés hydrauliques du milieu et se déforme. Ses changements de géométrie sont ressentis au puits par des changements de taux de rabattement. Selon le modèle GRF, un milieu homogène isotrope vérifie la relation suivante (Équation (2)) :

$$A(r) \sim r^{n-1} \quad (2)$$

Ainsi des systèmes avec une dimension d'écoulement radiale ($n = 2$) reflètent un milieu dont l'aire $A(r)$ grossit proportionnellement à r (Équation (2)). De telles conditions hydrodynamiques pourraient être produites lorsque $A(r)$ a la forme d'un cylindre, comme par exemple le modèle cylindrique-radial qui est celui considéré par Theis. La dimension d'écoulement linéaire ($n = 1$) reflète un milieu où la surface $A(r)$ n'évolue pas, ce qui pourrait être observé dans des aquifères allongés, longilignes et étroits de type « canal ou conduit ». La dimension d'écoulement sphérique ($n = 3$) exprime un système dont la surface $A(r)$ grandit proportionnellement à r^2 . Cette relation en r^2 est produite lorsque la surface équipotentielle au front de pression a la forme d'une sphère ou d'une portion de sphère (Moncada et al. 2005). L'interprétation physique de la dimension d'écoulement se conceptualise bien pour des valeurs de n entières, en revanche, pour des valeurs de n fractionnaires (non-entières), la conceptualisation du front de pression est plus difficile. Selon l'équation (1), les dimensions d'écoulement fractionnaires expriment un milieu où $A(r)$ évolue avec une puissance non-entière. Initialement, les valeurs de n fractionnaires étaient interprétées comme étant reliées à la géométrie de la source (Barker 1988) ou étant associées aux propriétés fractales des réseaux de fractures dans les milieux fracturés (Barker 1988, Polek, et al. 1989, Bangoy et al. 1992, Acuna et Yortsos 1995). Doe (1991) propose une interprétation conceptuelle non-fractale des dimensions d'écoulement fractionnaires. Il montre qu'une hétérogénéité des propriétés hydrauliques et/ou des variations de géométrie de la source ou de l'aquifère peuvent induire des valeurs de n non-entières. L'avantage fondamental du paramètre n est qu'il fournit un outil universel qui relie l'expansion du front de pression dans l'aquifère avec le taux de rabattement mesuré au puits (pentes du signal de $ds/d\log t$). Initialement, la définition de n avait été donnée par Barker

dans un milieu homogène, mais reprenant le modèle analytique d'Abbaszadeh et Cinco-Ley (1995) modélisant les écoulements à travers une faille verticale, de conductivité hydraulique finie et alimentée par la matrice. Rafini et Larocque (2012) ont montré que le concept de la dimension d'écoulement (Équation (2)) reste valide dans un modèle hétérogène induisant une séquence de n . Cette approche qui combine le concept de n avec l'approche *séquentielle des régimes d'écoulement* est un outil puissant qui retranscrit les variations de comportement hydraulique de l'aquifère dans l'espace et dans le temps, ce qui permet d'investiguer les géométries d'écoulement et la géologie autour des puits. Une telle approche est tout à fait originale par rapport aux approches conventionnelles puisqu'elle permet d'investiguer la géologie environnante au puits à partir du comportement hydraulique observé de l'aquifère en condition de pompage et non l'inverse, à savoir que les méthodes conventionnelles nécessitent de réaliser des hypothèses sur la géologie environnante avant de choisir le meilleur outil interprétatif de l'essai de pompage. Malgré son potentiel d'investigation, l'*analyse séquentielle des dimensions d'écoulement*, est encore très peu utilisée en pratique, du moins dans le domaine de l'hydrogéologie, même si elle l'est plus dans le domaine pétrolier.

Les problématiques actuelles en hydrogéologie nécessitent d'améliorer à la fois l'estimation des propriétés hydrauliques et le degré de précision de l'hétérogénéité des écoulements et des conditions structurales et géologiques des aquifères. Alors que les praticiens en hydrogéologie restent majoritairement tournés sur les méthodes conventionnelles basées sur le calage de courbes théoriques de type Theis, l'approche séquentielle des régimes d'écoulement est couramment employée dans l'industrie pétrolière et est au cœur des enjeux abordés dans les revues pétrolières (Ehlig-Economides 1988, Mattar 1997, Escobar et al. 2004b, Kuchuk et Biryukov 2013). Appliquer des modèles de type Theis à des régimes

d'écoulement non-radiaux implique une estimation peu précise voire erronée des propriétés hydrauliques compte-tenu que les hypothèses sont souvent inadaptées. L'analyse de la dérivée logarithmique du rabattement et des dimensions d'écoulement ne nécessite pas plus de mesures qu'une simple analyse d'essai de pompage (seules les mesures de s , de t et du débit Q sont nécessaires) mais apporte un potentiel diagnostique indéniable. En revanche, l'importante sensibilité de la dérivée-log du rabattement nécessite un traitement du signal, comme par exemple d'appliquer des algorithmes de déconvolution et/ou des algorithmes de lissage. Ces algorithmes permettent de corriger les variations du rabattement induites par les variations de débit lors de l'essai de pompage. Intégrer ces outils dans les études hydrogéologiques affinerait la compréhension des écoulements souterrains, amènerait une meilleure compréhension des systèmes et une meilleure précision dans l'estimation des propriétés hydrauliques, ce qui aiderait par exemple à déterminer les périmètres de protection de façon plus adaptée.

D'une manière générale, ce travail de recherche se propose d'améliorer la compréhension du signal hydrodynamique induit par un pompage, en régime transitoire. Plus précisément, il s'agit de déterminer la signification physique et hydraulique de l'évolution temporelle du rabattement et de sa dérivée logarithmique en adoptant une approche séquentielle de la dimension d'écoulement afin d'améliorer la caractérisation hydrodynamique et géologique des aquifères.

Actuellement, il existe un écart important dans le développement et l'application des outils diagnostiques entre les domaines de l'hydrogéologie et de l'industrie pétrolière. Renard (2005) prévoit cependant que les analyses graphiques diagnostiques (*diagnostic plots*) et l'analyse de la dérivée-log seront amenées à être couramment utilisées en hydrogéologie

dans les années à venir. Il fait d'ailleurs remarquer que la plupart des logiciels en hydrogéologie proposent déjà l'option « *diagnostic plot* ». L'objectif, dans un premier temps, est d'amener les outils diagnostiques couramment employés par l'industrie pétrolière (notamment l'analyse de la dérivée-log et la dimension d'écoulement) aux praticiens de l'hydrogéologie et de réaliser une revue de littérature récente de ces outils dans l'interprétation des essais de pompage dans le domaine de l'hydrogéologie et de l'industrie pétrolière. De plus, étant donné que ces outils diagnostiques sont amenés à être appliqués par les praticiens de l'hydrogéologie, il est donc important de bien illustrer et démontrer le potentiel de ces outils et d'en évaluer les limites.

Le premier chapitre présente quelques généralités en hydrogéologie afin d'amener des bases théoriques avant d'aborder les trois chapitres suivants qui se composent de trois articles de revue représentant trois contributions différentes afin de démontrer l'intérêt en hydrogéologie d'utiliser les outils diagnostiques présentés.

Le deuxième chapitre se consacre à réaliser un état de l'art des séquences de n et les modèles conceptuels associés afin de mettre à la disposition des praticiens un guide récent permettant d'améliorer l'interprétation qualitative et quantitative des essais de pompage au sein d'aquifères complexes (non theissiens).

Comme énoncé précédemment, le paramètre de la dimension d'écoulement est un outil essentiel afin d'investiguer le comportement hydrodynamique des aquifères mais son interprétation physique reste énigmatique pour la plupart des valeurs non-entières. Cette problématique a beaucoup été abordée par des simulations numériques mais encore peu d'études avec des données de terrain sont disponibles. Puisque la dimension d'écoulement s'estime empiriquement à partir de la dérivée-log du rabattement, le troisième chapitre a

pour objectif d'observer l'occurrence de n dans la nature, afin de i) vérifier l'applicabilité du modèle de Theis dans la nature en observant l'occurrence de ce type d'écoulement et ii) corrélérer, par une approche statistique, les valeurs de n aux contextes géologiques. Au final, cette étude vise à i) préciser la compréhension des conditions physiques (géométrie, hétérogénéité, effets liés au puits) et hydrauliques (conditions hydrauliques aux limites, directions préférentielles ou chenalisation des écoulements) qui génèrent une dimension non-entière et ii) préciser les contextes qui créent des séquences de dimensions d'écoulement. Ce travail s'appuie sur une base de données de dimension d'écoulement construite à partir d'essais de pompage à débit constant de longue et de moyenne durée (69 essais de pompage), réalisés dans des aquifères fracturés (carbonatés et granitiques), d'arènes granitique et de dépôts fluvio-glaciaires.

L'interprétation conceptuelle de la dimension sphérique $n = 3$ est généralement associée à un puits pénétrant partiellement l'aquifère. Pourtant, la base de données de n a mis en évidence des essais de pompage montrant un régime d'écoulement sphérique ($n = 3$) mais qui ne peuvent pas être interprétés avec le modèle à pénétration partielle. Le quatrième chapitre vise donc à modéliser numériquement un aquifère à substratum incliné, lequel exprime une dimension sphérique afin i) de proposer un modèle d'écoulement cohérent à l'un des essais de pompage observé dans la base de données de n et ii) de développer des équations empiriques afin d'améliorer la détermination des propriétés hydrauliques (transmissivité, emmagasinement) associées à un régime sphérique en contexte de substratum incliné. Cette dernière étude contribue également à présenter une méthodologie d'investigation numérique permettant, d'une part, de conceptualiser le sens physique de n ou d'une séquence de n dans le cas de modèles conceptuels encore jamais investigués et d'autre part, de proposer des solutions empiriques pour le calcul des propriétés

hydrauliques. Une telle méthodologie pourra ainsi s'appliquer à d'autres cas, d'autres modèles et elle permettra également d'explorer les cas de non-unicité des modèles lors d'expression d'un même signal hydraulique.

Les trois chapitres 2, 3, 4 sont présentés sous forme d'article de recherche. Au moment où cette thèse est présentée, l'article du chapitre 3 est publié dans la revue *Journal of Hydrology*, l'article du chapitre 4 est soumis dans la même revue et l'article du chapitre 2 (qui a été rédigé en dernier) est prêt à être soumis dans la revue *Water Resources Research* ou dans la revue *Journal of Hydrology*. Ainsi, il convient d'avertir le lecteur de cette thèse que dans la chronologie de la thèse, le premier article de synthèse qui est présenté dans le chapitre 2 fait référence à l'article du chapitre 3 parce que ce dernier a été publié avant l'article de synthèse. En effet, l'article de synthèse du chapitre 2 de la thèse a été rédigé en dernier puisqu'il nécessitait de s'être familiarisé avec l'état des connaissances et de la littérature au cours de toutes les années de la thèse.

Références

- Abbaszadeh, M., et Cinco-Ley, H. 1995. Pressure-transient behavior in a reservoir with a finite-conductivity fault [en ligne]. *SPE Formation Evaluation*, **10**(01) : 26–32. doi: 10.2118/24704-PA.
- Acuna, J.A., et Yortsos, Y.C. 1995. Application of fractal geometry to the study of networks of fractures and their pressure transient [en ligne]. *Water Resources Research*, **31**(3) : 527–540. doi: 10.1029/94WR02260.
- Bangoy, L.M., Bidaux, P., Drogue, C., Plégat, R., et Pistre, S. 1992. A new method of characterizing fissured media by pumping tests with observation wells [en ligne]. *Journal of Hydrology*, **138**(1–2) : 77–88. doi: 10.1016/0022-1694(92)90156-P.
- Barker, J.A. 1988. A generalized radial flow model for hydraulic tests in fractured rock [en ligne]. *Water Resources Research*, **24**(10) : 1796–1804. doi: 10.1029/WR024i010p01796.

- Bear, J., et Jacobs, M. 1965. On the movement of water bodies injected into aquifers [en ligne]. *Journal of Hydrology*, **3**(1) : 37–57. doi: 10.1016/0022-1694(65)90065-X.
- Bourdet, D., Ayoub, J.A., et Pirard, Y.M. 1989. Use of pressure derivative in well test interpretation [en ligne]. *SPE Formation Evaluation*, **4**(2) : 293–302. doi: 10.2118/12777-PA.
- Carrera, J. 1993. An overview of uncertainties in modelling groundwater solute transport [en ligne]. *Journal of Contaminant Hydrology*, **13**(1–4) : 23–48. doi: 10.1016/0169-7722(93)90049-X.
- Chapuis, R.P. 2007. Guide des essais de pompage et leurs interprétations [en ligne]. Bibliothèque et archives nationales du Québec, Québec (Canada). Disponible à http://www.mddelcc.gouv.qc.ca/eau/souterraines/guide_pompage/guide_pompage_1-4.pdf.
- Chow, V.T. 1952. On the determination of transmissibility and storage coefficients from pumping test data [en ligne]. *Eos, Transactions American Geophysical Union*, **33**(3) : 397–404. doi: 10.1029/TR033i003p00397.
- Cinco-Ley, H., Samaniego V., F., et Dominguez A., N. 1978. Transient Pressure Behavior for a Well With a Finite-Conductivity Vertical Fracture [en ligne]. *Society of Petroleum Engineers Journal*, **18**(04) : 253–264. doi: 10.2118/6014-PA.
- Cinco-Ley, H., et Samaniego-V., F. 1981. Transient pressure analysis: finite conductivity fracture case versus damaged fracture case [en ligne]. *Dans SPE Annual Technical Conference and Exhibition*, 4-7 October, 1981, San Antonio, Texas, USA, SPE-10179-MS. SPE Annual Technical Conference and Exhibition. doi: 10.2118/10179-MS.
- Cooper, H.H., Jr., et Jacob, C.E. 1946. A generalized graphical method for evaluating formation constants and summarizing well-field history [en ligne]. *Transactions, American Geophysical Union*, **27** : 526–534. doi: 10.1029/TR027i004p00526.
- Doe, T.W. 1991. Fractional dimension analysis of constant-pressure well tests [en ligne]. *Dans Society of Petroleum Engineers paper No. 22702*, SPE Annual Technical Conference and Exhibition, 6-9 October, 1991, Dallas, Texas, USA. p. 461–467. doi: 10.2118/22702-MS.
- Döll, P. 2009. Vulnerability to the impact of climate change on renewable groundwater resources: a global-scale assessment [en ligne]. *Environmental Research Letters*, **4**(3) : 035006. doi: 10.1088/1748-9326/4/3/035006.
- Eckhardt, K., et Ulbrich, U. 2003. Potential impacts of climate change on groundwater recharge and streamflow in a central European low mountain range [en ligne]. *Journal of Hydrology*, **284**(1–4) : 244–252. doi: 10.1016/j.jhydrol.2003.08.005.
- Eggleston, J., et Rojstaczer, S. 1998. Identification of large-scale hydraulic conductivity trends and the influence of trends on contaminant transport [en ligne]. *Water Resources Research*, **34**(9) : 2155–2168. doi: 10.1029/98WR01475.
- Ehlig-Economides, C. 1988. Use of the pressure derivative for diagnosing pressure-transient behavior [en ligne]. *Journal of Petroleum Technology*, **40**(10) : 1280–1282. doi: 10.2118/18594-PA.

- Escobar, F., Saavedra, N., Hernandez, C., Hernandez, Y., Pilataxi, J., et Pinto, D. 2004. Pressure and Pressure Derivative Analysis for Linear Homogeneous Reservoirs Without Using Type-Curve Matching [en ligne]. Society of Petroleum Engineers. doi: 10.2118/88874-MS.
- Gringarten, A.C., Ramey, H.J., et Raghavan, R. 1974. Unsteady-State Pressure Distributions Created by a Well With a Single Infinite-Conductivity Vertical Fracture [en ligne]. Society of Petroleum Engineers Journal, **14**(04) : 347–360. doi: 10.2118/4051-PA.
- Grubb, S. 1993. Analytical model for estimation of steady-state capture zones of pumping wells in confined and unconfined aquifers [en ligne]. Ground Water, **31**(1) : 27–32. doi: 10.1111/j.1745-6584.1993.tb00824.x.
- Hantush, M.S. 1956. Analysis of data from pumping tests in leaky aquifers [en ligne]. Transactions, American Geophysical Union, **37**(6) : 702. doi: 10.1029/TR037i006p00702.
- Horne, R.N. 1990. Modern well test analysis: a computer-aided approach. Petroway, Palo Alto, Calif.
- Huet, M. 2015, janvier. Comparaison de méthodes d'estimation de la recharge des aquifères : exemple de la région Charlevoix-Haute-Côte-Nord [en ligne]. masters, Université du Québec à Chicoutimi, Chicoutimi. Disponible à <http://constellation.uqac.ca/3828/> [cité le 16 janvier 2018].
- Karanta, G. 2002, octobre. Étude comparative de méthodes de détermination de périmètres de protection autour des ouvrages de captage dans les aquifères captifs fracturés du sud-ouest du Québec. [en ligne]. masters, Université du Québec, Institut national de la recherche scientifique, Québec. Disponible à <http://espace.inrs.ca/349/> [cité le 7 décembre 2015].
- Kruseman, G.P., et Ridder, N.A. de. 1994. Analysis and evaluation of pumping test data. 2. ed. (compl. rev.), repr. International Institute for Land Reclamation and Improvement, Wageningen.
- Kuchuk, F.J., et Biryukov, D. 2013. Pressure transient tests and flow regimes in fractured reservoirs [en ligne]. SPE Annual Technical Conference and Exhibition. Society of Petroleum Engineers, New Orleans, Louisiana, USA. doi: 10.2118/166296-MS.
- Mattar, L. 1997. Derivative Analysis Without Type Curves [en ligne]. Society of Petroleum Engineers. doi: 10.2118/97-51.
- Moncada, K., Tiab, D., Escobar, F.-H., Montealegre, M., Chacon, A., Zamora, R., et Nese, S.-L. 2005. Determination of vertical and horizontal permeabilities for vertical oil and gas wells with partial completion and partial penetration using pressure and pressure derivative plots without type-curve matching. CT&F - Ciencia, Tecnología y Futuro, **3**(1) : 77–94.
- Neuman, S.P. 1972. Theory of flow in unconfined aquifers considering delayed response of the water table [en ligne]. Water Resources Research, **8**(4) : 1031–1045. doi: 10.1029/WR008i004p01031.

- Paradis, D., Martel, R., Karanta, G., Lefebvre, R., Michaud, Y., Therrien, R., et Nastev, M. 2007. Comparative study of methods for WHPA delineation [en ligne]. *Ground Water*, **45**(2) : 158–167. doi: 10.1111/j.1745-6584.2006.00271.x.
- Polek, J., Karasaki, K., Long, J.C.S., et Barker, J. 1989. Flow to wells in fractured rock with fractal structure. *Dans Fractal Aspects of Materials*. Materials Research Society.
- Rafini, S., et Larocque, M. 2012. Numerical modeling of the hydraulic signatures of horizontal and inclined faults [en ligne]. *Hydrogeology Journal*, **20**(2) : 337–350. doi: 10.1007/s10040-011-0812-4.
- Renard, P. 2005. The future of hydraulic tests [en ligne]. *Hydrogeology Journal*, **13**(1) : 259–262. doi: 10.1007/s10040-004-0406-5.
- Renard, P., Glenz, D., et Mejias, M. 2009. Understanding diagnostic plots for well-test interpretation [en ligne]. *Hydrogeology Journal*, **17**(3) : 589–600. doi: 10.1007/s10040-008-0392-0.
- Scanlon, B.R., Healy, R.W., et Cook, P.G. 2002. Choosing appropriate techniques for quantifying groundwater recharge [en ligne]. *Hydrogeology Journal*, **10**(1) : 18–39. doi: 10.1007/s10040-001-0176-2.
- Taylor, R.G., Scanlon, B., Döll, P., Rodell, M., van Beek, R., Wada, Y., Longuevergne, L., Leblanc, M., Famiglietti, J.S., Edmunds, M., Konikow, L., Green, T.R., Chen, J., Taniguchi, M., Bierkens, M.F.P., MacDonald, A., Fan, Y., Maxwell, R.M., Yechieli, Y., Gurdak, J.J., Allen, D.M., Shamsudduha, M., Hiscock, K., Yeh, P.J.-F., Holman, I., et Treidel, H. 2013. Ground water and climate change [en ligne]. *Nature Climate Change*, **3**(4) : 322–329. doi: 10.1038/nclimate1744.
- Theis, C.V. 1935. The relation between the lowering of the piezometric surface and the rate and duration of discharge of a well using ground-water storage [en ligne]. *Transactions, American Geophysical Union*, **16** : 519–524. doi: 10.1029/TR016i002p00519.
- Tiab, D. 1993a. Analysis of pressure and pressure derivatives without type curve matching - IV. Flow and no-flow boundaries. to be submitted for presentation at the SPE Eastern Regional Meeting, Pittsburgh.
- Tiab, D. 1993b. Analysis of pressure and pressure derivatives without type-curve matching - V. Naturally Fractured Reservoirs. to be submitted for presentation at the SPE Eastern Regional Meeting, Pittsburgh.
- Tiab, D. 1993c. Analysis of pressure and pressure derivatives without type-curve matching - I. Skin and Wellbore Storage [en ligne]. *Society of Petroleum Engineers*. doi: 10.2118/25426-MS.
- Tiab, D. 1993d. Analysis of pressure and pressure derivative without type-curve matching - III. Vertically fractured wells in closed systems [en ligne]. *SPE Western Regional Meeting. Society of Petroleum Engineers, Anchorage, Alaska, USA*. doi: 10.2118/26138-MS.
- Tiab, D. 1994. Analysis of pressure and pressure derivative without type-curve matching: Vertically fractured wells in closed systems [en ligne]. *Journal of Petroleum Science and Engineering*, **11**(4) : 323–333. doi: 10.1016/0920-4105(94)90050-7.

- Todd, D.K. 1980. Groundwater hydrology. 2nd ed. JWiley, New York ; Toronto.
- Vorosmarty, C.J., Green, P., Salisbury, J., et Lammers, R.B. 2000. Global Water Resources: Vulnerability from Climate Change and Population Growth [en ligne]. *Science*, **289**(5477) : 284–288. doi: 10.1126/science.289.5477.284.
- Wada, Y., van Beek, L.P.H., Wanders, N., et Bierkens, M.F.P. 2013. Human water consumption intensifies hydrological drought worldwide [en ligne]. *Environmental Research Letters*, **8**(3) : 034036. doi: 10.1088/1748-9326/8/3/034036.
- Warren, J.E., et Root, P.J. 1963. The behavior of naturally fractured reservoirs [en ligne]. *Society of Petroleum Engineers Journal*, **3**(03) : 245–255. doi: 10.2118/426-PA.
- Wyssling, L. 1979. Eine neue formel zur Berechnung der Zuströmungsdauer (Laufzeit) des grundwassers zu einem grundwasser pumpwerk. *Eclogae Geologicae Helvetiae*, **72**(2) : 401–406.

CHAPITRE 1

CARACTÉRISATION ET MODÉLISATION HYDROGÉOLOGIQUE DES AQUIFÈRES

1.1 GÉNÉRALITÉS EN HYDROGÉOLOGIE

Étymologiquement, un aquifère est composé par le préfixe « aqu » qui vient du latin *aqua*, eau et du suffixe « fère » qui vient du latin *fer*, porter. Littéralement, le terme aquifère signifie « qui porte l'eau ». Selon le Glossaire international d'hydrogéologie (1978), un aquifère est défini par une formation réservoir qui contient de l'eau mobilisable et qui est suffisamment conductrice pour permettre un écoulement souterrain significatif et le captage d'une quantité appréciable d'eau souterraine. Cette définition met en exergue l'importance de comprendre, d'une part, les flux souterrains (circulation des fluides) et d'autre part, le système géologique (réservoir) pour gérer les ressources souterraines disponibles.

La connaissance de la structure physique de l'aquifère est donc primordiale afin de comprendre les vitesses et les directions d'écoulement. Selon que l'eau circule à travers une porosité d'interstices (également appelée porosité de pores, ou porosité primaire) ou circule à travers une porosité de fissures (communément appelée porosité secondaire), les vitesses et les chemins d'écoulement seront différents (Figure 1.1). Dans le cas du milieu poreux, l'eau circule à travers les pores interconnectés du milieu, alors que dans le cas d'un milieu fissuré, l'eau s'écoule à travers un réseau de fissures, de fractures ou de failles

interconnectées et ouvertes en plus de circuler avec une moindre facilité dans le milieu matriciel poreux.

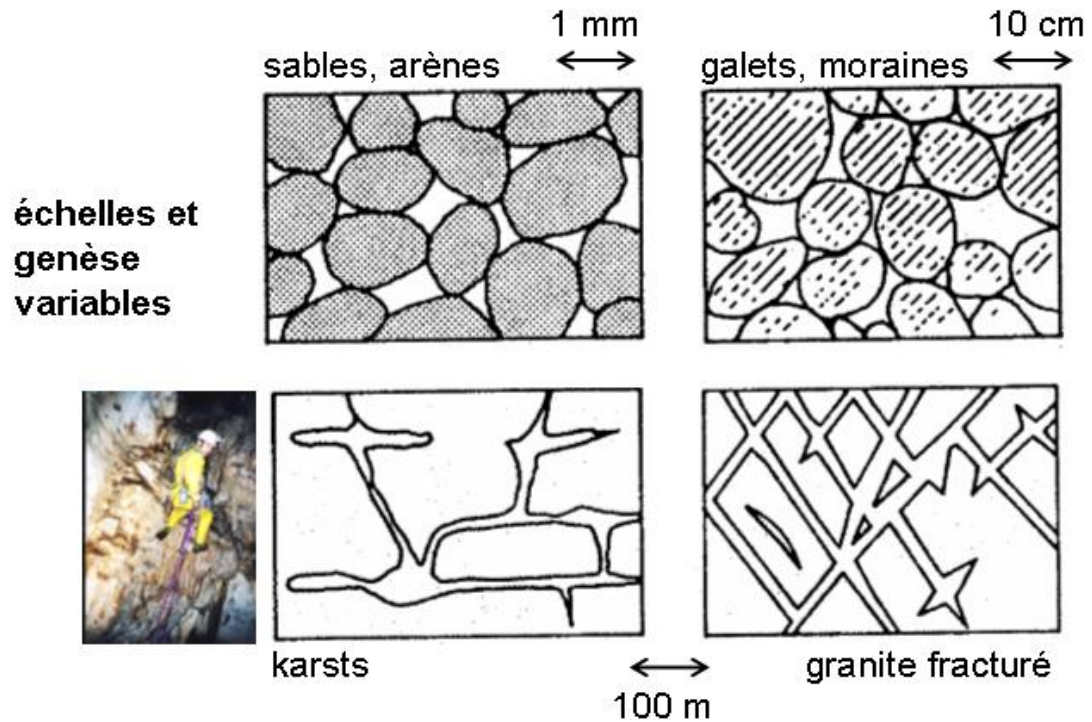


Figure 1.1 : Porosité rencontrée dans deux grands types de réservoirs : i) le milieu poreux (sable, arènes, grès, craie, galets, moraines, etc.), où l'on considère la porosité primaire, ii) le milieu fissuré (roche calcaire fissurée, roche cristalline, etc.), où l'on peut considérer à la fois, la porosité primaire (au sein de la matrice) et la porosité secondaire (dans les fissures) et iii) le milieu karstifié où l'on considère la porosité des drains, des fractures et de la matrice. (<http://www.isige.mines-paristech.fr>).

Le terme milieu discontinu regroupe des milieux dont le comportement hydrodynamique peut-être très différent. En effet, dans le cas d'aquifères fracturés, les discontinuités sont d'échelle mésoscopique (fractures). Lorsque la répartition spatiale de ces fractures est

uniforme et interconnecté, l'aquifère est assimilable à un milieu homogène équivalent ou un milieu à double porosité. Les failles sont quant à elles des structures macroscopiques qui génèrent une forte anisotropie hydraulique (Bense et Person 2006) et peuvent avoir une forte influence sur les écoulements souterrains. En effet, selon Caine et al. (1996) les failles peuvent agir comme des conduits, comme des barrières ou comme une combinaison conduit-barrière. La modélisation de ces structures nécessite donc une approche discrète, c'est-à-dire de les représenter explicitement.

1.2 LES DIFFÉRENTES APPROCHES POUR MODÉLISER UN AQUIFÈRE

L'hydrogéologie dispose de nombreux types de modèles pour représenter les aquifères.

- Les modèles **analogiques** qui se basent, sur une étude expérimentale en laboratoire afin de décrire des phénomènes hydrauliques.
- Les modèles **analytiques**, qui consistent à déterminer des solutions mathématiques à l'équation de diffusivité. Ceux-ci peuvent être **déterministes** ou **stochastiques**.
- Les modèles **numériques** qui permettent de modéliser les écoulements souterrains en discrétisant dans le temps et l'espace, l'équation de la diffusivité (aux dérivées partielles).

En hydrogéologie, la description des transferts de pression au sein d'un aquifère (il en va de même pour les transferts de masse et de chaleur), se basent, le plus souvent, sur des modèles fondés sur des équations mathématiques et des hypothèses simplificatrices. Il existe plusieurs approches pour aborder la modélisation d'un aquifère.

- **L'approche discrète** : pour les aquifères fracturés ou faillés, l'approche discrète repose sur une représentation précise et explicite du réseau de discontinuités, tel qu'il est observé *in situ* ou conceptualisé fictivement, et considère l'écoulement dans chaque fracture prise en compte. On suppose dans cette approche que la réponse hydraulique de l'aquifère peut être expliquée par la géométrie du réseau de discontinuités (hypothèse non vérifiée actuellement (Rafini 2008)) ainsi que les propriétés hydrauliques de chaque fracture. On dénombre actuellement de nombreux modèles discrets, à savoir, le modèle en plaques parallèles, le modèle à fracture verticale isotrope, le modèle à fracture horizontale isotrope, les modèles à fracture pseudo-anisotrope et anisotrope ainsi que des modèles considérant plusieurs fractures (Dewandel et al. 2018). Pour plus de détails sur ces modèles, il est possible de se référer aux thèses de De Dreuzy (1999) et de Rafini (2008). Dans cette approche, l'échelle modélisée est limitée face à l'ampleur du travail et la difficulté à caractériser les fractures (De Dreuzy 1999). Dans la zone concentrée autour d'un puits, il est possible de décrire le réseau de fractures de façon déterministe, par des méthodes diagraphiques ou hydrauliques.
- **L'approche stochastique** : les fractures qui ne sont pas directement observées sont couramment représentées par une **approche stochastique** (ou probabiliste). Celle-ci est basée sur une représentation statistique des propriétés du milieu (distributions statistiques de la forme, la longueur, l'orientation, la position, la densité et d'ouverture des fractures ainsi que la dimensionnalité du réseau d'écoulement) (Long et al., 1982, Dverstop et Andersson, 1989; Cacas et al., 1990b, cités par De Dreuzy (1999)). Utilisant le logiciel décrit par Rouleau (1988), Rouleau et Gale (1987) ont présenté la première application sur un cas réel de l'approche de modélisation de l'écoulement dans un réseau stochastique de fractures. Leur étude a porté sur un tunnel excavé au site de Stripa en Suède, ce site qui semble avoir servi

aussi à une application du modèle "GRF" proposé par Barker (1988). Cette approche est cependant, très simplifiée, en termes de géométrie et de propriétés hydrauliques des fractures et nécessite de connaître de nombreux paramètres.

- **L'approche hydraulique** : une autre approche, consiste à imposer une perturbation dans un aquifère, au moyen d'un pompage (ou d'une injection), et d'en observer la réponse hydraulique. En général, les essais hydrauliques sont réalisés car dans la plupart des cas, les connaissances sur le milieu ne sont pas suffisantes pour engager une modélisation avec les modèles déterministes. L'interprétation des essais hydrauliques a l'avantage de déterminer les paramètres hydrauliques *in situ*. Elle est d'ailleurs la méthode la plus communément adoptée par les hydrogéologues, afin de déterminer les propriétés hydrauliques d'un aquifère (e.g. Kruseman et al. 1973, Renard et al. 2009) et par les pétroliers, afin de caractériser un réservoir géologique (Mattar, 1994; Mattar, 2004; Anisur Rahman et Mattar, 2007; Anderson *et al.*, 2006). Cette méthode permet notamment de déduire des informations sur les propriétés macroscopiques du réservoir géologique (transmissivité, emmagasinement, limites, géométrie, hétérogénéité, etc.) et les propriétés hydrauliques du puits de pompage (efficacité du puits, défaut de scellement, captage partiel, etc.).

1.3 RÉALISATION D'UN ESSAI HYDRAULIQUE

Plusieurs raisons peuvent motiver la réalisation d'un essai de pompage, notamment :

- déterminer les caractéristiques physiques et hydrodynamiques *in situ* d'un réservoir (transmissivité, emmagasinement, hétérogénéité, géométrie, limites, disposition des couches géologiques, anisotropie). Le paramètre de la transmissivité doit être déterminé

- car il retranscrit la capacité du réservoir à fournir de l'eau.
- déterminer la productivité d'un puits et connaître les frontières de recharge ou les frontières imperméables de l'aquifère, dans le cadre d'une prospection sur les ressources en eau souterraines.
- déterminer les périmètres de protection à mettre en place autour du puits.
- obtenir des échantillons de fluide (afin de déterminer et contrôler la qualité de l'eau dans le cadre d'une alimentation en eau potable (AEP) par exemple).
- effectuer un suivi géochimique ou déterminer la nature du fluide pompé (gaz, huile), dans le cadre de recherche pétrolière.
- étudier le schéma de fonctionnement d'un aquifère (Roques 2013, Roques et al. 2014b, 2014a).

Dans le cadre de la présente étude, on s'intéressera à l'analyse des propriétés hydrauliques du réservoir.

Il existe plusieurs procédures afin de réaliser un essai hydraulique :

- l'essai de pompage peut être réalisé dans un seul puits. Le rabattement est parfois mesuré uniquement dans le puits de pompage ou mesuré également dans plusieurs piézomètres d'observation.
- le test d'interférence, qui consiste à pomper dans plusieurs puits en même temps. Le suivi du rabattement peut être effectué dans les différents puits de pompage et dans des piézomètres d'observation.

Pour les deux cas précédents, les essais peuvent être réalisés avec un débit de pompage constant ou par palier.

- le choc hydraulique (*slug test*) consiste à perturber l'aquifère au moyen d'une brusque modification de la charge hydraulique dans le puits. L'évolution de la charge hydraulique peut être mesurée dans le puits ou des piézomètres d'observation.
- le test avec obturateur (*packer test*), qui consiste à effectuer un test hydraulique sur une épaisseur restreinte de l'aquifère. Pour cela, la perturbation hydraulique s'effectue entre deux obturateurs qui isolent la zone test d'aquifère ciblée.
- L'étude de la remontée est également importante, peu importe l'essai de pompage réalisé, car elle fournit généralement le même type d'information qu'un pompage ainsi que des données moins bruitées, car non soumises aux variations non contrôlées du débit de la pompe.

La qualité d'un essai de pompage dépend de la qualité et de la précision des mesures du débit de pompage, du rabattement et du temps.

L'interprétation d'un essai de pompage se réalise en trois temps : un contrôle de la qualité des données mesurées de rabattement et de débit, une représentation graphique de la variation de ces données et leur interprétation à l'aide de modèles analytiques et/ou numériques.

1.4 INTERPRÉTATION DES ESSAIS DE POMPAGE

L'interprétation d'un essai de pompage se base sur le fait que la propagation de l'onde de pression induite par un pompage est influencée par le milieu traversé. Cette méthode est abondamment employée dans les domaines hydrogéologique et pétrolier. Il est donc possible de déterminer les propriétés hydrodynamiques d'un aquifère à partir de sa réponse

hydraulique à une perturbation anthropique, qui est en général représentée par l'évolution temporelle de la charge hydraulique mesurée au sein du puits et de piézomètres d'observation. Il est cependant important de garder à l'esprit qu'étant donné que la propagation de l'onde de pression, en régime transitoire est diffusive, les propriétés hydrauliques calculées par un essai de pompage, représentent une valeur moyenne des propriétés rencontrées et non une valeur localisée. En d'autres termes, le comportement d'un aquifère pompé à un temps t reflète l'ensemble des milieux affectés à ce stade t par la perturbation hydraulique. Les propriétés hydrauliques représentent une valeur moyenne pour les milieux déjà soumis à la perturbation au temps t .

Dans le monde des consultants en hydrogéologie, il est souvent admis que les conditions de terrain satisfont aux hypothèses de Theis (1935) pour interpréter les essais de pompage. Celles-ci stipulent entre autres que les écoulements induits par un pompage sont radiaux, que l'aquifère est homogène et captif. De nombreux auteurs ont cependant soulevé le manque de réalisme de ce modèle, dans le cas d'aquifères à géométrie variable (Smith et Vaughan 1985, Dal Soglio 2012), d'aquifères interconnectés (Chesnaux et al. 2012), d'aquifères hétérogènes (Geier *et al.*, 1996; Bowman *et al.*, 2013, Walker et Roberts, 2003), d'aquifères fracturés (Barker 1988, Kuusela-Lahtinen et al. 2003, Beauheim et al. 2004) et faillés (Rafini 2008, Rafini et Larocque 2012). En observant les rabattements dans un aquifère calcaire plissé et faillé, après un pompage de 24 h, Smith et Vaughan (1985) ont notamment observé que l'hypothèse des écoulements radiaux est complètement aberrante dans ce contexte (Figure 1.2).

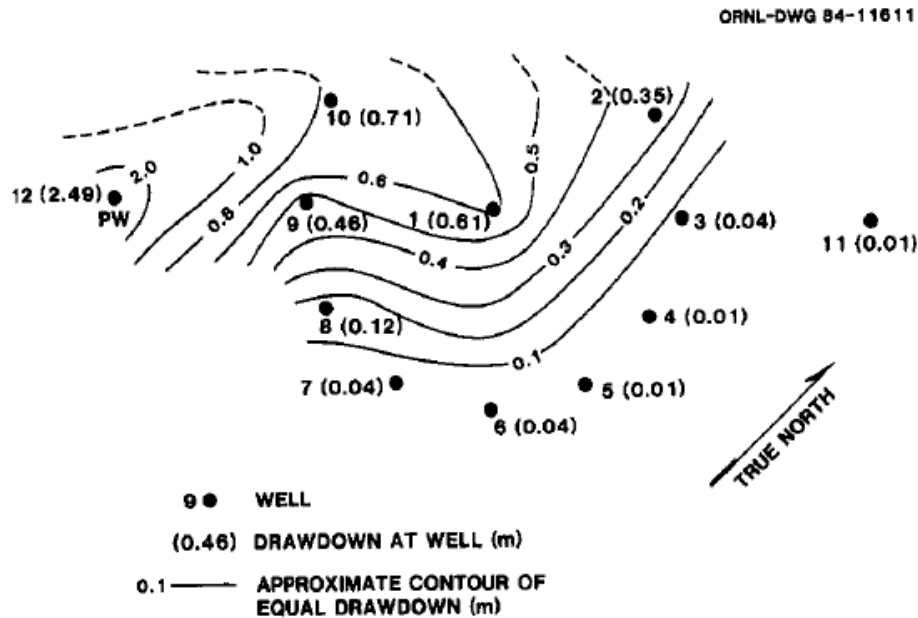


Figure 1.2 : Lignes de rabattement dans un aquifère calcaire faillé et plissé après un pompage de 24 heures ($Q = 3.29 \text{ L}\cdot\text{min}^{-1}$). (Smith et Vaughan 1985).

Ces trop fortes approximations mènent à une conceptualisation erronée de la géométrie d'écoulement, ce qui peut entraîner des erreurs d'interprétation des propriétés hydrauliques de l'aquifère étudié.

Une manière plus poussée d'interpréter les essais de pompage consiste à représenter des « *diagnostic plots* ». Ce nom n'a pas encore été traduit en français, on emploiera donc sa traduction littérale « analyses graphiques diagnostiques ». Cette approche est couramment utilisée par les pétroliers (Mattar 1994, 2004) et en voie de développement dans le domaine de l'hydrogéologie appliquée (Renard et al. 2009). Elle consiste à représenter les mesures de rabattement (m) ou de la pression (en Pa ou en psi) en fonction du temps, selon différents systèmes de coordonnées (Figure 1.3). Cette approche multi-coordonnées permet de faire

ressortir les différentes caractéristiques comportementales d'un milieu soumis à un essai de pompage (Mattar 2004), comme par exemple la signature des conditions hydrauliques aux frontières, le signal d'un aquifère à nappe libre, celui d'une contribution de la matrice, etc. Cette combinaison de graphiques aide ainsi à choisir le modèle analytique le plus approprié pour modéliser les mesures de rabattement (Renard et al. 2009).

The kangaroo in different coordinates

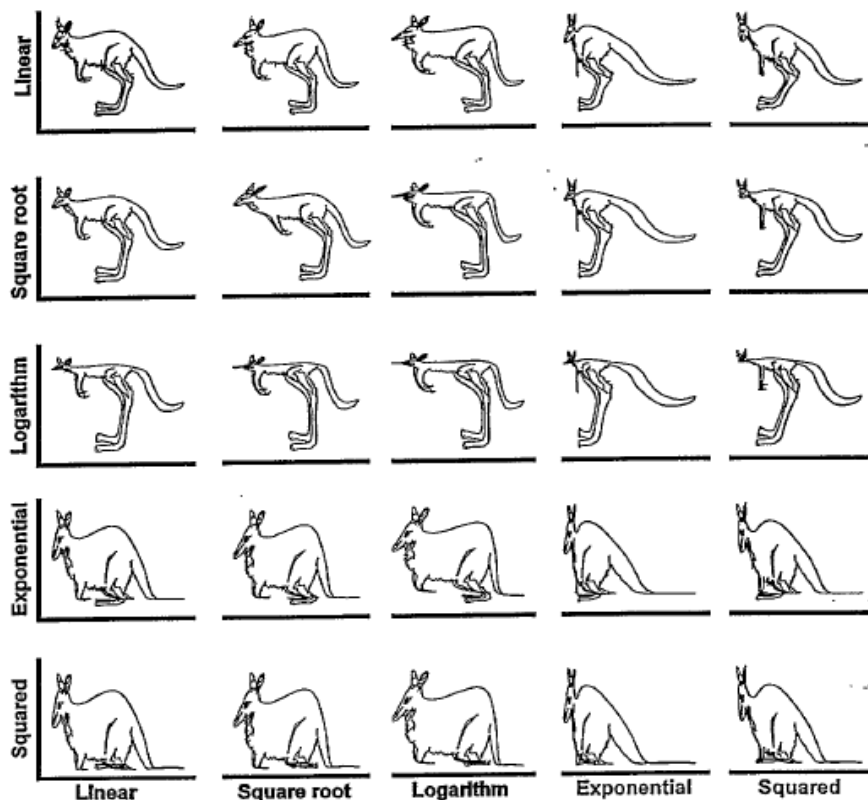


Figure 1.3 : Influence des systèmes de coordonnées sur la forme des courbes représentées du rabattement en fonction du temps lors d'un essai de pompage, a) exemple du « Kangaroo plot » (Mattar 2004).

Comme proposé par Bourdet *et al.* (1989), il est possible de représenter les rabattements de façon beaucoup plus éloquente en représentant sa « dérivée logarithmique ». Celle-ci consiste à représenter la dérivée du rabattement divisée par la dérivée du logarithme du temps en fonction du temps (sur un graphique à échelles log-log). Cette dernière représentation graphique est beaucoup plus sensible aux hétérogénéités (Doe 1991), à la géométrie du réservoir, au réseau de fractures (van Tonder *et al.* 2001) et aux frontières de recharge (Walker et Roberts 2003) rencontrés au cours du pompage. La Figure 1.4 montre une comparaison des signatures hydrauliques en rabattement et en dérivée logarithmique du rabattement pour un même essai de pompage dans différents aquifères. Cette figure illustre clairement la sensibilité plus importante de la dérivée logarithmique, aux conditions physiques et hydrodynamiques, par rapport à une simple représentation des rabattements. Nonobstant ses atouts, cette représentation en dérivée log du rabattement est encore peu utilisée en hydrogéologie, car son interprétation est difficile (Beauheim *et al.* 2004) et aussi peut-être parce que des pratiques bien ancrées sont plus difficiles à changer. La notoriété du signal de la dérivée logarithmique du rabattement dans la littérature pétrolière semble avoir réduit le terme *diagnostic plots* à un graphique log-log représentant à la fois les séries temporelles du rabattement et de la dérivée logarithmique du rabattement (Bourdet *et al.* 1989, Renard *et al.* 2009). Dans la suite de cette thèse, le terme « analyses graphiques diagnostiques » sera donc employé pour exprimer les séries temporelles de s et de $ds/d\log t$ affichées avec des axes log-log.

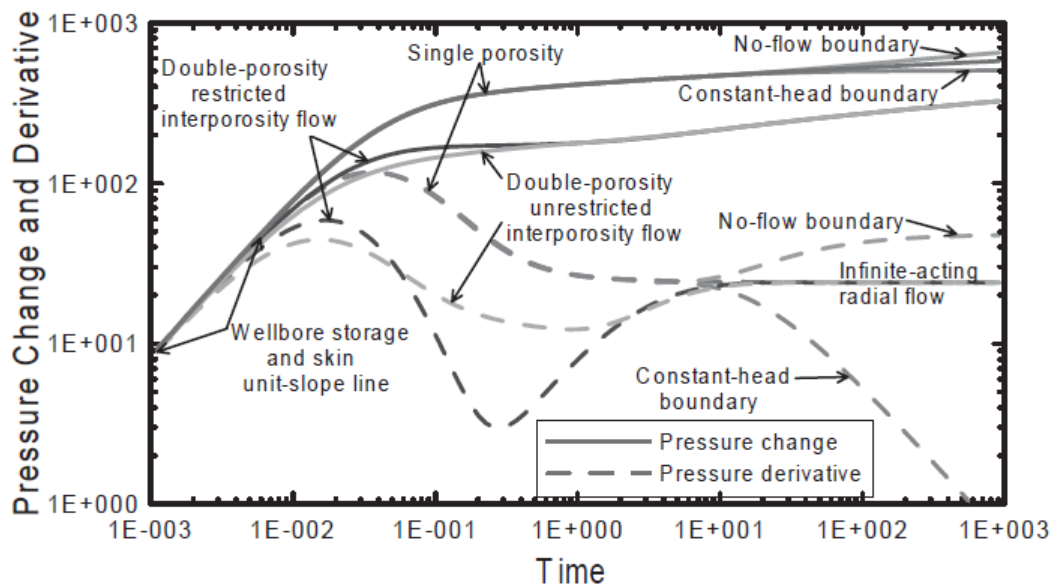


Figure 1.4 : Graphique diagnostique du rabattement (essai de pompage à débit constant) et de la dérivée logarithmique du rabattement en échelle log-log. Ce graphique met en avant le potentiel diagnostique de la dérivée logarithmique du rabattement. (Beauheim et al. 2004).

Une fois ces représentations graphiques réalisées, notamment celle de la dérivée log du rabattement, il est possible de déterminer graphiquement les propriétés hydrauliques du milieu par un calage de courbes théoriques issues de modèles analytiques (voir les sections 1.7.1 et 1.7.2). Ces courbes de calage sont obtenues en simplifiant l'équation de diffusivité, dans des hypothèses plus ou moins acceptables selon les contextes. En guise d'exemple, et de façon non exhaustive, on citera la solution de Theis (1935), la simplification de Cooper et Jacob (1946), Hantush et Jacob (1955), Neuman et Witherspoon (1969), Moench (1985), *etc.* ainsi que le modèle *Generalized Radial Flow* (Barker 1988) et le modèle *Generalized Darcy Law* (Atangana et Botha 2013). Des revues de modèles analytiques ont notamment été proposées par Kruseman et al. (1973), Chapuis (2007), Renard et al. (2009).

1.5 EFFETS DE LA STRUCTURE PHYSIQUE DU RÉSERVOIR SUR LES ÉCOULEMENTS

Lors d'un pompage, plusieurs paramètres liés à la structure physique et hydraulique de l'aquifère peuvent influencer la diffusion de l'onde équipotentielle de rabattement et donc influencer les rabattements mesurés au puits :

- la **géométrie** de l'aquifère (géométrie des formations géologiques ou des zones altérées ou fracturées),
- l'**hétérogénéité** de l'aquifère (variation de la conductivité hydraulique),
- des **connexions hydrauliques** entre les aquifères (des études ont notamment porté sur les risques de contaminations croisées entre les aquifères lors d'un pompage (Leveinen 2001, Chesnaux et al. 2012)),
- des **frontières hydrauliques** (frontière à charge imposée, frontière à limite imperméable),
- un **tassement** possible de l'aquifère en pompage. Ce phénomène se rencontre particulièrement en milieu poreux,
- les **effets de puits** (emmagasinement du puits, effets pariétaux),
- des **discontinuités** au sein de roches métamorphiques, ignées et carbonatées (failles, fractures, fissures) : orientation des failles (Rafini 2008), connectivité du réseau (Robinson 1983), distribution d'ouverture et de longueur des discontinuités.
- des relations géométriques entre le puits et l'aquifère (captage partiel).

Ces paramètres ne sont cependant pas forcément tous considérés dans l'interprétation des essais de pompage, car la résolution analytique de l'équation de diffusivité nécessite de poser des hypothèses plus ou moins fortes sur la conceptualisation de l'aquifère pompé. Pour plus de précision sur l'influence des conditions physiques et hydrauliques sur le rabattement, il est possible de se référer à la partie 1.7.2.3, qui aborde cette problématique à partir d'une *modélisation des écoulements radiaux généralisés*, telle que proposée par Barker (1988) (modèle présenté en 1.7.2.1).

1.6 ÉQUATION DE DIFFUSIVITÉ

L'une des équations les plus importantes en hydrogéologie, et à partir de laquelle découle la majorité des modèles analytiques en hydrogéologie, est l'équation de diffusivité (aussi appelée équation de continuité). Cette équation est obtenue en considérant un écoulement soumis à une variation de charge hydraulique, à travers un volume élémentaire. Pour cela, on stipule que les flux se conservent de part et d'autre du volume élémentaire et qu'ils respectent la loi de Darcy. L'équation est,

$$\vec{\nabla}(\bar{K}(x,t)\vec{\nabla}h) = S_s(x,t) \frac{\partial h}{\partial t} \pm f(x,t) \quad (1.1)$$

$\bar{K}(x)$ = tenseur de conductivité hydraulique [L/T]

h = charge hydraulique [L]

S_s = coefficient d'emmagasinement spécifique [L⁻¹]

f(x,t) = terme source

$\vec{\nabla}$ = vecteur gradient représenté par le signe nabla

La résolution analytique de cette équation est très complexe et nécessite de poser quelques hypothèses sur le régime d'écoulement et la structure physique de l'aquifère.

L'interprétation des essais hydrauliques en régime permanent nécessite un pompage de très longue durée afin d'atteindre une stabilisation des rabattements pouvant durer plusieurs semaines dans certains aquifères. Ces essais de pompage ont un coût élevé et nécessitent une maintenance fastidieuse (surveillance de la pompe de jour et de nuit, apport électrique...), c'est pourquoi les solutions analytiques en régime transitoire sont plus souvent utilisées pour modéliser les essais. De plus, les temps longs apportent plutôt des informations sur les limites hydrauliques de l'aquifère (Figure 1.4).

1.7 SOLUTIONS ANALYTIQUES DE L'ÉQUATION DE DIFFUSIVITÉ

1.7.1 MODÈLES D'INTERPRÉTATION DES ESSAIS DE POMPAGE

CONVENTIONNELS

Comme vu précédemment la caractérisation d'un aquifère en hydrogéologie appliquée consiste notamment à déterminer la transmissivité et l'emmagasinement de l'aquifère. La transmissivité étant la conductivité hydraulique intégrée sur l'épaisseur de l'aquifère. On présente ici seulement les solutions de Theis et de Cooper-Jacob car elles sont le plus conventionnellement utilisées en hydrogéologie appliquée, mais il existe de nombreux

autres modèles analytiques disponibles pour décrire la réponse hydraulique d'un aquifère à un pompage (Kruseman et al. 1973, Renard et al. 2009).

2.7.1.1 Solution analytique de Theis (1935)

En 1935, Theis propose une solution analytique de l'équation de diffusivité pour un aquifère conceptuel (Figure 1.5) dont les hypothèses sont :

- l'aquifère est homogène, isotrope et d'épaisseur uniforme dans la zone influencée par le pompage d'essai,
- l'extension latérale de l'aquifère est infinie, c'est à dire que le cône de rabattement ne se rapproche jamais d'une limite de l'aquifère,
- le puits est complet (c'est à dire qu'il pénètre entièrement l'aquifère) et l'eau arrive en écoulement horizontal sur toute l'épaisseur de la nappe,
- l'aquifère est limité à sa base par une couche imperméable horizontale,
- avant le pompage, la surface piézométrique est (presque) horizontale dans la zone influencée par le pompage,
- il n'y a pas de variation piézométrique avant le début de l'essai,
- toute modification de la position de la surface piézométrique est due uniquement au pompage,
- la loi de Darcy est applicable,
- l'eau a une densité et une viscosité constante,
- le débit pompé est constant,

- le puits a une efficacité de 100% et un diamètre infinitésimal, c'est à dire que l'emmagasinement dans le volume du puits peut être négligé,
- l'aquifère est à nappe captive (l'aquitard est donc supposé complètement imperméable = aquiclude),
- l'écoulement est en régime transitoire, c'est à dire que l'évolution du rabattement est non négligeable,
- l'eau provenant de l'emmagasinement est libérée instantanément avec la baisse de charge hydraulique,
- l'écoulement vers le puits se fait de manière radiale. Cette hypothèse suppose que le gradient hydraulique régional est négligé par rapport au gradient induit par le pompage.

Il est intéressant de noter que l'application du principe de superposition permet de prendre en compte les variations de débit. Aussi, les effets du puits, tels que les effets pariétaux (skin), les pertes de charge quadratiques et les effets capacitifs peuvent être pris en compte dans la solution analytique de Theis (1935).

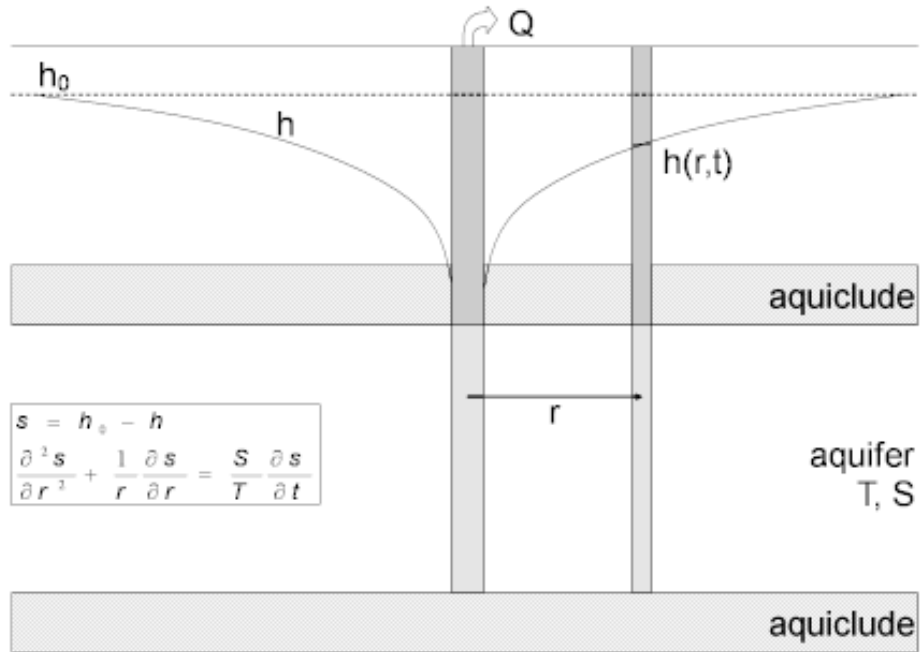


Figure 1.5 : Schéma conceptuel d'un aquifère captif pompé selon la solution analytique de Theis (1935). h_0 représente la charge hydraulique initiale de l'aquifère, $h(r,t)$ représente le profil de charge hydraulique induit par le pompage, T est la transmissivité de l'aquifère, S est l'emmagasinement de l'aquifère et r est la distance radiale. (tiré de <http://www.aqtesolv.com/>)

La solution de Theis s'écrit :

$$s = \frac{Q}{4\pi T} W(u) \quad (1.2)$$

avec
$$W(u) = -E_i(-u) = \int_u^\infty \frac{e^{-y}}{y} dy \approx -\lambda - \ln(u) - \sum_{n=1}^{\infty} \frac{(-1)^n u^n}{n(n!)} \quad (1.3)$$

et
$$u = \frac{r^2 S}{4Tt} \quad (1.4)$$

s = rabattement [L]

Q = débit de pompage [L^3T^{-1}]

T = transmissivité [L^2T^{-1}]

S = coefficient d'emmagasinement [-]

r = distance radiale au puits [L]

$W(u)$ = fonction exponentielle intégrale = $-E_i(-u)$

$\lambda \approx 0.57721$ = constante d'Euler

2.7.1.2 Simplification de Cooper-Jacob (1946)

En 1946, Cooper et Jacob présentent une simplification de la solution de Theis. Les hypothèses sont donc les mêmes que celles employées par Theis (1935) avec en plus, l'hypothèse que $u < 0.01$ (donc t est important et/ou r est faible). Cette méthode a l'avantage d'être plus directe dans la résolution graphique puisque la fonction exponentielle intégrale, $W(u)$, est simplifiée au strict minimum des deux premiers termes les plus significatifs de son développement en séries entières.

La solution analytique s'écrit,

$$s = \frac{Q}{4\pi T} \ln\left(\frac{2,25Tt}{r^2 S}\right) \quad (1.5)$$

$$s = \frac{2.3Q}{4\pi T} \log\left(\frac{2.25Tt}{r^2 S}\right)$$

La représentation des rabattements en fonction du temps en échelle semi-logarithmique (en base 10) donne donc une droite, dont la pente vaut : $\frac{2.3Q}{4\pi T}$.

2.7.1.3 Limites des modèles conceptuels conventionnels

Comme vu précédemment, l'interprétation des essais de pompage est réalisée par une méthode graphique. L'idée est de superposer une courbe analytique sur des données mesurées, dans un système de coordonnées (généralement log-log ou semi-log). Une fois que cette superposition est satisfaisante, il est possible d'estimer les propriétés hydrauliques de l'aquifère en déterminant les coordonnées d'un point arbitraire (qui représente le vecteur de translation entre les deux courbes) pour les deux graphiques.

Cette approche fait face à deux contraintes majeures :

- la non-unicité des modèles pour représenter une même évolution des rabattements. En effet, différents modèles produisent des courbes analytiques similaires : par exemple, la courbe en échelle log-log du modèle de limites à charge imposée et celle du modèle d'aquifère semi-captif (drainance d'un aquitard) sont similaires (Renard et al. 2009) même si les modèles sont différents.

- les hypothèses sur les directions d'écoulement sont très restrictives et ne sont pas applicables pour des aquifères complexes (hétérogènes, à géométrie variable, fracturés, faillés, karstifiés). En effet, comme vu en 1.4, l'hypothèse d'un flux radial est parfois trop contraignante pour pouvoir représenter correctement la dynamique réelle des écoulements. La détermination des paramètres hydrauliques avec les modèles conventionnels sera donc irréaliste et erronée. On notera cependant que les aquifères compartimentés verticalement induisent, aux temps longs, un rabattement suivant une droite dans un graphique semi-log dont la pente sera proportionnelle à la transmissivité des compartiments situés de part et d'autres de l'aquifère pompé (Butler Jr. 1988, Dewandel et al. 2014).

Le choix d'un modèle analytique approprié est ainsi déterminant pour estimer les propriétés hydrauliques, car pour chaque modèle les solutions sont développées pour représenter un phénomène en particulier et en supposant une certaine géométrie d'écoulement.

1.7.2 MODÈLES NON-CONVENTIONNELS D'INTERPRÉTATION DES ESSAIS DE POMPAGE

1.7.2.1 Modèle de Barker (1988)

C'est face à l'incapacité des modèles conventionnels à reproduire correctement les écoulements au sein d'un aquifère fracturé (mine de fer de Stripa en Suède), que Barker (1988) a développé le modèle *Generalized Radial Flow* (GRF). En effet, comme vu précédemment (1.7.1.1), les modèles conventionnels, tels que les solutions de Theis et de Cooper-Jacob, considèrent une géométrie d'écoulement radiale ($n = 2$) dans leurs hypothèses de base. On a également vu que ces hypothèses étaient indéniablement

inappropriées pour des aquifères hétérogènes, karstifiés, discontinus et à géométrie variable. Barker s'affranchit de ce problème en proposant un modèle qui prend en compte le paramètre de la **dimension d'écoulement n** . Le modèle GRF permet donc de généraliser les modèles conventionnels à des dimensions sphériques ($n = 3$), linéaires ($n = 1$) et fractionnaires (n non-entier). Cette dimension d'écoulement n'est donc pas préétablie comme c'est le cas des analyses conventionnelles, mais déterminée à partir des pentes des dérivées logarithmiques du rabattement en fonction du temps qui sont représentées par des droites en représentation log-log.

Le principe du modèle GRF repose sur une relation linéaire entre la surface équipotentielle $A(r)$ correspondant au front de diffusion des rabattements à une distance r et la dimension d'écoulement n (Équation (1.6)).

$$A(r) = b^{3-n} \frac{2\pi^{n/2}}{\Gamma(\frac{n}{2})} \times r^{n-1} \quad (1.6)$$

- $A(r)$: surface disponible aux écoulements à une distance r du puits
- b^{n-3} : étendue de la zone d'écoulement/épaisseur généralisée du domaine ;
 b = épaisseur de l'aquifère
- n : dimension d'écoulement, $n \geq 0$
- r : distance radiale au puits

Γ : fonction Gamma

La fonction Gamma est définie par (Équation (1.7)) :

$$\Gamma(-\nu, u) = \int_u^{\infty} x^{-(\nu+1)} e^{-x} dx \quad (1.7)$$

Le paramètre de la dimension d'écoulement n , est défini par Verbovšek (2011) comme étant l'expression de la géométrie des écoulements combinée aux variations des propriétés hydrauliques. Comme énoncé plus haut, le modèle GRF intègre des valeurs de dimensions d'écoulement, notamment $n = 1$ (écoulement linéaire), $n = 2$ (écoulement radial), $n = 3$ (écoulement sphérique) ainsi que des valeurs non-entières (également appelées : dimensions d'écoulement partielles ou fractionnaires). Ainsi, une seule équation permet de décrire les écoulements pour des géométries de n'importe quelle dimension (d'où les termes d'équation généralisée et de théorie généralisée de Barker).

Le modèle GRF est défini pour les hypothèses suivantes (Barker 1988) :

- la source est une « sphère » à n -dimensions (par exemple un cylindre fini à deux dimensions).
- l'écoulement est radial, dans un aquifère homogène et isotrope, et remplit un espace à n -dimensions ;
- la loi de Darcy est applicable ;
- les effets pariétaux (*skin effects*) sont infinitésimaux et l'emmagasinement du puits et des piézomètres est négligeable ;

En considérant la variation de volume entre deux surfaces équipotentiellles sous l'effet d'une variation de charge hydraulique Δh , pendant une période de temps Δt , Barker obtient une généralisation de l'équation de continuité pour des dimensions d'écoulement $n \neq 2$ (Équation(1.8)) :

$$\frac{K}{r^{n-1}} \frac{\partial}{\partial r} \left(r^{n-1} \frac{\partial h}{\partial r} \right) = S_s \frac{\partial h}{\partial t} \quad (1.8)$$

- K : conductivité hydraulique de l'aquifère [$L.T^{-1}$]
 r : distance radiale au puits [L]
 n : dimension d'écoulement
 h : charge hydraulique [L]
 S_s : emmagasinement spécifique de l'aquifère [L^{-1}]

En considérant quelques hypothèses, le rayon et l'emmagasinement du puits sont négligeables et l'aquifère a une extension latérale illimitée (c'est à dire que le cône de rabattement ne se rapproche jamais d'une limite de l'aquifère, on parle dans la littérature de *Infinite Acting Radial Flow* (IARF) (Beauheim et al. 2004)) et en appliquant la transformée de Laplace sur l'Équation(1.8), Barker exprime l'évolution de la charge hydraulique (dans le temps et l'espace) en fonction des paramètres du milieu (Équations (1.9) à (1.11)) :

$$h(r, t) = \frac{Qr^{2\nu}}{4\pi^{1-\nu}Kb^{3-n}} \Gamma(-\nu, u) \quad \nu < 1 \quad (1.9)$$

avec
$$u = \frac{S_s r^2}{4Kt} \quad (1.10)$$

et
$$\nu = 1 - \frac{n}{2} \quad (1.11)$$

L'équation (1.9) constitue une généralisation de la solution de Theis, car elle peut s'appliquer dans des contextes où l'écoulement n'est pas forcément radial (soit $n = 2$).

Barker a montré qu'il est possible de déterminer la dimension d'écoulement n , par simple lecture graphique de la dérivée logarithmique, lorsque celle-ci prend la forme d'une droite de pente p , donc le ν de l'équation (1.11) devient le p de l'équation (1.12) :

$$n = 2(1 - p) \quad (1.12)$$

Pour cela, il suffit de représenter sur un graphique en échelle log-log, la dérivée logarithmique du signal rabattement-temps en fonction du temps (Équation (1.11)), et d'y lire la pente.

$$\frac{\partial s}{\partial \ln(t)} = t \cdot \frac{\partial s}{\partial t} = \frac{\partial s}{2.3 \partial \log(t)} \quad (1.13)$$

La valeur de la dimension d'écoulement à un temps donné, se détermine en calculant la pente de la droite. Numériquement il est possible de calculer cette pente comme suit (Équation (1.14)) :

$$p = \frac{\log(s_b) - \log(s_a)}{\log(t_b) - \log(t_a)} \quad (1.14)$$

avec $t_a < t_b$

En régime transitoire, les dimensions d'écoulement observées lors d'un pompage sont directement liées à l'évolution de l'équipotentielle du front du rabattement qui se propage dans l'espace (Équation (1.6)). La dimension d'écoulement traduit ainsi l'influence de la structure physique (géométrie, faille, etc.) et hydraulique (propriétés du milieu, conditions aux limites) de l'aquifère ainsi que des conditions aux puits sur l'évolution transitoire en pompage (ou en injection) de la charge hydraulique. L'étude des variations de n dans le temps permet ainsi de suivre la configuration spatiale du réservoir. L'interprétation de la succession des phases d'écoulement (diagnostic des séquences de la dimension d'écoulement) permet donc de réaliser un « scan » de l'aquifère à partir d'un essai de pompage.

Rafini et Larocque (2012) ont d'ailleurs modélisé numériquement un aquifère composé d'une faille perméable verticale alimentée par la matrice et ils ont montré qu'il est possible de décomposer le signal hydraulique de la dérivée logarithmique du rabattement en portions spatio-temporelles caractéristiques. En effet, comme le montre la Figure 1.6, la dérivée logarithmique du rabattement est composée successivement de :

- (1) : un plateau dans les temps courts, qui correspond à un écoulement radial produisant une pente nulle de la dérivée-log ($n = 2$) ;
- (2) : un front de rabattement qui lorsqu'il rencontre la faille perméable verticale produit une pente unitaire négative reflétant une période de transition;
- (3) : un cône de rabattement se diffusant lentement dans la matrice et plus rapidement dans la faille, produisant une pente de la dérivée-log égale à 0.25 ($n = 1.5$) ;

(4) : un cône de rabattement qui se diffuse radialement au bout d'un certain temps, lorsque la faille et la matrice ont une contribution équivalente. Dans ce cas, la dérivée logarithmique du rabattement affiche un nouveau plateau avec une pente de la dérivée-log nulle ($n = 2$).

En utilisant l'équation du rayon d'influence ou les équations de Shapiro et al. (2003), il est donc théoriquement possible de localiser spatialement des failles, des changements de la géométrie ou des modifications importantes des propriétés hydrauliques en repérant le temps à partir duquel il y a une perturbation caractéristique du signal hydraulique de la dérivée logarithmique du rabattement.

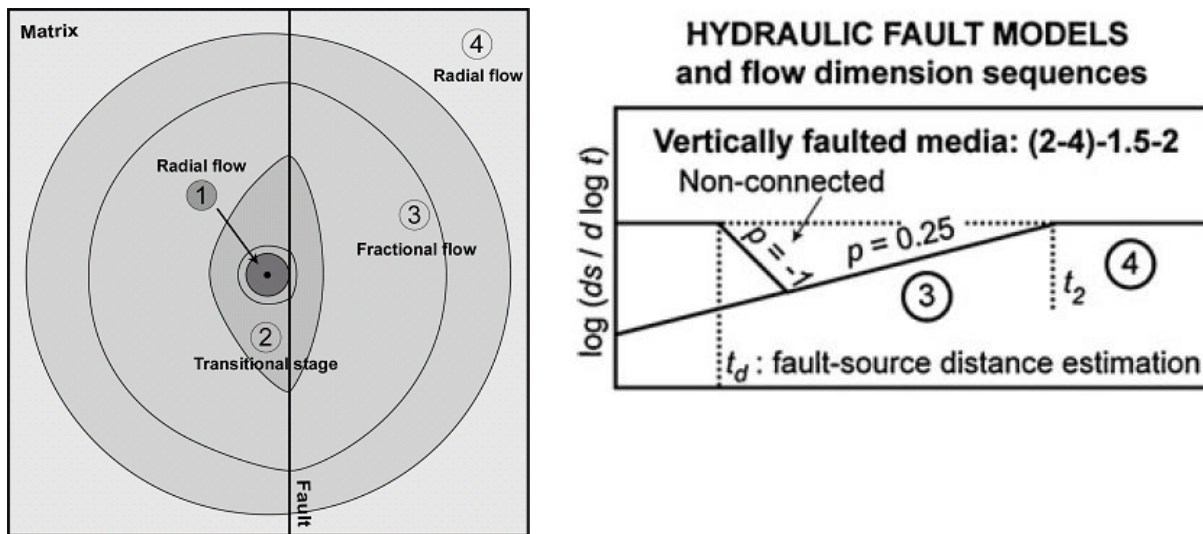


Figure 1.6 : Séquences diagnostiques de la dérivée logarithmique du rabattement pour une faille perméable verticale, non-connectée au puits de pompage (Rafini et Larocque 2009, 2012).

Le fait de considérer la dérivée logarithmique du rabattement accentue la sensibilité du signal. Une variation physique de l'aquifère, telle qu'un changement de la transmissivité, une modification de sa géométrie ou de ses conditions de recharge (connexions hydrauliques) vont engendrer des perturbations hydrauliques décelables sur un graphique log-log de $\partial s / \partial \ln t$ vs. t . Cette plus forte sensibilité du signal permet donc d'avoir une connaissance plus précise du milieu à partir d'un essai de pompage. Cependant, les incertitudes de mesure (liées à l'appareil et à l'opérateur) vont engendrer un bruit important sur les mesures de rabattement. De plus, des variations de débit de la pompe, une hétérogénéité diffuse aléatoire, des effets de marée, des changements barométriques ou des précipitations pendant le test peuvent induire de légères perturbations hydrauliques qui, accentuées sur un graphique logarithmique, peuvent engendrer une dispersion des données rendant difficile l'interprétation du signal hydraulique de l'aquifère.

Cette dispersion des mesures de la charge hydraulique liée au bruit instrumental associé aux perturbations hydrauliques « parasites » nécessite d'appliquer un algorithme de lissage afin d'augmenter le rapport signal/bruit (Bourdet et al. 1989, Spane et Wurtner 1993, Black 1994, Horne 1995, Veneruso et Spath 2006, cité par Renard et al. 2009).

1.7.2.2 Modèle de Doe (1991)

En 1991, Doe reprend les travaux de Barker (1988) et montre que des valeurs de n non-entières ne sont pas forcément expliquées par un milieu fractal, mais peuvent retranscrire des hétérogénéités ou des variations de la géométrie au sein d'un milieu euclidien. L'aire de la surface équipotentielle du front de rabattement est proportionnelle à la distance radiale

exposant n . En effet, il met en exergue que des dimensions d'écoulement non-entières, retranscrivent le caractère fractal d'un milieu si celui-ci est statistiquement homogène (*space-filling* : le milieu remplit l'ensemble de l'espace). En revanche, il montre également que des hétérogénéités, des variations de géométrie ou une combinaison des deux peuvent expliquer ces valeurs de n non-entières dans un milieu euclidien (Figure 1.7). Dans ce cas, la structure poreuse ne remplit pas totalement l'espace (*non-space filling*). Selon Doe, (1991), la dimension d'écoulement peut donc être interprétée par deux approches :

- $A(r) = \text{constante}, K(r) = K_0 r^m \text{ et } S_s(r) = S_{s0} r^m$
- $K(r) = \text{constante}, S_s(r) = \text{constante et } A(r) \sim r^{n-1}$

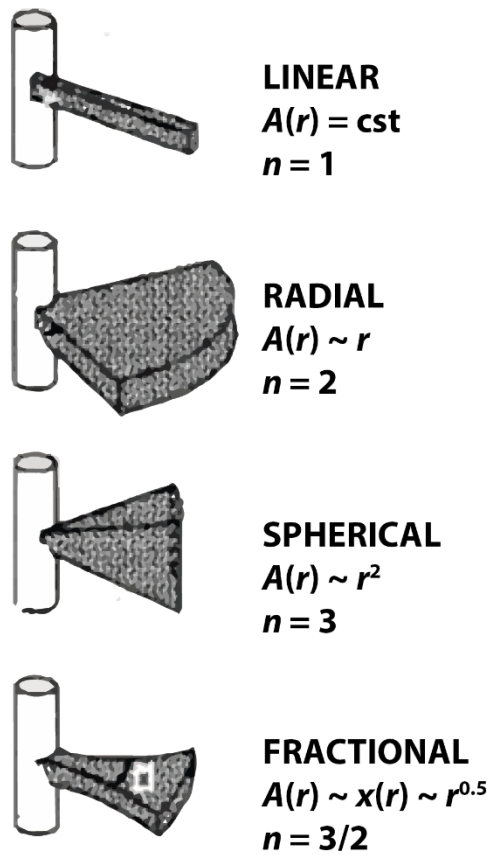


Figure 1.7 : Interprétation de la dimension d'écoulement en termes de géométrie de flux selon Doe, (1991), modifié de Doe (1991).

1.7.2.3 Signification physique et hydraulique des pentes de la dérivée logarithmique du rabattement et de la dimension d'écoulement selon le modèle GRF.

Cette partie a pour objectif de recenser les différents travaux qui ont été réalisés pour interpréter le signal hydraulique à partir de la dimension d'écoulement n .

Plusieurs travaux ont tenté de décrypter la signification physique du signal hydraulique en dérivée logarithmique. Selon les auteurs, les contextes expliquant des séquences ou des valeurs non-entières de la dimension d'écoulement diffèrent.

- Comme vu précédemment (1.7.2.2), selon le modèle de Doe (1991), les valeurs non-entières de n retranscrivent une **combinaison de géométries d'écoulement euclidiennes** ($n = 1, 2, 3$).
- Selon Barker (1988), cette dimension d'écoulement est liée à la **géométrie de la source** et au **caractère fractal du réseau de fractures**.
- En partant d'une modélisation fractale sur un DFN (*Discrete Fracture Network*) d'un aquifère fracturé, Cello et al. (2009), ainsi que Geier et al. (1992) et Winberg et al. (1996), cités par Dershowitz et al. (1998)) montrent un lien entre la **connectivité du réseau** de fractures (générée de façon fractale) et la dimension d'écoulement (Figure 1.9 et Figure 1.10). La Figure 1.10, présentée par Dershowitz et al. (1998), montre d'ailleurs la relation entre les variations de la surface d'écoulement (*flow path area*) en fonction de la distance au puits et la dimension d'écoulement n pour un aquifère fracturé.
- En suivant l'approche développée par Doe (1991), Bowman *et al.* (2013) simulent des écoulements au sein de conduits à forte transmissivité et de géométrie très simple. Ils montrent ainsi que des valeurs non-entières de n peuvent s'observer avec une **géométrie variable des conduits**.
- D'autres auteurs (Billaux et Gentier 1990, Jourde et al. 1998), interprètent les valeurs de dimension d'écoulement non-entières comme étant liées à la **densité de connexion de fractures selon un modèle de réseaux tubulaires**. En d'autres termes, pour un aquifère

fracturé, ils modélisent la chenalisation des écoulements due aux fractures grâce à un réseau tubulaire connecté, constitué de canaux unidimensionnels.

- Walker et Roberts (2003) investiguent, quant à eux, l'influence des conditions hydrauliques sur les dimensions d'écoulement. Ils montrent qu'un système radial influencé par des **conditions aux frontières** à charge imposée (condition de Dirichlet) donnera des valeurs de n de 4. Ils montrent également que pour un **aquifère semi-confiné**, la dimension d'écoulement dépend à la fois du temps et du facteur de drainance.
- Selon Chang et al. (2011), dans un milieu fracturé, les valeurs non-entières de n dépendent de **l'échelle d'observation**. Ils observent d'ailleurs que n augmente, presque linéairement entre le puits et un piézomètre d'observation.
- Verbovšek (2009, 2011) a cherché à expliquer la signification physique de la dimension d'écoulement par une approche statistique, en établissant des corrélations entre n et la lithologie, le degré de pénétration du puits, la proximité à une rivière, etc. Ses résultats ne montrent aucune corrélation entre tous les paramètres testés, mis à part le degré de pénétration du puits. La dimension d'écoulement est en général plus importante lorsque le puits pénètre partiellement l'aquifère. Il observe également que n est généralement plus important dans les formations intensément fracturées.
- Dal Soglio (2012) et Chesnaux et al. (communication personnelle) explorent l'interprétation des variations de n pour des aquifères granulaires. En simulant numériquement un aquifère granulaire dont la **géométrie** est conique, ils observent des dimensions d'écoulement sub-sphérique ($n > 2$). Ils simulent également l'influence de la **variation verticale et horizontale de la conductivité hydraulique** sur les signatures hydrauliques.
- Rafini et Larocque (2012), investiguent numériquement **l'influence des failles** et plus particulièrement de leur inclinaison sur la dimension d'écoulement. Ils observent une

séquence d'écoulement particulière de n , « 2 ; < 2 ; 2 » qui résulterait de l'interaction entre la matrice et une faille horizontale, à faiblement horizontale. Ils remarquent également une séquence de n , « 2 ; 1.5 ; 2 » qu'ils associent avec une faille verticale.

- Ji *et al.* (2013) abordent le problème sur le terrain en réalisant une étude précise de la densité de fracturation dans des puits (en aquifères rocheux fracturés), à partir d'un couplage de mesures diagraphiques. En réalisant des tests d'injection avec ballons obturateurs (*packer tests*), ils remarquent que la dérivée logarithmique du rabattement montre une signature hydraulique particulière, en forme de « bosse » lorsque le réseau de fractures n'est pas assez dense pour entretenir un écoulement dans le puits. Ce signal pourrait être associé à l'effet capacitif du puits. Ils concluent que l'étude de l'espacement des fractures, couplée à une analyse de la dérivée logarithmique, pourrait renseigner sur les régions fracturées et transmissives, au sein du puits étudié.
- Odling *et al.* (2013), interprètent les valeurs non-entières de n comme étant induites par une **pénétration partielle du puits**. Pour cela, ils se basent sur une étude des essais de pompage de 5 puits, situés dans des craies et ils obtiennent des dimensions d'écoulement partielles, sub-sphériques, comprises entre 2.2 et 2.4.
- Rafini *et al.* (2017) et Dewandel *et al.* (2014) ont investigué numériquement les séquences de la dimension d'écoulement dans des **aquifères contigus** (séparés verticalement ou horizontalement) **ayant des propriétés hydrauliques homogènes mais différentes**. Ils montrent que lorsque deux aquifères sont contigus, le signal révèle deux plateaux radiaux (la différence de hauteur entre les deux plateaux dépend du ratio de transmissivité entre les deux aquifères contigus).

Rafini (2008) a également testé numériquement l'influence de conditions hydrauliques aux frontières sur la dimension d'écoulement, dans un aquifère limité latéralement par 2 limites

imperméables et 2 limites à charge constante et dont le puits est à pénétration partielle. Il montre que pour des conditions aux limites à charge imposée et à flux nul telles qu'indiquées sur la Figure 1.8, le signal produit une **séquence de dimensions d'écoulement** : elle est d'abord sphérique ($n = 3$), puis radiale ($n = 2$), puis linéaire ($n = 1$) et tend enfin vers l'infini (pente qui tend vers zéro) lorsque le front de diffusion de l'onde de pression atteint les limites à charge imposée.

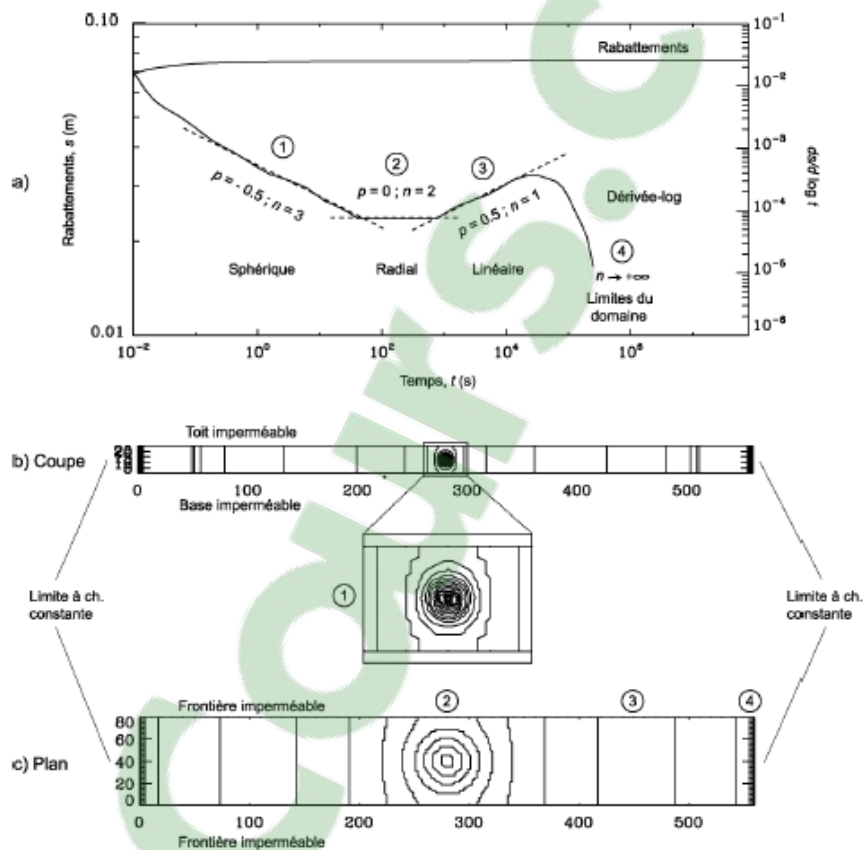


Figure 1.8 : Simulation numérique de l'influence de conditions hydrauliques aux frontières sur la dimension d'écoulement. (Rafini 2008).

Pour conclure, de nombreuses études, essentiellement numériques, ont tenté de déterminer les conditions physiques et hydrauliques induisant les différentes valeurs de n observées, les valeurs des pentes de la dérivée-log ou les valeurs des pentes semi-log du rabattement, qu'elles soient entières ou non-entières (par exemple, Bourdarot 1998, Bourdet 2002). Les figures 1.9 et 1.10 présentent une synthèse des liens entre les signatures hydrauliques et les modèles conceptuels associables (fracture linéaire, bilinéaire, écoulement sphérique, emmagasinement du puits, régime permanent, etc.).

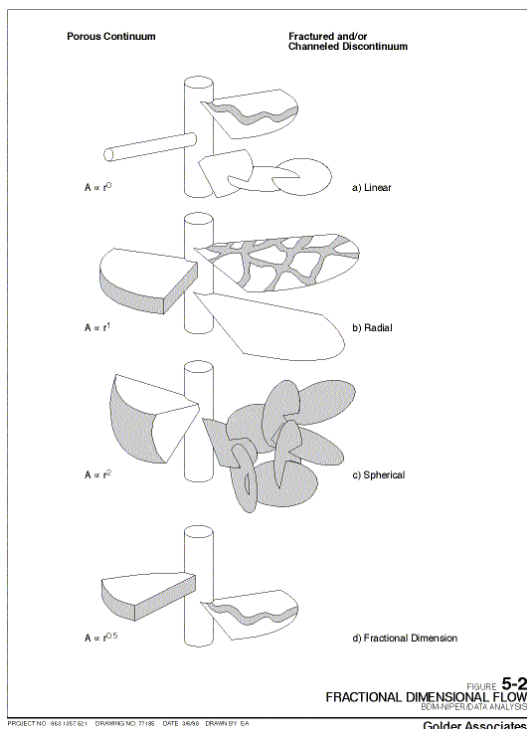


Figure 1.9 : Schémas conceptuels des relations entre les caractéristiques d'écoulement et la dimension d'écoulement. Tiré de Dershowitz et al., (1998).

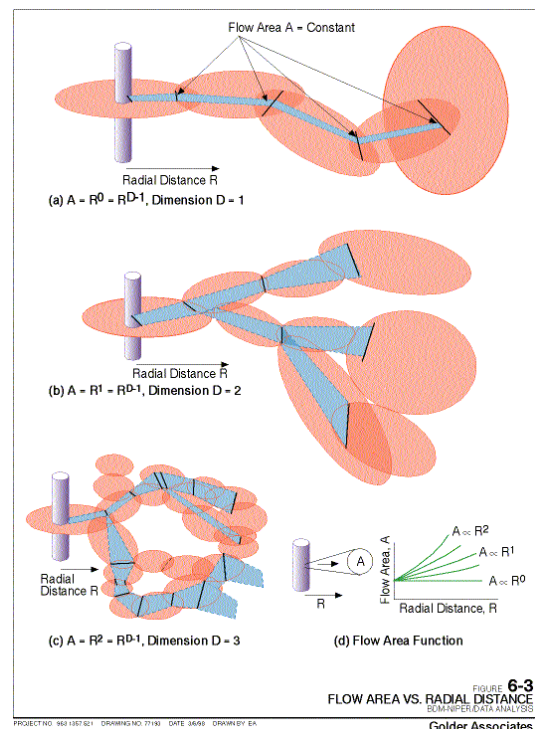


Figure 1.10 : Illustration de la relation entre l'aire d'écoulement (qui varie en fonction de la distance au puits r) et la dimension d'écoulement n , selon l'interprétation proposée par Doe, (1991). Tiré de Dershowitz et al., (1998).

1.7.3 DISCUSSION SUR LES MODÈLES ANALYTIQUES

De nombreux modèles existent actuellement pour décrire et caractériser les écoulements d'eau souterraine. Renard et al. (2009) ont d'ailleurs proposé une synthèse des « graphiques diagnostiques ». Certains auteurs (Mattar 1997, Kuusela-Lahtinen et al. 2003, Beauheim et al. 2004, Renard et al. 2009) préconisent une analyse couplée des rabattements et de la dérivée logarithmique des rabattements, car cette dernière est plus sensible aux propriétés du milieu. Le modèle permet de déterminer les différentes dimensions d'écoulement lors d'un pompage en considérant la dérivée logarithmique du rabattement. Cette analyse a donc l'avantage de considérer les différents régimes d'écoulement (transitoire, stationnaire) et de minimiser les hypothèses sur les géométries de flux, à la différence des modèles conventionnels très idéalisés qui ne considèrent en général qu'un seul régime et qu'une seule géométrie d'écoulement.

1.8 REVUE DES LOGICIELS INTÉGRANT L'ANALYSE DU SIGNAL $ds/d\ln(t)$ ET/OU L'ANALYSE DE LA DIMENSION D'ÉCOULEMENT

L'analyse de la dérivée-log du rabattement devenant de plus en plus populaire en hydrogéologie, elle est intégrée peu à peu au sein des logiciels d'interprétation d'essais de pompage. Voici une synthèse des logiciels permettant d'analyser et de lisser le signal de $ds/d\ln(t)$, de déterminer la dimension d'écoulement et/ou d'interpréter le signal hydraulique à partir du modèle GRF.

- **SIREN** : le logiciel SIREN (Système d'Interprétation des Régimes d'Écoulement en essais de Nappes) a été développé au sein du groupe de recherche R2Eau (Risque Ressource Eau) en partenariat avec le bureau de consultant LNA (Laforest Nova Aqua) dans l'objectif de proposer aux praticiens un outil permettant de visualiser la dérivée-log du rabattement et d'intégrer le concept de l'analyse séquentielle de la dimension d'écoulement dans l'interprétation qualitative et quantitative d'un essai de pompage. Pour améliorer le calage des pentes de la dérivée-log de s afin d'estimer les séquences de la dimension d'écoulement, le logiciel propose i) d'appliquer l'algorithme de lissage de Bourdet et al. (1989) et ii) d'interpréter les données de rabattement à partir d'un calage combiné des séries temporelles de s et de $ds/dlogt$ projetées respectivement sur un diagramme semi-logarithmique et log-log. Ce double calage permet de bénéficier des avantages de chacun des deux diagrammes. En effet, le diagramme semi-log de s vs t est peu sensible aux variations de débit mais il est également peu sensible aux régimes d'écoulement. En revanche, le diagramme log-log de $ds/dlogt$ vs t est très sensible aux fluctuations du débit de pompage, mais permet de détecter les régimes d'écoulement. Ce calage combiné permet de caler des courbes et des droites sur le signal de s et de caler des droites sur le signal de $ds/dlogt$. Le logiciel intègre plusieurs modèles conceptuels, notamment les plus communs (par exemple, les modèles radiaux de Theis (1935), Cooper et Jacob (1946)) et certains modèles conceptuels considérant des milieux hétérogènes (par exemple, le modèle bilinéaire à faille verticale alimentée par la matrice (Cinco-Ley et Samaniego 1981a, Abbaszadeh et Cinco-Ley 1995, Pulido et al. 2003, Rafini et Larocque 2009)). La version actuelle du code est encore en processus d'amélioration. Il est prévu de proposer une liste plus exhaustive de modèles conceptuels, d'intégrer une liste exhaustive de solutions analytiques, d'ajouter des algorithmes de lissage autres que celui de Bourdet et al. (1989)

et d'intégrer des algorithmes de déconvolution (Gringarten 2008, 2010, Kuchuk et al. 2010, Onur et Kuchuk 2012, Cumming et al. 2013).

- **AqteSolv** est l'un des logiciels des plus utilisés pour l'interprétation d'essais de pompage (essais de pompage à débit constant, *slug tests*, essais d'injection à charge constante). Le logiciel intègre l'analyse graphique diagnostique et permet un calage automatique des séries temporelles de s et de $ds/d\log t$. De nombreux modèles mathématiques sont disponibles pour l'interprétation séquentielle des régimes d'écoulement (y compris le modèle GRF (Barker 1988)) et l'estimation des propriétés hydrauliques de l'aquifère.
- L'équivalent d'AqteSolv dans l'industrie pétrolière est le logiciel **Saphir** (<https://www.kappaeng.com/software/saphir/overview>). Ce logiciel est spécialisé dans l'analyse transitoire des essais de pompage. Ce logiciel intègre des algorithmes de traitement du signal, notamment des algorithmes de déconvolution afin de corriger les variations du rabattement induites les fluctuations du débit. L'interprétation qualitative (identification du modèle conceptuels associé au signal) et quantitative (estimation des propriétés hydrauliques) du signal de la dérivée-log de s est réalisée à partir de calages automatiques de signatures théoriques issues de modèles analytiques. Enfin, ce logiciel propose des modèles numériques 2D et 3D afin de conceptualiser les écoulements dans divers contextes.
- **OUAIP** : Le logiciel OUAIP (Outil d'Aide à l'Interprétation des Pompages d'essais) est un programme disponible en accès libre à l'adresse <http://ouaip.brgm.fr/>. Ce logiciel, disponible en français et en anglais, a été réalisé par le BRGM afin d'interpréter les essais de pompage. Le logiciel permet de calculer les performances de l'ouvrage et de calculer les propriétés hydrauliques de l'aquifère (en pompage et en remontée). Ce logiciel intègre les solutions analytiques de Theis (1935), Hantush et Jacob (1955), Hantush (1964), Papadopoulos (1967)

et Gringarten et al. (1974). L'analyse peut être réalisée à partir des graphiques diagnostiques. L'algorithme de lissage de Bourdet et al. (1989) est également intégré. OUAIP permet également une simulation prédictive du rabattement induite par une chronique de pompage. Enfin, le logiciel OUAIP permet de prendre en compte, pour toutes les solutions : l'effet de limites, l'effet capacitif, les pertes de charges quadratiques, l'effet de skin et l'effet de vidange.

- **Hytool** : Le logiciel Hytool est une boîte à outil codée pour Matlab qui fournit un catalogue des solutions analytiques classiques pour interpréter les essais de pompage. Ce logiciel est proposé par Renard (2017) et est disponible gratuitement à l'adresse : <https://github.com/UniNE-CHYN/hytool>. Il inclut divers modèles conceptuels tels que les aquifères confinés et libres, les milieux à double-porosité, les milieux fractals et les failles verticales. Quelques solutions pour des essais à charge constante, des *slug tests*, des essais de pompage multiples sont également intégrés. Ce logiciel est utilisé pour l'enseignement à l'université de Neuchâtel (Suisse) et pour l'estimation des propriétés hydrauliques dans des projets de recherche (Mejias et al. 2009). Le code est modulable et permet à l'utilisateur d'ajouter de nouvelles solutions.
- **nSIGHTS** : Le logiciel nSIGHTS (n-dimensional Statistical Inverse Graphical Hydraulic Test Simulator) est proposé par la compagnie HydroResolution et offre également une interface pour l'analyse des essais de pompage. Le logiciel est disponible gratuitement à l'adresse suivante : <https://github.com/nsights/nSIGHTS>. Le logiciel intègre un catalogue exhaustif des outils d'analyse des essais de pompage. Entre autres, il permet ii) d'analyser des combinaisons d'essais de pompage à débit constant, d'essais d'injection à charge constante et des *slug tests*, ii) de diagnostiquer les dimensions d'écoulement non-radiales (Beauheim et al. 2004), iii) de représenter les séries temporelles du rabattement dans divers graphiques

spécialisés afin de faire ressortir différentes caractéristiques spécifiques. Le logiciel propose également plusieurs méthodes pour quantifier l'incertitude associée au calage de courbes théoriques issues de modèles analytiques aux données de terrain. Des algorithmes permettent de filtrer les effets barométriques et de marée. Enfin, toutes les informations disponibles (rabattement, dérivée-log du rabattement, changement de débit, etc.) peuvent être interprétées en même temps afin de contraindre le calage et l'estimation des paramètres. Une liste exhaustive des fonctionnalités du logiciel est disponible à l'adresse suivante : http://hydroresolutions.com/?page_id=442.

- Ramos et al. (2017) ont proposé un code permettant le lissage du signal de la dérivée-log du rabattement. Ce lissage est basé sur l'approche de régularisation variationnelle (*variational regularization approach*) qui permet de filtrer les faibles et les hautes fréquences de fluctuations. L'algorithme est implémenté dans une feuille de calcul Excel ainsi qu'un code Fortran. Ces deux outils sont disponibles gratuitement à l'adresse suivante : (<http://h2ogeo.upc.edu/en/investigation-hydrogeology/software>).

1.9 RÉFÉRENCES

- Abbaszadeh, M., et Cinco-Ley, H. 1995. Pressure-transient behavior in a reservoir with a finite-conductivity fault [en ligne]. SPE Formation Evaluation, **10**(01) : 26–32. doi: 10.2118/24704-PA.
- Anderson, D., Scotts, G.W., Mattar, L., Ilk, D., et Blasingame, T. 2006. Production Data Analysis--Challenges, Pitfalls, Diagnostics [en ligne]. Society of Petroleum Engineers. doi: 10.2118/102048-MS.
- Anisur Rahman, N.M., et Mattar, L. 2007. New analytical solution to pressure transient problems in commingled, layered zones with unequal initial pressures subject to step changes in production rates [en ligne]. Journal of Petroleum Science and Engineering, **56**(4) : 283–295. doi: 10.1016/j.petrol.2006.10.002.

- Atangana, A., et Botha, J.F. 2013. A generalized groundwater flow equation using the concept of variable-order derivative [en ligne]. *Boundary Value Problems*, **2013**(1) : 1–11. doi: 10.1186/1687-2770-2013-53.
- Barker, J.A. 1988. A generalized radial flow model for hydraulic tests in fractured rock [en ligne]. *Water Resources Research*, **24**(10) : 1796–1804. doi: 10.1029/WR024i010p01796.
- Beauheim, R.L., Roberts, R.M., et Avis, J.D. 2004. Well testing in fractured media: flow dimensions and diagnostic plots [en ligne]. *Journal of Hydraulic Research*, **42**(sup1) : 69–76. doi: 10.1080/00221680409500049.
- Bense, V.F., et Person, M.A. 2006. Faults as conduit-barrier systems to fluid flow in siliciclastic sedimentary aquifers [en ligne]. *Water Resources Research*, **42**(5) : n/a–n/a. doi: 10.1029/2005WR004480.
- Billaux, D., et Gentier, S. 1990. *Numerical and Laboratory Studies of Flow in a Fracture*. A Balkema, Rotterdam.
- Black, J.H. 1994. Hydrogeology Of Fractured Rocks – A Question Of Uncertainty About Geometry [en ligne]. *Applied Hydrogeology*, **2**(3) : 56–70. doi: 10.1007/s100400050049.
- Bourdarot, G. 1998. *Well testing: : interpretation methods*. Editions Technip, Paris.
- Bourdet, D. 2002. *Well Test Analysis: The Use of Advanced Interpretation Models: Handbook of Petroleum Exploration and Production*. Elsevier Science.
- Bourdet, D., Ayoub, J.A., et Pirard, Y.M. 1989. Use of pressure derivative in well test interpretation [en ligne]. *SPE Formation Evaluation*, **4**(2) : 293–302. doi: 10.2118/12777-PA.
- Bowman, D.O., Roberts, R.M., et Holt, R.M. 2012. Generalized radial flow in synthetic flow systems [en ligne]. *Groundwater*, **51**(5) : 768–774. doi: 10.1111/j.1745-6584.2012.01014.x.
- Butler Jr., J.J. 1988. Pumping tests in nonuniform aquifers — The radially symmetric case [en ligne]. *Journal of Hydrology*, **101**(1–4) : 15–30. doi: 10.1016/0022-1694(88)90025-X.
- Caine, J.S., Evans, J.P., et Forster, C.B. 1996. Fault zone architecture and permeability structure [en ligne]. *Geology*, **24**(11). doi: 10.1130/0091-7613(1996)024<1025:FZAAPS>2.3.CO;2.
- Cello, P.A., Walker, D.D., Valocchi, A.J., et Loftis, B. 2009. Flow Dimension and Anomalous Diffusion of Aquifer Tests in Fracture Networks [en ligne]. *Vadose Zone Journal*, **8**(1) : 258–268. doi: 10.2136/vzj2008.0040.
- Chang, Y.-C., Yeh, H.-D., Liang, K.-F., et Kuo, M.-C.T. 2011. Scale dependency of fractional flow dimension in a fractured formation [en ligne]. *Hydrology and Earth System Sciences*, **15**(7) : 2165–2178. doi: 10.5194/hess-15-2165-2011.
- Chapuis, R.P. 2007. *Guide des essais de pompage et leurs interprétations* [en ligne]. Bibliothèque et archives nationales du Québec, Québec (Canada). Disponible à

http://www.mddelcc.gouv.qc.ca/eau/souterraines/guide_pompage/guide_pompage_1-4.pdf.

- Chesnaux, R., Dal Soglio, L., et Rafini, S. communication personnelle. A numerical analysis to illustrate the usefulness of diagnostic plots in characterizing the hydraulic properties of heterogeneous granular aquifers.
- Chesnaux, R., Rafini, S., et Elliott, A.-P. 2012. A numerical investigation to illustrate the consequences of hydraulic connections between granular and fractured-rock aquifers [en ligne]. *Hydrogeology Journal*, **20**(8) : 1669–1680. doi: 10.1007/s10040-012-0912-9.
- Cinco-Ley, H., et Samaniego-V., F. 1981. Transient Pressure Analysis for Fractured Wells [en ligne]. *Journal of Petroleum Technology*, **33**(09) : 1749–1766. doi: 10.2118/7490-PA.
- Cooper, H.H., Jr., et Jacob, C.E. 1946. A generalized graphical method for evaluating formation constants and summarizing well-field history [en ligne]. *Transactions, American Geophysical Union*, **27** : 526–534. doi: 10.1029/TR027i004p00526.
- Cumming, J.A., Wooff, D.A., Whittle, T., Crossman, R.J., et Gringarten, A.C. 2013. Assessing the non-uniqueness of the well test interpretation model using deconvolution [en ligne]. *Dans Society of Petroleum Engineers paper No. 164870, EAGE Annual Conference & Exhibition incorporating SPE Europec, 10-13 June, London, UK.* doi: 10.2118/164870-MS.
- Dal Soglio, L. 2012. Simulation numériques d'essai de pompage pour le diagnostic des discontinuités structurales et des hétérogénéités des aquifères de dépôts. MSc., Université du Québec de Chicoutimi, Chicoutimi.
- De Dreuzy, J.-R. 1999. Analyse des propriétés hydrauliques des réseaux de fractures. Discussion des modèles d'écoulement compatibles avec les principales géométries. Thèse Doctorat, France.
- Dershowitz, W.S., Foxford, T., et Doe, T. 1998. FRDFNT: Research Report, Fracture Data Analysis Technology [en ligne]. Disponible à <http://www.fracturedreservoirs.com/niper/database/REPORTS/FracSys98/FracSys98.htm#TopOfPage> [cité le 3 novembre 2013].
- Dewandel, B., Aunay, B., Maréchal, J.C., Roques, C., Bour, O., Mougine, B., et Aquilina, L. 2014. Analytical solutions for analysing pumping tests in a sub-vertical and anisotropic fault zone draining shallow aquifers [en ligne]. *Journal of Hydrology*, **509** : 115–131. doi: 10.1016/j.jhydrol.2013.11.014.
- Dewandel, B., Lanini, S., Lachassagne, P., et Maréchal, J.-C. 2018. A Generic analytical solution for modelling pumping tests in wells intersecting fractures [en ligne]. *Journal of Hydrology*, **559** : 89–99. doi: 10.1016/j.jhydrol.2018.02.013.
- Doe, T.W. 1991. Fractional dimension analysis of constant-pressure well tests [en ligne]. *Dans Society of Petroleum Engineers paper No. 22702, SPE Annual Technical Conference and Exhibition, 6-9 October, 1991, Dallas, Texas, USA.* p. 461–467. doi: 10.2118/22702-MS.

- Geier, J.E., Doe, T.W., Benabderrahman, A., et Hassler, L. 1996. Generalized radial flow interpretation of well tests for the site-94 project [en ligne]. Disponible à <http://dspace.library.dc-uoit.ca/uoit/handle/dcuoit/902> [cité le 25 octobre 2013].
- Gringarten, A. 2008. From Straight Lines to Deconvolution: The Evolution of the State of the Art in Well Test Analysis [en ligne]. *SPE Reservoir Evaluation & Engineering*, **11**(1). doi: 10.2118/102079-PA.
- Gringarten, A.C. 2010. Practical use of well-test deconvolution [en ligne]. *Dans Society of Petroleum Engineers paper No. 134534, SPE Annual Technical Conference and Exhibition, 19-22 September, Florence, Italy.* doi: 10.2118/134534-MS.
- Gringarten, A., Ramey, H.J., et Raghavan, R. 1974. Unsteady-State Pressure Distributions Created by a Well With a Single Infinite-Conductivity Vertical Fracture [en ligne]. *Society of Petroleum Engineers Journal*, **14**(04) : 347–360. doi: 10.2118/4051-PA.
- Hantush, M.S. 1964. Hydraulics of wells. *Dans Advances in Hydroscience. Academic Press. Sous la direction de V.T. Chow. New York.* p. 281–442. Hantush, M.S., et Jacob, C.E. 1955. Non-steady radial flow in an infinite leaky aquifer [en ligne]. *Eos, Transactions American Geophysical Union*, **36**(1) : 95–100. doi: 10.1029/TR036i001p00095.
- Ji, S.-H., Lee, D.H., Yeo, I.W., Park, K.-W., et Koh, Y.-K. 2013. Derivative-Assisted Classification of Fractured Zones Crossing a Deep Borehole [en ligne]. *Groundwater*. doi: 10.1111/gwat.12035.
- Jourde, H., Bidaux, P., et Pistre, S. 1998. Fluid flow modelling in orthogonal fracture networks: influence of pumping well location on the hydrodynamic response of the modelled aquifer. *Bulletin De La Societe Geologique De France*, **169**(5) : 635–644.
- Kruseman, G., De Rider, N., et Meilhac, A. 1973. Interprétation et discussion des pompages d'essai [en ligne]. *International Institute for landreclamation and improvement, Wageningen, Bulletin 11, 2nd edition.* Disponible à <http://library.wur.nl/WebQuery/wurpubs/fulltext/72326>.
- Kuchuk, F.J., Onur, M., et Hollaender, F. 2010. *Pressure Transient Formation and Well Testing: Convolution, Deconvolution and Nonlinear Estimation.* Elsevier.
- Kuusela-Lahtinen, A., Niemi, A., et Luukkonen, A. 2003. Flow dimension as an indicator of hydraulic behavior in site characterization of fractured rock [en ligne]. *Ground Water*, **41**(3) : 333–341. doi: 10.1111/j.1745-6584.2003.tb02602.x.
- Leveinen, J. 2001. Conceptual and analytical modeling of fracture zone aquifers in hard rock - Implications of pumping tests in the Pohjukansalo well field, east-central Finland [en ligne]. *Geological Survey of Finland, Nuclear Waste Disposal Research. YST-105.* Disponible à <http://arkisto.gtk.fi/yst/yst-105.pdf> [cité le 11 novembre 2013].
- Long, J.C.S., Remer, J.S., Wilson, C.R., et Witherspoon, P.A. 1982. Porous Media Equivalents for Networks of Discontinuous Fractures [en ligne]. *Water Resources Research*, **18** : 645–658. doi: 10.1029/WR018i003p00645.
- Mattar, L. 1994. Practical Well Test Interpretation [en ligne]. *Society of Petroleum Engineers.* doi: 10.2118/27975-MS.

- Mattar, L. 1997. Derivative Analysis Without Type Curves [en ligne]. Society of Petroleum Engineers. doi: 10.2118/97-51.
- Mattar, L. 2004. Well test interpretation [en ligne]. Calgary, Alberta, Canada. Disponible à <http://www.spe.org/training/courses/WTI.php>.
- Mejias, M., Renard, P., et Glenz, D. 2009. Hydraulic testing of low-permeability formations: A case study in the granite of Cadalso de los Vidrios, Spain [en ligne]. *Engineering Geology*, **107**(3–4) : 88–97. doi: 10.1016/j.enggeo.2009.05.010.
- Moench, A.F. 1985. Transient Flow to a Large-Diameter Well in an Aquifer With Storative Semiconfining Layers [en ligne]. *Water Resources Research*, **21**(8) : 1121–1131. doi: 10.1029/WR021i008p01121.
- Neuman, S.P., et Witherspoon, P.A. 1969. Theory of flow in a confined two aquifer system [en ligne]. *Water Resources Research*, **5**(4) : 803–816. doi: 10.1029/WR005i004p00803.
- Odling, N.E., West, L.J., Hartmann, S., et Kilpatrick, A. 2013. Fractional flow in fractured chalk; a flow and tracer test revisited [en ligne]. *Journal of Contaminant Hydrology*, **147** : 96–111. doi: 10.1016/j.jconhyd.2013.02.003.
- Onur, M., et Kuchuk, F. 2012. A New Deconvolution Technique Based on Pressure-Derivative Data for Pressure-Transient-Test Interpretation [en ligne]. *SPE Journal*, **17**(1). doi: 10.2118/134315-PA.
- Papadopoulos, I.S., et Hilton H. 1967. Drawdown in a well of large diameter [en ligne]. *Water Resources Research*, **3**(1) : 241–244. doi: 10.1029/WR003i001p00241.
- Pulido, H., Samaniego, F., River, J., et Camacho, R. 2003. Decline Curve Analysis in a Naturally Fractured Reservoir with a Finite-Conductivity Fault [en ligne]. Stanford Geothermal Workshop. Stanford, USA. Disponible à https://pangea.stanford.edu/ERE/db/IGAstandard/record_detail.php?id=96.
- Rafini, S. 2008. Comportement hydraulique des milieux faillés [The hydraulic behaviour of faulted environments]. [en ligne]. PhD, Université du Québec à Montréal, Montréal. Disponible à <http://www.archipel.uqam.ca/1684/> [cité le 1 juillet 2013].
- Rafini, S., Chesnaux, R., et Ferroud, A. 2017. A numerical investigation of pumping-test responses from contiguous aquifers [en ligne]. *Hydrogeology Journal*, **3**(25) : 877–894. doi: 10.1007/s10040-017-1560-x.
- Rafini, S., et Larocque, M. 2009. Insights from numerical modeling on the hydrodynamics of non-radial flow in faulted media [en ligne]. *Advances in Water Resources*, **32**(8) : 1170–1179. doi: 10.1016/j.advwatres.2009.03.009.
- Rafini, S., et Larocque, M. 2012. Numerical modeling of the hydraulic signatures of horizontal and inclined faults [en ligne]. *Hydrogeology Journal*, **20**(2) : 337–350. doi: 10.1007/s10040-011-0812-4.
- Ramos, G., Carrera, J., Gómez, S., Minutti, C., et Camacho, R. 2017. A stable computation of log-derivatives from noisy drawdown data: COMPUTATION OF NOISY LOG-DERIVATIVES [en ligne]. *Water Resources Research*, **53**(9) : 7904–7916. doi: 10.1002/2017WR020811.

- Renard, P. 2017. Hytool: an open source matlab toolbox for the interpretation of hydraulic tests using analytical solutions [en ligne]. *The Journal of Open Source Software*, **2**(19) : 441. doi: 10.21105/joss.00441.
- Renard, P., Glenz, D., et Mejias, M. 2009. Understanding diagnostic plots for well-test interpretation [en ligne]. *Hydrogeology Journal*, **17**(3) : 589–600. doi: 10.1007/s10040-008-0392-0.
- Robinson, P.C. 1983. Connectivity of fracture systems-a percolation theory approach [en ligne]. *Journal of Physics A: Mathematical and General*, **16**(3) : 605–614. doi: 10.1088/0305-4470/16/3/020.
- Roques, C. 2013. Hydrogéologie des zones de faille du socle cristallin : implications en terme de ressources en eau pour le Massif Armoricaïn [en ligne]. Rennes 1. Disponible à <http://www.theses.fr/2013REN1S138> [cité le 12 novembre 2014].
- Roques, C., Aquilina, L., Bour, O., Maréchal, J.-C., Dewandel, B., Pauwels, H., Labasque, T., Vergnaud-Ayraud, V., et Hochreutener, R. 2014a. Groundwater sources and geochemical processes in a crystalline fault aquifer [en ligne]. *Journal of Hydrology*, **519** : 3110–3128. doi: 10.1016/j.jhydrol.2014.10.052.
- Roques, C., Bour, O., Aquilina, L., Dewandel, B., Leray, S., Schroetter, J., Longuevergne, L., Le Borgne, T., Hochreutener, R., Labasque, T., Lavenant, N., Vergnaud-Ayraud, V., et Mougin, B. 2014b. Hydrological behavior of a deep sub-vertical fault in crystalline basement and relationships with surrounding reservoirs [en ligne]. *Journal of Hydrology*, **509** : 42–54. doi: 10.1016/j.jhydrol.2013.11.023.
- Rouleau, A. 1988. A numerical Simulator for Flow and Transport in Stochastic Discrete Fracture Networks. Inland Waters Directorate, Ottawa, Technical Bull.(155) : 204.
- Rouleau, A., et Gale, J.E. 1987. Stochastic discrete fracture simulation of groundwater flow into an underground excavation in granite [en ligne]. *International Journal of Rock Mechanics and Mining Sciences & Geomechanics*, **24**(2) : 99–112. doi: 10.1016/0148-9062(87)91929-2.
- Shapiro, S.A., Patzig, R., Rothert, E., et Rindschwentner, J. 2003. Triggering of Seismicity by Pore-pressure Perturbations: Permeability-related Signatures of the Phenomenon [en ligne]. *pure and applied geophysics*, **160**(5–6) : 1051–1066. doi: 10.1007/PL00012560.
- Smith, E.D., et Vaughan, N.D. 1985. Aquifer Test Analysis in Nonradial Flow Regimes: A Case Study [en ligne]. *Ground Water*, **23**(2) : 167–175. doi: 10.1111/j.1745-6584.1985.tb02789.x.
- Theis, C.V. 1935. The relation between the lowering of the piezometric surface and the rate and duration of discharge of a well using ground-water storage [en ligne]. *Transactions, American Geophysical Union*, **16** : 519–524. doi: 10.1029/TR016i002p00519.
- van Tonder, G.J., Botha, J.F., Chiang, W.-H., Kunstmann, H., et Xu, Y. 2001. Estimation of the sustainable yields of boreholes in fractured rock formations [en ligne]. *Journal of Hydrology*, **241**(1–2) : 70–90. doi: 10.1016/S0022-1694(00)00369-3.

- Verbovšek, T. 2011. Hydrogeology and Geochemistry of Fractured Dolomites—A case study of Slovenia [en ligne]. *Dans* Aquifers: formation, transport, and pollution. Nova Science Publishers, Hauppauge, N.Y. p. 87–147. Disponible à http://www.geo.ntf.uni-lj.si/tverbovsek/papers/Aquifers%20-%20Formation%20Transport%20and%20Pollution_pageproof.pdf [cité le 4 novembre 2013].
- Walker, D.D., et Roberts, R.M. 2003. Flow dimensions corresponding to hydrogeologic conditions. *Water resources research*, **39**(12) : 1349.

CHAPITRE 2

Ce chapitre 2 est écrit sous la forme d'un article de recherche. Il vise à présenter un état de l'art de l'analyse des séquences de la dimension d'écoulement ainsi que des modèles analytiques associés afin de proposer un catalogue de modèles comportementaux théoriques pour l'interprétation des aquifères non-uniformes par une approche inverse. Pour cela, ce chapitre se propose de regrouper les modèles conceptuels dans un même cadre hydrodynamique universel (théorie de n) permettant d'utiliser un même schéma interprétatif pour l'interprétation de essais de pompage (revue pétrolière et en hydrogéologie). Pour chaque valeur de n , une synthèse des modèles interprétatifs, de leur réalisme et de leurs limites est proposée. Enfin, ce chapitre propose une méthodologie et des recommandations pour l'interprétation des essais de pompage à débit constant. Le manuscrit de cette section a été soumis à la revue *Journal of Hydrology*.

**USING FLOW DIMENSION SEQUENCES TO INTERPRET NON-UNIFORM
AQUIFERS WITH CONSTANT-RATE PUMPING-TESTS: A REVIEW**

Anouck Ferroud*, Silvain Rafini and Romain Chesnaux

*Research Group R2Eau, Centre d'études sur les ressources minérales, Université du
Québec à Chicoutimi, 555, boulevard de l'Université, Chicoutimi (Québec), Canada G7H
2B1*

Revue visée : *Journal of Hydrology*.

2.1 ABSTRACT

Today it is still common practice to analyse pumping tests assuming Theissian conditions, resulting in interpretations that are at best grossly approximated, if not erroneous, with potentially negative impacts on the quality of water resource management. Over the last several decades, numerous technological advances in hydrogeology have been developed that make it possible to perform more realistic analyses of heterogeneous, non-purely Theissian flow systems (e.g. aquifers with non-uniform geometry and/or hydraulic properties). For this study a catalog of available behavioral flow models was compiled from the literature and consolidated into a unique interpretative scheme. This is based on two first-order flow modelling breakthrough developments derived from research works: the derivative analysis (Bourdet et al., 1983) and the flow dimension theory (Barker, 1988). Each derivative type-curve is segmented and converted into a sequence of stable flow dimensions, in order to integrate a large panel of models into a comprehensive conceptual hydrodynamic and interpretative framework. This allowed us to conduct a thorough discussion on a range of different hydraulic conditions and their associated most common responses to constant-rate pump tests, namely, the linear, bilinear, radial, and spherical flow regimes and various sequential combinations of these elementary flow regimes. The relevance of the catalogued behavioral flow models is examined based on the realism of their postulates and on their frequency of occurrence in the field. The proposed diagnostic methodology makes it possible to further refine the interpretation of pumping tests and to routinely detect complex aquifer conditions.

Keywords: transient tests; flow dimension; diagnostic plots; numerical modeling; non-Theis aquifers

2.2 INTRODUCTION

Groundwater resources are subjected to growing pressure due to increasing population, industrial development and climate changes. The decline in water quality and/or quantity is becoming an issue of global concern (Behmel et al., 2016). Applied hydrogeology must cope with new scientific and environmental issues related to sustainability management of resources, stricter water quality legislation, and emerging industrial activities such as geothermal energy, radionuclide in situ repositioning and carbon sequestration. Groundwater investigation tools are being called upon to respond to these new concerns; they should have the capability of providing more precise routine assessments of the hydraulic properties of real aquifers. This challenge, in many instances, requires an understanding of their complex, heterogeneous, non-uniform or discontinuous nature. It appears evident that more hydrogeology research is needed to develop more precise aquifer modeling tools for practitioners. The issue is not only to improve the quantitative estimation of the bulk hydraulic properties of aquifers, but also to develop realistic, qualitative conceptualizations of heterogeneous flow conditions.

The analytical flow models that are commonly used today are overly simplified with a high degree of idealization, which makes it impossible to realistically represent the complexity of aquifers in nature. This leads to gross assessments of the hydraulic properties of aquifers.

Although it appears that customary practices in modeling are slowly changing, most hydrogeology practitioners are still interpreting most cases of constant-rate pumping tests by matching theoretical type-curves obtained from Theis (Theis, 1935) and Theis-derived models (Cooper and Jacob, 1946). Merely by routinely fitting these type-curves, practitioners are positing that pumping tests produce a cylindrical-radial flow regime in an Infinite Acting Radial Flow (IARF) model, thus ignoring, in most cases, the flow regime that is really occurring within the aquifer. Indeed, numerous studies (Audouin et al., 2008; Ferroud et al., 2018; Kuusela-Lahtinen et al., 2003; Leveinen, 2000; Lods and Gouze, 2004; Maréchal et al., 2004; Odling et al., 2013; Verbovšek, 2011, 2009) have reported from field investigations that the flow regimes occurring in real media are actually much more complex and diversified than what is modeled by the trivial Theis-derived cylindrical radial flow regime. Ferroud et al. (2018) observed that 88% of 69 pumping tests exhibited multi-stage derivative signatures, and 69% of 121 interpreted flow regimes were non-radial (the database was composed of constant-rate pumping tests performed in various geological settings). Despite this, all of the compiled tests had been interpreted by practitioners using the Theis/CJ models. In cases where flow regimes are in actual fact non-radial, applying an overly idealized interpretation model would lead to serious consequences, among which are the following (Ferroud et al., 2018; Le Borgne et al., 2004; Rafini et al., 2017):

- 1) simplifying the behaviour of the system to an extreme degree and disregarding the real geometry of flow;

- 2) ignoring the presence of several 1D, 2D or 3D hydraulic objects with non-equal properties, which may actually be governing the aquifer's global hydrodynamics at various pumping times;
- 3) in low-conductivity contexts, overestimating the hydraulic properties of the pumped domain and missing the presence of distal and/or discrete conductive domains which may be exerting a predominant role in supplying water to the well over some pumping time-windows;
- 4) missing the presence of partial or non-uniform boundaries, or erroneously interpreting hydraulic frontiers that are non-existent;
- 5) globally, dismissing most of the diagnostic potential of the time-drawdown signal;
- 6) poorly assessing the impact of the disruption that is applied to the aquifer, leading to erroneous delineation of water-productive wellhead protection areas, erroneous estimates of sustainable pumping rates, etc.

It should be noted that in this study, the term "flow regime" refers to a specific form of transient drawdown response of the aquifer to pumping; it does not relate to the laminar versus turbulent flow conditions as defined by the Reynold number.

As mentioned by Ferroud et al. (2018), when applying a model which assumes a flow regime outside the bounds of the real flow regime observed during the pumping test, this leads to an erroneous estimation of hydraulic properties. For instance, it was numerically shown that when applying the Theis model (which is based on a cylindrical-radial flow regime

assumption) to interpret a derivative signal has a linear flow regime, the estimation of K is overestimated of 89 %. Similarly, when applying the Theis model to interpret a spherical flow regime, then the estimation of K is underestimated by 100%.

Several pioneering publications have introduced advances in the interpretation of transient tests by means of analyzing the drawdown log-derivative time series $ds/d\log t$, more commonly referred to in the petroleum literature as the pressure derivative $t.dp/dt$. These are Bourdet et al. (1983), Chow (1952) and Tiab and Kumar (1980a). The drawdown log-derivative time series analysis was early recognized as a major improvement in pumping test interpretation, due to its drastically enhanced sensibility to flow conditions, allowing for the detection of various forms of non-uniform, heterogeneous or bounded reservoirs (Gringarten, 2008). The gain in diagnostic potential is illustrated by the following theoretical examples, where the derivative analysis makes it possible to avoid certain misinterpretations of hydraulic boundary which would have resulted from the use of the Cooper-Jacob drawdown-semi-log plot approach (Ehlig-Economides, 1988): i) a linear flow regime succeeding a prior radial flow regime generates an increase of drawdown rate that may be misinterpreted as a no-flow boundary (Ferroud et al., 2018); ii) an aquifer with an inclined substratum (IS), or two contiguous aquifers, both induce a strong decrease of drawdown rate after various durations of pumping time (pseudo-stabilisation) that may be misinterpreted as a constant-head boundary (Rafini et al., 2017).

Numerous analytically-derived predictive behavioral models have been proposed in the literature, providing a panel of derivative type-curves related to various forms of well and reservoir conditions. The diagnostic plots approach (Renard, 2005) calls upon these models

to diagnose hydraulic conditions by means of a two-step analysis: 1) firstly, a qualitative diagnosis where the appropriate conceptual model is selected based on the similarity between observed and theoretical signals; and 2) secondly, a quantitative diagnosis where the aquifer's specific hydraulic parameters are derived from matching the observed response to the selected model's type-curves, generally using best-fitting codes (Gringarten, 1987a; Kuusela-Lahtinen et al., 2003; Leveinen et al., 1998; Verbovšek, 2009).

This type-curve matching approach was criticized by Mattar (1999) for its lack of precision. Mattar and Tiab alternatively proposed a *sequential analysis* in which the derivative signal is decomposed into a sequence of straight lines that are interpreted separately from each other as successive flow regimes (Mattar, 1999; Tiab, 1995, 1994, 1993a, 1993b, 1993c, 1993d, 1989). Based on this sequential analysis approach, the Tiab's Direct Synthesis (TDS) makes it possible to graphically estimate the hydraulic properties of the aquifer using the slopes, intercepts, starting and ending times of $ds/dlogt$ plot on a bilog graph.

On this graph, a straight derivative response implies, from a hydrodynamic standpoint, that the flow dimension parameter n is constant, since n is defined (for drawdown recorded at the pumping well and after very short pumping times) by $n = 2(1-p)$ where p is the slope of $ds/dlogt$ on a bilog plot.

Applying the flow dimension theory to Mattar's straight derivative analysis provides us with a general hydrodynamic conceptual framework. This framework stipulates that n , at any time and space in the flow domain, represents the transient evolution of the shape of the pressure-front pulse that is diffusing throughout the aquifer during pumping (Barker, 1988; Doe, 1991). Note that this theory has been shown to be rather universal, with validity ranges

extending beyond the strict postulates of Barkers' GRF model (Rafini et al., 2017; Rafini and Larocque, 2009), as explained in the following chapter. Any stabilization of the flow dimension reflects a hydrodynamic stabilization during the transient test, which implies a spatial-temporal window where hydraulic conditions are unchanging and the reservoir's governing parameters T and S are constant. In natural media, most derivative responses obtained from constant rate tests are composed of a sequence of several segments with stable flow dimensions, as reported by Ferroud et al. (2018) from various geological environments. When the values of the flow dimension change, this reflects changing hydraulic conditions as the cross-flow surface extends throughout the flow domain. To a certain extent, these changes provide a "scan" of aquifer conditions. In heterogeneous aquifers, complex signatures are produced whose interpretation is not necessarily possible using conventional type-curve matching methods.

This article is a review of diverse analyses and interpretations of flow regimes proposed in both the petroleum and the hydrogeological literature. The majority of Oil and Gas articles address the flow regime analysis by recognizing specific $ds/d\log t$ slopes without using the flow dimension parameter. This review converts the flow regime slopes into flow dimension values, and sorts these values into various hydrodynamic signatures. Emphasis is placed on considering the sequences of several flow regimes that, when combined, are predicted to represent various specific hydraulic conditions. Based on a review of petroleum engineering and hydrogeology research and authors, we submit a catalog of certain specific conceptual flow models that have been associated with certain specific flow regimes, or sequences of flow regimes. The hydrodynamics of each conceptual model is explained in

regards to the fundamental relationship between n and the transient geometry of the front pulse as it propagates into the flow domain.

This article is a current “state-of-the-art” review of advanced analysis methodologies that combine the derivative signatures and the flow dimension sequences for the qualitative and quantitative interpretation of aquifers. This more evolved methodology is no more difficult to apply and does not require more data than a conventional pumping test analysis, although it holds dramatically greater potential. This article proposes the use of this methodology as a powerful diagnostic tool to improve accuracy in hydrogeological and petroleum studies. First, we describe and discuss in detail the concepts of flow dimension and sequential analysis. Emphasis is placed on derivative data preprocessing, flow dimension theory and sequential analysis. We then review the known conceptual models, distinguishing between mono- and multi-stage models. Finally, we discuss the n -sequential methodology, including advanced topics and limitations such as the various hydraulic meanings of multi-stage sequences and the issue of non-unique interpretations.

2.3 BACKGROUND

2.3.1 DATA PROCESSING AND DENOISING OF THE DERIVATIVE SIGNAL

The interpretation of a derivative signal may be compromised by poor quality data (Nobakht and Mattar, 2009; Rouboutsos and Stewart, 1988). Since the time series is highly sensitive to any subtle drawdown variation, it frequently appears noisy due to various factors, including operational imprecision, pumping rate fluctuations (Kuchuk, 1990), wind effects,

earth tides, barometric fluctuations or precipitation. To cope with these problems and to avoid misinterpretations in the recognition of real flow regimes, a pre-processing and smoothing of data are often required.

First, it is suggested to remove the outliers (Nobakht and Mattar, 2009). Secondly, an algorithm is applied to correct the derivative signal for pumping rate adjustments and/or wellbore storage. Various algorithms have been proposed to this end in the literature (e.g., convolution, deconvolution, variational regularization, multirate). Ideally, the drawdown and the pumping rate are simultaneously measured in order to correct the derivative signal for pumping rate fluctuations.

The convolution is a mathematical operation applied to two functions: a flow rate function and an impulse response. This produces a third function: the wellbore pressure (or drawdown). The impulse response represents the theoretical pressure response for a specific conceptual model, which is mostly based on a radial flow regime. In other words, the convolution integral produces the wellbore pressure as a forward problem using the measured flow rate data and the constant-rate pressure behavior of the system. Based on the Duhamel principle of superposition (Duhamel, 1833; Kuchuk et al., 2010), various convolution algorithms are available in the literature. For instance, the pressure-pressure convolution uses different pressure (or drawdown) data, recorded at two different spatial locations, in order to interpret a pressure signal lacking a flow rate measurement or with an unreliable flow rate (Denney, 2003; Onur et al., 2004). The limit of the convolution method is that it needs to assume a conceptual model: convolution overwhelmingly postulates a

radial flow regime, which is unsuitable in most real-world tests as explained above (Rouboutsos and Stewart, 1988). Conversely, the deconvolution is an algorithm-based process that aims at finding the solution of a convolution equation. The deconvolution is an inverse method that reconstructs an equivalent constant-rate drawdown response. In other words, the variable-rate drawdown is converted into an extrapolated equivalent constant-rate drawdown. This processing has the advantage that it does not need to assume a specific conceptual model. The deconvolution method corrects the rate-altered data and transforms it into constant-rate data, which makes more data available for the interpretation (Gringarten, 2010). In addition, the deconvolution process allows more accurate and unique interpretations: it reduces the non-uniqueness of a well test interpretation by reducing the uncertainties of observed data and also by reducing the multitude of possible derivative signatures that fit to observed noisy data (Cumming et al., 2013). The deconvolution process also helps in identifying the conceptual model (Gringarten, 2008; von Schroeter et al., 2001) and produces much better estimations of hydraulic properties and boundary conditions by producing clearer transformed derivative data (Gringarten, 2008). In the time between the publication of the papers by Kuchuk and Ayestaran (1985) and Stewart et al. (1983), which introduced the process of deconvolution to the petroleum industry, and today, many deconvolution algorithms have been proposed in the petroleum literature using different operational techniques (e.g., analytical deconvolutions, discrete numerical deconvolution without measurement noise, deconvolution with constraints, nonlinear least-squares pressure-rate deconvolution) (among others: Birsoy and Summers (1980), Bourdet et al. (1983), Obeahon et al. (2014), Onur and Kuchuk (2012), Pimonov et al. (2010) and von Schroeter et al., 2001)). For more details about convolution and deconvolution codes, the

reader is invited to read the review of Kuchuk et al. (2010). It should be noted that deconvolution algorithms cannot reconstruct the drawdown data if the pumping test is influenced by some interferences from other wells nearby or if the aquifer is influenced by leakage effects (Wang, 2010).

Various differentiation algorithms have been used to increase the signal/noise ratio of derivative time series. Escobar et al. (2004) evaluated the performance of seven algorithms (Bourdet, Clarck, Horne, Simons, Spline, Van Golf-Racht, first-degree and second-degree polynomials), and concluded that the Spline, Bourdet and Horne functions are the most suitable to analyze derivative data. Recently, Ramos et al. (2017) proposed a variational regularization method based on frequency filtering.

2.3.2 BACKGROUND OF THE FLOW DIMENSION SEQUENTIAL ANALYSIS

2.3.2.1 THE LOG-DERIVATIVE ANALYSIS

Over the last three decades, it has been routine practice for Oil and Gas theoreticians and practitioners to use the logarithmic derivative (log-derivative) pressure time-series to analyze flow conditions in natural reservoirs, after pioneering works by Bourdet et al. (1983), Mattar and Zaoral (1992) and Tiab and Kumar (1980b). The log-derivative analysis was first introduced into the hydrogeology literature by Chow (1952) and refined by Karasaki et al. (1988), Spane and Wurstner (1993) and Spane (1993), and has since remained in the theoretical realm. However, a recently growing interest is to be noted (Avci et al., 2013; Beauheim et al., 2004; Bowman et al., 2012; Cheng and Ni, 2009; Dewandel et al., 2011;

Gringarten, 2008; Hammond & Field, 2014; Onur et al., 2007; Ramos et al., 2017; Renard et al., 2009; Samani et al., 2006; Sun et al., 2015; Xiao & Xu, 2014).

The bilogarithmic projection of the drawdown log-derivative versus time makes it possible to distinguish between changes in flow regime caused by subtle variations in aquifer conditions (e.g., Issaka and Ambastha (1999)), changes which are less visible on drawdown-only plots. In Figure 1, the late flow regime is identified and characterized by a change in the log-derivative slope. The drawdown-only response only makes it possible to diagnose a departure from the early Theis function, or eventually to fit a Theis function to the late stage, which would be inappropriate, as the derivative signal clearly indicates that this is a non-radial flow regime (the derivative slope is different from 0).

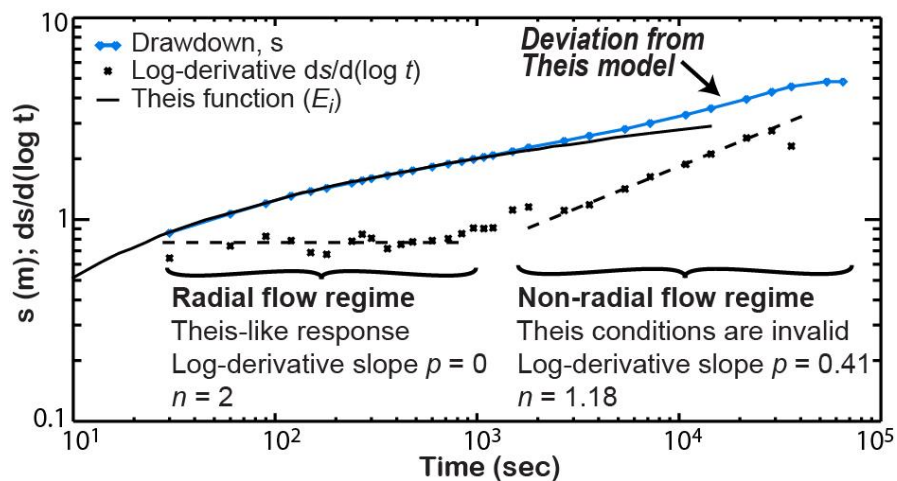


Figure 2.1. Example of real drawdown data displaying two successive radial and non-radial flow regimes.

The principle of universally interpreting various types of flow regimes from bilog plots of the drawdown log-derivative vs time was formalized by Bourdet et al. (1983). Other classic diagnostic plots include s , $\log(s)$ or $\log(ds/d\log(t))$ vs $\log(t^{0.5})$ or $\log(t^{0.25})$, where distinct diagrams were used for identifying specific flow regimes (for reviews on the approaches, see Bourdet (2002), Gringarten, (2008), Kruseman and Ridder (1994), Renard et al. (2009) and Verweij (1995)). Notably, Renard et al. (2009) effectively promoted the analysis of the $ds/d\log t$ signal in hydrogeology by highlighting its helpfulness in providing more detailed aquifer interpretations.

Recently, some research works have submitted the β -derivative signal, which is the derivative of the logarithm of the drawdown with respect to the logarithm of time, plotted on a bilog plot (Equation (2.1)) (Hosseinpour-Zonoozi, 2006; Idorenyin et al., 2011; Ilk et al., 2007; Shahamat et al., 2015). This β -analysis is not expected to replace the derivative analysis, but it is another tool that provides a unique characterization of flow regimes with a “power law” function, such as wellbore storage, reservoir boundaries with either a closed aquifer (circle, rectangle, etc.), with 2-parallel faults or with 3-perpendicular faults, or in fractured media with either an infinite-conductivity vertical fracture or a finite-conductivity vertical fracture (Hosseinpour-Zonoozi, 2006).

$$\frac{d\log(s)}{d\log(t)} = \frac{1}{s} t \frac{ds}{dt} \quad (2.1)$$

2.3.2.2 THE SEQUENTIAL INTERPRETATION

The sequential approach consists in identifying successive flow regimes occurring over the duration of the derivative signal of a constant-rate pumping test. A critical issue is now raised: what is the proper identification of what is called « a flow regime »? At a given pumping time, the derivative response may either reflect the occurrence of a real, settled and constant flow regime in the aquifer, or a transition between two successive flow regimes. For instance, the numerical modeling conducted by Rafini and Larocque (2012) showed that a non-connected well located close to a vertical finite-conductivity fault produces a derivative signal composed of several successive flow regimes appearing in this order: radial – transition – bilinear. The radial and bilinear flow regimes relate to, the diffusion of the pressure front pulse throughout the matrix and the leaky fault, while the transition stage does not reflect any of the properties of the aquifer, strictly speaking. In order to correctly identify a stable flow regime, the derivative data must exhibit a straight line, which implies that flow conditions are hydrodynamically stable, under the influence of some hydraulic objects whose properties may be calculated. A flow regime transition, in most cases, is a short time-period during which several heterogeneities are interacting in an inconsistent manner, thus generating unsettled hydrodynamic conditions. We submit that the two following primary criteria are required to confidently derive a flow regime: the stability of n (derivative straight line) and its duration which must be of at least one log-cycle (Beauheim et al., 2004). Where derivative straight segments are shorter than one log-cycle, it is not possible to reliably infer unique hydraulic properties.

The flow dimension theory (Barker, 1988) corroborates Tiab's and Mattar's approach as it predicts that the slope of a pumping-well drawdown-derivative time series will stabilize after very early pumping time (corresponding to the asymptotic portion of Barker's GRF model). Due to its homogeneous, continuous and infinite-acting flow idealization, the GRF predicts a unique constant-slope segment. In nature, the great majority of cases produce a series of several straight segments (Ferroud et al., 2018).

The concept of flow dimension diagnostic plots was later introduced by Beauheim et al. (2004) and Beauheim and Roberts (1998). This concept merges the flow dimension theory with the straight-line sequential analysis promoted by Tiab and Mattar. Pressure derivative time series are decomposed into sequences of flow regimes marked by constant flow dimensions that can be either sublinear ($n < 1$), linear ($n = 1$), bilinear ($n = 1.5$), radial ($n = 2$), spherical ($n = 3$), hyperspherical ($n > 3$) or fractional (n is a non-integer). Positive and negative unit slopes also are commonly identified, which are classically interpreted as representing internal and external hydraulic boundaries rather than flow dimensions but may also represent transient behaviors.

Theoretically, unrestricted multi-stage responses (i.e., several successive distinct flow regimes) can be analyzed and interpreted as a succession of stable hydraulic conditions occurring in the aquifer as the pulse "scans" through it. These distinct conditions reflect the temporary predominance of various hydraulic objects, boundaries, non-uniformities, or any heterogeneities on the aquifer response. The identification of a sequence of flow regimes essentially constitutes a hydraulic diagnosis (for instance in Figure 2.1, the n sequence is 2 – 1.18). The process of determining the sequence of flow regimes makes it possible to then

proceed to a qualitative interpretation of these regimes. This consists in selecting the appropriate conceptual flow model(s), considering the knowledge of the hydrogeological context. In many cases, the hydraulic properties associated with the successive aquifer conditions may then be quantified using the conceptual flow models that are reviewed in this article. However, this process presents two important limitations: we lack understanding of several specific flow regimes and associations of flow regimes; also certain conceptual models predict similar flow dimensions, leading to the so-called issue of non-unique diagnostics. This last problem is partially attenuated by studying the sequences of flow dimensions as a whole rather than separately.

2.3.2.3 HYDRODYNAMIC FRAMEWORK OF THE FLOW DIMENSION THEORY

Based on the GRF model (Barker, 1988), the flow dimension, n , represents the area, A , formed by the depressurization front pulse (cross-flow area), through the following power-law relationship (Equation (2.2)):

$$A(r) \sim r^{(n-1)} \quad (2.2)$$

where r is the distance traveled by the pressure front pulse starting from the source. Because r is a function of time t , this equation can be written as $A(t) \propto r(t)^{(n-1)}$, where $r(t)$ refers to the diffusive regime. Under normal Fickian diffusive conditions, $r \propto t^{0.5}$, which yields $A(t) \propto t^{(n-1)/2}$. As a premise, our conception of the flow dimension is that, from a hydrodynamic

perspective, it directly represents the temporal evolution of the cross-flow area during the hydraulic test in such a manner that, when the depressurization front around a pumping well expands outward over time, it encounters hydraulic heterogeneities of various natures and topological dimensions (irregularly shaped boundaries, faults, channels, connections to other aquifers etc.) that modify flow conditions and that will influence the observed flow dimension. This behavior is expected both in hard-rock aquifers that typically consist of complex discontinuous geometries, and in granular aquifers, which are characterized by internal complexities and relatively short-scale hydraulic compartmentalization (e.g., fluvial and alluvial sediments (Corbett et al., 2012)). This conception of the flow dimension fundamentally diverges from the common premise that this parameter reflects some specific and non-trivial scheme of scaling invariance of the hydraulic properties (see discussion below in this section and in section 3.10).

For multi-well sets, Rafini (2008) submitted that a general homogeneous response may be sought by using bilog plots with GRF-normalized derivative data $d(s/r^{(2-n)}) / d\log t$ versus standard normalized time t/r^2 . In systems inducing successive flow regimes with different flow dimensions, these normalized plots must be analyzed independently for each flow regime. A deeper explanation on the flow dimensional analysis of multi-well datasets brings us to the complex issue of the spatial homogeneity of flow dimensions at a pumping-field scale, which is beyond the scope of this publication.

Flow regimes with $n = 1$ (linear flow) represent one-dimensional pressure transfers restricted to corridors in such a manner that the lateral propagation of the cross-flow area, A , is

prevented. Thus, A remains constant: $A \sim r^{(1-1)}$. In the case of $n = 2$, a radial flow, the cross-flow area proportionally varies with r . The simplest radial flow case is the cylinder-shaped cross-flow area of the classical Theis aquifer: $A = 2\pi r$. Note that *radial flow* does not necessarily imply a cylindrical Theis-type flow; it simply means that $A \sim r$. Any value of n different from 2 is referred to as *non-radial* flow. The case of $n = 3$ corresponds to a spherical flow regime, with the most simple form being a sphere-shaped cross-flow: $A = 4\pi r^2$. Again, a spherical flow regime does not automatically imply sphere-shaped cross-flow surfaces, and $A \sim r^2$ may result from other flow conditions (e.g., a variable-thickness aquifer, as explained below). Non-integer values of the flow dimension are referred to as *fractional flow* behaviors, which can be induced by any hydraulic or geometric structure generating a non-specific time-variable cross-flow area with respect to Equation (2.2).

Figure 2.2 presents a summary of published theoretical flow regimes and their associated flow dimensions, n .

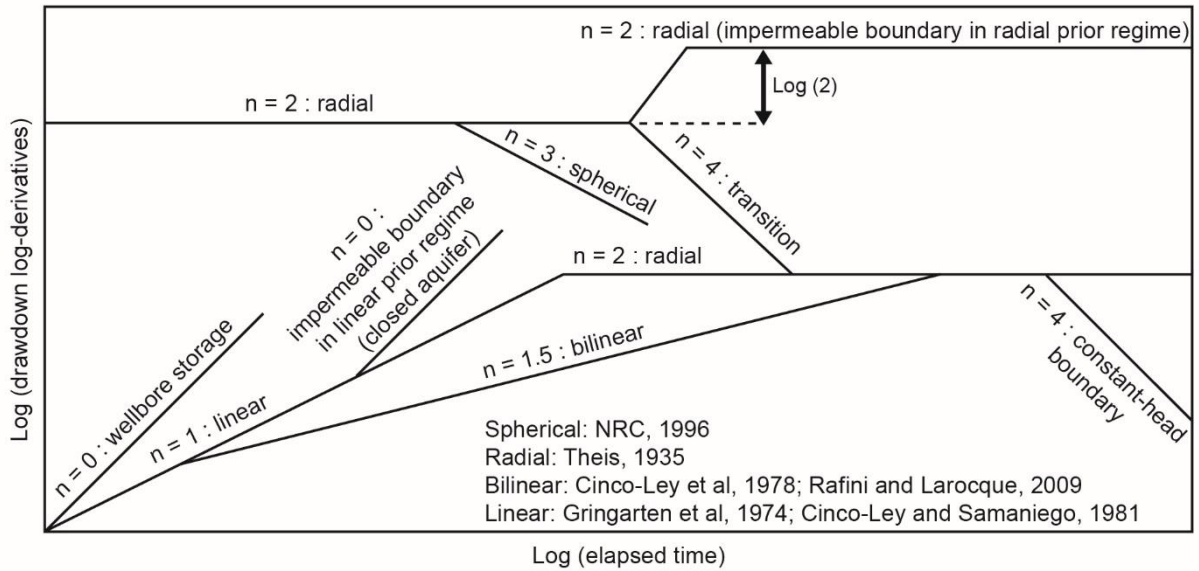


Figure 2.2. Summary of published theoretical flow regimes and their associated flow dimensions, n (modified from Ehlig-Economides et al. (1994)).

The flow dimension is not an intrinsic property of an aquifer, because it results from the combined effects of aquifer conditions and the topological dimension of the source. The source is cylindrical in conventional well-test cases but spherical (point-source) in packer-test configurations or when the screen length is very short in comparison to the aquifer thickness (Escobar et al., 2012a; Moncada et al., 2005). In an ideal, continuous, homogeneous and infinite-acting GRF aquifer, n is governed by the dimension of the source (Barker, 1988). Conversely, even if the source is cylindrical, the presence of many types of large-scale heterogeneities generate flow regime changes whereby the flow dimension is modified. Not all heterogeneity types produce flow dimension changes: in order for such a change to occur, the fundamental power-law relationship between the front pulse area and

the distance it travels from the source (Equation (2.2)) must be modified in a stable manner. Moreover, the influence of heterogeneities on the drawdown response is equally tempered by the size of the heterogeneity and its distance to the pumping well. A small-scale discontinuity, such as a single joint located near the pumping well, can alter an aquifer's response to a pumping test as drastically as a major multi-kilometer fault zone located far from the well. The former case affects the early-time response, whereas the latter affects late-time stages. This phenomenon is governed by the heterogeneity scale relative to the volume of the aquifer supplying the well, *i.e.*, the size of the "cone" of depression. When interpreting a conceptual model using drawdown data, it is important to remember that the heterogeneity dimensions are directly related to the absolute log-time of their occurrence on drawdown curves.

The most significant contribution of the GRF model lies in the theory of the flow dimension, which provides a universal formulation of the relationships between the expansion rate of the transmissive area A (depressurization front) and drawdown rate variations (drawdown log-derivative slope). While analytical models based on the assumption of a radial flow regime imply that the drawdown log-rate increases linearly during the pumping test ($n = 2$), the flow dimension theory widens the pumping test interpretation to non-linear expansion modes and non-constant drawdown log-rates. $n < 2$ and $n > 2$, respectively, represent flow regimes with increasing and decreasing drawdown log-rates as a function of pumping time. Purely from the standpoint of groundwater management, $n < 2$ and $n > 2$ hence reflect, respectively, poor-potential and high-potential aquifers. The flow dimension analysis substantially expands the interpretative framework and diversity of real flow responses that

can be modeled, allowing for a lesser degree of idealization and a higher degree of accuracy in representing real aquifer complexity.

From a physical standpoint, the GRF model proposes a relatively restrictive vision of the flow dimension, due to strong hydraulic and geometrical assumptions. A GRF aquifer is continuous, homogeneous and laterally infinite, and its flow geometry forms an n -dimension symmetrical pattern around the source, which is in itself n -dimensional. Thus, in theory, n remains constant during the entire transient test. Although mathematically robust, this model contains several physical paradoxes that have been subject to debate, including the meaninglessness of non-integer dimension sources, which explains why the n parameter has seldom found a practical use despite its powerful potential (Equation (2.2)).

It quickly became obvious that the flow dimension theory, which posits a relationship between the drawdown rate at time t and the cross-flow area expansion rate at distance $r(t)$ from the pumping well, is a rather universal law extending beyond the strict postulates stated by Barker (1988), namely where the dimensionality of flow is not only governed by the dimensionality of the source. Beginning with Doe (1991), several authors have explored this avenue for decades, notably deciphering the use of n for drawdown interpretations in fractured-network aquifers that were pumped via a conventional two-dimensional source (e.g., Jourde et al. (2002), Kuusela-Lahtinen et al. (2003), Leveinen (2000) and Leveinen et al. (1998)). More recently, Rafini and Larocque (2009) noted the versatility of the flow dimension theory by quantitatively verifying that the $n = 1.5$ fractional flow regime, obtained from numerical flow simulations in a vertical conductive fault embedded in an aquifer, occurred in accordance with the fundamental definition of n given in Equation (2.2), although

such discontinuum lies, by definition, outside of the GRF assumptions. Rafini and Larocque (2009) quantified the growth of the cross-flow area $A(r)$ induced by transient interactions between the hydraulic units (the fault and the aquifer) and confirmed that $A(r)$ grows following a power-law relationship with an exponent equal to 0.5. This value corresponds, using Equation (2.2), to a flow dimension equal to 1.5, thus corroborating the flow dimension as calculated from drawdown log-derivative slope 0.25. Expanding Barker's concept, Doe (1991) found that the flow dimension relates to the evolution of the transmissivity as a function of distance r that may actually correspond either to a purely geometrical expansion of the cross-flow surface restricted by the geometry of some constant-conductivity conduits embedded into a no-flow matrix (non-space-filling case of Bowman et al. (2012); Doe (1991)), or to a sole conductivity increase (space-filling case of Doe (1991)), or to a combination of both. The former, i.e., the power-law increase of the cross-flow section of some constant-conductivity conduits, was later numerically simulated by Bowman et al. (2012). The latter, i.e., the power-law conductivity-increase case, has long been debated through the GRF-derived fractal models (Acuna and Yortsos, 1995; Chang and Yortsos, 1990; Walker et al., 2006).

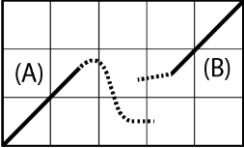
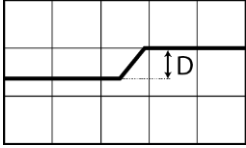
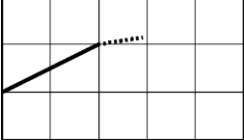
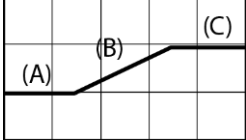
2.4 REVIEW OF FLOW DIMENSIONS WITH KNOWN CONCEPTUAL MODELS

The quality of the hydrodynamic analysis and the accuracy of the estimation of an aquifer's hydraulic properties depend on the relevance of the selection of an appropriate conceptual model to interpret the pumping test signatures.

This section presents an extensive catalog (Table 2.1) of conceptual flow models in various types of non-uniform aquifers. These models have been published by numerous authors over several decades of research in the fields of petroleum engineering and water resources. The predicted theoretical behaviors are displayed in terms of flow dimension sequences. The majority of these models were developed by analytically resolving the diffusivity problem according to various hydraulic and geometrical postulates; the remaining minority are empirical models derived from numerical experiments. In the opinion of the authors, these approaches both are relevant for the theoretical investigation of predictive flow responses. Each has its respective strengths and weaknesses. While the empirical numerical approach is criticized for its generalization that is deemed to be difficult to constrain, it has the major advantage of allowing the representation of complex, 3-dimensional flow systems in a realistic fashion (i.e., weaker geometrical idealisation of flow). On the contrary, the analytical approach commonly involves strong simplifying premises on the flow problem for mathematical-suitability purposes, which also impact the generalization (often poorly addressed). In most cases, these postulates come to either simplifying the geometry of flow and boundaries (internal or external), and/or to splitting (and recombining) the complex flow problem into several solvable forms restricted to some time- or space-domains. To conclude, the manner the problem is formulated strongly commands, in itself, the flow response of the analytical model, leading to models bounded by editorial choices, rather than universal.

Compiling these models allowed performing a thorough review and discussion of the different approaches used by the authors to conceptualize the hydrodynamics associated with the various flow regimes.

Table 2.1. Summary of drawdown log-derivative signatures and their associated conceptual models.

Flow dimension	Log-derivative response (bilog plots)	Conceptual model	Flow dimension	Log-derivative response (bilog plots)	Conceptual model
1	 <p>Unit-positive slope</p>	<p>(A). Early time: wellbore ⁽³⁸⁾</p> <p>(B). Late time: impermeable boundaries in all four directions ^(11, 13, 27, 38), referred to as closed reservoir, pseudo-steady state and depleting reservoir</p>	14		<p>- Impermeable vertical frontier</p> <p>$D = \log(2) \rightarrow$ single linear frontier ⁽¹⁶⁾</p> <p>$D > \log(2) \rightarrow$ dual linear frontiers ⁽⁴⁾, with D inversely proportional to the angle between the two frontiers</p> <p>- Aquifer cross-cut by a weakly-inclined finite-conductivity fault ⁽³⁴⁾</p>
2	 <p>1</p>	<p>-2D conduits</p> <p>Early and medium time: infinitely conductive fracture (matrix-related linear regime) ⁽¹⁸⁾ or finite-conductivity fault with high diffusivity contrast or a skin effect delaying pressure</p>	15		<p>Layered (glacio-) fluvial channels or deep-sea fan systems with micro-cross flow within the deposits ⁽⁸⁾. (A) Early radial flow through the fluvial media, (B) linear flow ("ramp effect") due to a low vertical conductivity and a reducing of the lateral connectivity (meandering environments)</p>

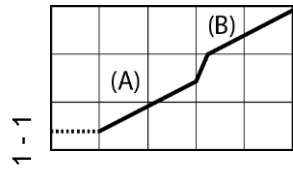
transfers to the matrix (fault-related linear regime) ⁽⁶⁾.

-1D conduits

Medium or late time: (Glacio-)fluvial channel ⁽²⁶⁾, elongated reservoir (corridor) ^(11, 12, 15, 29, 32), intersection of 2D conduits.

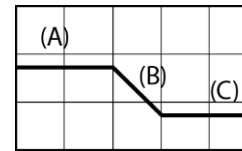
and/or transmissivity (braided environments). (C) steady-state value of the effective permeability.

3



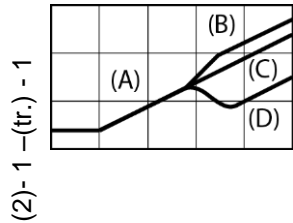
Semi-infinite corridor (dual linear flow model ^(11,13)): an impermeable boundary is reached (B) in a linear flow model (A). The intercept of the later linear regime is double that of the early one.

16



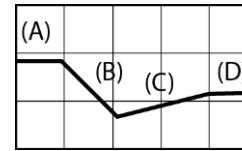
Contiguous aquifers: presence of a lateral, blind (non-pumped), more transmissive flow domain ⁽³³⁾. Early (A) and late (C) radial flow regimes reflect, respectively, the pumped (less transmissive) and non-pumped aquifers (more transmissive). The transitional stage (B) slope is -1.

4



T-shaped channel ⁽²⁸⁾: two perpendicular channels or the two channels are parallel but have different diameters (Deltaic environments). (A) Linear flow through the first channel. The second channel width is thinner (B), or equal (C) or greater (D) than the first one.

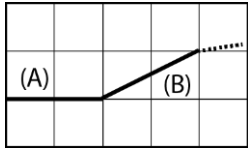
17



Contiguous aquifers with faulted interface: flow domains with a conductive fault at the interface ⁽³³⁾ Early (A) and late (D) radial flow regimes reflect, respectively, the pumped and non-pumped aquifers. (C) bilinear flow regime. The transitional stage (B) slope is -1.

5

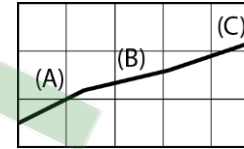
2 - 1



Large channel ^(11, 13): radial flow (A) settles before the lateral impermeable boundaries are reached (linear flow, B). (Glacio-) fluvial channel, elongated reservoir

18

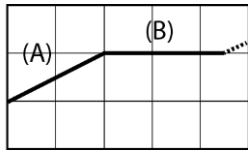
1 - 1.5 - 1.3



Finite-conductivity vertical fault influenced by a linear flow associated with an external drainage boundary ⁽²⁵⁾: Early linear flow in the fault ⁽⁵⁾, followed by a leaky fault bilinear flow (B) (6), the late time trilinear flow reflects the flow behavior of the leaky fault when the an external drainage boundary is felt (C). This constant-head boundary is conceptualized by linear flow within the matrix (parallel to the vertical fault).

6

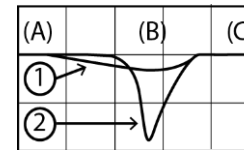
1 - 2



Sub-metric fracture in a fractured rock aquifer ⁽⁹⁾. Linear flow (A) (early times), induced by a sub-metric fracture followed by a radial flow (B) when the individual effect of a single fracture is diluted by the general behavior of the fractured aquifer.

19

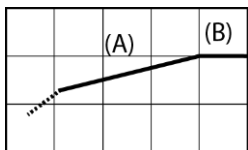
2 - 2



Double porosity model ^(3, 40): equivalent homogeneous system with a fracture network supplied by the matrix. (A) radial flow in the fracture network. (B) interporosity flow (the matrix starts supplying the fractures). (C) radial flow in the fractures that are supplied by the matrix

7

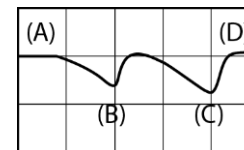
1.5 - (2)



Aquifer cross-cut by a strongly inclined finite-conductivity fault ^(6, 35). Leaky fault $n = 1.5$ (bilinear) flow (A). Late radial flow (B) occurs after the matrix signature has masked the

20

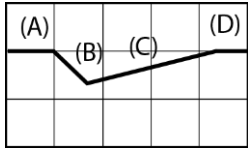
2 - 2 - 2



Triple porosity model ⁽¹⁰⁾: (A) and (D) have similar interpretations to that of cell 19. The depressions (B) and (C) are associated with the interporosity of the two domains in the matrix.

fault signature. The well is connected to the fault.

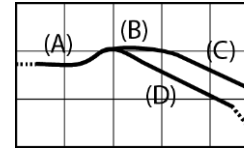
8



Aquifer cross-cut by a strongly inclined finite-conductivity fault; the fault is *not connected* to the wellbore (not intercepted) ^(1, 35). (A, D) The matrix properties prevail (early and late plateau are equal), (C), $n = 1.5$ stage due to interactions between the fault and the matrix. (B) is a transitional stage with slope lower than or equal to -0.5.

2 - (tr.) - 1.5 - 2

21



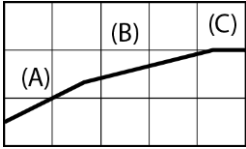
Semi-infinite variable thickness aquifer (vertical wedge) ⁽¹⁷⁾ either the substratum or the confining layer is inclined. (A) early radial flow, (B) second radial flow regime occurs when the pressure wave reaches the wedge (l) (Figure 2.14c). Note that the low hydraulic conductivity K and/or small angle of the wedge induces α (C). Rather, high K and/or wide α lead to (D).

Aquifer with a pinch-out boundary (wedge) (Figure 2.13a) ^(23, 28): (A) early radial flow and (D) a spherical flow regime induced by the pinch-out (wedge) boundary. The spherical flow regime is only observed if the well is close enough from the pinch-out boundary.

2 - 3

9

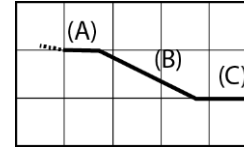
1 - 1.5 - (2)



Aquifer cross-cut by a strongly inclined finite-conductivity fault ^(5, 6). Early fault-related linear regime (A) possibly caused by the fault's skin effects or internal layering in the fault's architecture. Leaky fault bilinear flow (B). Late radial flow (C) occurs after the matrix signature has masked the fault signature. The well is connected to the fault.

22

(2) - 3 - 2

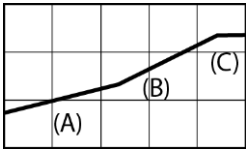


Water-receiving borehole height substantially shorter than the aquifer thickness: partially completing/penetrating well ^(14, 19, 30), packers tests ⁽³¹⁾. (A) Early radial flow around the pumping well, (B) spherical flow regime due to the increase of the cross flow area in the thick aquifer (point source model). (C) Late radial flow when the top and bottom boundaries are reached.

-Cross-connexion to an outer aquifer layer (fracture, gap in the confining layer).

10

1.5 - 1 - (2)

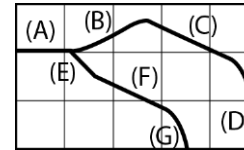


Aquifer cross-cut by a strongly inclined finite-conductivity fault ^(6, 38). Matrix-related linear regime (B) (fault acts as a planar source) barely realistic. Late radial flow (C) occurs after the matrix signature has masked the fault signature. The well is connected to the fault.

23

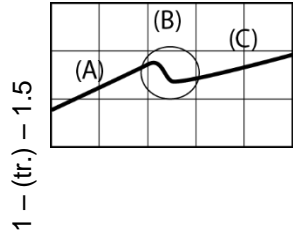
(2) - 1 - 3

(2) - (tr.) - 3



Elongated aquifer which is influenced by a constant head boundary (CHB) ⁽³⁶⁾ In a semi-infinite channel influenced by a CHB, the position of the well influences the n -sequence: After the early radial flow ($n = 2$) (A), the signal shows either a negative slope (E) if the pressure wave reaches first the CHB, or a linear flow regime ($n = 1$) (B) if the two lateral impermeable boundaries (channel) are reached first. (C) and (F) represent the dipolar flow regime ($n = 3$)

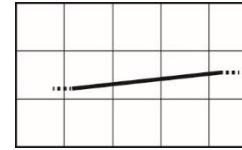
11



Aquifer cross-cut by a strongly inclined finite-conductivity fault with regulated interporosity transfer ⁽³⁹⁾. Fault-related linear flow ⁽⁶⁾ (A), followed by a “hump” in the derivative signal (B) due to an interporosity skin effect, followed by a leaky fault $n = 1.5$ flow stage. The well is connected to the fault. (Figure 2.10b).

24

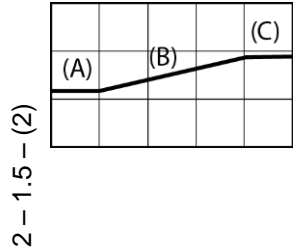
n non-integer



reflecting the “CHB influenced linear flow”. (D) and (G) reflect the reach of all the CHB.

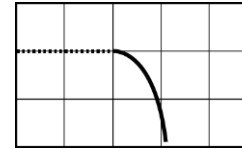
Fractal fracture network flow models ⁽²⁾, or non-stabilized flow regime (erroneous interpretation of a straight segment)

12

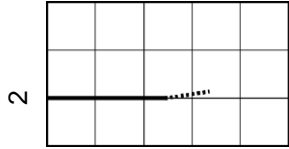


Aquifer cross-cut by a weakly inclined finite-conductivity fault ⁽³⁴⁾: (A) Early radial flow occurs before the top and bottom aquifer boundaries are reached (fault-related radial flow), (B) fault-related $n = 1.5$ flow stage, (C) late radial flow (matrix-related radial flow) occurs after the fault response has been masked by the matrix signature. The well is connected to the fault.

25



Recharge boundary ⁽²²⁾ or infinite leaky multilayer aquifer ⁽²¹⁾.



This aquifer, Infinite Acting Radial Flow (IARF), Cooper-Jacob approximation valid ^(37, 7). Systems in which the front-pulse grows proportionally to its distance from the source.

(1) (Abbaszadeh and Cinco-Ley, 1995)
 (2) (Barker, 1988)
 (3) (Barenblatt et al., 1960)
 (4) (Beauheim and Roberts, 1998)
 (5) (Cinco-Ley et al., 1978)
 (6) (Cinco-Ley and Samaniego-V., 1981a)
 (7) (Cooper and Jacob, 1946)
 (8) (Corbett et al., 2012)
 (9) (Doe, 1991)
 (10) (Escobar, Saavedra, Escorcía, et al., 2004)
 (11) (Escobar et al., 2004c)
 (12) (Escobar et al., 2007)
 (13) (Escobar and Montealegre-M, 2007)

(14) (Escobar et al., 2012a)
 (15) (Escobar et al., 2012b)
 (16) (Fenske, 1984)
 (17) (Ferroud et al., 2016)
 (18) (Gringarten et al., 1974)
 (19) (Gringarten and Ramey, 1975)
 (20) (Hantush, 1960)
 (21) (Hantush and Jacob, 1955)
 (22) (Horne, 1995)
 (23) (Horne and Temeng, 1982)
 (24) (Kruseman and de Ridder, 1994)
 (25) (Lee and Brockenbrough, 1986)

(26) (Massonnat et al., 1993)
 (27) (Mattar, 1999)
 (28) (Mijinyawa and Gringarten, 2008)
 (29) (Miller, 1962)
 (30) (Moncada et al., 2005)
 (31) (National Research Council Staff, 1996)
 (32) (Nutakki and Mattar, 1982)
 (33) (Rafini et al., 2017)
 (34) (Rafini and Larocque, 2012)
 (35) (Rafini and Larocque, 2009)
 (36) (Sui et al., 2007)
 (37) (Theis, 1935)
 (38) (Tiab, 2005)
 (39) (Valdes-Perez et al., 2011)
 (40) (Warren and Root, 1963)

2.4.1 THE LINEAR FLOW REGIME: $n = 1$

The flow dimension $n = 1$ implies a cross-flow area that remains practically constant as the pressure wave travels through the aquifer. Although commonly interpreted as the response produced by a fracture, the linear regime can also take place in any channelized, narrow, alluvial or fractured contexts.

When diagnosed over very short time frames, i.e., when the volume of depressurized aquifer is low (meter scale), a linear flow regime can represent a small-scale (measuring one meter or less) conductive fracture in the close vicinity of the pumping well. This is due to the high diffusivity of the fracture and the consequent rapid propagation of the depressurization front compared to the embedding matrix which is nearly non-depressurized at very early stages. Here, the matrix drawdown diffusion surrounding the fracture is so small compared with diffusion in the fracture that the cross-flow area propagating into the matrix remains negligible compared to the fracture's section. The total cross-flow area, A , hence remains practically equal to the fracture's section, generating a linear regime with respect to Eq. 2.2. The association commonly made between linear flow responses and larger, aquifer-scale vertical fractures embedded in a less conductive matrix is based on analytical solutions by Gringarten et al. (1974) and Cinco-Ley and Samaniego-V. (1981a). However, this interpretation is non-unique as explained above. The proper interpretation of an aquifer-scale fault would require the association of this signal with a subsequent $n = 1.5$ stage (1 – 1.5 sequence) (Table 2.1, cell 9), which is a much more unequivocal response as explained in sections below.

Two different types of linear flow regimes indicating the presence of a fracture have been proposed in the petroleum literature (Figure 2.3a-b). Gringarten et al. (1974) solved a *matrix-related linear flow* problem developing around a fracture which is infinitely conductive (Figure 3b). In this linear flow model, the pressure along the fracture is constant and uniform, leading to the fracture acting as a vertical planar source. Pressure gradients develop in the matrix surrounding the fracture, and generate one-directional flow perpendicular to the fault. Afterwards, Cinco-Ley et al. (1978) and Cinco-Ley and Samaniego-V. (1981a) solved a *fault-related linear flow* problem, occurring prior to the bilinear ($n = 1.5$, see below) flow regime into finite-conductivity aquifer-scale fractures or fault zones. By contrast, this linear flow regime posits that the depressurization practically is restricted to the fracture or the fault zone, and does not penetrate the matrix only negligibly (Figure 2.3a). This flow configuration is similar, on a hydrodynamic standpoint, to that described in the previous section for submetric fractures: the cross-flow area penetrating into the matrix is negligible in comparison to the fracture's section which hence is the predominant cross-flow area, leading to the linear flow. Top and bottom limits must be reached such that drawdown propagation is strictly horizontal and one-dimensional in the fracture. Such flow conditions may occur in natural cases where temporary flow restriction into the fracture occurs, either due to a high diffusivity contrast, *i.e.*, a practically impermeable matrix, or to a very strong skin effect delaying pressure transfers to the embedding matrix. The latter could possibly be due to mineral precipitations on the fault's rock walls.

There are two different types of tectonically-induced hydraulic objects occurring into hard-rock aquifers, fractures and faults, whose distinction is critical within the scope of reservoirs interpretation. It appears necessary to clarify semantical standards from hydrogeology, hydraulics and hydrocarbon reservoirs research fields, in regards to the structural geology terminology. In the conception of the pumping-tests hydraulics classical literature (numerous references in this chapter), a fracture refers to a low-thickness single discontinuity (some models posit zero-thickness) with a finite lateral extension, where laminar-flow occurs between two parallel planar walls (Poiseuille flow). These objects are hydraulic drains, it may be modelled singly – rather than as a network – when one fracture predominates the response of the system, which typically occurs at early times (when the pumping-test scale is low, see further discussion in sections 4.1 and 4.2). By contrast, hydrocarbon reservoir and regional hydrogeology researchers commonly refer to faults zones as hydraulic barriers or drains (Aydin, 2000; Bense et al., 2013; Knipe et al., 1998) consisting in tabular objects with non-negligible thickness (often multi-metric) and a large lateral extension (practically infinite on the scale of pumping test investigations). Their complex multilayered internal architecture (Dick et al., 2016; Faulkner et al., 2010; Herve Jourde et al., 2002) produces a hydraulic compartmentation where, typically, external layers (damage zones) are highly diffusive due to increased fracturing intensity, and core layers have a low diffusivity due to grain size reduction (fault gouges; e.g., Micarelli et al. (2006)). The relative importance of these contrasting-diffusivity layers is strongly variable in the nature, leading to a large spectrum of faults hydraulic properties from barriers to drains (Antonellini and Aydin, 1994; Aydin, 2000; Caine et al., 1996; Knipe et al., 1998).

On the standpoint of pumping-tests hydraulics, it is questionable that any real fracture may validate Gringarten's infinite-conductivity assumption of uniform and constant – instantly equilibrated – pressures into the discontinuity (matrix-related linear flow regime explained above, early-time solution of Gringarten et al. (1974)); this is indeed inconsistent with both *in-situ* measurements (e.g., packer-tests, flow-meter profiles inversion; Paillet (1998), Paillet et al. (1987)) and laboratory experimental data (Durham and Bonner, 1994; Engelder and Scholz, 2013; Pyrack-Nolte et al., 1987; Raven and Gale, 1985; Witherspoon et al., 1980). However, it is absolutely certain that this postulate is not applicable to faults zones. On the other hand, Cinco-Ley's both early-time linear and medium-time bilinear solutions (Cinco-Ley and Samaniego-V., 1981a) explicitly solve the transient flow problem into a finite-conductivity discontinuity. Since the latter is represented as a tabular highly conductive darcyan flow domain in itself, this conceptual model is likely applicable to both fully penetrating fractures and fault drains, which exert a similar influence on the aquifer response to pumping tests (Rafini and Larocque, 2012, 2009). It is likely that the above-mentioned hydraulic compartmentation of multilayered faults is significant in generating the early-time linear flow regime (fault-related linear flow, (Cinco-Ley et al., 1978; Cinco-Ley and Samaniego-V., 1981a)). In the fracture case, transitions from fracture- to matrix-related flow regimes during the pumping test may relate to the reaching of the fracture's finite extension as predicted by Cinco-Ley et al. (1978) and Cinco-Ley and Samaniego-V. (1981a); however, Rafini and Larocque (2009) explained that this transition naturally occurs, irrespective of the finite or infinite extension of the discontinuity, as a direct consequence of the diffusion slow-down (see details below). Herein, the term *fault* is used by default for any finite-conductivity

highly diffusive tabular darcyan flow domain of low – but non-negligible – thickness on an aquifer-scale, and penetrating totally the aquifer.

On the standpoint of pumping tests hydraulics, it is questionable that any real fracture may validate Gringarten's infinite-conductivity assumption of uniform and constant – instantly equilibrated – pressures into the discontinuity (matrix-related linear flow regime explained above, early-time solution of Gringarten et al. (1974)); however, it is absolutely certain that this postulate is not applicable to faults. By contrast, the Cinco-Ley's model (fault-related linear flow regime and bilinear flow regime (Cinco-Ley et al., 1978; Cinco-Ley and Samaniego-V., 1981a)), explicitly solves the transient darcyan flow problem into a finite-conductivity discontinuity. Since the latter is represented as a tabular flow domain in itself, this conceptual model is likely applicable to both fractures and fault drains, which exert a similar influence on the aquifer response to pumping tests (Rafini and Larocque, 2012, 2009). In the fracture case, transitional times between successive fracture- to matrix-related flow regimes produced during the pumping test may relate to the finite extension of the fracture as predicted by Cinco-Ley et al. (1978) and Cinco-Ley and Samaniego-V. (1981a); however, Rafini and Larocque (2009) explained that this transition naturally occurs, for any finite-conductivity fracture or fault and irrespective of its extension, as a direct consequence of the fault-diffusion slow-down (see details below). As a consequence, the finite or infinite lateral extension of conceptual finite-conductivity fractures and faults is not a distinctive feature on a hydraulic standpoint. In this article, the word *fault* will be used by default to describe a finite-conductivity and infinite-acting tabular flow domain of low thickness in comparison to the pumping test investigation scale.

A linear flow regime may also be produced by a highly conductive channel (one-dimensional conduit) into the fracture plane (Figueiredo et al., 2016) or at the intersection of two conductive fractures (Gringarten, 2008) (Table 2.1, cell 2).

Linear flow regimes also occur very frequently in granular aquifer contexts (Ferroud et al., 2018), in an elongated aquifer such as an esker, i.e., a grossly homogeneous isotropic aquifer laterally confined between two parallel impermeable or low-conductive boundaries in such a manner that the flow is restricted to a corridor (e.g., Escobar et al. (2004c), Escobar and Montealegre (2006) and Escobar and Montealegre-M (2007)). Note that if the well is far from the lateral boundaries, a radial flow regime would settle prior to the linear flow, leading to the diagnostic sequence $n = 2 - 1$ (Table 2.1, cell 2). Additionally, the linear response has been reported in highly channelized fluvial systems (e.g. braided and/or meandering systems) (Corbett et al., 2012) and deep sea fans (Escobar et al., 2004c). According to Corbett et al. (2012), a linear flow can be induced by a cross flow behavior, namely a flow within a layer, and not between layers (Table 2.1, cell 15). This flow behavior is presented under the name “ramp effect” and is explained below in section 3.5. Finally, the linear flow regime has also been reported within fractured corridors or large permeable veins (Dewandel et al., 2011).

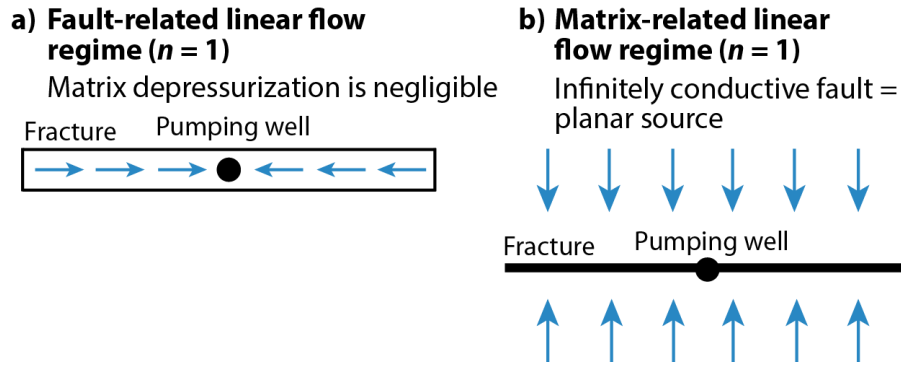


Figure 2.3. Conceptual flow models associated with faulted and fractured rock aquifers with a linear flow regime within a) a finite-conductivity fault or fracture (see text for semantical explanations) and b) an infinite-conductivity fracture.

In a previous study (Ferroud et al., 2018), we analyzed a flow dimension database composed of 69 pumping tests and we observed that the linear flow regime is mostly observed in fractured crystalline rock aquifers when the rock is very sparsely fractured (Figure 2.4a) and in fluvio-glacial deposits (Figure 2.4b). In the case of crystalline rocks, the documented occurrences of fractures reported in well logs, combined with knowledge of the structural context, suggest the presence of a steeply dipping and productive fault embedded in a slightly fractured matrix. The linear flow regime displayed in Figure 2.4a may hence adequately be interpreted using the vertical finite-conductivity fault model. The linear flow regime observed in the fluvio-glacial deposit may, however, reflect either a narrow aquifer (Escobar et al., 2004c) or a meandering and/or braided environment (Corbett et al., 2012). In this case, more field investigations would be needed to distinguish between these models.

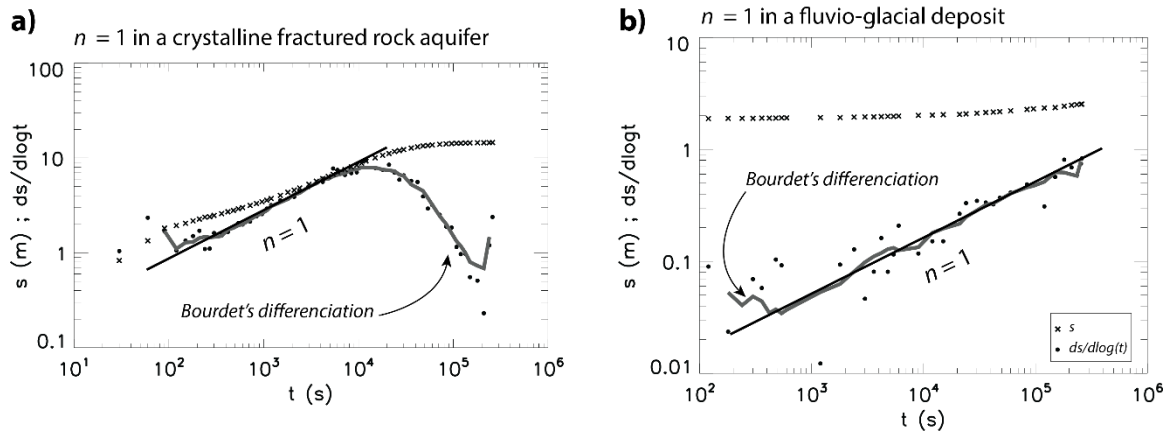


Figure 2.4. Diagnostic plots and interpretations of a constant-rate pumping test inducing a linear and conducted in a fractured rock aquifer a) and in a fluvio-glacial deposit b).

2.4.2 MULTI-LINEAR COMBINATIONS

Sequence $n = 1 - 1$

Mijinyawa and Gringarten (2008) proposed a conceptual model to reproduce the flow behavior in a deltaic environment (river-dominated deltas). This environment is composed of a distributary channel system (Olariu and Bhattacharya, 2006) (Figure 2.5). According to Olariu and Bhattacharya (2006), these distributary channels represent channel bifurcations that have characteristic sedimentary structures of unidirectional effluent flow. These network patterns may be formed in deep-sea fans (Damuth et al., 1983; Posamentier and Kolla, 2003), alluvial fans and delta plains. Mijinyawa and Gringarten (2008) proposed two conceptual models. In the first case, the model is composed of two perpendicular channels (Figure 2.5b), while the second model is composed of two successive channels with a non-

equal diameter (Figure 2.5c). In both cases (Figure 2.5a and Figure 2.5b), a second linear flow regime is observed when the diameter of the second channel is greater than the first one. These numerical results emphasise the non-uniqueness of the derivative signature, because the two different configurations of the branches (Figure 2.5b and Figure 2.5c) produce similar responses. The position of the second linear flow regime on a derivative signal plot depends on the ratio of diameters between the two branches. As shown in Table 2.1, cell 4, if the second channel is thicker than the first one, its transmissivity will be greater, and the line showing this second linear flow regime will be shown lower on the plot ((D) in Table 2.1, cell 4); if the second channel is thinner, the second linear slope will be higher than the first ((B) in Table 2.1, cell 4).

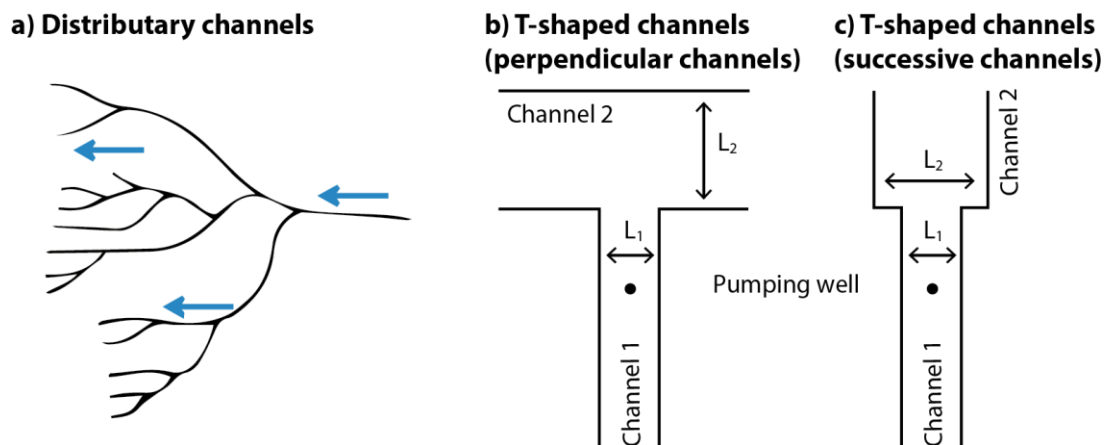


Figure 2.5. a) Conceptual model of a distributary channel in a deltaic environment, b) T-shaped channel in a perpendicular arrangement modelled by Mijinyawa and Gringarten (2008) to reproduce the flow behavior of a distributary channel system c) Two successive channels with a non-equal diameter to reproduce the flow behavior of a distributary channel system.

Our database (Ferroud et al., 2018) shows that the n -sequence 1 – 1 has not been observed in alluvial deposits, but rather in a crystalline fractured rock aquifer and a carbonate rock aquifer. New, more detailed conceptual models in fractured rock aquifers are thus needed in order to interpret the sequence $n = 1 – 1$. The shift of the linear slope shown in Figure 2.6 may reflect the moment when the pressure wave reaches another fracture having greater hydraulic conductivity.

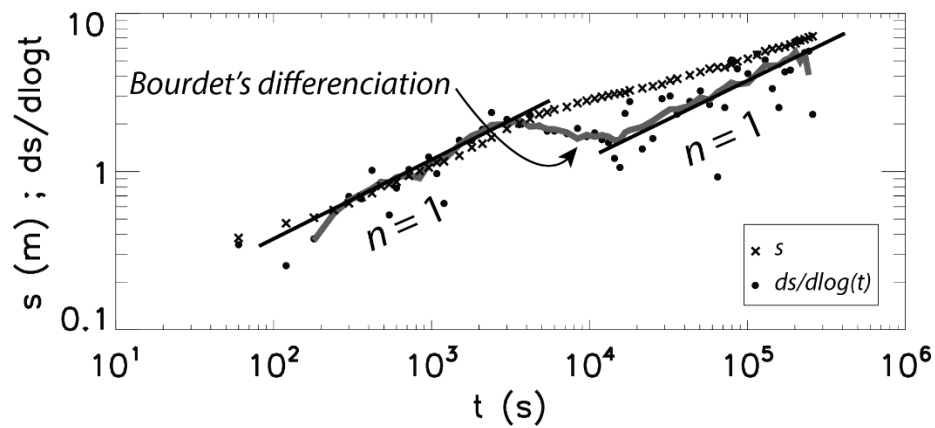


Figure 2.6. Diagnostic plots and interpretations of a constant-rate pumping test conducted in a crystalline fractured rock aquifer: example of a n -sequence 1 – 1.

2.4.3 THE RADIAL FLOW REGIME: $n = 2$

Although far from being ubiquitous, the radial flow regime remains the regime most frequently observed in natural media, regardless of geological context (Ferroud et al., 2018). It occurs as often in fractured as in granular media.

Radial flow may correspond to the classic Theis conditions (also named infinite acting radial flow (IARF)), but this is not the only possible interpretation, because the confirmation of radial behavior only requires that the conditions of $A \propto r$ be verified. This may not occur only in purely Theis-type cylindrical equipotential surfaces. Radial flow may also be produced in a wide range of aquifer configurations, including discontinuous porosities: dense Euclidean fracture-network aquifers (corresponding, for instance, to the early radial stage of the so-called dual porosity model) or aquifers cross-cut by a weakly inclined single conductive fault (before the front pulse reaches the top and bottom boundaries) (Gringarten et al., 1974; Rafini and Larocque, 2012) (Figure 2.7). Regardless of the aquifer conditions, the radial flow model makes it possible to derive an apparent transmissivity T_{app} which is inversely proportional to the plateau elevation of the derivative signal a , as given by Cooper-Jacob solution: $T_{app} = 2.3Q/4\pi a$. The physical meaning of T_{app} , however, varies depending on the conceptual model, as explained over this section.

Radial flow also typically occurs at a very late pumping time, when the cone of depression is so large that heterogeneities such as fractures and faults in bedrock aquifers are small compared to the volume of the depressurized aquifer. Numerical modelling works by Meier et al. (1998) and Sánchez-Vila et al. (1999) have validated the applicability of the Cooper-Jacob solution in a heterogeneous domain producing a radial flow regime with diffuse transmissivity fields and concentric heterogeneous storage conditions. Since the effects of single heterogeneities are diluted, the hydraulic properties calculated from such a late radial regime represent the bulk aquifer properties.

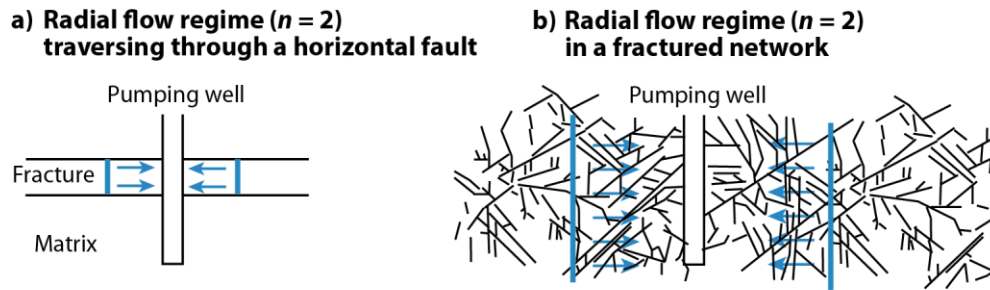


Figure 2.7. Examples of fractured rock conceptual models that induce a radial flow regime ($n = 2$).

Our flow dimension database (Ferroud et al., 2018) emphasizes that most long-term radial flow regimes are observed in carbonate rock aquifers. This may indicate that the bedding plane fractures of the carbonate rock analysed in the database are well-connected and contribute to the flow.

2.4.4 MULTI-RADIAL COMBINATIONS

Two successive radial flow regimes may be produced in a variety of different aquifer settings: dual porosity, unconfined aquifer, impermeable frontiers, leaky aquifers, aquifers with variable-transmissivity lateral flow domains (transitional stage with a negative unit slope of $ds/d\log t$), multilayered aquifers or an aquifer cross-cut by a weakly inclined finite-conductivity fault (Figure 2.7a-b). These conceptual models are described in the following sections. Critical features for identifying appropriate conceptual models are: whether the late plateau is higher or lower than the early plateau, and the shape of the transitional stage.

Sequence $n = 2 - 2$ with late plateau higher than the early plateau

The most common interpretation of this sequence is a single, linear, impermeable barrier. In this case, the elevation of the late plateau is twice that of the early plateau (equivalent to doubling the drawdown slope on a classic semi-log plot) (Table 2.1, cell 14). This is due to the fact that, after reaching the frontier, the pressure wave propagates into a space half the size of the full space; i.e., the apparent transmissivity is halved. Compartmented aquifers models (Butler Jr. and Liu, 1991; Dewandel et al., 2014; Rafini et al., 2017) with the non-pumped compartment less transmissive than the pumped one, generate responses similar to no-flow boundary systems – a limiting case – when the diffusivity contrast between both compartments exceed one order of magnitude, practically (Rafini et al., 2017). Drawdown derivative sequences displaying two successive radial flow regimes, with the second plateau greater than twice the early plateau, are seldom reported in field investigations. Two distinct conceptual flow models associated with such a sequence have been submitted in the literature: the multiple impermeable frontiers model, and the weakly-inclined finite-conductivity model.

The derivative signature in a flow model with multiple impermeable vertical frontiers has been analysed by Beauheim and Roberts (1998), Mijinyawa and Gringarten (2008) and van Poolen (1965). This signature presents a second plateau, whose Y-intercept is higher than the Y-intercept of the first plateau. It signals a decrease in the flowing surface after the pressure wave has reached one or several vertical no-flow boundaries. In such a

generalized concept of multiple impermeable frontiers, the ratio x , which is greater than 2, between the levels of the second and the first plateaus, reflects a decrease in the transmissive surface by an equal factor. Primarily, this signature makes it possible to diagnose systems with two vertical frontiers forming a wedge with an angle β , with $\beta = 360 T_{app} / T$ where T is the “real” transmissivity of the aquifer as given by the early radial plateau, and T_{app} is the apparent transmissivity given by the second radial plateau (Beauheim and Roberts, 1998). Similarly, Mijinyawa and Gringarten (2008) observed that the narrower the semi-infinite channel with non-parallel frontiers, the greater the stabilisation of the second plateau.

The derivative signature of a weakly inclined (or horizontal) fault embedded in an isotropic conductive matrix also induces two plateaus, with the second plateau greater than double the elevation of the first plateau (Rafini and Larocque, 2012). The fault and the matrix are both connected to the pumping well. The first plateau reflects a cylindrical-radial flow within the fault which is much more transmissive than the matrix, in a fashion grossly similar to that illustrated in Figure 2.7a. The second plateau occurs when the fault no longer exerts influence on the transient hydrodynamics, and pressure diffusion into the entire system is governed by the matrix properties. The elevations of the first and second plateaus are strictly related to the hydraulic transmissivities of the fault and the matrix. The transition stage (positive slope of the derivative signal) relates to the fault inclination.

A criterion that may make it possible to distinguish between the conceptual model for multiple impermeable frontiers and that for a weakly inclined fault may be the shape of the transitional stage between the two plateaus. In the weakly inclined fault aquifer, the

transitional stage reflects a balancing flow period in which the signal of the fault is progressively masked by the signal of the matrix. Rafini and Larocque (2012) demonstrated that, due to transient hydrodynamic interactions between the fault and the surrounding matrix, the less inclined the fault, the higher the slope of the derivative during the transitional stage and the shorter its duration. On another hand, in the model for multiple impermeable frontiers, transitions may form prolonged stages over time, as frontiers are successively reached one after another. To conclude, in many cases, using the shape of the transitional stage to distinguish between both models is not a straightforward process. Knowledge of the geological context (primarily, fractured rock versus granular aquifer contexts) remains the most valuable information for this purpose.

Sequence $n = 2$ – (transition) – 2 with late plateau lower than the early plateau

Recently, Rafini et al. (2017) analysed the pressure front pulse behavior in an aquifer composed of two linearly contiguous homogeneous domains with non-equal hydraulic properties. They showed that, when the pumping well is located in the less transmissive media (domain A), the pressure wave will diffuse preferentially through the most transmissive domain (domain B). This flow behavior results in a derivative signal composed of 1) a first plateau ($n = 2$) representing the radial diffusion of the pressure wave in domain A; 2) a transitional stage (unit-negative slope) after the pressure wave reaches the vertical limit between both domains; and 3) a late plateau controlled by the hydraulic transmissivity

of the domain B (Table 2.1, cell 16). Since the transmissivity of domain B is greater than the transmissivity of domain A, the elevation of the second plateau is lower than that of the first.

Sequence $n = 2$ – (transition) – 2 with both plateaus at the same elevation

The dual-porosity models proposed by Barenblatt et al. (1960), Kazemi (1969) and Warren and Root (1963) model fractured aquifers where the conductive matrix and the fracture network form two hydraulic continua. The fractured aquifer is represented by an equivalent continuum in which there is no explicit fracture and the matrix blocks are contributing as local source terms. The hydraulically active fractures in the network must be dense and sufficiently connective, and their sizes must be small enough, compared to the scale of investigation, for the pressure to diffuse in a practically radial multi-directional fashion and for the transient effects of individual fractures to be diluted in the bulk network radial response. These models idealize the fractured aquifer by means of a 3D Euclidean fractured network, in which the fractures provide the hydraulic conductivity of the system while the matrix provides the storage capacity. This model predicts type-curves composed of two plateaus with equal elevations (same hydraulic transmissivity) separated by a depression of the derivative signal which represents the interporosity flow function, during which the pressures of each of the two media tend to balance each other out (Gringarten, 1987b) (Table 2.1-cell 19). Note that the shape of this depression depends on the flow type between the matrix and the fracture. Gringarten (1987a) illustrated that flow models with a pseudo-steady state interporosity flow (there is interporosity skin that restricts the flow between the

matrix and the fractured media) will induce a V-shaped depression of the derivative signal (Warren and Root, 1963), whereas flow models with an transient interporosity flow will induce an open U-shaped depression (Moench, 1984). The interporosity flow coefficient is defined as the ratio of the permeability of the matrix to that of the fractures. However, the relevancy of the dual-porosity model is deeply undermined by Kuchuk and Biryukov (2014, 2013, 2012). By combining semi-analytical solutions (Kuchuk and Biryukov, 2013, 2012), field data (Kuchuk and Biryukov, 2015, 2014) and numerical modelling of flow through a discretely fractured and faulted reservoir (containing arbitrary distributed finite and/or infinite-conductivity faults and/or fractures) (Biryukov and Kuchuk, 2012), these authors point to a lack of validity of the dual-porosity model.

As initially submitted by Barenblatt et al. (1960) and Warren and Root (1963), the dual-porosity model assumes that the matrix is homogeneous and uniform throughout the entire system. Abdassah and Ershaghi (1986) later revisited this restrictive assumption and introduced the triple-porosity model in order to represent the fracture-matrix flow behavior in a more realistic way. This conceptual model considers two, rather than one, matrix domains with different properties (interporosity and storage capacity). The model assumes that the flow takes place in the fractures towards the well, no flow occurs between the two matrix domains and the matrices act as sources to supply the fractures (the well is not supplied by the matrices). Abdassah and Ershaghi (1986) proposed two conceptual models: horizontal matrix layers separated by fractures (strata model) and blocks which are uniformly distributed and which are separated by orthogonal fractures (block model). Escobar et al. (2004b) adapted the derivative analysis to the triple-porosity model by using Tiab's method.

The type-curve of this model shows two radial flow regimes separated by two humps (Table 2.1, cell 20). It should be noted, however, that if the relevancy of the dual-porosity model is questionable, the triple-porosity model is even more debatable and doubtful. Neither the double-porosity signature nor the triple porosity signature has been reported in our flow dimension database (Ferroud et al., 2018).

2.4.5 LINEAR – RADIAL COMBINATIONS

Sequence $n = 2 - 1 - 2$

Fluvial deposits (e.g., braided and/or meandering environments) are systems which are formed by the transport and deposition of sediments in river channels. This deposition creates layered systems in which the communication between layers controls the flow. This type of environment produces a specific derivative signature. If the communication between layers is laterally and vertically restricted, a “ramp effect” signal may be observed (Table 2.1, cell 15, segment B). This flow regime expresses a one-directional flow within the layers. In other words, lateral micro-cross flow within fluvial deposits produces a linear flow dimension observed over at least one log-cycle when there is no vertical permeability and a poor lateral connectivity between facies. A linear flow is observed because the transmissivity decreases laterally, due to the heterogeneity of layers that constrains the flow in one direction (Corbett et al., 2012). The late times radial flow dimension reflects the effective hydraulic conductivity when the entire heterogeneous system contributes. The n -sequence of this conceptual model is 2 - 1 - 2 (Table 2.1, cell 15).

Sequence $n = 2 - 1$

The n -sequence $2 - 1$ is typically generated in a large corridor bounded by two parallel no-flow lateral boundaries. The early radial flow regime settles as the pressure front pulse increases radially around the pumping well, while the linear regime starts after the lateral boundaries have been reached (Rafini, 2008, p. 76) (Table 2.1, cell 5).

Note that this sequence $n = 2 - 1$ was commonly observed, with a short-duration early radial flow regime, in our flow dimension database (Ferroud et al., 2018) in fluvio-glacial deposits. This sequence is associated either with a narrow aquifer (Table 2.1, cell 5) or with the first portion of the ramp effect ($n = 2 - 1 - 2$, Table 2.1, cell 15) proposed by Corbett et al. (2012). This n -sequence has also been observed in granites by Dewandel et al. (2011).

2.4.6 THE “BILINEAR” FLOW REGIME: $n = 1.5$

The $n = 1.5$ behavior, commonly referred to as the so-called bilinear flow regime, is produced by a steeply inclined finite-conductivity fault embedded into an aquifer, as demonstrated analytically by Cinco-Ley and Samaniego-V. (1981a) and numerically by Rafini and Larocque (2012, 2009). The fact that the fault's conductivity is finite rather than infinite accounts for the pressure gradients in the fault. This case contrasts with previously mentioned infinite-conductivity fault models where the water pressure in the fault is approximated to be uniform in such a manner that it behaves as a planar source (see matrix-related linear flow regime, in the preceding section). The finite-conductivity fault model

describes transient flow into two darcyan flow domains, i.e., the fault and the matrix, and their interactions. The authors showed that, for reasons relating to flow geometry, the $n = 1.5$ flow regime occurs only if the diffusion into the fault is strictly one-directional, which means that the pressure front pulse must have reached the top and bottom boundaries. In other words, the entire vertical extension of the fault must be depressurized. This explains why this flow regime is rarely produced by weakly inclined faults unless the embedding aquifer is very thin. Strictly speaking, the $n = 1.5$ regime is generated when there are transient interactions between a two-dimensional (fault) and a three-dimensional (matrix) hydraulic object with contrasting properties. The initial flow scheme associated with this conceptual model as submitted by Cinco-Ley and Samaniego-V. (1981a) is depicted in Figure 2.8a. It assumes two simultaneous one-dimensional sets of stream lines, one occurring in the fault and the other one in the embedding matrix perpendicularly to the fault. Although this idealization was analytically necessary because it reduces an unsolvable, complex two-dimensional problem into two one-dimensional solvable problems, it remains unrealistic because any pressure gradient into the fault would instantly cause stream lines into the matrix to be non-parallel (Rafini, 2008). A later numerical study (Rafini and Larocque, 2009) re-examined in detail the hydrodynamics associated with the $n = 1.5$ flow regime. It demonstrated that this flow regime is not restricted to such idealized geometry of stream lines. The flow regime occurring in the matrix is not a linear one, nor is the flow geometry one-dimensional, as explained in Figure 2.8b. The hydrodynamic conditions indicated by $n = 1.5$ consist in a slowing-down of the diffusive regime $r(t)$ in the fault as a consequence of water being supplied from the matrix (Rafini and Larocque, 2009). In such a case, the front pulse evolves into the fault according to $r \propto t^{0.25}$ rather than according to $r \propto t^{0.5}$ as it

would in a normal –fickian– diffusive regime. The authors demonstrated that the simultaneous occurrence of normal and abnormal diffusive regimes in the matrix and in the fault, respectively, lead to an aquifer-scale pressure front-pulse surface A growing proportionally to $r^{0.5}$, which explains the flow dimension equal to 1.5, according to the definition of this parameter (Eq. 1).

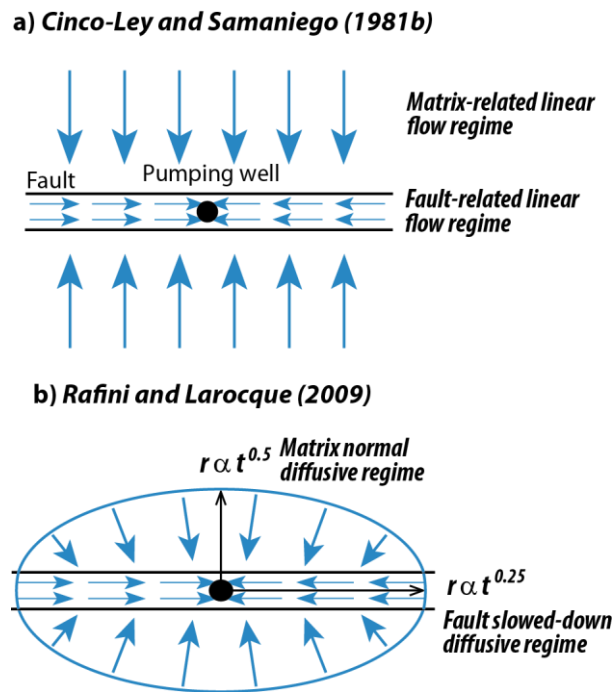


Figure 2.8. Evolution of the “bilinear” $n = 1.5$ conceptual flow model.

Our flow dimension database emphasizes that the bilinear flow regime ($n = 1.5$) is mostly observed in faulted rock aquifers where the matrix is highly fractured (Figure 2.9), which

confirms the relevancy of the vertical leaky fault model (Cinco-Ley and Samaniego-V., 1981a).

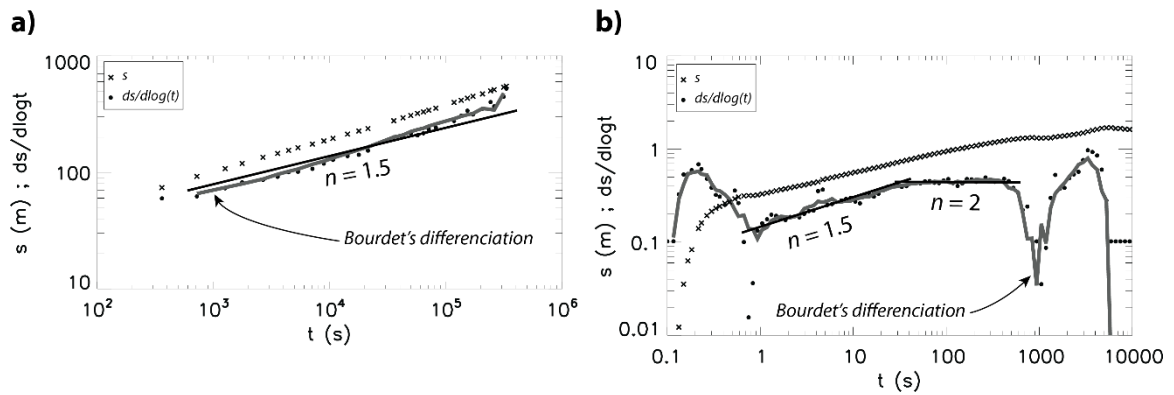


Figure 2.9. Examples of a leaky vertical faults. a) Diagnostic plots and interpretations of a constant-rate pumping test given by Tiab (2005) (Example 2), b) Diagnostic plots and interpretations of a constant-rate pumping test (6.5 days) conducted in the P-8 well located in a Chasy carbonate rock aquifer of Sainte-Anne-des-Plaines (Quebec, Canada).

In accordance with this generalized conception, the $n = 1.5$ fractional regime may actually be produced by any steeply inclined tabular thin aquifer surrounded by a less conductive unit – a fractured dyke embedded into a massive granite, or a conductive layer in a verticalized sedimentary sequence, etc.

Recently, Valdes-Perez et al. (2011) proposed a bilinear flow model with a transient interporosity transfer (TIT) between the matrix (which the authors refer to as the “fractured bulk” and which considers matrix, vugs, micro and meso fractures) and the fault (which the authors refer to as the dominant fracture). This conceptual model is composed of a well that intercepts a finite conductive vertical fracture in a double-porosity aquifer with an

interporosity skin. (Figure 2.10b). The interporosity skin restricts the interaction between the fault and the matrix; it may consist in a zone of damage with mineral-filled fractures. In this conceptual model, the predicted early linear regime represents the restriction of flow in the fracture in a fashion similar to that explained in section 3.1; it is followed by a short transition reflecting the interactions between the fractured network and the dominant fracture, and a late bilinear flow regime induced by the fault-matrix transient interactions as explained in the previous section (Table 2.1, cell 18).

It should be noted that Butler Jr. and Liu (1991) have stated that a $n = 1.5$ fractional regime observed at very early time is associated with a low-conductivity vertical fracture (Gringarten (1985) cited by Butler Jr. and Liu (1991)), whereas when observed at moderate to late times, a linear flow regime represents a leaky vertical finite conductivity fault, as explained above. These authors defined the fault as a linear strip of one material embedded in a matrix having different hydraulic properties.

In all circumstances, the $n = 1.5$ behaviour essentially does not represent an “infinite-acting” regime, as it is due to the transient hydrodynamic interactions between hydraulic objects, as explained above.

Sequence $n = 1.5 - 2$

A late radial flow regime occurring after the $n = 1.5$ corresponds to a matrix-related flow regime (Cinco-Ley and Samaniego-V., 1981a; Rafini and Larocque, 2009). Strictly speaking, it is established after the diffusion into the matrix has become greater than the diffusion into the fault. In other words, the fault becomes invisible from a hydrodynamic standpoint; its

effect is “diluted” into the large volume of depressurized aquifer (Rafini and Larocque, 2009). The apparent transmissivity given by the plateau elevation strictly is that of the matrix (Table 2.1, cell 7).

Sequence $n = 2 - (\text{transition}) - 1.5$

Abbaszadeh and Cinco-Ley (1995) described the case of a finite-conductivity fault-matrix system in which the fault is not directly pumped, as it is not intercepted by the wellbore. This leads to the settlement of an early, matrix-related, radial flow corresponding to the time before the fault is reached by the pressure front-pulse (Rafini and Larocque, 2009). During this early stage, the apparent transmissivity as derived by the plateau elevation is that of the matrix. A transitional stage with a characteristic negative unit slope takes place between early radial and late $n = 1.5$ flow regimes, whose duration increases with the conductivity ratio between the fault and the matrix (Table 2.1, cell 8).

Sequence $n = 2 - 1.5$

Rafini and Larocque (2012) concluded from numerical experiments that the $n = 1.5$ flow regime may be generalized to inclined faults, which would be reflected by the settlement of an early radial flow regime prior to the $n = 1.5$ stage without any transitional negative unit slope stage. This corresponds to the time lapse during which the pressure front pulse propagates into the fault in a radial fashion from the point of interception with the wellbore, before reaching the aquifer’s top and bottom boundaries. In this case, the early radial flow regime is fault-related, which means that the plateau elevation is inversely proportional to the fault’s transmissivity (Table 2.1, cell 12).

Sequence $n = 1 - 1.5 - 1.3$

Lee and Brockenbrough (1986) proposed an analytical solution based on the trilinear flow regime ($n = 1.3$) to interpret a finite-conductivity vertical fracture intercepting a pumping well (Table 2.1, cell 18). This conceptual model assumes three perpendicular linear flow regimes: one into the fracture, one into the matrix, perpendicular to the fracture and restricted to a region directly surrounding the fracture, and one also into the matrix, perpendicular to the latter and infinite-acting (Lee and Brockenbrough, 1986) (Figure 2.10c, Table 2.1, cell 18). These authors predict the early sequence 1 – 1.5, previously introduced by Cinco-Ley and Samaniego-V. (1981a), and which corresponds to a transient flow depressurization in the fracture only ($n = 1$), then simultaneously in the fracture and the matrix, as discussed in the previous section. Their original contribution, though, is the prediction of a late $n = 1.3$ flow regime, referred to as the trilinear regime. They observed that the curves generated by the solutions of Cinco-Ley et al. (1978) and the curves generated by the trilinear flow model are equivalent for the linear and bilinear sequence. According to Lee and Brockenbrough (1986), the advantage of the trilinear flow model lies in its ability to provide a solution that is valid from the early time signal (linear and bilinear flow regime sequence) to the pseudoradial flow regime (boundary-dominated flow regime). According to Azari et al. (1990), the trilinear flow model has the advantage of smoothly linking the fracture flow to the pseudoradial solution. Finally, the trilinear conceptual flow model is of a higher degree of idealization than the bilinear model, which has previously been criticized by Rafini and Larocque (2009) and revised for its lack of realism (Figure 2.10).

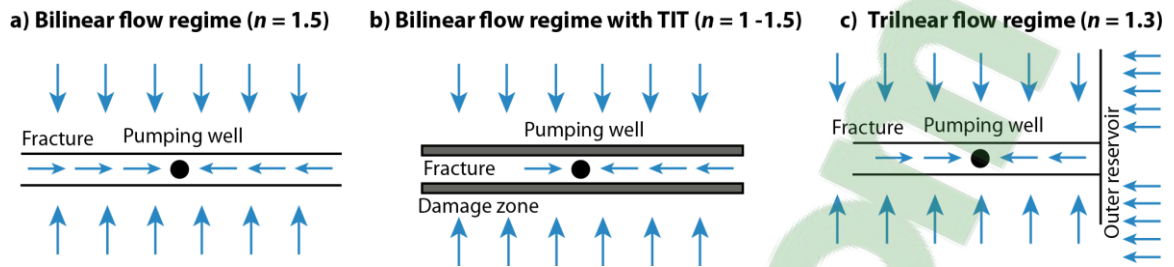


Figure 2.10. a) bilinear flow model for a vertical finite conductivity fault (Cinco-Ley and Samaniego-V., 1981b; Rafini and Larocque, 2009); b) bilinear flow model for a vertical finite conductivity fault with a transient interporosity transfer (TIT) between the fault and the matrix (Valdes-Perez et al., 2011); c) trilinear flow model of a leaky vertical finite conductivity fault and a linear flow induced by an external drainage (Lee and Brockenbrough, 1986).

2.4.7 THE SPHERICAL FLOW REGIME: $n = 3$

Conceptually, the spherical flow regime is primarily attributed to a point-source: equipotential surfaces are spheres that grow outwards according to $A(r) \sim 4\pi r^2$, leading to $n=3$ following Equation (2.2). This occurs when the portion of borehole that is receiving groundwater is significantly shorter than the aquifer thickness. Barker (1988) interprets $n = 3$ as being induced by a point source. The spherical flow regime is thus expected to be observed i) in thick granular systems or thick fractured media where the pumping well partially penetrates the aquifer; ii) in partially completed aquifers; iii) during a packer test (the pumping test is considered as a point source (Escobar et al., 2012a; Moncada et al., 2005); in an fractured aquifer where a well is pumping a partially penetrating (finite-extension) fracture (Dewandel et al., 2018). In these conceptual models, the cross-flow area diffuses as a sphere (partially

completed aquifer or point source) or a hemisphere (partially penetrated aquifer). However, Rafini et al. (2014) and Ferroud et al. (2016) showed that a spherical flow regime may also be produced in an aquifer with an increasing thickness (inclined substratum or confining layer), as explained in the section below. In this conceptual model, the cross-flow area grows as a portion of a sphere. It should be noted that spherical flow regimes are associated with a slowdown of the drawdown.

2.4.8 RADIAL – SPHERICAL COMBINATIONS

Sequence $n = (2) - 3 - 2$

When the spherical flow is associated with a later radial stage (3 – 2 sequence), this may suggest a point source (Barker, 1988) (Table 2.1, cell 22). The spherical or hemispherical flow regime is generated when pumping between packers (Gringarten and Ramey, 1975; National Research Council Staff, 1996, p. 255; Rafini, 2008), or in cases of short-screen, partial-completion and partial-penetration wellbores (Figure 2.11) (Moncada et al., 2005; Razminia et al., 2016; Yildiz and Bassiouni, 1990). Three-dimensional pressure diffusion occurs before the horizontal top and bottom boundaries are reached, leading to a $n = 3$ flow regime (Figure 2.11). The late radial stage takes place after these boundaries have been reached, due to the horizontal diffusion. The ending time of spherical flow, and transition to the late radial flow regime, provide insights on the aquifer thickness (Moncada et al., 2005). It should be noted that, when the water-receiving borehole height – either screened or open – remains significant (from a practical standpoint, more than a few meters), a radial stage

occurs at the earliest pumping time, prior to the settlement of the spherical flow regime. This early radial flow regime, which is generally short and masked by the wellbore storage, reflects the cylindrical radial diffusion of the pressure front pulse around the length of the open zone of the well.

In this model, the spherical flow regime is short-lived. Its duration depends on the ratio between the water-receiving borehole height and the aquifer thickness. It is very short in cases of partially completed wells with large screen or open borehole heights, while it lasts much longer in the context of packer tests. Note that, the vertical anisotropy has effects on the duration of the spherical flow regime.

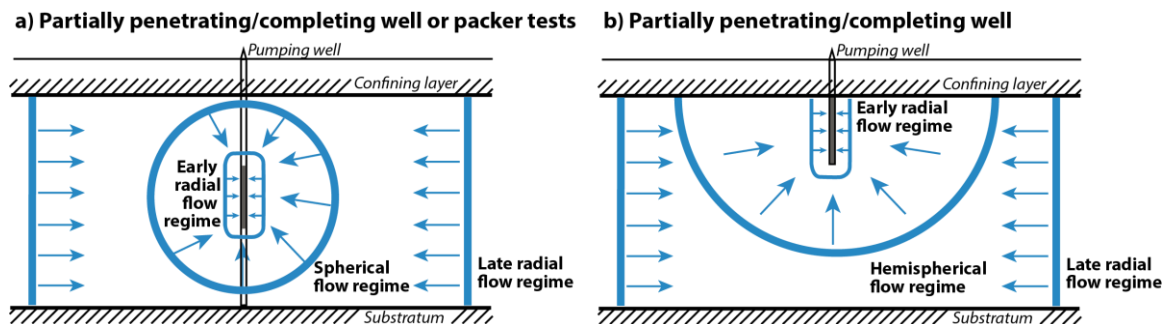


Figure 2.11. Conceptual flow model of a confined aquifer with short-screen length, partial completion or partial completion borehole.

Finally, it is worth noting that such a flow configuration can also occur when an external aquifer is connected to the pumped layer through a localized, “point-like”, pathway (Bourdet, 2002). As illustrated in Figure 2.12, real world examples are: a localized gap in the confining

layer (Figure 12a), a pumped hard-rock aquifer connected to an overlying granular aquifer (non-pumped) through a 1D hydraulic conduit (intersection of two conductive fractures, or conductive channel into a fault) (Figure 2.12b), or a conductive fault cross-cutting a (glacio-)fluvial channel at the base of the overlying sedimentary pile. Note that a late radial stage may also occur in such configurations (Figures 2.12 a and b), which has not been represented.

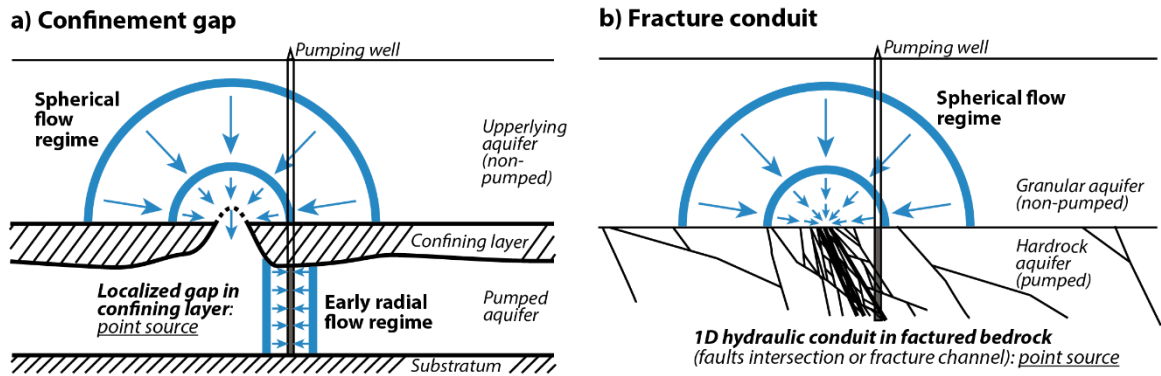


Figure 2.12. Examples of locally leaky aquifers; spherical flow regime.

Sequence $n = (2) - 2 - 3$

Initially, Horne and Temeng (1982) interpreted the spherical flow regime as being related to a conceptual model influenced by a pinch-out boundary (the upper and the lower confining beds form a wedge with an angle θ , Figure 2.13). In this conceptual model, the derivative signal shows a short early radial flow dimension ($n=2$), followed by a spherical flow regime

($n=3$). More recently, Mijinyawa and Gringarten (2008) remarked that this n -sequence 2-3 is only observed if the well is close to the pinch-out (Figure 2.13a) (Table 2.1, cell 21). It should be noted that Mijinyawa and Gringarten (2008) observed that if the well is far away from the pinch-out (Figure 2.13b), the spherical regime will not be visible: the derivative signal shows two plateaus (sequence $n = 2 - 2$) (Table 2.1, cell 14). The first plateau expresses the radial diffusion of the cross-flow area in the constant-thickness aquifer. The second plateau (which is double the first plateau) is produced by the attainment of the pinch-out boundary, which acts as the signal of a single vertical no-flow boundary. More recently, Rafini et al. (2014) and Ferroud et al. (2016) showed numerically that the spherical flow regime can also be observed in an aquifer having an inclined substratum.

Conversely to the partially penetrated/completed aquifer with a n -sequence 2 -3 -2, the 2 – 2 – 3 sequence reflects the signal of an aquifer of variable thickness (inclined substratum or wedge aquifer (Ferroud et al., 2016; Rafini et al., 2014)), as illustrated in Figure 2.14. The front pulse surface can be conceptually decomposed into the three components A_1 , A'_1 and A_2 . Due to the inclined substratum, a portion of cylinder A_{1-loss} is truncated. A_1 and A'_1 grow in a normal radial fashion while A_2 , a portion ($\alpha/360$) of the sphere radius of $r(t)$, grows in a spherical fashion. In early times, before the pressure front pulse reaches the corner (Figure 2.14a), the equivalence between A_{1-loss} and A_2 and after the pressure wave reaches the corner (Figure 2.14b), the predominance of A_1 and A'_1 leads to a sequence of two radial flow regimes. Once the surface area A_2 becomes greater than A_1 , a truncated hemispherical flow regime ($n = 3$) occurs. Depending on the proximity of the pumping to the corner, the early radial stage tends to be short-lived. The second radial stage depends on the well length, the

inclination of the substratum and the hydraulic conductivity of the aquifer. The late spherical flow regime is infinite-acting as it lasts until the end of pumping if no boundary is met.

Note that the wedge-like aquifer solution developed by Hantush (1962) does not predict such spherical behavior due to the postulate that the shape of substratum's inclination follows an exponential function.

Our flow dimension database emphasizes that the spherical flow regime has been commonly observed in thick granular aquifers (Figure 2.15), which confirms the relevancy of the partially penetrated/completed model. One pumping test also showed a spherical flow regime in an inclined substratum (IS) aquifer context.

a) Well close to a pinch-out boundary b) Well further away from a pinch-out boundary



Figure 2.13. Conceptual flow model of a confined aquifer with a well located a) close to; and b) further away - from a pinch-out boundary (modified from Horne and Temeng (1982) and Mijinyawa and Gringarten (2008)).

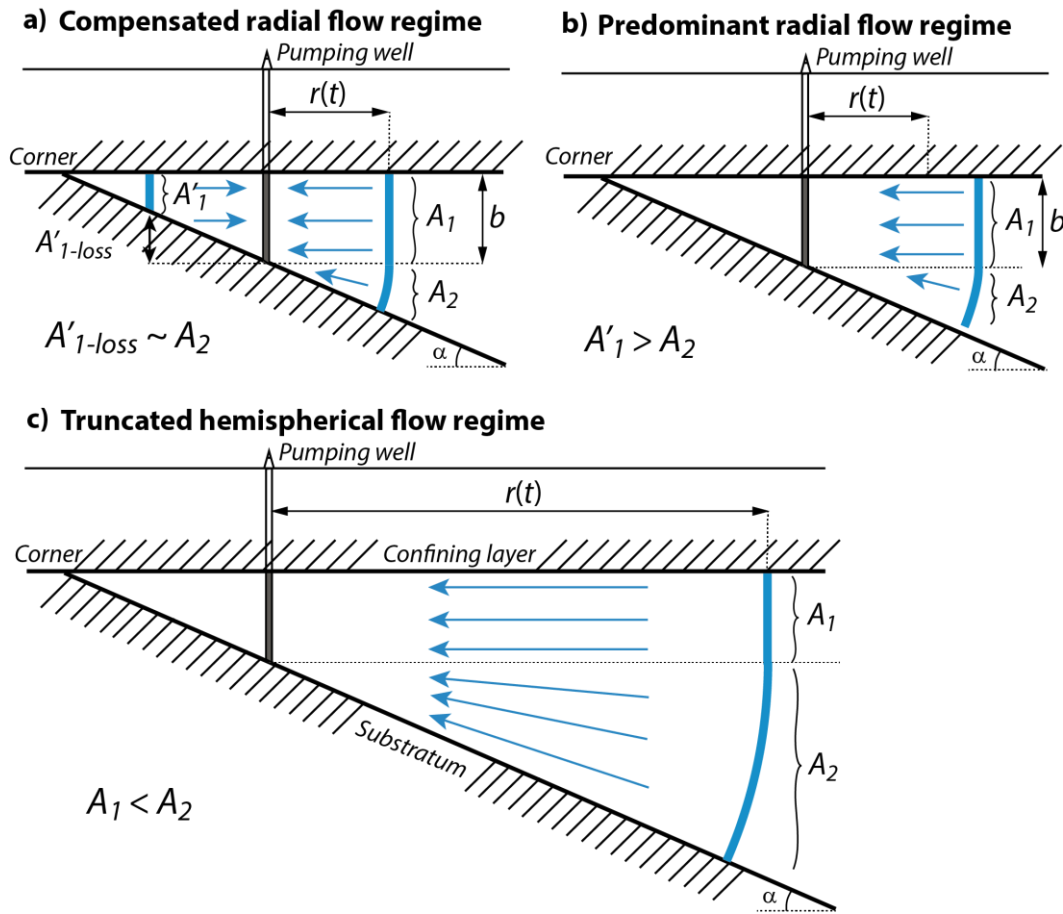


Figure 2.14. Conceptual flow model of a confined aquifer with inclined substratum; a) early compensated radial flow regime ($n = 2$); b) predominant radial flow regime ($n = 2$); c) late infinite acting spherical regime ($n = 3$).

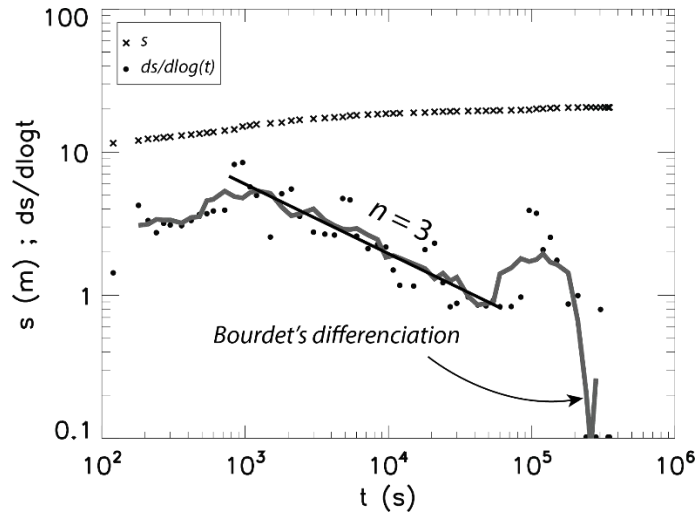


Figure 2.15. Diagnostic plots and interpretations of a constant-rate pumping test conducted in a thick alluvial deposit: example of a signal of a partially penetrated well ($n=3$).

2.4.9 LINEAR – SPHERICAL COMBINATIONS

Sequences $n = (2) - 1 - 3$ and $n = (2) - 4 - 3$

When associated with a previous linear flow dimension, the spherical flow regime can represent a flow regime of a long and narrow (elongated) aquifer that is influenced by a constant head boundary (Sui et al., 2007). The conceptual model is composed of an elongated aquifer, bounded laterally by two no-flow boundaries and one constant-head boundary perpendicular to the elongated direction and a constant-rate pumping well near the constant head boundary. Sui et al. (2007) observed that the flow regime induced by a constant-head boundary depends on the shape of the aquifer and on the position of the well in the model. If the well is closest to the constant-head boundary, the pressure front pulse

firstly grows radially, inducing a radial flow regime (IARF, $n = 2$), then reaches the constant-head boundary, inducing a dipolar flow regime (unit-negative derivative signal) and then diffuses between the two lateral no-flow boundaries, inducing a dipole linear flow regime ($n = 3$). The n -sequence of this configuration is $n = 2 - 4 - 3$ (Table 2.1, cell 23). If the distance between the well and the no-flow boundaries is shorter than the distance between the well and the constant-head boundary, the derivative signal will show a radial flow regime ($n = 2$), followed by a linear flow regime ($n = 1$), followed by a dipole linear flow regime ($n = 3$). The n -sequence of this configuration is $n = 2 - 1 - 3$. When the pressure wave reaches the far constant-head boundary, the derivative signal drops to $-\infty$. Note that the linear ($n = 1$) and the dipolar ($n = 4$) flow regimes are not necessarily observed depending on the configuration of the system. Note that, when the wellbore storage effect is observed, the early radial flow regime may be masked.

2.4.10 FRACTIONAL FLOW REGIMES: NON-INTEGER n

The non-integer n values were initially interpreted as being related to fractal properties of the fractured media (Acuna and Yortsos, 1995; Barker, 1988; Chang and Yortsos, 1990). However, from a geological perspective, the fractal theory applied to natural fracture networks is limited to restricted scale of ranges (e.g., Hardacre and Cowie (2003) and Nicol et al. (1996)), and the finite limits of the hydraulic model, noted by Acuna and Yortsos (1995), would hardly permit the fractional response to develop. Walker et al. (2006) noted that fractional responses may relate to heterogeneity fields with fractal properties. de Dreuzy et

al. (2004) and de Dreuzy and Davy (2007) have observed fractional n values in models with local scaling of transmissivity in non-stationary multifractal correlation patterns (such as Sierpinski- and percolation-like fractal media). In 1991, Doe extends the interpretation of fractional n values to non-fractal geometries which are not space-filling. Following this concept, Rafini and Larocque (2009) numerically demonstrated how the $n = 1.5$ fractional flow response was generated by an aquifer crosscut by a single leaky fault which is non-fractal by definition. Based on our current knowledge, fractional flow dimensions can only be reproduced by a slowing-down of the drawdown diffusion regime $r(t)$ either due to the fractal properties of the medium (Acuna and Yortsos, 1995; Barker, 1988) or to the transient interactions between Euclidean faults and matrix hydraulic units.

Real derivative signatures in fractured rock aquifers have shown successive integer and non-integer n values which compromise the homogeneity assumption of the fractal model (Ferroud et al., 2018; Rafini, 2008). Figure 2.1 depicts a sequence of radial flow dimension and a fractional flow dimension. The radial flow conditions during the first 10^3 seconds of pumping make it difficult to interpret the late fractional regime with a fractal model because it implies the presence of non-fractal characteristic length scales. Furthermore, the succession of different fractional flow regimes on a single response poses the issue of the spatial superposition of two infinite-acting fractal continua, which is conceptually inextricable. In addition, the flow dimension database compiled by Ferroud et al. (2018) emphasized fractional n values in alluvial deposits (Figure 2.16), which are by their very essence non-fractured and non-faulted, implying that other avenues must be considered to interpret these non-integer n values.

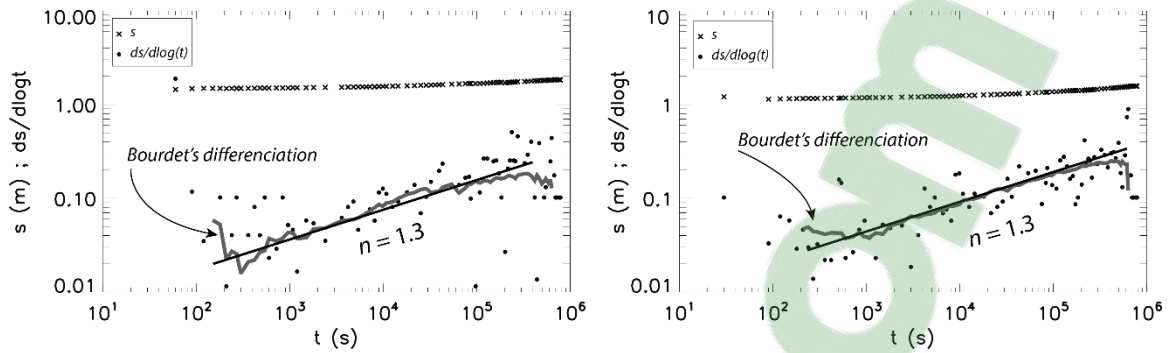


Figure 2.16. Diagnostic plots and interpretations of a constant-rate pumping test conducted in fluvio-glacial deposits (eskers) (Val d'Or, Quebec, Canada): example of a fractional flow dimension.

2.4.11 BOUNDARY FLOW REGIMES

A positive unit slope of the drawdown log-derivative signal may represent wellbore storage effects (e.g., Tiab (2005)) or impermeable boundaries in every direction (also named closed reservoir or depleted reservoir (Gringarten, 2008; Mattar, 1997), which occur respectively at the shortest and at the latest pumping time. Finally, derivative signatures tending to zero or negative unit slopes represent constant-head boundaries in the IARF model (e.g., Walker and Roberts (2003)) or represent a transitional time period (Rafini and Larocque, 2012, 2009; Sui et al., 2007).

2.5 DISCUSSION

2.5.1 THE HYDRAULIC SIGNIFICANCE OF MULTI-STAGE SEQUENCES

In most cases, the natural responses obtained from field investigations display successions of several time periods with different values of n (Ferroud et al., 2018; Rafini, 2008) such as illustrated in Figure 2.1. The typical temporal interpretation of pumping test data stipulates that early-stage responses are controlled by wellbore storage or skin effects, mid-stage responses are an expression of the aquifer properties, and late-stage responses mark the boundary effects (e.g., Leveinen (2001, 2000)). Although this principle remains generally true, the sequential interpretations discussed here make it possible to state that aquifer properties frequently provide multistage responses in themselves. This is due to the existence of various types of “major” or “minor diffuse” heterogeneities or non-uniformities within the aquifer that successively exert a dominant influence on the macroscale flow regime over various time periods. The terms “major” and “minor diffuse” here are time-dependent attributions, as they relate to the ratio between the size of heterogeneities and the investigation scale, i.e., the volume of depressurized aquifer that increases as pumping persists.

Diffuse minor heterogeneity fields, typically conceptualized as an unknown $K(x,y,z)$ distribution function, are not likely to modify the flow dimension unless they follow a scale-invariance statistic function, which brings us to the long-debated fractal models discussed above (Cello et al., 2009; Walker et al., 2006). These fields likely behave like continua after a critical pumping time range where the investigation scale exceeds that of single

heterogeneities by a greater enough amount for those heterogeneities situated into the depressurized volume of aquifer constituting a statistically representative sample of the distribution function. In other words, the bulk conductivity stabilizes with scale. Conversely, at a given pumping time and space, the macroscale aquifer behavior may be influenced by some “major” heterogeneities or non-uniformities, whose magnitude of size is more or less equal to or greater than the investigation scale, and hence of restricted number. In such cases, non-uniform flow will be generated, and a non-radial flow regime will eventually settle. Such heterogeneities may be finite-conductivity hydraulic objects with contrasting topological dimension (patch, conduit, fault, matrix region), or boundaries linearly or irregularly shaped, single or multiple, finite- or infinite-conductivity (substratum inclination, pinchout boundary, lateral lithological domain with variable thickness or conductivity, localized connections to other aquifers, partially leaky strata etc.). It is worth noting that short-lived flow regimes are more likely produced by the former heterogeneity type while the latter is prone to generate “infinite acting” regimes.

In real-life pumping test conditions, hydraulic objects ranging in sizes exceeding a meter or a decameter are likely being considered “major” at least during the restricted time-range during which they exert a singular influence on flow geometry (before the pumping investigation scale grows much greater than their own size). During that period of time when they deterministically impact the aquifer response, they must be explicitly conceptualized in the flow model. Their influence may then evolve over time as the scale of the investigation increases, and they will eventually be better represented as belonging to a “minor diffuse” heterogeneity field. An example is the 1 – 2 flow dimension sequence obtained from a sub-

metric fractures network (Doe, 2002): the early linear stage reflects the influence of a single fracture connected to the wellbore, hence influencing the drawdown response as though it were a “major” heterogeneity whose properties can be explicitly calculated. The late radial regime occurs when a large portion of the network is depressurized, behaving like a radial continuum.

It is a general rule that early time flow regimes (after wellbore storage effects) reflect the minor scale hydraulic conditions, since a restricted flow domain is sampled (depressurized), while late flow regimes are the expression of larger scale, bulk aquifer properties, commonly considered more reliable for practical purposes. At the extreme, and somehow schematically, the early times likely inform on the porosity conditions (fracture or interstitial porosity) while the late times investigate the aquifer geometrical conditions (leakage, connexions to other flow domains, boundaries etc.). Indeed, an early linear flow regime undoubtedly points to the presence of secondary type porosity, dominated by fractures, while late time linear flow regime may indicate an elongated aquifer (fluvial channel, tabular reservoir). The latter conceptual interpretation is more robust, though, if radial regime occurs prior to the late linear one, leading to the sequence 2 – 1, due to the Theissian cylindrical diffusion before the sides of the channel are reached.

It rises from this observation that two factors are meaningful at the conceptual interpretation stage: the time at which the flow regime occurs, and its duration. As said above, flow regimes produced by transient interactions between hydraulic objects are more likely generating short-lived regimes. Following the previous example, the linear flow regime settling into an elongated aquifer is infinite-acting, which is not the case of any fracture-related linear flow

regime. Moreover, a fracture-related linear flow regime cannot occur in late time since it is unrealistic that the fault's cross-sectional surface could be predominant over the cross-flow area evolving in the rest of the flow domain unless it is impermeable.

Successive flow regimes may also correspond to various expressions of the same hydraulic object, at different pumping times and spatial scales. An example already mentioned above is the 1 – 2 sequence that may be conceptually interpreted as an Euclidean conductive fracture network with early linear flow regime expressing sub-meter scale pressure diffusion into a single fracture without matrix depressurization, and later radial stage occurring when the volume of investigation scale is sizeable over the length of the fractures, i.e., the network behaves like a continuum.

Theoretically, changes in flow regimes that relate to the attainment of new non-uniformities – flow domain, distal fault, top or bottom borders, new conditions, far-field water supply etc., – may be succeeding each other in a perfectly independent fashion until the occurrence of drawdown stabilization, aquifer de-saturation, or the end of pumping. This leads to multistage responses for which each regime or sequence may be analyzed independently (Hammond and Field, 2014).

2.5.2 INFLUENCE OF HYDRAULIC DOMAINS WITH NON-EQUAL FLOW AND TOPOLOGICAL DIMENSIONS

Successive flow regimes express flow domains or objects that succeed each other in exerting a sensitive and predominant control on the macroscale aquifer response. They successively govern the global transient diffusion mode of the front pulse, in other words, the exponent of Equation (2.2) power-law relationship. In the example of the fault-matrix system producing the flow dimension sequence 1.5 – 2, both stages correspond to time periods during which the fault and the matrix, respectively, exert a dominant control on the aquifer's response. The two successive flow regimes are caused by a change in interactive mode between the two flow units: fault and matrix produce pressure front-pulse envelopes with, respectively, a pseudo-disc-shape A_1 and cylinder-shape A_2 , diffusing in different modes ($A_1 \propto r^{0.5}$; $A_2 \propto r$) such that their respective flow dimensions are 1.5 and 2. The macroscale flow dimension of the aquifer recorded at the pumping well is 1.5, then 2, each value expressing a time period during which the total surface $A = A_1 + A_2$ is controlled successively by A_1 and then by A_2 , hence changing the Equation (2.2) power-law exponent and the flow dimension (see Rafini and Larocque (2009) for a deeper demonstration). This conducts to the general result that, where flow units with different dimension are present in the aquifer and produce surfaces A_n growing at different power-law rates with r , the polynomial form of $A_{total} = \sum_n A_n$ is such that a single surface A_n predominates over others at a given pumping time and space. Due to this polynomial form, in no circumstances may the resulting exponent of $A_{total}(r)$ power-law relationship be a combination of individual exponents $A_n(r)$. In other words, the aquifer flow dimension can never be a mathematical

combination (product, average, etc.) of flow dimensions produced by individual hydraulic objects, contrary to what may have been stated. The flow dimension that is measured on a derivative signal is an apparent value reflecting the predominant flow behavior rather than a mean value of the flow dimensions related to hydraulic object in the aquifer.

Finally, it is worth noting that the position of the well relative to the aquifer configuration is essential and may significantly influence the derivative signal and the n -sequence. For instance, Sui et al. (2007) showed that if a well is close to the constant-head boundary of an elongated aquifer, the n -sequence 2 – 4 – 3 occurs, while if the well is far from the constant-head boundary and the pressure front pulse reaches the lateral impermeable boundaries of the elongated aquifer before the constant-head boundary, the n -sequence 2 – 1 – 3 will be observed.

2.5.3 LIMITATIONS

Issue of non-unique interpretations

Analyzing the drawdown-log derivative signal helps to improve the interpretation of pumping tests by reducing the non-unicity of the drawdown signatures; however, it remains that different flow behaviors can produce the same flow dimension. For instance, Ferroud et al. (2018) observed that the same flow dimension value can be observed in various geological contexts, such as carbonate rock aquifers, crystalline rock aquifers and alluvial deposits. For instance, they observed a linear flow regime in both fractured rock aquifers and alluvial

deposits. This study, with its catalogue of flow regimes, also emphasizes the issue of non-unicity, because various conceptual models may produce an identical flow dimension value. For instance, the spherical flow regime ($n = 3$) can be produced in a partially penetrated aquifer (Escobar et al., 2012a; Moncada et al., 2005), in an aquifer of increasing thickness (IS aquifer) (Ferroud et al., 2016; Rafini et al., 2014) and in a narrow aquifer influenced by a constant head boundary (Sui et al., 2007). Similarly, the linear flow regime is produced by 1) an infinite hydraulic conductivity fault (Gringarten et al., 1974; Gringarten and Ramey, 1975); 2) a finite hydraulic conductivity fault (Abbaszadeh and Cinco-Ley, 1995; Cinco-Ley et al., 1978; Cinco-Ley and Samaniego-V., 1981b); 3) an elongated aquifer (Escobar et al., 2004c), 4) an alluvial system (micro-cross flow in the sediment) (Corbett et al., 2012); and 5) a deltaic environment (distributary channel system) (Mijinyawa and Gringarten, 2008).

Analysing the sequence of flow regimes helps to choose an appropriate conceptual model by countering the non-unicity of the derivative signal. For instance, the n -sequence 2 - 3 - 2 expresses a partially penetrated aquifer, whereas the n -sequence 2 - 2 - 3 refers to an aquifer with an inclined substratum. This study aims at listing and summarizing the main type curves of the various conceptual models presented in the literature in order to help the practitioner in interpreting pumping test data.

Finally, it is worth noting that conducting a proper aquifer interpretation requires a comprehensive approach in which the derivative response is analysed with respect to the geological environment. Field knowledge, typically from geological or geophysical surface or log surveys, in many instances may prove helpful in selecting between several non-unique flow models which all fit the observed data.

Issue of the quality of derivative data and the subjectivity of interpretations

Noise in data: As mentioned previously, the relevancy of the selection of the conceptual model is based on the quality of the derivative signal. If the signal is too noisy, the determination of the flow regimes will be uncertain and therefore the selection of the conceptual model doubtful. Deconvolution/convolution algorithms are available to reduce noise induced by flow rate variations, while differentiation algorithms are deemed efficient to reduce Gaussian noise (instrumental noise, random diffuse heterogeneity) (see section 2.1).

Duration of the pumping test: The longer the pumping test, the larger the volume of aquifer that is investigated and therefore, the more likely that the more numerous flow regimes will be detected. It should be kept in mind that, unless the hydraulic boundaries are reached, the derivative signature is possibly not complete. Indeed, if the pumping test is not long enough to detect all the sequences of the type-curve or if drawdown data are missing or too noisy, only one portion of the theoretical type-curve is observed or detected. For instance, with the sequence $n = 1.5 - 2$, we cannot conclude that the well is connected to the fault. However, the sequence $2 - (\text{negative unit slope}) - 1.5 - 2$ makes it possible to detect the effect of a leaky vertical fault that is non-connected to the source. It is thus important to combine the analysis of the derivative signal with all the available field information (Liang et al., 2012; Massonnat and Bandiziol, 1991). Once the relevant conceptual model is chosen, the hydraulic properties may be estimated.

Determination of the flow regimes: The determination of flow dimensions by analysing straight lines in the derivative signal presents several challenges: the derivative signal must attain a “real” stabilization; in some cases, the transitional flow regime may be observed over a long duration due to, for instance, a low hydraulic conductivity. These small variations during the transitional stage may be mistakenly interpreted as a flow regime. When aquifers are very heterogeneous, it is possible that the derivative signal may never become stable, thus expressing only transitional stages. As stated by Beauheim et al. (2004) and Rafini et al. (2017), a proper estimation of the flow dimension should be determined from a constant straight line of the derivative signal that lasts at least one log cycle.

The interpretation of flow regimes uses successive linear regressions on derivative straight lines, into several time windows. The recognition of these time windows, and the confidence these provide in the interpretation of flow dimensions, remains a sensitive aspect of the approach that may, in some cases, still present some uncertainties. If the effects of pumping-rate changes have not been removed from the derivative signal, a manual interpretation is recommended rather than any automated process for optimizing regression coefficient sequences. Indeed, the quality of regressions is not the only component of a proper interpretation of flow regimes: a manual analysis of derivative data makes it possible to identify pumping rate interruptions or changes, to award less weight or significance to certain noisy sections presenting obviously increased data instability – either instrumental, due to a localized highly diffuse heterogeneity field, or other sources. Furthermore, the manual interpreter may benefit from derivative differentiation without being misled by it, in other

words to stick to raw data. We finally submit that a simultaneous fit on both s and $ds/d\log t$ significantly contributes to reducing the level of subjectivity when interpreting flow regimes.

2.5.4 SUMMARY OF THE PROPOSED METHODOLOGY

The proposed methodology consists in:

1. Pre-processing the data in order to correct the variable-rate drawdown into constant-rate drawdown and to reduce the noise by using deconvolution/ convolution and/or differentiation codes.

If data pre-processing is not possible, the recognition of various noise types, such as pump arrests/instabilities or imprecise drawdown manual measurement is recommended.

2. Identifying the flow regimes as successive straight lines on the log-log plot of the derivative response:

Specific attention must be paid to the stability of the slope and the critical duration of the slope-stable segment. It is important to keep in mind that, as the pressure front pulse propagates, the volume of depressurized aquifer increases and thus the scale of detected heterogeneity increases.

3. Fitting with real data:

The determination of the flow dimension is improved by simultaneously fitting the signal segments of s and $ds/dlogt$, respectively, on a semi-log and on a log-log plot. This approach combines the advantages of both plots: the semi-log plot of s is not very sensitive to both pumping rate changes and flow regime, whereas the log-log plot of $ds/dlogt$ is very sensitive to both pumping rate changes and flow regime. This combined fitting of s and $ds/dlogt$ increases the objectivity of the flow dimension determination. It should be noted that this approach is all the more useful when data pre-processing is not possible and the derivative signal is noisy. For instance, when the derivative signal is noisy, it is sometimes difficult to confidently adjust the vertical position of the straight line. In such cases, adjusting the s signal on a semi-log plot proves very helpful. Note that the combined approach may be assisted by manually or automatically optimizing the correlation coefficients independently into each segment and on both plots.

4. Choosing a conceptual model

Because several conceptual models may produce a same derivative signal, it is important to have some information about the geological settings (Liang et al., 2012; Massonnat and Bandiziol, 1991). In addition, as explained previously, analysing the sequence of flow regimes will help to attenuate the non-unicity of the derivative signal.

5. Doing extra geological studies

If possible, consider doing extra studies to determine the nature and the configuration of the heterogeneity, such as geophysical surveys (e.g., georadar, Time Domain Electromagnetic

Method, seismic methods), or drilling (e.g., to investigate a buried esker), etc.

2.6 CONCLUSION

This contribution deciphers the methodology that consists in using the sequential analysis of flow dimensions for the interpretation of pumping test data in complex aquifers. The relevance of performing hydraulic investigations in real aquifers using models with variable degrees of idealization has been discussed, and the need for innovative tools able to model more complex flow conditions was mentioned. Our sequential interpretative methodology was described in detail. This paper provides an extensive review of diagnostic responses and their associated conceptual models which have been published in the hydrogeology and petroleum industry literature.

Ferroud et al. (2018) demonstrated that non-radial behaviors are generally predominant in natural aquifer responses to transient pump tests, in various geological environments. They noted that common drawdown interpretations are not capable of accurately representing the transient geometry of flow occurring in aquifers, as non-radial flow models remain seldom used and still insufficient to explain fractional flow behaviors. Such conclusions tell us that continued research efforts should be devoted to the flow dimension approach. The fact that the flow dimension theory remains valid beyond GRF aquifer conditions must now be considered a consensual premise. In this view, further works should focus on 1) identifying the multistage dimensional responses of various types of complex, irregular and realistic aquifer conditions, from numerical experiments on synthetic objects along with field

verification; 2) investigating flow dimensional responses from multi-well datasets, i.e., constraining the spatial distribution of this parameter in various types of heterogeneous flow configurations; 3) last but not least, understanding the still-enigmatic fractional flow regimes, which are extensively reported in nature (Ferroud et al., 2018; Rafini, 2008). Most research efforts focused on fractal approaches, which remain unsatisfactory in many geological contexts and did not prove successful in providing conclusive outcomes. In spite of the negative effects of this unfruitful avenue on the perceptions some researchers have had regarding flow dimension analysis, we submit that this approach still has the potential of providing significant and substantial future advances in the field of interpretation of complex aquifers, similar in significance to Bourdet's breakthrough derivative approach published in the 1980's.

2.7 ACKNOWLEDGMENTS

The authors would like to thank the National sciences and engineering research council of Canada (NSERC-Individual discovery grants program) and the Fonds de recherche du Québec - Nature et technologies (FRQNT-New university researchers start up program) grant programs held by Prof. Romain Chesnaux for their financial contribution in supporting this study. We also thank the municipalities of Charlevoix-Haute-Côte-Nord (Quebec) and the environmental government of Quebec (MDDELCC, Développement durable, Environnement et Lutte contre les changements climatiques) for their financial support. Proofreading of the manuscript has been kindly performed by Josée Kaufmann.

2.8 REFERENCES

- Abbaszadeh, M., Cinco-Ley, H., 1995. Pressure-transient behavior in a reservoir with a finite-conductivity fault. *SPE Form. Eval.* 10, 26–32. <https://doi.org/10.2118/24704-PA>
- Abdassah, D., Ershaghi, I., 1986. Triple-Porosity Systems for Representing Naturally Fractured Reservoirs. *SPE Form. Eval.* 1, 113–127. <https://doi.org/10.2118/13409-PA>
- Acuna, J.A., Yortsos, Y.C., 1995. Application of fractal geometry to the study of networks of fractures and their pressure transient. *Water Resour. Res.* 31, 527–540. <https://doi.org/10.1029/94WR02260>
- Antonellini, M., Aydin, A., 1994. Effect of Faulting on Fluid Flow in Porous Sandstones: Petrophysical Properties. *AAPG Bull.* 78, 355–377.
- Audouin, O., Bodin, J., Porel, G., Bourbiaux, B., 2008. Flowpath structure in a limestone aquifer: multi-borehole logging investigations at the hydrogeological experimental site of Poitiers, France. *Hydrogeol. J.* 16, 939–950. <https://doi.org/10.1007/s10040-008-0275-4>
- Avcı, C.B., Şahin, A.U., Çiftçi, E., 2013. A new method for aquifer system identification and parameter estimation. *Hydrol. Process.* 27, 2485–2497. <https://doi.org/10.1002/hyp.9352>
- Aydin, A., 2000. Fractures, faults, and hydrocarbon entrapment, migration and flow. *Mar. Pet. Geol.* 17, 797–814. [https://doi.org/10.1016/S0264-8172\(00\)00020-9](https://doi.org/10.1016/S0264-8172(00)00020-9)
- Azari, M., Wooden, W.O., Coble, L.E., 1990. A Complete Set of Laplace Transforms for Finite-Conductivity Vertical Fractures Under Bilinear and Trilinear Flows. *Society of Petroleum Engineers*. <https://doi.org/10.2118/20556-MS>
- Barenblatt, G.I., Zheltov, I.P., Kochina, I.N., 1960. Basic concepts in the theory of seepage of homogeneous liquids in fissured rocks [strata]. *J. Appl. Math. Mech.* 24, 1286–1303. [https://doi.org/10.1016/0021-8928\(60\)90107-6](https://doi.org/10.1016/0021-8928(60)90107-6)
- Barker, J.A., 1988. A generalized radial flow model for hydraulic tests in fractured rock. *Water Resour. Res.* 24, 1796–1804. <https://doi.org/10.1029/WR024i010p01796>
- Beauheim, R.L., Roberts, R.M., 1998. Flow-dimension analysis of hydraulic tests to characterize water-conducting features, in: *Water-Conducting Features in Radionuclide Migration, GEOTRAP Project Workshop Proceedings, Barcelona, Spain, June 10-12, 1998*. Paris, France: OECD NEA. 287-294. ISBN 92-64-17124-X.
- Beauheim, R.L., Roberts, R.M., Avis, J.D., 2004. Well testing in fractured media: flow dimensions and diagnostic plots. *J. Hydraul. Res.* 42, 69–76. <https://doi.org/10.1080/00221680409500049>
- Behmel, S., Damour, M., Ludwig, R., Rodriguez, M.J., 2016. Water quality monitoring strategies — A review and future perspectives. *Sci. Total Environ.* 571, 1312–1329. <https://doi.org/10.1016/j.scitotenv.2016.06.235>
- Bense, V.F., Gleeson, T., Loveless, S.E., Bour, O., Scibek, J., 2013. Fault zone hydrogeology. *Earth-Sci. Rev.* 127, 171–192. <https://doi.org/10.1016/j.earscirev.2013.09.008>

- Biryukov, D., Kuchuk, F.J., 2012. Transient pressure behavior of reservoirs with discrete conductive faults and fractures. *Transp. Porous Media* 95, 239–268. <https://doi.org/10.1007/s11242-012-0041-x>
- Birsoy, Y.K., Summers, W.K., 1980. Determination of Aquifer Parameters from Step Tests and Intermittent Pumping Data. *Ground Water* 18, 137–146. <https://doi.org/10.1111/j.1745-6584.1980.tb03382.x>
- Bourdet, D., 2002. *Well Test Analysis: The Use of Advanced Interpretation Models: Handbook of Petroleum Exploration and Production*. Elsevier Science.
- Bourdet, D., Whittle, T., Douglas, A., Picard, Y., 1983. A new set of types curves simplifies well test analysis. *World Oil*, Gulf Publishing Company 196, 95–106.
- Bowman, D.O., Roberts, R.M., Holt, R.M., 2012. Generalized radial flow in synthetic flow systems. *Groundwater* 51, 768–774. <https://doi.org/10.1111/j.1745-6584.2012.01014.x>
- Butler Jr., J.J., Liu, W.Z., 1991. Pumping tests in non-uniform aquifers — the linear strip case. *J. Hydrol.* 128, 69–99. [https://doi.org/10.1016/0022-1694\(91\)90132-2](https://doi.org/10.1016/0022-1694(91)90132-2)
- Caine, J.S., Evans, J.P., Forster, C.B., 1996. Fault zone architecture and permeability structure. *Geology* 24. [https://doi.org/10.1130/0091-7613\(1996\)024<1025:FZAAPS>2.3.CO;2](https://doi.org/10.1130/0091-7613(1996)024<1025:FZAAPS>2.3.CO;2)
- Cello, P.A., Walker, D.D., Valocchi, A.J., Loftis, B., 2009. Flow Dimension and Anomalous Diffusion of Aquifer Tests in Fracture Networks. *Vadose Zone J.* 8, 258–268. <https://doi.org/10.2136/vzj2008.0040>
- Chang, J., Yortsos, Y.C., 1990. Pressure-transient analysis of fractal reservoirs. *SPE Form. Eval.* 5, 31–38. <https://doi.org/10.2118/18170-PA>
- Cheng, W., Ni, J., 2009. The pumping test data analyses of andesite rock blocks aquifer with varied hydraulic boundaries by generalized radial flow model, in: *Soils and Rock Instrumentation, Behavior, and Modeling*. American Society of Civil Engineers, pp. 64–71.
- Chow, V.T., 1952. On the determination of transmissibility and storage coefficients from pumping test data. *Eos Trans. Am. Geophys. Union* 33, 397–404. <https://doi.org/10.1029/TR033i003p00397>
- Cinco-Ley, H., Samaniego V., F., Dominguez A., N., 1978. Transient Pressure Behavior for a Well With a Finite-Conductivity Vertical Fracture. *Soc. Pet. Eng. J.* 18, 253–264. <https://doi.org/10.2118/6014-PA>
- Cinco-Ley, H., Samaniego-V., F., 1981a. Transient pressure analysis: finite conductivity fracture case versus damaged fracture case, in: *SPE Annual Technical Conference and Exhibition*, 4-7 October, 1981, San Antonio, Texas, USA, SPE-10179-MS. Presented at the SPE Annual Technical Conference and Exhibition. <https://doi.org/10.2118/10179-MS>
- Cinco-Ley, H., Samaniego-V., F., 1981b. Transient Pressure Analysis for Fractured Wells. *J. Pet. Technol.* 33, 1749–1766. <https://doi.org/10.2118/7490-PA>

- Cooper, H.H., Jr., Jacob, C.E., 1946. A generalized graphical method for evaluating formation constants and summarizing well-field history. *Trans. Am. Geophys. Union* 27, 526–534. <https://doi.org/10.1029/TR027i004p00526>
- Corbett, P.W.M., Hamdi, H., Gurav, H., 2012. Layered fluvial reservoirs with internal fluid cross flow: a well-connected family of well test pressure transient responses. *Pet. Geosci.* 18, 219–229. <https://doi.org/10.1144/1354-079311-008>
- Cumming, J.A., Wooff, D.A., Whittle, T., Crossman, R.J., Gringarten, A., 2013. Assessing the non-uniqueness of the well test interpretation model using deconvolution, in: Society of Petroleum Engineers Paper No. 164870, EAGE Annual Conference & Exhibition Incorporating SPE Europec, 10-13 June, London, UK. <https://doi.org/10.2118/164870-MS>
- Damuth, J.E., Kolla, V., Flood, R.D., Kowsmann, R.O., Monteiro, M.C., Gorini, M.A., Palma, J.J.C., Belderson, R.H., 1983. Distributary channel meandering and bifurcation patterns on the Amazon deep-sea fan as revealed by long-range side-scan sonar (GLORIA). *Geology* 11, 94. [https://doi.org/10.1130/0091-7613\(1983\)11<94:DCMABP>2.0.CO;2](https://doi.org/10.1130/0091-7613(1983)11<94:DCMABP>2.0.CO;2)
- de Dreuzy, J.-R., Davy, P., 2007. Relation between fractional flow models and fractal or long-range 2-D permeability fields. *Water Resour. Res.* 43. <https://doi.org/10.1029/2006WR005236>
- de Dreuzy, J.-R., Davy, P., Erhel, J., de Brémond d’Ars, J., 2004. Anomalous diffusion exponents in continuous two-dimensional multifractal media. *Phys. Rev. E* 70. <https://doi.org/10.1103/PhysRevE.70.016306>
- Denney, D., 2003. Pressure-Pressure Convolution Analysis Using Wireline Formation Tester Data. *J. Pet. Technol.* 55, 45–46. <https://doi.org/10.2118/0503-0045-JPT>
- Dewandel, B., Aunay, B., Maréchal, J.C., Roques, C., Bour, O., Mougín, B., Aquilina, L., 2014. Analytical solutions for analysing pumping tests in a sub-vertical and anisotropic fault zone draining shallow aquifers. *J. Hydrol.* 509, 115–131. <https://doi.org/10.1016/j.jhydrol.2013.11.014>
- Dewandel, B., Lachassagne, P., Zaidi, F.K., Chandra, S., 2011. A conceptual hydrodynamic model of a geological discontinuity in hard rock aquifers: Example of a quartz reef in granitic terrain in South India. *J. Hydrol.* 405, 474–487. <https://doi.org/10.1016/j.jhydrol.2011.05.050>
- Dewandel, B., Lanini, S., Lachassagne, P., Maréchal, J.-C., 2018. A Generic analytical solution for modelling pumping tests in wells intersecting fractures. *J. Hydrol.* 559, 89–99. <https://doi.org/10.1016/j.jhydrol.2018.02.013>
- Dick, P., Wittebroodt, C., Courbet, C., Sammaljarvi, J., Esteve, I., Matray, J.-M., Siitari-Kauppi, M., Voutilainen, M., Dauzères, A., 2016. The internal architecture and permeability structures of faults in shale formations. pp. 219–229. <https://doi.org/10.1346/CMS-WLS-21.17>
- Doe, T.W., 2002. Generalized dimension analysis of build-up and pressure interference tests (International Progress Report No. IPR-02-70). Stockholm Suède.
- Doe, T.W., 1991. Fractional dimension analysis of constant-pressure well tests, in: Society of Petroleum Engineers Paper No. 22702, SPE Annual Technical Conference and Exhibition,

6-9 October, 1991, Dallas, Texas, USA, Formation Evaluation & Reservoir Geology. pp. 461–467. <https://doi.org/10.2118/22702-MS>

- Duhamel, J., 1833. Memoire sur la methode generale relative au mouvement de la chaleur dans les corps solides plonge dans les milieux dont la temprature varie avec le temps. *J. L'École Polytech.* 14, 20–77.
- Durham, W.B., Bonner, B.P., 1994. Self-propping and fluid flow in slightly offset joints at high effective pressures. *J. Geophys. Res. Solid Earth* 99, 9391–9399. <https://doi.org/10.1029/94JB00242>
- Ehlig-Economides, C., 1988. Use of the pressure derivative for diagnosing pressure-transient behavior. *J. Pet. Technol.* 40, 1280–1282. <https://doi.org/10.2118/18594-PA>
- Ehlig-Economides, C.A., Hegeman, P. (Schlumberger O.S., Clark, G. (Schlumberger O.S., 1994. Three Key Elements Necessary for Successful Testing. *Oil Gas J. U. S.* 92:30.
- Engelder, T., Scholz, C.H., 2013. Fluid Flow Along Very Smooth Joints at Effective Pressures Up to 200 Megapascals, in: Carter, N.L., Friedman, M., Logan, J.M., Stearns, D.W. (Eds.), *Geophysical Monograph Series*. American Geophysical Union, Washington, D. C., pp. 147–152. <https://doi.org/10.1029/GM024p0147>
- Escobar, F.H., Corredor, C.M., Gomez, B.E., Cantillo, J.H., Prent, L.A., 2012a. Pressure and pressure derivative analysis for slanted and partially penetrating wells. *Asian Res. Publ. Netw. ARPN* 7, 932–938.
- Escobar, F.H., Hernández, Y.A., Hernández, C.M., 2007. Pressure transient analysis for long homogeneous reservoirs using TDS technique. *J. Pet. Sci. Eng.* 58, 68–82. <https://doi.org/10.1016/j.petrol.2006.11.010>
- Escobar, F.H., Montealegre, M., 2006. Effect of well stimulation on the skin factor in elongated reservoirs. *CTF - Cienc. Tecnol. Futuro* 3, 109–119.
- Escobar, F.H., Montealegre-M, M., 2007. A complementary conventional analysis for channelized reservoirs. *CTF - Cienc. Tecnol. Futuro* 3, 137–146.
- Escobar, F.H., Navarrete, J.M., Losada, H.D., 2004a. Evaluation of Pressure Derivative Algorithms for Well-Test Analysis. *Society of Petroleum Engineers*. <https://doi.org/10.2118/86936-MS>
- Escobar, F.H., Rojas, M.M., Bonilla, L.F., 2012b. Transient-rate analysis for long homogeneous and naturally fractured reservoir by the TDS technique. *J. Eng. Appl. Sci.* 7, 353–370.
- Escobar, F.H., Saavedra, N., Escorcía, G., Polania, J., 2004b. Pressure and Pressure Derivative Analysis without Type-Curve Matching for Triple Porosity Reservoirs. *Society of Petroleum Engineers*. <https://doi.org/10.2118/88556-MS>
- Escobar, F.H., Saavedra, N., Hernandez, C., Hernandez, Y., Pilataxi, J., Pinto, D., 2004c. Pressure and Pressure Derivative Analysis for Linear Homogeneous Reservoirs Without Using Type-Curve Matching. *Society of Petroleum Engineers*. <https://doi.org/10.2118/88874-MS>
- Faulkner, D.R., Jackson, C.A.L., Lunn, R.J., Schlische, R.W., Shipton, Z.K., Wibberley, C.A.J., Withjack, M.O., 2010. A review of recent developments concerning the structure, mechanics

- and fluid flow properties of fault zones. *J. Struct. Geol., Fault Zones* 32, 1557–1575. <https://doi.org/10.1016/j.jsg.2010.06.009>
- Fenske, P.R., 1984. Unsteady drawdown in the presence of a linear discontinuity, in: Rosenshein, J.S., Bennett, G.D. (Eds.), *Water Resources Monograph*. American Geophysical Union, Washington, D. C., pp. 125–145.
- Ferroud, A., Chesnaux, R., Rafini, S., 2018. Insights on pumping well interpretation from flow dimension analysis: The learnings of a multi-context field database. *J. Hydrol.* 556, 449–474. <https://doi.org/10.1016/j.jhydrol.2017.10.008>
- Ferroud, A., Chesnaux, R., Rafini, S., 2016. Numerical investigations of the spherical flow regimes induced by constant-rate pumping tests, in: 43rd IAH Congress, September 25-29, 2016 Montpellier, France.
- Figueiredo, B., Tsang, C.-F., Niemi, A., Lindgren, G., 2016. Review: The state-of-art of sparse channel models and their applicability to performance assessment of radioactive waste repositories in fractured crystalline formations. *Hydrogeol. J.* 1–16. <https://doi.org/10.1007/s10040-016-1415-x>
- Gringarten, A., 2010. Practical use of well-test deconvolution, in: *Society of Petroleum Engineers Paper No. 134534*, SPE Annual Technical Conference and Exhibition, 19-22 September, Florence, Italy. <https://doi.org/10.2118/134534-MS>
- Gringarten, A., 2008. From Straight Lines to Deconvolution: The Evolution of the State of the Art in Well Test Analysis. *SPE Reserv. Eval. Eng.* 11. <https://doi.org/10.2118/102079-PA>
- Gringarten, A., 1987a. Type-Curve Analysis: What It Can and Cannot Do. *J. Pet. Technol.* 39, 11–13. <https://doi.org/10.2118/16388-PA>
- Gringarten, A., 1987b. How To Recognize “Double-Porosity” Systems From Well Tests. *J. Pet. Technol.* 39, 631–633. <https://doi.org/10.2118/16437-PA>
- Gringarten, A., 1985. Interpretation of transient well test data, in: Dawe, R.A., Wilson, D.C. (Eds.), *Developments in Petroleum Engineering-1*. Elsevier Applied Science Publishers, London and New York, pp. 133–196.
- Gringarten, A., Ramey, H.J., 1975. An Approximate Infinite Conductivity Solution for a Partially Penetrating Line-Source Well. *Soc. Pet. Eng. J.* 15, 140–148. <https://doi.org/10.2118/4733-PA>
- Gringarten, A., Ramey, H.J., Raghavan, R., 1974. Unsteady-State Pressure Distributions Created by a Well With a Single Infinite-Conductivity Vertical Fracture. *Soc. Pet. Eng. J.* 14, 347–360. <https://doi.org/10.2118/4051-PA>
- Hammond, P.A., Field, M.S., 2014. A reinterpretation of historic aquifer tests of two hydraulically fractured wells by application of inverse analysis, derivative analysis, and diagnostic plots. *J. Water Resour. Prot.* 06, 481–506. <https://doi.org/10.4236/jwarp.2014.65048>
- Hantush, M.S., 1962. Flow of ground water in sands of nonuniform thickness: 3. Flow to wells. *J. Geophys. Res.* 67, 1527–1534. <https://doi.org/10.1029/JZ067i004p01527>

- Hantush, M.S., 1960. Modification of the theory of leaky aquifers. *J. Geophys. Res.* 65, 3713–3725. <https://doi.org/10.1029/JZ065i011p03713>
- Hantush, M.S., Jacob, C.E., 1955. Non-steady radial flow in an infinite leaky aquifer. *Eos Trans. Am. Geophys. Union* 36, 95–100. <https://doi.org/10.1029/TR036i001p00095>
- Hardacre, K., Cowie, P., 2003. Variability in fault size scaling due to rock strength heterogeneity: a finite element investigation. *J. Struct. Geol.* 25, 1735–1750. [https://doi.org/10.1016/S0191-8141\(02\)00205-5](https://doi.org/10.1016/S0191-8141(02)00205-5)
- Horne, R.N., 1995. *Modern well test analysis: a computer-aided approach*. Petroway.
- Horne, R.N., Temeng, K.O., 1982. Recognition and Location of Pinchout Boundaries by Pressure Transient Analysis. *J. Pet. Technol.* 34, 517–519. <https://doi.org/10.2118/9905-PA>
- Hosseinpour-Zonoozi, N., 2006. Development of the β -pressure derivative (MSc.). Texas A&M University, Texas, USA.
- Idorenyin, E., Okouma Mangha, V., Mattar, L., 2011. Analysis of Production Data Using the Beta-Derivative. Society of Petroleum Engineers. <https://doi.org/10.2118/149361-MS>
- Ilk, D., Hosseinpor-Zonoozi, N., Amini, S., Blasingame, T.A., 2007. Application of the Beta-Integral Derivative Function to Production Analysis, in: SPE 107967, 2007 SPE Rocky Mountain Oil and Gas Technology Symposium, Denver, Colorado, USA.
- Issaka, M., Ambastha, A., 1999. A Generalized Pressure Derivative Analysis For Composite Reservoirs. *J. Can. Pet. Technol.* <https://doi.org/10.2118/99-13-57>
- Jourde, Herve, Flodin, E.A., Aydin, A., Durlafsky, L.J., Wen, X.-H., 2002. Computing permeability of fault zones in eolian sandstone from outcrop measurements. *AAPG Bull.* 86.
- Jourde, H., Pistre, S., Perrochet, P., Drogue, C., 2002. Origin of fractional flow dimension to a partially penetrating well in stratified fractured reservoirs. New results based on the study of synthetic fracture networks. *Adv. Water Resour.* 25, 371–387. [https://doi.org/10.1016/S0309-1708\(02\)00010-6](https://doi.org/10.1016/S0309-1708(02)00010-6)
- Karasaki, K., Long, J.C.S., Witherspoon, P.A., 1988. Analytical models of slug tests. *Water Resour. Res.* 24, 115–126. <https://doi.org/10.1029/WR024i001p00115>
- Kazemi, H., 1969. Pressure Transient Analysis of Naturally Fractured Reservoirs with Uniform Fracture Distribution. *Soc. Pet. Eng. J.* 9, 451–462. <https://doi.org/10.2118/2156-A>
- Knipe, R.J., Jones, G., Fisher, Q.J., 1998. Faulting, fault sealing and fluid flow in hydrocarbon reservoirs: an introduction, in: Jones, G., Fisher, Q.J., Knipe, R.J. (Eds.), *Faulting, Fault Sealing and Fluid Flow in Hydrocarbon Reservoirs*, Special Publications. London, pp. vii–xxi.
- Kruseman, G.P., de Ridder, N.A., 1994. *Analysis and evaluation of pumping test data*, 2. ed. (compl. rev.), repr. ed, ILRI publication. International Institute for Land Reclamation and Improvement, Wageningen.
- Kuchuk, F.J., 1990. Applications of Convolution and Deconvolution to Transient Well Tests. *SPE Form. Eval.* 5, 375–384. <https://doi.org/10.2118/16394-PA>

- Kuchuk, F.J., Ayestaran, L., 1985. Analysis of Simultaneously Measured Pressure and Sandface Flow Rate in Transient Well Testing (includes associated papers 13937 and 14693). J. Pet. Technol. 37, 323–334. <https://doi.org/10.2118/12177-PA>
- Kuchuk, F.J., Biryukov, D., 2015. Pressure-Transient Tests and Flow Regimes in Fractured Reservoirs. SPE Reserv. Eval. Eng. 18, 187–204. <https://doi.org/10.2118/166296-PA>
- Kuchuk, F.J., Biryukov, D., 2014. Pressure-Transient Behavior of Continuously and Discretely Fractured Reservoirs. SPE Reserv. Eval. Eng. 17, 82–97. <https://doi.org/10.2118/158096-PA>
- Kuchuk, F.J., Biryukov, D., 2013. Pressure transient tests and flow regimes in fractured reservoirs. Presented at the SPE Annual Technical Conference and Exhibition, Society of Petroleum Engineers, New Orleans, Louisiana, USA. <https://doi.org/10.2118/166296-MS>
- Kuchuk, F.J., Biryukov, D., 2012. Transient Pressure Test Interpretation from Continuously and Discretely Fractured Reservoirs. Society of Petroleum Engineers. <https://doi.org/10.2118/158096-MS>
- Kuchuk, F.J., Onur, M., Hollaender, F., 2010. Pressure Transient Formation and Well Testing: Convolution, Deconvolution and Nonlinear Estimation. Elsevier.
- Kuusela-Lahtinen, A., Niemi, A., Luukkonen, A., 2003. Flow dimension as an indicator of hydraulic behavior in site characterization of fractured rock. Ground Water 41, 333–341. <https://doi.org/10.1111/j.1745-6584.2003.tb02602.x>
- Le Borgne, T., Bour, O., de Dreuzy, J.R., Davy, P., Touchard, F., 2004. Equivalent mean flow models for fractured aquifers: Insights from a pumping tests scaling interpretation. Water Resour. Res. 40, W03512. <https://doi.org/10.1029/2003WR002436>
- Lee, S.-T., Brockenbrough, J.R., 1986. A New Approximate Analytic Solution for Finite-Conductivity Vertical Fractures. SPE Form. Eval. 1, 75–88. <https://doi.org/10.2118/12013-PA>
- Leveinen, J., 2001. Conceptual and analytical modeling of fracture zone aquifers in hard rock - Implications of pumping tests in the Pohjukansalo well field, east-central Finland (No. YST-105). Geological Survey of Finland, Nuclear Waste Disposal Research.
- Leveinen, J., 2000. Composite model with fractional flow dimensions for well test analysis in fractured rocks. J. Hydrol. 234, 116–141. [https://doi.org/10.1016/S0022-1694\(00\)00254-7](https://doi.org/10.1016/S0022-1694(00)00254-7)
- Leveinen, J., Rönkä, E., Tikkanen, J., Karro, E., 1998. Fractional flow dimensions and hydraulic properties of a fracture-zone aquifer, Leppavirta, Finland. Hydrogeol. J. 6, 327–340. <https://doi.org/10.1007/s100400050156>
- Liang, H., Lin, S., Huang, T., Chen, D., Tom Kuo, M., 2012. Identifying the flow dimension in fractured rock using an interference test. J. Pet. Gas Eng. 3, 114–123.
- Lods, G., Gouze, P., 2004. WTFM, Software for Well Test Analysis in Fractured Media Combining Fractional Flow with Double Porosity and Leakance Approaches. Comput Geosci 30, 937–947. <https://doi.org/10.1016/j.cageo.2004.06.003>

- Maréchal, J.C., Dewandel, B., Subrahmanyam, K., 2004. Use of hydraulic tests at different scales to characterize fracture network properties in the weathered-fractured layer of a hard rock aquifer. *Water Resour. Res.* 40, W11508. <https://doi.org/10.1029/2004WR003137>
- Massonnat, G.J., Bandiziol, D., 1991. Interdependence Between Geology and Well Test Interpretation. Society of Petroleum Engineers. <https://doi.org/10.2118/22740-MS>
- Massonnat, G.J., Norris, R.J., Chalmette, J.-C., 1993. Well test interpretation in geologically complex channelized reservoirs. Presented at the SPE Annual Technical Conference and Exhibition, Society of Petroleum Engineers, Houston, Texas, USA. <https://doi.org/10.2118/26464-MS>
- Mattar, L., 1999. Derivative analysis without type curves. *J. Can. Pet. Technol.* 38. <https://doi.org/10.2118/99-13-63>
- Mattar, L., 1997. Derivative Analysis Without Type Curves. Society of Petroleum Engineers. <https://doi.org/10.2118/97-51>
- Mattar, L., Zaoral, K., 1992. The primary pressure derivative (PPD) a new diagnostic tool in well test interpretation. *J. Can. Pet. Technol.* 31. <https://doi.org/10.2118/92-04-06>
- Meier, P.M., Carrera, J., Sánchez-Vila, X., 1998. An evaluation of Jacob's Method for the interpretation of pumping tests in heterogeneous formations. *Water Resour. Res.* 34, 1011–1025. <https://doi.org/10.1029/98WR00008>
- Micarelli, L., Benedicto, A., Wibberley, C.A.J., 2006. Structural evolution and permeability of normal fault zones in highly porous carbonate rocks. *J. Struct. Geol.* 28, 1214–1227. <https://doi.org/10.1016/j.jsg.2006.03.036>
- Mijinyawa, A., Gringarten, A., 2008. Influence of Geological Features on Well Test Behavior. Society of Petroleum Engineers. <https://doi.org/10.2118/113877-MS>
- Miller, F.G., 1962. Theory of Unsteady-State Influx of Water in Linear Reservoirs. *J Inst Pet* 48, 365–379.
- Moench, A.F., 1984. Double-porosity models for a fissured groundwater reservoir with fracture skin. *Water Resour. Res.* 20, 831–846. <https://doi.org/10.1029/WR020i007p00831>
- Moncada, K., Tiab, D., Escobar, F.H., Montealegre, M., Chacon, A., Zamora, R., Nese, S.-L., 2005. Determination of vertical and horizontal permeabilities for vertical oil and gas wells with partial completion and partial penetration using pressure and pressure derivative plots without type-curve matching. *CTF - Cienc. Tecnol. Futuro* 3, 77–94.
- National Research Council Staff, 1996. *Rock Fractures and Fluid Flow: Contemporary Understanding and Applications*. National Acad. Press, Washington, DC.
- Nicol, A., Walsh, J.J., Watterson, J., Gillespie, P.A., 1996. Fault size distributions — are they really power-law? *J. Struct. Geol.* 18, 191–197. [https://doi.org/10.1016/S0191-8141\(96\)80044-7](https://doi.org/10.1016/S0191-8141(96)80044-7)
- Nobakht, M., Mattar, L., 2009. Diagnostics of data quality for analysis of production data, in: Society of Petroleum Engineers Paper No. 2009-137, Canadian International Petroleum Conference, 16-18 June, Calgary, Alberta, USA. <https://doi.org/10.2118/2009-137>

- Nutakki, R., Mattar, L., 1982. Pressure Transient Analysis of Wells in Very Long Narrow Reservoirs. Presented at the SPE Annual Technical Conference and Exhibition, Society of Petroleum Engineers. <https://doi.org/10.2118/11221-MS>
- Obeahon, P.P., Sedgwick, A., Okereke, O., 2014. Practical application of multi rate deconvolution, in: Society of Petroleum Engineers Paper No. 172446, SPE Nigeria Annual International Conference and Exhibition, 5-7 August, Lagos, Nigeria. <https://doi.org/10.2118/172446-MS>
- Odling, N.E., West, L.J., Hartmann, S., Kilpatrick, A., 2013. Fractional flow in fractured chalk; a flow and tracer test revisited. *J. Contam. Hydrol.* 147, 96–111. <https://doi.org/10.1016/j.jconhyd.2013.02.003>
- Olariu, C., Bhattacharya, J.P., 2006. Terminal Distributary Channels and Delta Front Architecture of River-Dominated Delta Systems. *J. Sediment. Res.* 76, 212–233. <https://doi.org/10.2110/jsr.2006.026>
- Onur, M., Cinar, M., Aksoy, N., Serpen, U., Satman, A., 2007. Analysis of well tests in Afyon Ömer-Gecek geothermal field, Turkey, in: Proceedings, Thirty-Second Workshop on Geothermal Reservoir Engineering Stanford University. Stanford, California.
- Onur, M., Hegeman, P.S., Kuchuk, F.J., 2004. Pressure/Pressure Convolution Analysis of Multiprobe and Packer-Probe Wireline Formation Tester Data. *SPE Reserv. Eval. Eng.* 7, 351–364. <https://doi.org/10.2118/88994-PA>
- Onur, M., Kuchuk, F.J., 2012. A New Deconvolution Technique Based on Pressure-Derivative Data for Pressure-Transient-Test Interpretation. *SPE J.* 17. <https://doi.org/10.2118/134315-PA>
- Paillet, F.L., 1998. Flow modeling and permeability estimation using borehole flow logs in heterogeneous fractured formations. *Water Resour. Res.* 34, 997–1010. <https://doi.org/10.1029/98WR00268>
- Paillet, F.L., Hess, A.E., Cheng, C.H., Hardin, E., 1987. Characterization of Fracture Permeability with High-Resolution Vertical Flow Measurements During Borehole Pumping. *Groundwater* 25, 28–40. <https://doi.org/10.1111/j.1745-6584.1987.tb02113.x>
- Pimonov, E., Ayan, C., Onur, M., Kuchuk, F.J., 2010. A New Pressure/Rate-Deconvolution Algorithm To Analyze Wireline Formation-Tester and Well-Test Data. *SPE Reserv. Eval. Eng.* 13, 603–613. <https://doi.org/10.2118/123982-PA>
- Posamentier, H.W., Kolla, V., 2003. Seismic Geomorphology and Stratigraphy of Depositional Elements in Deep-Water Settings. *J. Sediment. Res.* 73, 367–388. <https://doi.org/10.1306/111302730367>
- Pyrack-Nolte, L.J., Myer, L.R., Cook, N.G.W., Witherspoon, P.A., 1987. Hydraulic and mechanical properties of natural fractures in low permeability rocks (No. LBL-22118). University of California, Lawrence Berkeley Laboratory, Earth Sciences Division, Berkeley, California 94120.
- Rafini, S., 2008. Comportement hydraulique des milieux faillés [The hydraulic behaviour of faulted environments]. (PhD). Université du Québec à Montréal, Montréal.

- Rafini, S., Chesnaux, R., Dal Soglio, L., 2014. A numerical analysis to illustrate the usefulness of drawdown log-derivative diagnostic plots in characterizing the heterogeneity of non-Theis aquifers, in: 2014 GSA Annual Meeting, October 19-22, 2014 Vancouver, British Columbia, Canada.
- Rafini, S., Chesnaux, R., Ferroud, A., 2017. A numerical investigation of pumping-test responses from contiguous aquifers. *Hydrogeol. J.* 3, 877–894. <https://doi.org/10.1007/s10040-017-1560-x>
- Rafini, S., Larocque, M., 2012. Numerical modeling of the hydraulic signatures of horizontal and inclined faults. *Hydrogeol. J.* 20, 337–350. <https://doi.org/10.1007/s10040-011-0812-4>
- Rafini, S., Larocque, M., 2009. Insights from numerical modeling on the hydrodynamics of non-radial flow in faulted media. *Adv. Water Resour.* 32, 1170–1179. <https://doi.org/10.1016/j.advwatres.2009.03.009>
- Ramos, G., Carrera, J., Gómez, S., Minutti, C., Camacho, R., 2017. A stable computation of log-derivatives from noisy drawdown data: COMPUTATION OF NOISY LOG-DERIVATIVES. *Water Resour. Res.* 53, 7904–7916. <https://doi.org/10.1002/2017WR020811>
- Raven, K.G., Gale, J.E., 1985. Water flow in a natural rock fracture as a function of stress and sample size. *Int. J. Rock Mech. Min. Sci. Geomech. Abstr.* 22, 251–261. [https://doi.org/10.1016/0148-9062\(85\)92952-3](https://doi.org/10.1016/0148-9062(85)92952-3)
- Razminia, K., Razminia, A., Dastkhan, Z., 2016. A Comprehensive Solution for Partially Penetrating Wells with Various Reservoir Structures. *J. Oil Gas Petrochem. Technol.* 3, 43–58.
- Renard, P., 2005. The future of hydraulic tests. *Hydrogeol. J.* 13, 259–262. <https://doi.org/10.1007/s10040-004-0406-5>
- Renard, P., Glenz, D., Mejias, M., 2009. Understanding diagnostic plots for well-test interpretation. *Hydrogeol. J.* 17, 589–600. <https://doi.org/10.1007/s10040-008-0392-0>
- Rouboutsos, A., Stewart, G., 1988. A Direct Deconvolution or Convolution Algorithm for Well Test Analysis. Society of Petroleum Engineers. <https://doi.org/10.2118/18157-MS>
- Samani, N., Pasandi, M., Barry, D., 2006. Characterizing a heterogeneous aquifer by derivative analysis of pumping and recovery test data. *J. Geol. Soc. Iran* 1, 29–41.
- Sánchez-Vila, X., Meier, P.M., Carrera, J., 1999. Pumping tests in heterogeneous aquifers: An analytical study of what can be obtained from their interpretation using Jacob's Method. *Water Resour. Res.* 35, 943–952. <https://doi.org/10.1029/1999WR900007>
- Shahamat, M.S., Mattar, L., Aguilera, R., 2015. Analysis of Decline Curves on the Basis of Beta-Derivative. *SPE Reserv. Eval. Eng.* 18, 214–227. <https://doi.org/10.2118/169570-PA>
- Spane, F., Wurstner, S., 1993. DERIV: A computer Program for Calculating Pressure Derivatives for Use in Hydraulic Test Analysis. *Ground Water* 31.
- Spane, F.A., Jr., 1993. Selected hydraulic test analysis techniques for constant-rate discharge tests (No. PNL-8539). Pacific Northwest Laboratory, Richland, Washington, USA.

- Stewart, G., Wittmann, M.J., Meunier, D., 1983. Afterflow Measurement and Deconvolution in Well Test Analysis. Presented at the SPE Annual Technical Conference and Exhibition, San Francisco, CA. October 5-8, 1983, Society of Petroleum Engineers. <https://doi.org/10.2118/12174-MS>
- Sui, W., Mou, J., Bi, L., Deng, J., Ehlig-Economides, C.A., 2007. New Flow Regimes for Well Near Constant Pressure Boundary. Society of Petroleum Engineers. <https://doi.org/10.2118/106922-MS>
- Sun, X., Xu, Y., Lin, L., 2015. The diagnostic plot analysis of artesian aquifers with case studies in Table Mountain Group of South Africa. *Hydrogeol. J.* 23, 567–579. <https://doi.org/10.1007/s10040-014-1203-4>
- Theis, C.V., 1935. The relation between the lowering of the piezometric surface and the rate and duration of discharge of a well using ground-water storage. *Trans. Am. Geophys. Union* 16, 519–524. <https://doi.org/10.1029/TR016i002p00519>
- Tiab, D., 2005. Analysis of pressure derivative data of hydraulically fractured wells by the Tiab's Direct Synthesis technique. *J. Pet. Sci. Eng.* 49, 1–21. <https://doi.org/10.1016/j.petrol.2005.07.001>
- Tiab, D., 1995. Analysis of pressure and pressure derivative without type-curve matching — Skin and wellbore storage. *J. Pet. Sci. Eng.* 12, 171–181. [https://doi.org/10.1016/0920-4105\(94\)00040-B](https://doi.org/10.1016/0920-4105(94)00040-B)
- Tiab, D., 1994. Analysis of pressure and pressure derivative without type-curve matching: Vertically fractured wells in closed systems. *J. Pet. Sci. Eng.* 11, 323–333. [https://doi.org/10.1016/0920-4105\(94\)90050-7](https://doi.org/10.1016/0920-4105(94)90050-7)
- Tiab, D., 1993a. Analysis of pressure and pressure derivatives without type-curve matching - I. Skin and Wellbore Storage. Society of Petroleum Engineers. <https://doi.org/10.2118/25426-MS>
- Tiab, D., 1993b. Analysis of pressure and pressure derivative without type-curve matching - III. Vertically fractured wells in closed systems. Presented at the SPE Western Regional Meeting, Society of Petroleum Engineers, Anchorage, Alaska, USA. <https://doi.org/10.2118/26138-MS>
- Tiab, D., 1993c. Analysis of pressure and pressure derivatives without type curve matching - IV. Flow and no-flow boundaries. to be submitted for presentation at the SPE Eastern Regional Meeting, Pittsburgh.
- Tiab, D., 1993d. Analysis of pressure and pressure derivatives without type-curve matching - V. Naturally Fractured Reservoirs. to be submitted for presentation at the SPE Eastern Regional Meeting, Pittsburgh.
- Tiab, D., 1989. Direct Type-Curve Synthesis of Pressure Transient Tests. Society of Petroleum Engineers. <https://doi.org/10.2118/18992-MS>
- Tiab, D., Kumar, A., 1980a. Application of the p'D Function to Interference Analysis. *J. Pet. Technol.* 32, 1,465-1,470. <https://doi.org/10.2118/6053-PA>

- Tiab, D., Kumar, A., 1980b. Detection and location of two parallel sealing faults around a well. *JPT J. Pet. Technol.* 32, 1701–1708.
- Valdes-Perez, A.R., Pulido, H., Cinco-Ley, H., Galicia-Muñoz, G., 2011. A new bilinear flow model for naturally fractured reservoirs with transient interporosity transfer, in: *PROCEEDINGS, Thirty-Sixth Workshop on Geothermal Reservoir Engineering Stanford University, Stanford, California, January 31 - February 2, 2011, SGP-TR-191.*
- van Poolen, H.K., 1965. Drawdown Curve give angle between intersecting faults. *Oil Gas J.*
- Verbovšek, T., 2011. Hydrogeology and Geochemistry of Fractured Dolomites—A case study of Slovenia, in: *Aquifers: Formation, Transport, and Pollution.* Nova Science Publishers, Hauppauge, N.Y., pp. 87–147.
- Verbovšek, T., 2009. Influences of Aquifer Properties on Flow Dimensions in Dolomites. *Ground Water* 47, 660–668. <https://doi.org/10.1111/j.1745-6584.2009.00577.x>
- Verweij, J.M., 1995. Analysis of pumping test data from hard rock aquifers (TNO report No. GG R-95-39(A)), Institute of Applied Geoscience, The Netherlands.
- von Schroeter, T., Hollaender, F., Gringarten, A., 2001. Deconvolution of well test data as a nonlinear total least squares problem, in: *Society of Petroleum Engineers Paper No. 71574, SPE Annual Technical Conference and Exhibition, 30 September-3 October, 2001, New Orleans, Louisiana, USA.* <https://doi.org/10.2118/71574-MS>
- Walker, D.D., Cello, P.A., Valocchi, A.J., Loftis, B., 2006. Flow dimensions corresponding to stochastic models of heterogeneous transmissivity. *Geophys. Res. Lett.* 33, L07407. <https://doi.org/10.1029/2006GL025695>
- Walker, D.D., Roberts, R.M., 2003. Flow dimensions corresponding to hydrogeologic conditions. *Water Resour. Res.* 39, 1349.
- Wang, F., 2010. Processing and Analysis of Transient Pressure from Permanent Down-hole Gauges (Ph.D.). Institute of Petroleum Engineering, Heriot-Watt University, Edinburgh, United Kingdom.
- Warren, J.E., Root, P.J., 1963. The behavior of naturally fractured reservoirs. *Soc. Pet. Eng. J.* 3, 245–255. <https://doi.org/10.2118/426-PA>
- Witherspoon, P.A., Wang, J.S.Y., Iwai, K., Gale, J.E., 1980. Validity of Cubic Law for fluid flow in a deformable rock fracture. *Water Resour. Res.* 16, 1016–1024. <https://doi.org/10.1029/WR016i006p01016>
- Xiao, L., Xu, Y., 2014. Diagnostic Analysis of Pumping Tests Using Derivative of $dlgs/dlgt$ with Case Study. *Groundwater* n/a-n/a. <https://doi.org/10.1111/gwat.12175>
- Yildiz, T., Bassiouni, Z., 1990. Transient Pressure Analysis in Partially-Penetrating Wells. *Petroleum Society of Canada.* <https://doi.org/10.2118/90-02>

CHAPITRE 3

L'étude proposée dans ce chapitre 3 est présentée sous forme d'article. Elle vise à améliorer la compréhension du sens physique de la dimension d'écoulement n à partir d'une approche de terrain. Ce travail a permis d'établir un portrait de l'occurrence de la dimension d'écoulement dans divers contextes géologiques, tels que des socles rocheux granitique et carbonatés (faillé et/ou fracturés), des arènes granitiques et des dépôts fluvio-glaciaires. Les résultats montrent entre autres, une grande diversité des valeurs de n et des relations statistiques entre des valeurs de n et des contextes géologiques. Nous remercions spécialement Dr. Tomas Doe, pour sa relecture de fond ainsi que ses commentaires pertinents qui ont permis l'aboutissement de cet article.

**INSIGHTS ON PUMPING WELL INTERPRETATION FROM FLOW
DIMENSION ANALYSIS: THE LEARNINGS OF A MULTI-CONTEXT FIELD
DATABASE**

Anouck Ferroud*, Romain Chesnaux and Silvain Rafini

Research Group R2Eau, Centre d'études sur les ressources minérales, Université du Québec à Chicoutimi, 555, boulevard de l'Université, Chicoutimi (Québec), Canada G7H 2B1

Ferroud, A., Chesnaux, R., et Rafini, S. 2018. Insights on pumping well interpretation from flow dimension analysis: The learnings of a multi-context field database [en ligne]. *Journal of Hydrology*, **556** : 449–474. doi: 10.1016/j.jhydrol.2017.10.008.

3.1 ABSTRACT

The flow dimension parameter n , derived from the Generalized Radial Flow model, is a valuable tool to investigate the actual flow regimes that really occur during a pumping test rather than suppose them to be radial, as postulated by the Theis-derived models. A numerical approach has shown that, when the flow dimension is not radial, using the derivative analysis rather than the conventional Theis and Cooper-Jacob methods helps to estimate much more accurately the hydraulic conductivity of the aquifer. Although n has been analysed in numerous studies including field-based studies, there is a striking lack of knowledge about its occurrence in nature and how it may be related to the hydrogeological setting. This study provides an overview of the occurrence of n in natural aquifers located in various geological contexts including crystalline rock, carbonate rock and granular aquifers. A comprehensive database is compiled from governmental and industrial sources, based on 69 constant-rate pumping tests. By means of a sequential analysis approach, we systematically performed a flow dimension analysis in which straight segments on drawdown-log derivative time series are interpreted as successive, specific and independent flow regimes. To reduce the uncertainties inherent in the identification of n sequences, we used the proprietary SIREN code to execute a dual simultaneous fit on both the drawdown and the drawdown-log derivative signals. Using the stated database, we investigate the frequency with which the radial and non-radial flow regimes occur in fractured rock and granular aquifers, and also provides outcomes that indicate the lack of applicability of Theis-derived models in representing nature. The results also emphasize the complexity of

hydraulic signatures observed in nature by pointing out n sequential signals and non-integer n values that are frequently observed in the database.

Keywords: Diagnostic plot; drawdown log-derivative signal; flow dimension; Theis-derived models; complex aquifers; field data.

3.2 INTRODUCTION

The discrepancy between the complexity of real flow behavior and the simplicity of analytical flow models makes the interpretation of transient well tests an ambiguous and imprecise task. Hydrogeology practitioners routinely interpret constant-rate pumping tests by matching theoretical type-curves obtained from Theis-derived models, thus ignoring the real flow regime that occurs during the test and neglecting the idealized Theis assumptions that suppose a totally penetrating well, the homogeneity of the aquifer and the infinite acting radial flow. This matching procedure, or “fit”, requires the practitioner to make the implicit postulate that the flow regime is cylindrical-radial. The term “flow regime” refers here to the pressure behavior and does not relate to any laminar or turbulent flow regimes, as defined by the Reynold number. While cylindrical-radial flow is a common pumping test response, the careful examination of well test results from a variety of geologic environments reveals that other, non-cylindrical-radial flows are also common and that they may change over the course of a well test. Theis-derived models are only valid for cylindrical-radial flow. Their application to systems with non-cylindrical-radial behaviors may lead to a significant degree of error, leading to a poor understanding of the hydrodynamic behavior of the aquifer and

requiring a substantial degree of approximation when estimating the aquifer's hydraulic properties. As stated by Le Borgne et al. (2004), the estimation of the transmissivity T and the storage coefficient S depend directly on the flow dimension value as $T = b^{3-n}.K$ and $S = b^{3-n}.S_s$. This paper uses an extensive database of both fractured and non-fractured environments to show that non-cylindrical-radial flow regimes are widespread, and must be considered in the analysis of well test data.

One of the fundamental issues in hydrogeology is the capability of estimating aquifer's hydraulic parameters in a more representative and accurate manner. For instance, hydraulic conductivity (K) is an essential parameter used to characterize groundwater flow fields, predict contaminant transport (Carrera 1993, Rozemeijer et al. 2010, Barlow et Coupe 2012) and delineate wellhead protection areas (WHPA) (Bear et Jacobs 1965, Wyssling 1979, Todd 1980, Grubb 1993). It is essential to reduce the degree of uncertainty of K because this value controls the size, shape and location of wellhead capture zones (Bhatt 1993, Forster et al. 1997, Fadlelmawla et Dawoud 2006, Paradis et al. 2007, Barry et al. 2009).

In 1989 in the petroleum literature, Bourdet et al. proposed that in addition to plotting the pressure data p , practitioners and modellers should also plot the pressure derivative signal $dp/dlogt$. This is easily implemented in hydrogeology in the form of the drawdown log-derivative signal $ds/dlogt$ (Renard et al. 2009). Rather than using a simple drawdown signal s , the derivative approach makes the signal much more sensitive to small variations of drawdown. The diagnostic plots, representing the combined plots of both s and $ds/dlogt$ versus time, are thus used in particular to improve the interpretation of constant-rate pumping tests. Two different methods can be employed to interpret this derivative signal:

matching type curves over the entire signal or decomposing the signal into straight lines. In the first method, an analytical flow model is selected and its theoretical curve is matched to the derivative data. The match is generally performed using automatic best-fitting codes (Leveinen et al. 1998, Kuusela-Lahtinen et al. 2003, Verbovšek 2009). To select the analytical model that most suitably represents the real flow regime, $ds/d\log t$ is considered. The second method is a straight-line analysis that consists in decomposing the hydraulic signal into straight lines that are interpreted separately from each other in terms of their hydrodynamic behavior. Usually plotted on a log-log scale, the diagnostic plots make it possible to better take into consideration the heterogeneity of aquifers. Using this sequential approach of flow regimes, the hydraulic properties of the aquifer can be estimated according to the TDS (Tiab's Direct Synthesis) philosophy (Tiab 1994, 1995). This approach, chiefly used in the petroleum literature, establishes equations based on the intersections points and slopes of the $ds/d\log t$ straight lines to estimate the parameters of the well and of the aquifer that control the flow regime. Petroleum researchers developed equations for specific conceptual models established in view of determining parameters such as: permeability, skin factor, wellbore storage coefficient, hydraulic conductivity of fractures, half-fracture length and drainage area (Tiab 2005, Escobar et al. 2007, 2010, 2012b).

The flow dimension is a parameter proposed by Barker in 1988. It expresses the evolution of the shape of the pressure-front pulse as it diffuses through the aquifer during the transient stage of pumping. The flow dimension identifies, by a value $n = 2$, the occurrence of a cylindrical-radial flow regime during the pumping test, associated with a zero slope of $ds/d\log t$ when plotted on the log-log axis. The non-cylindrical-radial flow dimensions are

easily recognised when $ds/dlogt$ displays a rising straight line (positive slope) for $n < 2$, and a declining straight line (negative slope) for $n > 2$. The interpretation of pumping tests, supposing cylindrical-radial flow, is thus performed more accurately and swiftly by easily detecting when the Theis-derived assumptions are suitable. This better compliance with assumed and real flow geometries may reduce uncertainties in the determination of hydraulic properties. As stated by Black (1994), if the flow dimension is assumed to be 2 while in fact it is closer to 1, the hydraulic diffusivity will be underestimated. Furthermore, for the specific case of $n = 2$, K is directly estimated from the y-axis intercept of $ds/dlogt$ on log-log scales (Barker 1988). For cases where a vertical fault produces a bilinear flow regime ($n = 1.5$), Rafini and Larocque (2009, 2012) developed an equation that makes it possible to estimate K graphically, without type-curve matching. The most significant advantage of the flow dimension lies in the fact that it provides a relationship between the drawdown log-derivative signal and the flow regime occurring during the pumping test, for any hydrodynamic circumstance (cylindrical-radial and non-cylindrical -radial flow regimes). The $ds/dlogt$ approach significantly improves the transient test interpretation method because makes it possible to investigate the flow regimes detected by the transient test, instead of assuming them. Despite its diagnostic potential for interpreting transient well tests, the n parameter is still seldom used, due to the difficulty of relating the flow dimension values to conceptual aquifer conditions such as flow patterns and geological settings. So far, only a few values of n have been assigned a physical interpretation, and thus its diagnostic potential remains only partially exploited.

Advances in the conceptual understanding of n have been achieved through several numerical modelling studies. These studies concentrate on the influence exerted by various configurations or mechanisms on the $ds/d\log t$ signal. We may mention research works that have focused on: the geometry of the boundaries (Beauheim et Roberts 1998, Walker et Roberts 2003, Escobar et al. 2005, 2007), the wellbore effects (Jourde et al. 2002b, Escobar et al. 2012a), the properties of fractured rock (Jourde et al. 2002a, Cello et al. 2009) and the properties of faults (Abbaszadeh and Cinco-Ley, 1995; Cinco-Ley et al., 1978; Gringarten et al., 1974; Rafini and Larocque, 2012, 2009). These studies contributed to the evolution of the physical conceptualization of flow regimes. They proposed specific conceptual models to interpret the flow geometry, the configuration of the hydraulic properties and the boundary conditions of a specific flow regime sequence.

In the literature, the flow dimension parameter is sporadically used to characterise the hydraulic properties of aquifers (Leveinen et al. 1998, Liang et al. 2012). Only a few studies have described the frequency of occurrence of n in nature: one in dolomite (Verbovšek 2009, 2011), one in fractured limestone (Audouin et Bodin 2008), one in fractured crystalline rock (Kuusela-Lahtinen et al. 2003, Audouin et Bodin 2008) and one in weathered crystalline rock (Maréchal et al. 2004). Other studies have provided specific case study analyses: one in granitic and carbonate rocks (Bangoy et al. 1992), one in poorly-weathered crystalline rock (Leveinen 2000), sixteen in evaporite deposits (Beauheim et Roberts 2002) and five in fractured rock aquifers (Lods et Gouze 2004).

These studies showed that the majority of n values lie within a range of 1 to 3 and that the radial flow dimension is seldom observed (Table 3.4). The authors (Kuusela-Lahtinen et al.

2003, Audouin et Bodin 2008, Verbovšek 2009) each analyzed only one geological family. They limited themselves to correlating the distribution of n with the geology, but did not propose a hypothesis regarding the conceptual model or the geological facies that provide the water supply and control the flow regimes. Furthermore, the majority of the wells analyzed in these studies belong to the same aquifer. The observations and conclusions of these studies should be examined by comparing aquifers in various locations.

This article proposes to open novel perspectives as it examines the distribution of n in various geological environments in nature. We examine constant-rate pumping tests (lasting 3.1 days on average) performed in various aquifers composed of fluvio-glacial deposits, crystalline and carbonate rocks. This study has two main objectives: i) to survey the suitability of Theis and Theis-derived model assumptions for reproducing flow dimensional behaviors in natural aquifers, ii) to provide objective and comprehensive records of occurrences of natural flow dimension, with insights on the relationships between n and the features of various different aquifers. Over the last three decades, flow dimensions have been subjectively reported in the literature in the context of introductions of published articles describing specific interpretative models. The real distribution of flow dimension values in various types of natural media have remained undocumented, even though flow dimension undoubtedly constitutes a key and reliable indicator of the physical attributes of an aquifer. Comparing flow dimension distribution patterns against their associated geological frameworks will provide insights about their possible conceptual interpretation. This study is the first to attempt to perform a statistical analysis of the flow dimensions observed in nature, based on a sequential derivative analysis, and to provide an initial portrait of the flow

dimension distribution in both fractured rock aquifers and fluvio-glacial deposits. In an n -sequential analysis, the log-log plot of the drawdown log-derivative signal is considered a diagnostic tool. It is used to help interpret the flow geometry, the aquifer geometry and the heterogeneity of hydraulic properties, all there of which are detected as the pressure front pulse expands through the aquifer. We will firstly review the basic concepts of the GRF model, and then propose a reinterpretation of transient pumping tests conducted in wells. To this end we will use a database derived from 69 constant-rate pumping tests (lasting 3.1 days on average) conducted in the framework of consulting projects for municipal groundwater supplies in the Province of Quebec, Canada, in France and in Tunisia. A flow-dimension-sequence diagnostic approach is adopted for this reinterpretation of pumping tests, meaning that each slope of the drawdown log-derivative signal is interpreted as a specific and independent flow regime. Such analysis may be efficiently performed using the proprietary SIREN code, specifically designed to routinely interpret flow dimension sequences by simultaneously fitting drawdown and drawdown log-derivative data, respectively, on semi-log and log-log plots. This approach combines the advantages of both plots: the former is weakly influenced by pumping rate changes but grossly insensitive to flow regime, the latter is highly sensitive to flow regime changes but subject to strong noise effects due, for instance, to pumping rate instabilities. This study aims at contributing to our understanding of the physical interpretation of n through a statistical analysis of its natural occurrences in various geological media and by comparing the hydrodynamic interpretation of n against the conceptual models of the geology surrounding the wells. Finally, some ideas will be discussed regarding current practices in hydrogeology and the diagnostic potential of an approach which combines conventional plots, drawdown log-derivative plots and flow

dimension analysis. While an extensive review of interpretative models using log-derivative analysis is beyond the scope of this paper, existing flow regime sequences will be investigated in detail and compared to the theoretical and geological conceptual models.

3.3 THEORY AND PRACTICE

3.3.1 CONVENTIONAL ANALYSIS

The Theis model (1935) describes a transient cylindrical-radial flow, induced by a constant-rate pumping test within a confined, homogeneous, isotropic, horizontal-slab, totally screened and laterally infinite aquifer. In such conditions, also called Infinite Acting Radial Flow (IARF) conditions, the pressure front diffuses radially in the form of concentric circles (Figure 3.1). The pressure front pulse generates an equipotential cross-flow surface $A(r)$ which grows radially in the shape of a cylinder (Figure 3.1), producing the ideal cylindrical-radial flow conditions referred to as Theis aquifers. A distinction must be made between the Theis model and the concept of radial flow regime, which strictly describes the proportional relationship between the cross-flow surface A and the travelled distance r from the pumping well, regardless of the shape of this surface. Most analytical solutions published during the three last decades in the petroleum literature, and classically used in the diagnostic plot approach (Bourdet et al. 1983, Renard et al. 2009), account for some variations on the cylindrical-radial flow theme, including either its combination with some external sources (unconfined aquifers; leaky aquifers as described by Hantush (1956, 1960), some specific overlaying of several Theis aquifers (dual-porosity models; leaky aquifers as described by

Neuman et Witherspoon (1969). These models actually describe various types of radial flow regimes, which in itself does not signify that the flow geometry they are modelling remains ideally cylindrical-radial. In this study, these models will hereafter be referred to as Theis-derived models.

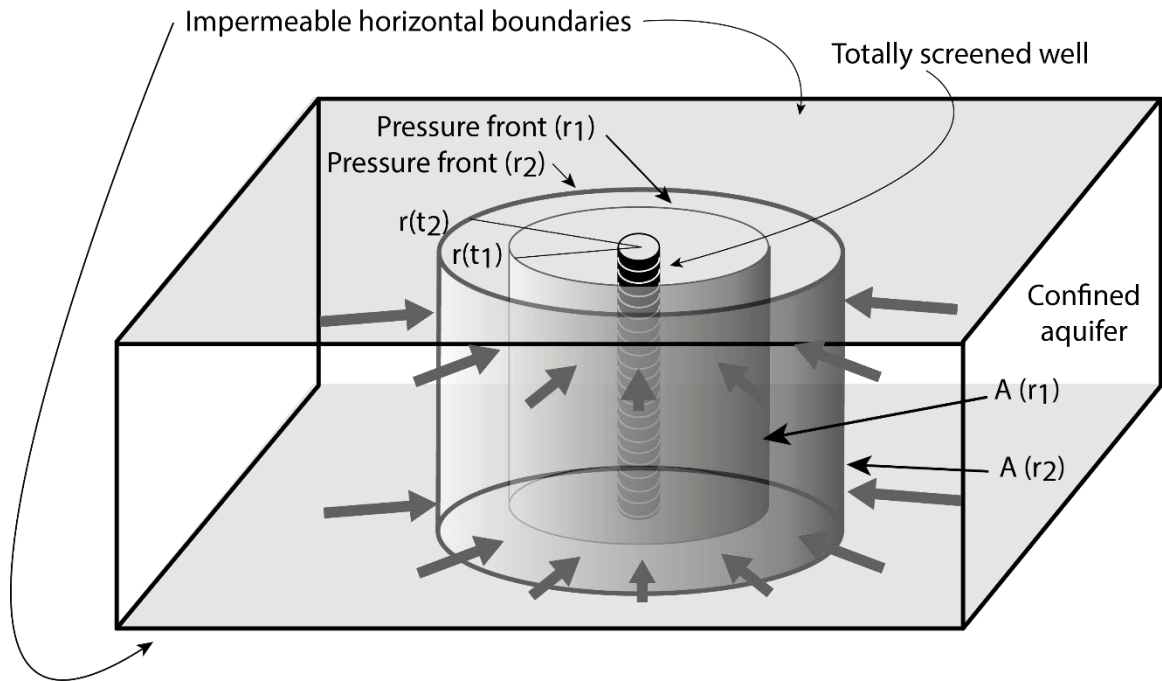


Figure 3.1: Conceptual Theis model (1935) representing its main assumptions. The thick arrows represent the flow induced by the pumping test. In these IARF conditions, the cross-flow area $A(r)$ extends radially in the form of cylinders and the pressure front pulse expands radially in the form of concentric circles having a radius $r(t)$. This flow behavior is called the cylindrical-radial flow regime.

In a system characterized by a diffuse short-scale field of heterogeneities, T and S may be averaged over the cross-flow area $A(r)$, making it possible to estimate the properties of the aquifer as being continuous and homogeneous. When the pressure front pulse reaches a large-scale heterogeneity within the aquifer, its shape may be deformed, leading to modifications in the equipotential surface growth pattern. The cylindrical-radial flow regime assumption can no longer be applied, rendering any Theis-derived model irrelevant.

Numerical modelling by Meier et al. (1998) and Sánchez-Vila et al. (1999) showed that for late-time drawdown and under cylindrical-radial flow conditions, the Cooper-Jacob approximation allows a good approximation of transmissivity but an erroneous estimation of storage coefficient in systems with a diffuse heterogeneity field and a radially convergent flow (Meier et al. 1998, Pechstein et al. 2016). These studies validated the applicability of the Cooper-Jacob model in specific heterogeneous domains with diffuse transmissivity fields and a concentric heterogeneous storage, conditions that allow the establishment of a cylindrical-radial flow regime. Meier et al. (1998) concluded their study by explaining that further numerical studies with three-dimensional flow conditions are needed to analyze flow behavior in aquifers with variable thicknesses. Cases of an increasing aquifer thickness (Dal Soglio 2012, Rafini et al. 2014) or a partially screened or a partially penetrated aquifer (Moncada et al. 2005, Escobar et al. 2012a, Ferroud et al. 2015a) have been numerically documented to produce spherical flow regimes. In these non-cylindrical-radial conditions, Theis-derived approaches are undoubtedly unsuitable.

3.3.2 THE GENERALIZED RADIAL FLOW MODEL

3.3.2.1 *Basic concepts*

The *Generalized Radial Flow (GRF)* model was proposed by Barker in 1988, in response to the inability of conventional models to reproduce the flow within the fractured aquifer of Stripa mine (Barker 1988). The concept of the GRF model is based on a proportional relationship between $A [L^2]$, the cross-flow area and r^{n-1} , the radial distance from the borehole of the pressure front pulse to the power of the flow dimension minus one (Equation (3.1)):

$$A(r) \sim r^{n-1} \quad (3.1)$$

The parameter n is a value “that must be determined empirically and which may not have an integer value” (Barker 2007). n reflects the rate by which the cross-flow area changes as a function of the distance from the well. As the pressure front pulse extends outwards and reaches heterogeneities within the aquifer, it may be deformed in such a manner that Equation (3.3) is modified, inducing changes in the flow dimension. The sequences of n thus reflect flow regime changes induced by some variations in the physical or hydraulic features in the aquifer. Short pumping tests, because they induce only a limited cross-flow area expansion in the aquifer, mainly reflect wellbore effects and a small proportion of the aquifer in the vicinity of the well. It is the long-term pumping tests that may more accurately reflect the aquifer signal *sensu stricto* and the influence of boundary conditions.

The term “flow regime” thus refers to the behavior of the pressure front pulse as it moves through the aquifer. It is worth noting that the sequential analysis we employ in this study is an extension of the GRF model, since Barker (1988) defined media with constant n values

assuming homogeneous conditions. By verifying the validity of Barker's equation (Equation (3.1)) in a non-uniform, faulted aquifer, Rafini and Larocque (2009, 2012) proved that n is a valuable tool for interpreting the successive flow regimes that occur during a medium- or long-term pumping test, even if the aquifer does not have GRF-like properties in accordance with Barker's postulates. Each value of n independently observed at different times during the pumping test represents the dominant flow regime felt at that time by the pressure front pulse as it diffuses throughout the aquifer around the well at a distance $r(t)$.

Using the *GRF* concept, Barker (1988) introduced the flow dimension n in the diffusivity equation. The generalized diffusivity equation is written as (Equation (3.2)):

$$\frac{K}{r^{n-1}} \frac{\partial}{\partial r} \left(r^{n-1} \frac{\partial h}{\partial r} \right) = S_s \frac{\partial h}{\partial t} \quad (3.2)$$

where K [LT^{-1}] is the hydraulic conductivity, r [L] is the radial distance from the borehole at time t [T], n is the flow dimension, S_s [L^{-1}] is the specific storage and h [L] is the hydraulic head.

Based on Equation (3.2), using the Laplace transform tables and supposing constant head boundaries, a zero initial head and a long time t or a short distance r , Barker predicts the hydraulic head distribution as (Equation (3.3)):

$$h(r, t) = \frac{Q}{4\pi^{1-v} K b^{3-n} \nu} \left[\left(\frac{4Kt}{S_s} \right)^v - \Gamma(1-v) r^{2v} \right] \quad \nu \neq 0 \quad (3.3)$$

$$v = 1 - \frac{n}{2} \quad (3.4)$$

With b the extent of the flow zone [L] and Γ the gamma function. Note Equation (3.3) is the asymptotic form of GRF's general solution (valid for u small enough with $u = S_s r^2 / 4Kt$), which is an incomplete gamma function.

Equation (3.3) can be rewritten with a time-dependent term Ct^v and time-independent term C' as:

$$h(t) = Ct^v + C' \quad (3.5)$$

with

$$C = \frac{Q}{4\pi^{1-v} K b^{3-nv}} \left(\frac{4K}{S_s} \right)^v \quad (3.6)$$

and

$$C' = \frac{-Q}{4\pi^{1-v} K b^{3-nv}} \Gamma(1-v) r^{2v} \quad (3.7)$$

Deriving Equation (3.5) with respect to time shows that the drawdown log-derivative $ds/d\log t$ time series (Equation (3.8)) displayed on a log-log plot forms a straight line with slope v , providing a mean of a straightforward graphic determination of the flow dimension using Equation (3.4).

$$\frac{ds}{d\log t} = \frac{t}{2.3} \frac{ds}{dt} = \frac{C}{2.3} vt^{\nu} \quad (3.8)$$

From a practical standpoint, when interpreting drawdown time series at the pumping well, the asymptotic condition is reached very early and can be considered valid during the whole aquifer-related response beyond the early influence of the wellbore effects. Note that in the petroleum literature, this asymptotic flow behavior is also named « infinite acting behavior ». According to Equations (3.4) and (3.8), the derivative signal depends on Q , K , S_s , b and n . Thus, any modification of these parameters will be felt by the derivative signal. Note that only changes of K and S_s will temporarily invalidate the asymptotic assumption of the derivative signal (Equation (3.3) is valid when u is small enough). Yet, straight derivative segments represent a sufficient proof of the validation of the asymptotic assumption. Before the pressure front pulse reaches the hydraulic boundaries, each straight-line segment is associated with a n value and represents a flow period during which Q , K , S_s and b are constant and/or uniform. As stated by Beauheim et al. (2004) and Rafini et al. (2017), we suggest that the flow dimension should be estimated from a constant straight line of $ds/d\log t$ that lasts at least one log-cycle.

We favor this graphic approach (Equation (3.8)) without type-curve matching because it allows us to decompose the signal in a sequence of successive flow regimes associated to specific geological facies and flow behaviors. Because n is directly determined from the $ds/d\log t$ straight line slopes, which implies that it can assume any integer and non-integer value, it is a valuable parameter for statistically analyzing the flow regimes of natural aquifers.

3.3.2.2 Conceptual interpretation of n

The main known flow dimensions (interpreted using Equation (3.1)) are briefly summarized in this section. For further details, the reader is invited to refer to the original papers.

$n = 0$ ($v = 1$)

Observed early in the pumping test, this unit slope line of the drawdown log-derivative refers to wellbore effects (skin and wellbore storage) (Tiab 1993c, Mattar 1997). Observed late in the pumping test, this flow regime may express the attainment of a stagnant state (“pseudo-steady-state flow” as described by Mattar, 1997), achieved when all the outer boundaries are no-flow boundaries, i.e., when the reservoir depressurizes without spatial diffusion of drawdown.

$n = 1$ ($v = 0.5$)

The linear flow implies that the cross-flow area remains constant as the pressure wave travels through the aquifer. Such conditions are observed in long and narrow systems which may be found: i) in granular channelized aquifers (fluvial and deep sea fans) (Escobar et al. 2004b, Escobar et Montealegre-M 2007, Escobar et al. 2010, Corbett et al. 2012); ii) in fractured media containing an infinite-conductivity vertical fault (Gringarten et Witherspoon 1972, Gringarten et al. 1974), iii) in fractured rocks with a finite-conductivity one-dimensional conduit formed by the intersection of fractures and iv) in karst systems (Maréchal et al.

2008). A linear flow can also be observed in a planar fracture with channeling or preferred flow paths (Tsang et Neretnieks 1998).

$n = 2 (v = 0)$

The radial flow regime is observed when the cross-flow area grows proportionally to the radial distance r . Such a condition can be produced by a cylindrical-radial flow regime. This flow regime is generally associated with a homogeneous and isotropic aquifer of uniform thickness, but other conceptual models may produce a radial flow dimension. Heterogeneous media may also produce a radial flow regime, such as a well located close to a vertical fault, when the matrix supply masks the signature of the fault (Cinco-Ley et al., 1978; Rafini and Larocque, 2009) or an orthogonal discontinuity network (Jourde et al., 1998).

$n = 3 (v = -0.5)$

The spherical flow regime is observed when the cross-flow area expands proportionally to r^2 . According to Equation (3.4), a spherical flow dimension is represented by a -0.5 negative slope of $ds/d\log t$ which reflects a drawdown rate deceleration that may be observed early in the pumping test, when the screen is very short relative to the aquifer. For instance, a spherical flow regime can be induced by a point source (between packers), by a partially penetrating well, by a partially completed well or by a restricted producing interval (Culham 1974, Moncada et al. 2005, Escobar et al. 2012a, Ferroud et al. 2015a).

$n = \text{non-integer}$

The fractional (non-integer) flow regimes, which are frequently exhibited by field data diagnostic plots, have long been interpreted as being related to the geometry of the source (Barker 1988) or to the fractal properties of the fractured media (Barker 1988, Polek, et al. 1989, Chang et Yortsos 1990, Bangoy et al. 1992, Acuna et Yortsos 1995). By analysing fractured systems that are generated from a fractal model using a Discrete Fracture Network, other authors (Geier et al. 1996, Winberg 2000, Cello et al. 2009) showed that there exists a relationship between the flow dimension parameter and the connectivity of fractures. Other authors (Billaux et Gentier 1990, Jourde et al. 1998) interpreted the fractional flow dimension to be related to the connectivity of fractures in an orthogonal fracture network in tabular stratified aquifers. In 1991, the interpretation of fractional flow dimensions was widened to involve new considerations. In fact, Doe (1991) opened the fractional flow dimension definition to non-fractal geometries which are not space-filling. In other words, Euclidian configurations, with heterogeneity either in conductivity or geometry or a combination of both, can produce non-integer values of n . Bowman et al. (2012) simulated the flow through high-transmissivity conduits characterized by non-radial and simple geometries. By means of the flow dimension concepts developed by Doe (1991), Bowman et al. (2012) showed that the variability of conduit shape can generate non-integer flow dimensions such as 0.8, 1.2 and 1.6. In addition, the bilinear flow regime ($n = 1.5$) has been reported to reflect the signal of a finite-conductive fault supplied by the matrix. Such a configuration has been demonstrated analytically by Abbaszadeh and Cinco-Ley (1995) and then corroborated numerically by Rafini and Larocque (2009). The karst systems are also

known to generate fractional flow dimension values that generally range between 0 and 1 (Maréchal et al. 2008, Giese et al. 2017). Finally, Walker and Roberts (2003) suggested that the flow dimension depends on the form of the nonstationary transmissivity (for instance, an aquifer presenting an exponential variation of thickness).

3.4 DATA AND METHOD

3.4.1 COMPILATION OF A PUMPING-WELL TEST DATABASE

A database mainly composed of 69 pumping-well tests (with a mean duration of 3.1 days ranging from 0.2 to 14.7 days) and of local geological information has been established (Table 3.1). Most of the compiled data come from pumping-well tests conducted in the framework of municipal groundwater supply investigations in the province of Quebec (Canada) regions of Charlevoix-Haute-Côte-Nord (CHCN), Saguenay-Lac-Saint-Jean (SLSJ) (Chesnaux et al. 2011) and Abitibi-Temiscamingue (ABTE) (Nadeau et al. 2015). Additional data were obtained from i) south-eastern Quebec (Mirabel) (Nastev et al. 2004); ii) various locations in France (regions of the Alps, Midi-Pyrénées, Nord-Pas-de-Calais and Loire); iii) the database *Banque de données du sous-sol* compiled by the *Bureau de Recherches Géologiques et Minières* (BRGM) and iv) in northern Tunisia.

3.4.2 DATA PRE-PROCESSING

Log-derivative data are typically very noisy; this may be due to datalogger or operator complications, pumping rate variations, random diffuse heterogeneity fields and tidal or recharge effects. We therefore smooth the data using the algorithm of Bourdet et al. (1989) which has proven to be one of the most efficient in filtering noise without deteriorating the hydraulic signature (Escobar et al. 2004a). The differentiation equation is:

$$\frac{ds_i}{dX_i} = \frac{\left(\frac{\Delta s_1}{\Delta X_1} \Delta X_2 + \frac{\Delta s_2}{\Delta X_2} \Delta X_1 \right)}{(\Delta X_1 + \Delta X_2)} \quad (3.9)$$

with: $\Delta s_1 = s_i - s_1$; $\Delta s_2 = s_i - s_2$; $\Delta X_1 = X_i - X_1$; $\Delta X_2 = X_i - X_2$ and $X = \log(t)$.

Equation (3.9) uses 3 points: the next and previous points (1 and 2) of point i which are the first to be separated by a minimum length of L . The length can thus be adjusted until the noise is attenuated and the signal is no longer distorted.

The drawing of straight lines is performed manually by considering the differentiation curves for various L values (Equation (3.9)). Furthermore, the simultaneous dual fits performed with SIREN are such that when derivative data are too noisy or disrupted, the drawdown fit makes it possible to attenuate the uncertainties inherent in the assessment of derivative linear regressions.

In order to quantify the quality of each manual fit, the coefficient of determination R^2 is calculated between the differentiated points and the regression line, defined manually.

Figure 3.2-A displays the effects of pumping rate adjustments (at 55, 243 and 3390 minutes) on the s and $ds/dlogt$ responses. On the upper plot, s shows a slight translation of the signal for each of the three changes of pumping rate Q . The rate values are unfortunately not mentioned in the consultant's report but the increase of the drawdown signature suggests an increase of Q for each adjustment. On the lower plot, the $ds/dlogt$ signal shows a small number of extreme and noisy data when the pumping rate is increased but afterwards, the initial flow regime is rapidly recovered. The flow dimension value is thus not influenced by variations in the constant pumping rate.

Figure 3.2-B shows the effects of an interruption in pump operation (between 3 and 4 minutes) on the s and $ds/dlogt$ responses. On the upper plot, s displays a reduction of drawdown associated with an increase of hydraulic head in the well, until the pump is restarted (approximately 10 minutes). Derivative data show a pseudo-spherical flow regime ($n = 2.6$), which is totally disrupted by the pump interruption. Indeed, between 3 and 10 minutes (Figure 3.2-B), the pumping stops and induces a recovery of the signal yielding negative data of the derivative which are not visible on a log-log plot. When the pump restarts, the general trend is rapidly recovered, with no evidence of pump disturbance (straight line in Figure 3.2). In both case studies (Figures 3.2-A and B), the derivative signal quickly returns to normal due to the high hydraulic conductivity of the alluvial deposit, which is estimated in the order of $3,5 \times 10^{-5}$ m/s. Note that this value is estimated from a

conventional cylindrical-radial flow dimension model, and therefore, it is not properly estimated in the case of an aquifer that instead induces a spherical flow dimension.

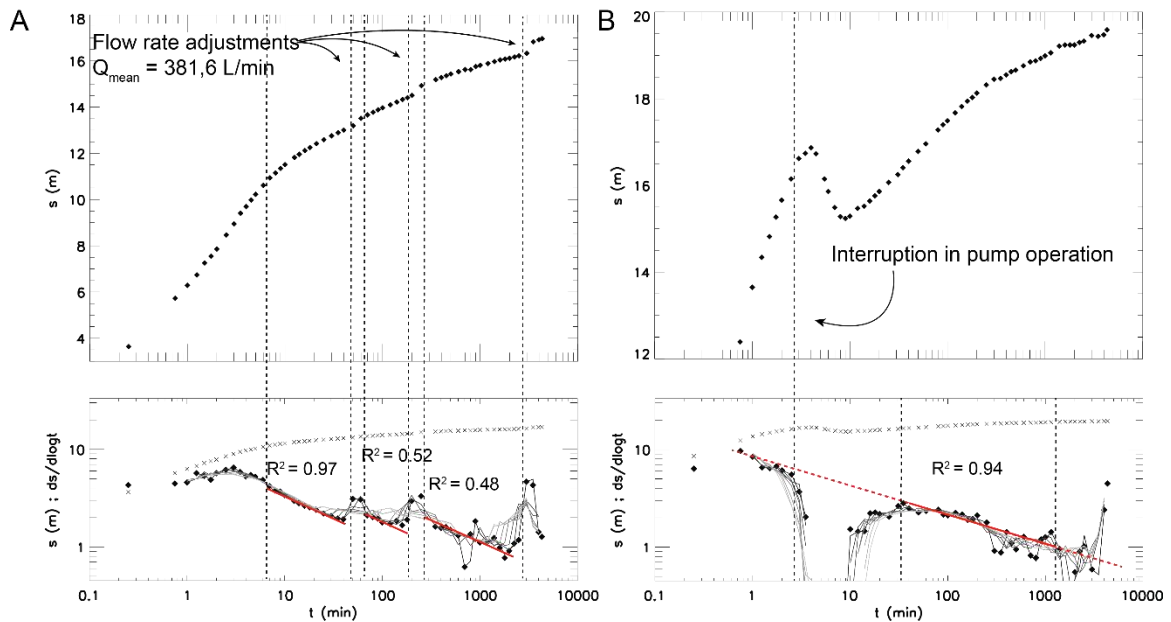


Figure 3.2: Diagnostic plots of two pumping tests performed in two wells in alluvial deposits showing A) the effects of pumping rate adjustments and B) the effect of a temporary interruption of the pump on the s and $ds/dlogt$ signals. The diamond shapes represent the drawdown log-derivative signal and the “x” shapes represent the drawdown signal. The grey lines, derived from the algorithm of Bourdet et al. (1989), represent seven data smoothings for L ranging between 0.2 and 0.8. The R^2 value represents the coefficient of determination between the derivative data and the regression line.

Numerical simulations were conducted in order to confirm these field observations and to clarify the flow regime behavior when the hydraulic test is affected by pumping rate changes or by a pump shut-down. The four columns of Figure 3.3 show the drawdown and drawdown-

log derivative signals of four different conceptual models, which are generated in confined conditions using the HydroGeoSphere code (Therrien et al. 2010). Each of the four conceptual models generates distinct flow dimension sequences. From left to right of Figure 3.3, the n -sequences are: cylindrical-radial to linear ($n = 2 - 1$), bilinear to cylindrical-radial ($n = 1.5 - 2$), simply cylindrical-radial ($n = 2$) and spherical to cylindrical-radial ($n = 3 - 2$). The cylindrical-radial-linear n -sequence is obtained by generating a flow within a conduit. The bilinear to cylindrical-radial n -sequence is obtained by a well connected to a finite-conductive vertical fault supplied by the matrix. The cylindrical-radial flow regime is modelled with a conventional Theis aquifer. The spherical-radial n -sequence is induced by a well that partially penetrates the aquifer. From top to bottom, Figure 3.3 shows the semi-log plot of the drawdown (CP_1, CP_2, CP_3 and CP_4), the drawdown log-derivative signal without pump disturbance (A_1, A_2, A_3 and A_4), the derivative signal when pumping rate increases occur (B_1, B_2, B_3 and B_4) and the signal that is disturbed by a pump shut-down (C_1, C_2, C_3 and C_4). For both the change in pumping rate and the pump shut-down, similarly to the field observations in Figure 3.2, the general trend of the derivative signal is rapidly recovered after the disturbance has stopped. In other words, the flow dimension value is temporarily disrupted by the pumping-rate disturbances but is not dependent on the pumping rate. Even when the test is altered during a short time period when a pumping rate change occurs, the general trend of the flow regime is not impacted. Furthermore, the step rate adjustments are generally observable during the test (induced peak noise) and have been considered in the interpretation of flow regimes.

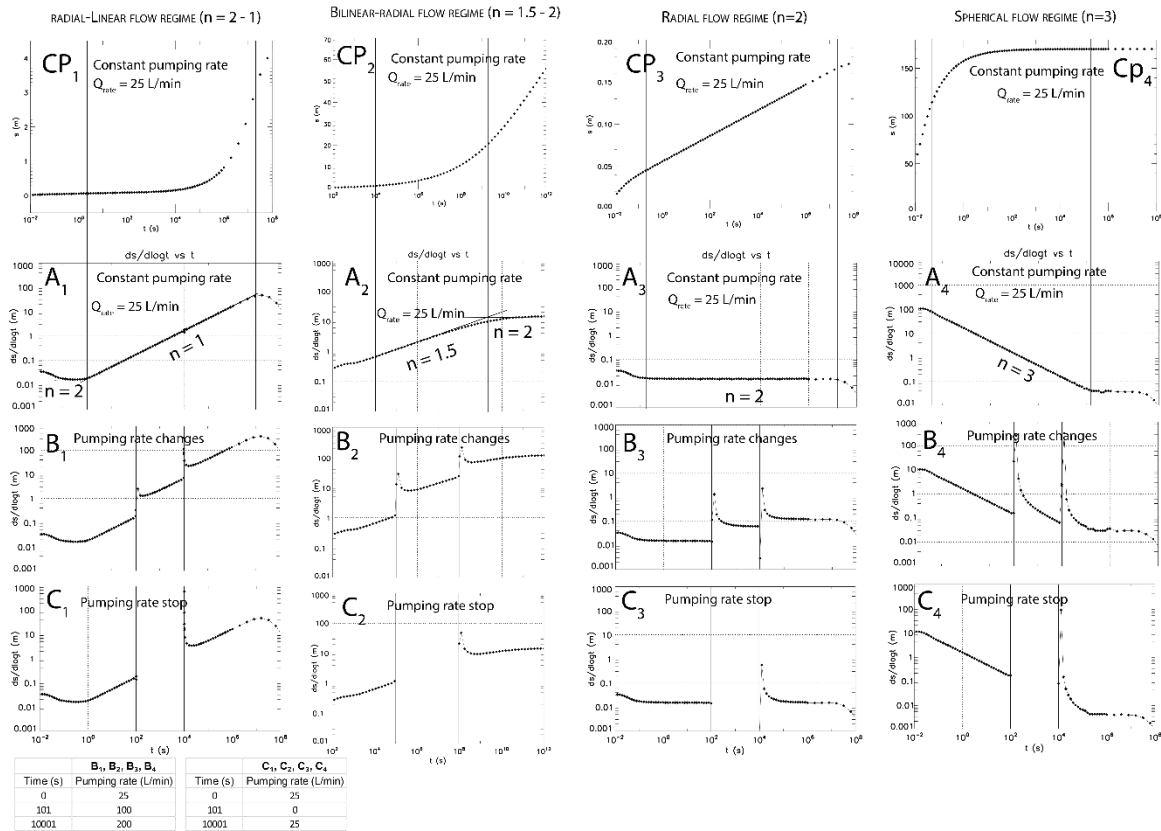


Figure 3.3: Derivative signals of 4 conceptual models (one for each column) modeled numerically using HydroGeoSphere (Therrien et al. 2010). Respectively, the first, second, third and fourth column represent a radial-linear, bilinear-radial, radial and spherical-radial n -sequence. Respectively, the first, second, third and fourth line represent a semi-log plot of the s with a constant-rate pumping test (CP_{*i*}), the derivative signal with a constant-rate pumping test (A_{*i*}), the derivative signal with 3 increased adjustments of the pumping rate (B_{*i*}) and a derivative signal disrupted by a pump shut-down (C_{*i*}).

As described by Equations (3.6) and (3.8), besides the hydraulic properties K and S_s of the aquifer and the extent of the flow zone b , the pumping rate Q is also a parameter that influences the derivative signal. We conducted several numerical tests to observe the impacts of the drift of the pumping rate on the flow dimension value. Figure 3.4-A shows

numerical results of three situations of the drawdown-log derivative signatures of a cylindrical-radial flow model obtained in three different pumping rate conditions. In one case, the pumping rate is constant and in the two other cases we model a gradual drift of the pumping rate. In fact, the pump performance depends on the well head level. Figure 3.4-A shows that the power law variation of the pumping rate influences the value of the flow dimension. The linear variation of the pumping rate induces an apparent flow dimension value which can be very different from the flow dimension of the equivalent constant-rate model. The slopes of the derivative signal and the pumping rate are practically identical (Figure 3.4-A). According to the GRF model (Barker, 1988), the derivative signal is given by Equations (3.6) and (3.8). Because C is proportional to Q , when the pumping rate varies according to a power law (*i.e.*, $Q = Q_0 \cdot t^a$), Equation (3.8) can be written as (Equation (3.10)):

$$\frac{ds}{d \log t} = \frac{C' \cdot v \cdot t^v \cdot Q_0 \cdot t^a}{2.3} = \frac{C' \cdot v \cdot Q_0 \cdot t^{(v+a)}}{2.3} \quad (3.10)$$

With C' written as (Equation (3.11)):

$$C' = \frac{1}{4\pi^{1-v} K b^{3-n} v} \left(\frac{4K}{S_s} \right)^v \quad (3.11)$$

With a the slope of the power law pumping rate drift $Q(t) = Q_0 \cdot t^a$. Thus, the slope p of the derivative response plot on a log-log graph is (Equation (3.12)):

$$p = a + v = 1 + a - \frac{n}{2} \quad (3.12)$$

Consequently, the apparent flow dimension n_{app} induced by a power law pumping rate drift can be written as (Equation (3.13)),

$$n_{app} = n - 2a \quad (3.13)$$

For instance, in Figure 3.4-A, the slope of the increasing power law pumping rate a is equal to 0.38 and the related slope of the derivative signal is equal to 0.44, inducing an apparent flow dimension of $n_{app} = 1.12$ (calculated from Equation (3.8)) instead of $n = 2$, which is the flow dimension of the constant-rate model. The apparent flow dimension calculated from Equation (3.14) with the power exponent a of the variable flow rate is equal to $n_{app} = 1.24$. We observe a slight difference between the observed apparent flow dimension equal to 1.12 and the calculated apparent flow dimension equal to 1.24. These numerical tests are only a preliminary study which aims at issuing a warning to practitioners when interpreting the flow dimension, because pumping rate drifts can influence the flow dimension value. Obviously, further work is needed to suitably address the issue of pumping rate drift. In particular, other pumping rate drift behaviours should be analysed. Unfortunately, the possible distortion of the flow dimension in the database due to pumping rate changes cannot be verified because pumping rate changes during the pumping test were not sufficiently monitored.

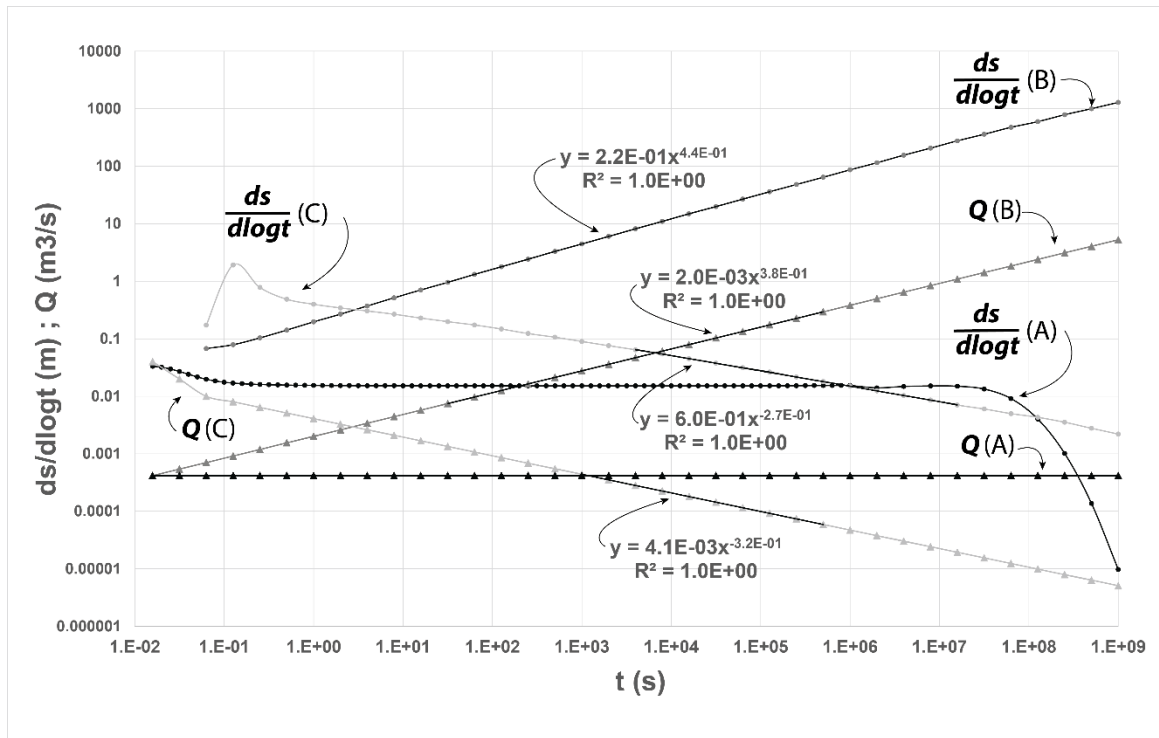


Figure 3.4: A) 3 derivative signals associated with 3 different behaviours of the pumping rate of a same cylindrical-radial flow model modeled numerically using HydroGeoSphere (Therrien et al. 2010). The flow model is composed of an isotropic constant thickness aquifer bounded by constant head boundaries pumped by a vertical well located in the center. The solid lines with dots represent the drawdown log-derivative responses of the cylindrical-radial flow model induced by a particular pumping condition represented by dashed lines with triangles. $Q(A)$ and $ds/dlogt(A)$ are the curves of a constant rate pumping test and the associated derivative response, $Q(B)$ and $ds/dlogt(B)$ are the curves of an increasing power law pumping rate and the associated derivative response, and $Q(C)$ and $ds/dlogt(C)$ are the curves of a decreasing power law pumping rate and the associated derivative response.

3.4.3 GEOLOGICAL CONTEXTS

A distribution of lithological types in each investigated area is provided in Table 3.1. 49 % of the database originates from pumping test data compiled by Rafini (2008) and 51 % from

data collected within the framework of the PACES project (*Programme d'acquisition de connaissances sur les eaux souterraines*, a groundwater knowledge-acquisition program funded by the Ministry of Environment of Quebec and in part directed by the *Université du Québec à Chicoutimi*).

The Quebec bedrock is mainly composed of Precambrian crystalline rocks, essentially orthogneisses, paragneisses, granitic intrusions, anorthosite, and charnockites (Rondot 1989). The crystalline rocks are disconformably overlaid by non-deformed sedimentary deposits composed, from depth to surface, of limestone to limy limestone, sandstone and shale (Lemieux et al. 2003). The limestones generally display a tabular lamination and may include clay interbeds. The carbonate rocks are today found only in the valleys or topographic depressions, where they have been protected from the intense erosion that occurred during the late Quaternary glaciations. The crystalline bedrock is interspersed by a complex fault system generated by various successive geological events dating from the Precambrian, some of which have been reactivated during the late Mesozoic opening of the Atlantic Ocean (Tremblay et al., 2003; Tremblay and Lemieux, 2001). Thick sand and gravel horizons overlaying the bedrock are found throughout the province of Quebec as the result of the late Quaternary glaciations, though most deposits are related to events that occurred since the Last Glacial Maximum (~ 20 ka). Various glacial and fluvio-glacial structures, such as tills, terminal and lateral moraines, eskers, kame, fluvio-glacial deltas, kettles, drumlins and floodplains compose the alluvial landscape of the region. The glacial retreat generated numerous eskers, particularly widespread in the Abitibi-Temiscamingue region (Quebec). These deposits, established by intra-glacial meltwater streams in ice tunnels, generally

present a channelized structure and a stream-rate stratification (Levasseur 1995). Marine transgression and regression events led to the deposition of fluvio-marine horizons that are represented by a confining clay layer above the fluvio-glacial sediments (Levasseur 1995).

In northern Tunisia, pumping tests were performed exclusively in carbonate rock aquifers composed of limestones from the Eocene period. That region is characterised by thick stratified strata and finely laminated carbonate rocks (Rafini 2004). The media is affected by faults formed during the Upper Jurassic and the Cretaceous and reactivated during the Pyrenean and Alpine compressions. The fractured media manifests a negligible karstification and a low matrix porosity.

The carbonate rocks studied in France are located in Alpine and Pyrenean forelands, composed of dolomite, limestone and marls. The crystalline media, located in the regions of Lozère and Loire (France), are characterised by a deeply weathered surficial horizon composed of granitic sand and clay-rich materials whose general hydrodynamic behavior have been explained in detail by Lachassagne (2008), Lachassagne et al. (2011) and Dewandel et al. (2011). Some wellbore loggings have reached a horizon composed of fissured rocks or compact rocks underlying the pumped granitic sand aquifer (BRGM database).

Table 3-1: Long-term pumping tests included in the pooled database: location of wells and observed lithology.

	Number of observations							Total %
	All sources	CHCN (Quebec)	SLSJ (Quebec)	Mirabel (Quebec)	ABTE (Quebec)	Tunisia	France	
Alluvial deposits	22	6	8	1	7	0	0	32%
Crystalline rocks	19	9	2	2	0	0	6	28%
Carbonates	28	2	1	14	0	2	9	41%
Total	69	17	11	17	7	2	15	100%

3.4.4 COMPARISON OF HYDRAULIC PROPERTY VALUES ESTIMATED FROM VARIOUS MODELS

In this section, the conventional Theis and Cooper-Jacob methods and a derivative analysis based on the cylindrical-radial flow regime are applied in various conceptual models. Some models display a long-term radial flow regime, whereas others show a sequence of radial and non-radial flow regimes. This analysis, composed of numerical and field data, aims at comparing the estimated hydraulic properties and to appreciate their degree of uncertainty when using the analytical models derived from the cylindrical-radial flow regime assumption.

Four conceptual models are modeled with a constant-rate pumping test. These conceptual models generate the following n -sequences: radial-linear, bilinear-radial, single-stage radial and spherical-radial flow regimes that are described in section 3.4.2. The parameter

estimation is performed using a manual type-curve matching: the Theis method (Theis 1935), and two graphical analyses: the Cooper-Jacob semi-log method (Cooper et Jacob 1946) and the radial derivative analysis. The Theis and the Cooper-Jacob solutions are described in Kruseman et de Ridder (1994). The cylindrical-radial derivative analysis estimates the hydraulic conductivity for a cylindrical-radial flow regime using the following equation (Equation (3.14) which is derived from equation (3.2)):

$$K = \frac{2.3Q}{m4\pi b} \quad (3.14)$$

with m [L] the Y-intercept of the radial flow dimension on a log-log plot of $ds/d\log t$ and b [L] the thickness of the cylindrical-radial cross-flow area. For each conceptual model, the log-log plot of the drawdown derivative signal is analysed in order to identify the radial portion of the signal and to determine m .

The values of the hydraulic conductivity K are shown in Table 3.2. The gray lines in Table 3.2 represent the relative errors between the above K value and the modeled K value. The simplified diagrams of the Table 3.2 represent, from left to right, the semi-log plot of s vs t of the linear, the bilinear, the cylindrical-radial and the spherical flow dimension. When the conceptual model induces a single-stage cylindrical-radial flow regime, the three methods give a good approximation of K (the relative error ranges between 0% and 6%, Table 3.2). For the radial-linear, bilinear-radial and spherical-radial flow regimes, the type-curve matching and the graphical analysis of conventional methods are difficult to apply because the cylindrical-radial flow regime represents only a small portion of the entire signal.

The Cooper-Jacob plot of the linear flow (Figure 3.3-CP₁) emphasizes two slopes. The first slope slightly underestimates K (-13%), whereas the second slope strongly underestimates K (-99%) or can be inadequately interpreted as a no-flow boundary. The derivative signal shows a short cylindrical-radial flow regime at early times before the long-term linear flow regime. This early times cylindrical-radial flow, reflecting the cylindrical diffusion of the cross-flow area before reaching the impermeable wall of the conduits, makes it possible to accurately estimate K with a relative error of -1% (Table 3.2). Similarly, the semi-log plot of the spherical flow regime shows two slopes for the same flow regime. Both strongly underestimate K , probably because, in addition to not complying with the cylindrical-radial flow regime, the thickness that is investigated by the cross-flow area is different from the real thickness of the aquifer. The derivative signal (Figure 3.3-A₄) shows a short radial flow regime at late times (unnoticeable in the semi-log plot of s). The radial flow regime, representing the reach of both the bottom and the top of the aquifer, makes it possible to estimate a good approximation of K with a relative error of 11% (Table 3.2). Overestimating the hydraulic conductivity of the matrix K_m using the Theis and Cooper-Jacob models for the bilinear conceptual model is not surprising because these models assume a homogeneous aquifer and do not take into account the hydraulic conductivity of the fault K_f . The radial flow regime that is observed after the bilinear flow regime (Figure 3.3-A₄) represents the “matrix-related radial flow regime” (Rafini and Larocque, 2012). This radial stage gives a good approximation of K_m using Equation (3.14). The Cinco-Ley et al. (1978) solution developed for the vertical fault has the advantage of producing a value for K_f . To conclude, the K values estimated from the radial derivative analysis are close to the modeled K value. The relative errors are respectively 0%, -1%, 4% and -25% for the radial, radial-linear, the bilinear-radial

and the spherical-radial conceptual models. The derivative signal has the advantage of clearly highlighting the radial flow regime by a flat horizontal slope of $ds/dlogt$.

Table 3-2: Hydraulic conductivity modeled and estimated from the Theis, Cooper-Jacob and radial derivative analysis for 4 conceptual models generating a radial-linear, a bilinear-radial, a radial and a spherical-radial flow regime. The grey lines represent the relative errors of the overlying K values. The derivative signals of the 4 conceptual models are shown in Figure 3 (linear- A_1 , bilinear- A_2 radial- A_3 and spherical- A_4). The simplified graphs represent, from left to right, the semi-log plot of s vs t of the radial-linear, the bilinear-radial, the radial and the spherical-radial flow dimensions.

Flow regime		Radial-linear	Bilinear-radial	Radial	Spherical-radial
n -sequence		$n = 2 - 1$	$n = 1.5 - 2$	$n = 2$	$n = 3 - 2$
K (m/s) modeled		1.0E-05	-	1.0E-05	1.0E-05
K(matrix) (m/s) modeled for the bilinear-radial conceptual model ($n = 1.5 - 2$) *K(fault)_modeled = 1.0E-2 m/s ; bf = 2 m			1.0E-08		
K (m/s) estimated with the Theis method		1.9E-05 89%	9.5E-08 847%	9.5E-06 -5%	1.9E-08 -100%
K (m/s) estimated with the Cooper-Jacob method	Semi-log plot of s vs t				
	First slope of s (ρ_1)	8.7E-06 -13%	7.4E-07 7267%	1.0E-05 0%	4.4E-09 -100%
	Second slope of s (ρ_2)	9.3E-08 -99%	1.3E-08 26%	- -	1.1E-06 -89%
K (m/s) estimated with the radial derivative analysis	0 slope of $ds/dlogt$	9.9E-06 -1%	1.1E-08 12%	1.0E-05 0%	1.1E-05 11%
	K_matrix (m/s) estimated with the Cinco-Ley et al. (1978) solution for $n = 2$	0 slope of $ds/dlogt$	- -	4.9E-09 -51%	- -
K_fault (m/s) estimated with the Cinco-Ley et al. (1978) solution for $n = 1.5$	0.25 slope of $ds/dlogt$ -> K_f	- -	6.46E-06 -52%*	- -	- -

We also analysed two sets of field data (obtained from the Sainte-Anne and the Saint-Eustache wells) in order to compare the K values estimated from the four methods that were used in the previous section (Table 3.3). The wells are installed in fractured carbonate rocks. Field observations (such as packer tests) have highlighted the presence of conductive structures (Lemieux et al. 2006). The two derivative signatures (Figure 3.5) show a multi-staged signal composed of the characteristic n -sequence 4-1.5-2, reflecting a non-connected vertical fault media (Rafini, 2008, Rafini and Larocque, 2012). The K values estimated for the two pumping tests are close, regardless of the method used. This similarity in the results is probably related to the fact that the hydraulic conductivities of the matrix and of the fault are close to each other or the transmissivity of the fault is negligible compared to the transmissivity of the matrix.

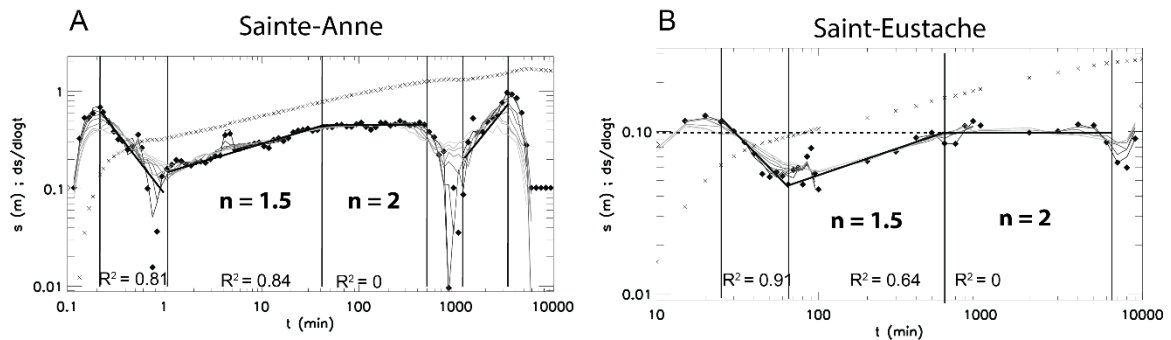


Figure 3.5: Diagnostic plots and flow regime interpretations in fractured rock aquifers. A: constant-rate pumping test (6.5 days) conducted in the P-8 well located in a Chasy carbonate rock aquifer of Sainte-Anne-des-Plaines (Charlevoix, Quebec, Canada). B: constant-rate pumping test (6.5 days) conducted in the SE6 well located in the aquifer of Saint-Eustache composed of the Beauharnois rock unit (Mirabel, Quebec, Canada). The diamond shapes represent the drawdown log-derivative signal and the “x”

shapes represent the drawdown signal. The R^2 value represents the coefficient of determination between the derivative data and the regression line.

Table 3-3: Hydraulic conductivity values estimated from the Theis and Cooper-Jacob methods and the radial derivative analysis and for the n-sequence $n = 1.5 - 2$.

		Saint-Anne	Saint-Eustache
<i>n</i> -sequence		$n = 4 - 1.5 - 2$	$n = 4 - 1.5 - 2$
<i>K</i> (m/s) estimated with the Theis method	First fit	5.3E-04	5.2E-05
<i>K</i> (m/s) estimated with the Cooper-Jacob method	First slope of <i>s</i>	4.1E-04	4.2E-05
	Second slope of <i>s</i>	5.4E-04	3.5E-05
<i>K</i> (m/s) estimated with the radial derivative analysis	0 slope of $ds/dlogt$	4.8E-04	3.6E-05
<i>K</i> _matrix (m/s) estimated with the with the Cinco-Ley et al. (1978) solution for $n = 2$	0 slope of $ds/dlogt$	2.1E-04	1.6E-05
<i>T</i> _fault (m ² /s) estimated with the Cinco-Ley et al. (1978) solution for $n = 1.5$	0.25 slope of $ds/dlogt \rightarrow Tf$	8.4E-03	3.4E-03

3.5 RESULTS AND DISCUSSION

3.5.1 FLOW DIMENSION VERSUS THEIS ANALYSIS: CASE STUDIES

This section describes two different situations that illustrate the benefits of using flow dimension analysis in addition to drawdown-only conventional interpretations to better characterize the flow regimes induced by a pumping test.

Case study 1

Figure 3.6 represents the semi-log plot of the drawdown signal (upper plots) and the log-log plot of the drawdown log-derivative signal (lower plots) of a 3-day constant-rate pumping test conducted in the glacio-fluvial deposits of the Senneterre esker (Abitibi-Temiscamingue, Quebec, Canada). Despite the noise of the drawdown log-derivative signal between 100 min and 4230 min, the SIREN code makes it possible to assuredly fit a sub-radial ($1 < n < 2$) flow dimension by fitting at the same time both the semi-log plot of the drawdown (which is much less noisy), and the lower plot of the drawdown log-derivative signal. Using the traditional (Cooper et Jacob 1946) method, the drawdown signal is interpreted by drawing two straight lines (Figure 3.6a): a first line from 0.3 to 230 minutes and the second line from 230 to 4320 minutes. The second straight line, whose slope is roughly double that of the first line, might be interpreted as a second media with a lesser transmissivity or as the attainment of impermeable boundary conditions. In a first approximation, these two successive straight lines appear as an acceptable linear regression. But, when visualizing the effect of the fit of these two supposed radial flow regimes (upper plot of Figure 3.6a) on a log-log plot of $ds/d\log t$ (lower plot of Figure 3.6a), we see two distinct horizontal straight lines which are obviously an inappropriate representation of the existing data points.

As shown in Figure 3.6b, fitting a 0.35 straight line slope ($n = 1.3$, Equation (3.4)) onto the $ds/d\log t$ signal, resulting in a convex curve on the semi-log plot of s , represents the real data much more accurately.

The pumping test is performed in an esker, a fluvio-glacial sedimentary feature that typically contains channels (Escobar et al. 2004b, Corbett et al. 2012). Such channels impede the cross-flow area to laterally expand during drawdown diffusion. Remaining constant in these alluvial conduits, the flow dimension of eskers is expected to be linear. However, each of the seven derivative signals of eskers that have been analysed in this database showed a sub-radial flow dimension ($n = 1.3$, see below). We interpret this sub-radial flow dimension to be related to leakage coming from the surrounding deposits and that supplies the highly transmissive esker conduit. This assumption is further explained in the general discussion section.

Using the (Cooper et Jacob 1946) model in this case would lead the practitioner to interpret the data as representing a Theis aquifer bounded by an impermeable boundary (Ferris 1949). But, Cooper-Jacob is not a valid model to interpret this pumping test. Rather, the flow dimension analysis, which fits the data and the conceptual model much more closely, is able to detect the presence of a linear flow regime.

This case study illustrates how the identification of flow regime sequences rather than the trivial postulate of a radial flow regime may substantially improve the diagnosis of the aquifer's hydraulic properties, a diagnosis which exerts numerous practical implications on resource management (e.g., a wellhead protection area (WHPA) delineation).

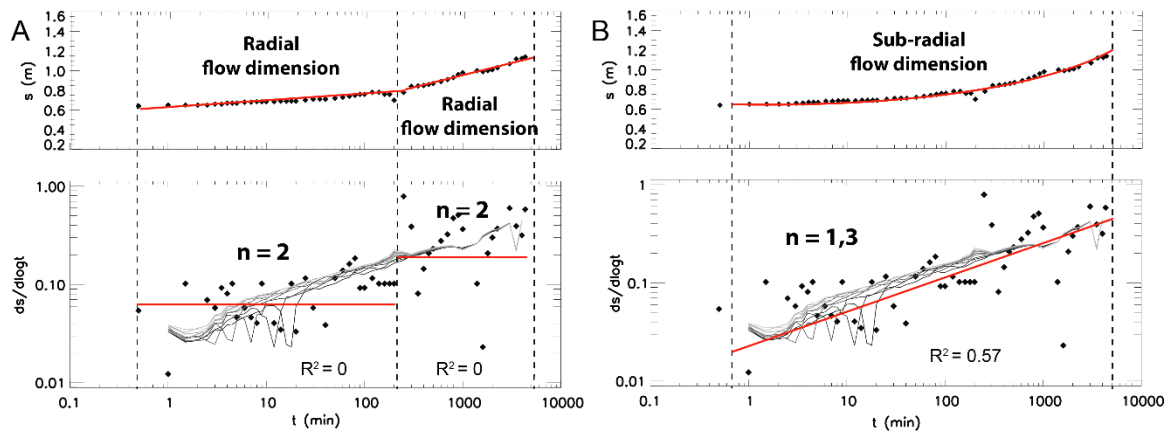


Figure 3.6: Diagnostic plots and interpretations of a constant-rate pumping test conducted in the PP-1 well located in the fluvioglacial deposits of the Senneterre esker (Abitibi-Temiscamingue, Quebec, Canada). In the upper part of figures a) and b): Semi-log plot of the drawdown s ; in the lower part: log-log plot of the drawdown-log derivative $ds/d\log t$. A) Example of a conventional interpretation assuming radial flow regimes, B) Demonstration of a more accurate interpretation of the pumping test using a $ds/d\log t$ log-log plot. The grey lines, derived from the algorithm of Bourdet et al. (1989), represent seven data smoothings for L ranging between 0.2 and 0.8. The R^2 value represents the coefficient of determination between the derivative data and the regression line.

Case study 2

Figure 3.7 represents 3 different examples of pumping test interpretations of a 6.5 day constant-rate pumping test performed in a carbonate rock aquifer in the Sainte-Anne-des-Plaines site (Mirabel, Quebec, Canada). The same methodology as the one that is used in case study 1 is adopted. The reliability of the fitting of the s data (upper plots of Figure 3.7-a-b-c) is checked by analysing the match with the $ds/dlogt$ signal (lower plots of Figure 3.7-a-b-c). As shown in Figure 3.7-a and b, neither a long radial flow regime (from 1,8 to 400 minutes, Figure 3.7a), neither two successive radial flow regimes (one from 1,5 to 30 minutes and another from 30 to 400 minutes, Figure 3.7b) can adequately reproduce the trend of both the s and $ds/dlogt$ signatures. Even if the match of 1 or 2 radial flow regimes seems to be a rather good approximation on the semi-log plot of s , the linear regression is visibly inconsistent on a $ds/dlogt$ log-log plot.

A much more suitable fit of s and $ds/dlogt$ is presented in Figure 3.7c where the signal is divided in a sequence of flow regimes with various n values. On a semi-log plot of s , values of $n < 2$, $n > 2$, and $n = 2$ show respectively a convex, a concave and a straight curve reflecting a rising, a declining or a static drawdown rate. Conceptually, these flow regimes can be related to transmissivity patterns. Bowman et al. (2012) showed numerically that $n < 2$ and $n > 2$ may be generated by conduit geometry in which the cross-sectional area respectively decreases and increases as a power function of distance. Finally, for $n = 2$, the derivative horizontally straightens and the drawdown signal displays a straight line, indicating no change in the drawdown rate, which agrees with the Cooper-Jacob model.

The $ds/dlogt$ signal displays a sequence of integer and non-integer flow regimes (Figure 3.7c): a fractional flow regime ($n = 1.5$ from 1.8 to 40 minutes), followed by a radial flow regime ($n = 2$ from 40 to 500 minutes). This n sequence composed of $n = 1.5$ and $n = 2$ has been numerically shown by Rafini and Larocque (2012 p. 201) to be generated by the presence of a vertical finite-conductivity fault embedded into an aquifer, and not directly connected to the pumping well. The $n = 1.5$ segment represents a bilinear flow regime indicating that the pressure front pulse expands through a media composed by a finite-conductive fault and the fractured rock continuous-like matrix (Abbaszadeh and Cinco-Ley 1995; Rafini and Larocque, 2009). In other words, during the constant-rate pumping test, the fault that is supplying the well is at the same time supplied by the matrix, inducing a diffusion deceleration that is responsible for the fractional flow regime occurrence (Rafini and Larocque, 2009). The radial flow is observed following the bilinear flow regime and indicates that the pressure front pulse diffusion through the matrix is dominant over the pressure front pulse diffusion through the fault. The influence of the fault is thus totally masked by the matrix's hydraulic response, which predominates over the aquifer's response. So far, the leaky vertical fault is the only flow model that has been documented to interpret $n = 1.5$. If the area of the cross flow undergoes a change which is proportional to $r^{0.5}$, this will produce a value of n equal to 1.5.

This case study provides another example showing that interpreting pumping test data using the traditional drawdown analysis on semi-log plots leads the practitioner to miss most of the information and to perform an invalid or low-quality hydrodynamic diagnosis. Such inappropriate interpretation of flow will induce inaccuracies in the estimation of the aquifer's

hydraulic properties. For instance, assuming a radial flow ($n = 2$) in a homogeneous media while the aquifer is, in fact, composed of a vertical fault that generates a bilinear flow ($n = 1.5$), would lead the practitioner to overestimate the matrix's transmissivity, to ignore the presence of a water-bearing fault or to underestimate the fault's transmissivity.

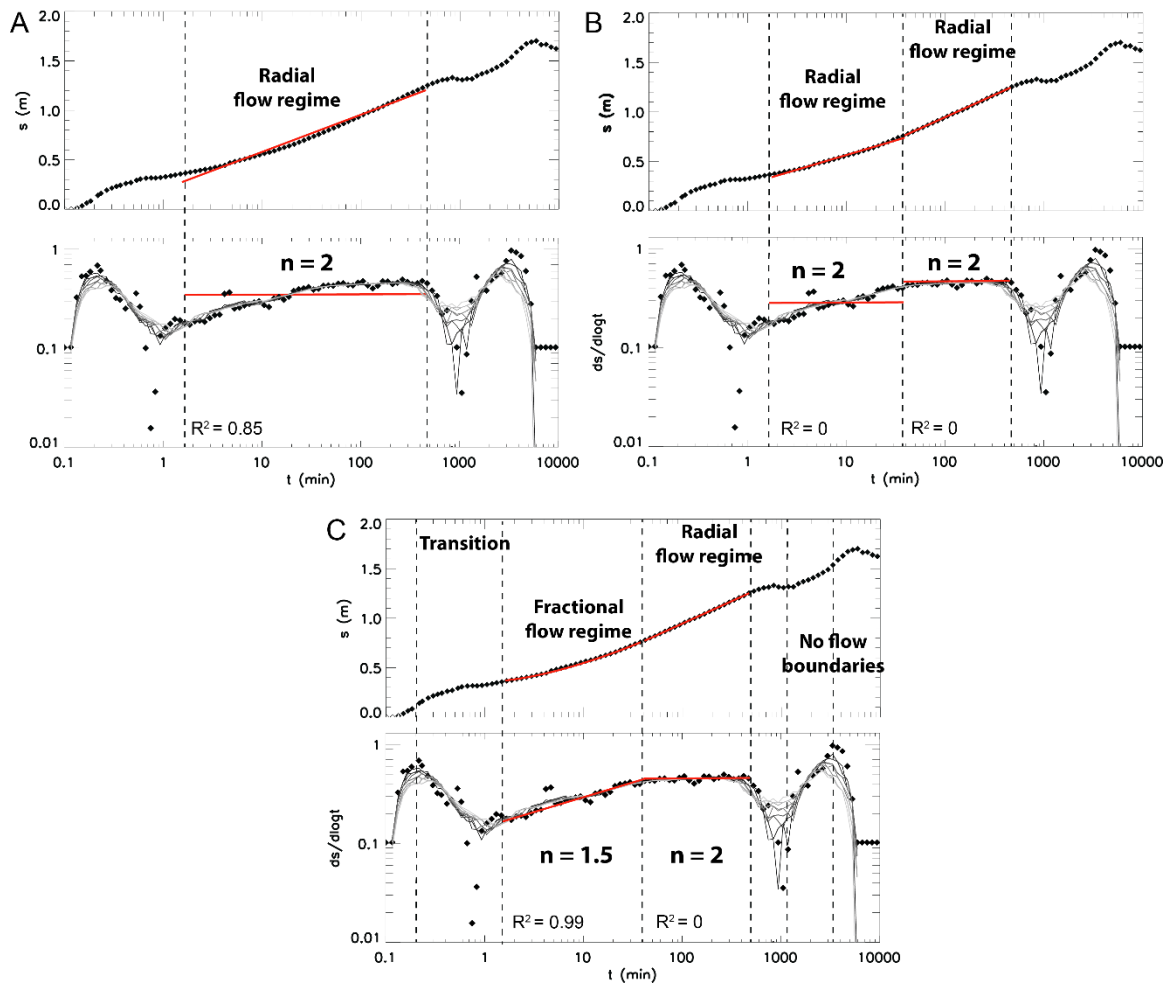


Figure 3.7: Diagnostic plots and interpretations of a constant-rate pumping test (6.5 days) conducted in the P-8 well located in a Chazy carbonate rock aquifer of Sainte-

Anne-des-Plaines (Quebec, Canada). In the upper part of Figures A), B) and C): Semi-log plot of the drawdown s ; in the lower part of the same figures: log-log plot of the drawdown-log derivative $ds/d\log t$. a) Hydrodynamic analysis assuming one radial flow regime, b) Hydrodynamic analysis assuming a sequence of two radial flow regimes, c) Hydrodynamic analysis assuming a sequence of a fractional and a radial flow regime. The grey lines, derived from the algorithm of Bourdet et al. (1989), represent seven data smoothings for L ranging between 0.2 and 0.8. The R^2 value represents the coefficient of determination between the derivative data and the regression line.

3.5.2 THE OCCURRENCES OF FLOW DIMENSION IN NATURAL AQUIFERS

The scope of this section is to provide an overview of the occurrence of flow dimension in nature and to compare the values of n against their geological settings in order to obtain insights into the physical meaning of flow dimension in terms of what it can tell us about the hydrogeological settings and features. Note that only derivative slopes which rigorously correspond to a flow dimension are retained. Slopes more likely relating to transitions and boundary effects (no-flow or constant head) were not included in the database. In fact, as defined by Barker (1988), the flow dimension must reflect the properties of a volume of aquifer investigated by the cross-flow area. This definition of the flow dimension will be covered in the discussion section.

3.5.2.1 Analysis of the entire database

3.5.2.1.1 Flow dimension values

The database contains data from 69 well tests conducted in three different geological environments, in roughly the same proportions: crystalline rocks (19 pumping tests), carbonate rocks (28 pumping tests) and alluvial deposits (22 pumping tests). The pumping tests were performed on average during 2.5 days (63% of the tests ranged from 2 to 4 days). The four shortest well tests lasted 4 hours, 5.5 hours, 12 hours and 15 hours, whereas the four longest well tests lasted 7.1 days, 8 days, 9.1 days and 14.7 days.

Analysis of the data from these 69 pumping tests provided flow dimension distribution values ranging between 0.2 and 3.5, with a mean value of 1.7 and a standard deviation of 0.4. Other studies have also analyzed the frequency of occurrence of the flow dimension from field data (Table 3.4). The frequencies of occurrence of n posited by the studies of (Bangoy et al. 1992, Kuusela-Lahtinen et al. 2003, Audouin et Bodin 2008, Verbovšek 2009, 2011) bring valuable insight as to how n occurs in fractured rock aquifers. Each of these 4 studies, however, is restricted to only one or two fractured rock settings and used n as a tool for refining the characterization of fractured media or to help in selecting the analytical model. Only one (Verbovšek 2009, 2011) presented a statistical study aiming to analyse the influence of several parameters on n , such as the lithological properties of dolomites, their age, the topographical settings, the degree of penetration of the wells, etc. His study analyzes the statistical occurrence of n in a single geological setting, the dolomites. Our study compared n to various environments such as crystalline and carbonate fractured rocks, weathered crystalline rocks and fluvio-glacial deposits in order to better understand

the relationship between n and the local geological features. Because statistical studies examine and manipulate direct field information, they contribute information in parallel to numerical studies and make it possible to enrich our physical interpretation of n .

Because the data used for the studies of Table 3.4 were obtained by means of various different methodologies to conduct pumping tests (packer test, slug test, pumping test) and a wide diversity of procedures to determine flow dimensions (manual and automated type-curve matching of s or $ds/dlogt$, sequential analysis of $ds/dlogt$), the studies should be compared with caution. Indeed, the pumping test duration scale is different for all studies, implying that the portion of each aquifer investigated by the pressure front pulse is no doubt variable. We should remember that short-term pumping test studies are only capable of expressing wellbore effects and the behavior of the aquifer in the area closest to the well.

Table 3-4: Summary of studies analyzing the frequency of occurrence of the flow dimension n .

Type of test	Range of n	Geological setting	Nb of pumping wells	Duration of the pumpig test	Location of pumping tests	Methodology	Reference
Pumping test	$0,2 < n < 1,34$	Granitic rock and carbonate rock aquifers	2 pumping wells, 12 observation piezometers	25 h (granitic rock aquifer), < 10 h (carbonate rock aquifer)	Pyrenee (southern France), Terrieu (France)	Type-curve fittings	Bangoy et al. (1992)
Hydraulic tests	76% of the data showed fractal n , with $1 < n < 2$	54 fractured aquifers	126 well tests		Korean		Hamm (1995)
Three multiple constant rate pumping tests	$1,6 < n < 2$ for the pumped fracture zone and $n = 1,45 - 1,5$ in the neighboring one	Poorly weathered crystalline rocks. No flow in the crystalline matrix. Intense fracturing along subvertical Precambrian shear zones	3 pumping wells, 4 observation piezometers	6 h of pumping	Leppavirta (south-central Finland)	Best-fitting curve based on an analytical model with fractional flow dimensions	Leveinen (2000)
Pressure-pulse, constant-pressure flow, pressure-recovery tests	$1 < n < 3$	Evaporite deposits	16 hydraulic tests	not determined	Waste Isolation Pilot Plant of the Delaware Basin (New Mexico)	Type-curve fitting	Beauheim et Roberts (2002)
2 m and 10 m constant pressure injection test	$1,6 < n < 2,5$	Low conductivity crystalline rock aquifer	5 pumping wells, 175 constant-pressure injection tests	around 1 hour or less	Romuvaara (Suede)	Type-curve fitting of ds/dlogt (FRACDIMQ algorithm, Doe et Geier 1990)	Kuusela-Lahtinen et al. (2003a)
Constant-rate pumping tests	$n = 1,6$	Crystalline aquifer (preferential weathering of a subvertical fractured zone)	106 m ³ per year since 1991 as the main water supply for a town of 20,000 inhabitants	3 pumping tests, whose duration was 5, 13 and 88 days, with sampling rates as short as 1 min, giving a scale range of 4–5 orders of magnitude in time	Ploemeur	Best-fitting of both s and ds/dlogt	le Borgne et al (2004)
Step drawdown test	2,25	Fractured limestones	1 pumping well	approximately 150 min	Montpellier University yard (France)	Type-curve fitting of the semi-logarithmic plot of the drawdown data (with a leakage model)	Lods et Gouze (2004)
Pumping tests	0,7	Fractured rock (harzburgite massif)	1 pumping well	approximately 80 hours	Ophiolitic complex of Oman	Type-curve fitting of the semi-logarithmic plot of the drawdown data (with a double porosity model)	Lods et Gouze (2004)
Pumping tests	1,7	Fractured rock (gabbros)	1 pumping well, 3 observation piezometers	around than 80 hours	Ophiolitic complex of Oman	Type-curve fitting of the semi-logarithmic plot of the drawdown data	Lods et Gouze (2004)
Pumping tests	1,8	Fractured granites	1 pumping well, 3 observation piezometers	around 16 hours	South Centre of India	Type-curve fitting of the semi-logarithmic plot of the drawdown data (with a model composed of a fracture and a matrix)	Lods et Gouze (2004)
Pumping tests	1,45	Fractured granites	1 pumping well, 1 observation piezometer	less than 20 hours of pumping	South Korea	Type-curve fitting of the semi-logarithmic plot of the drawdown data (with a leakage model)	Lods et Gouze (2004)
Pumping tests	$1,2 < n < 2$	Weathered crystalline rock aquifer (3 m of underlying horizontally fractured-weathered layer)	34 pumping wells/observation wells	around 1 day	Maheshwaram watershed (India)	Type-curve fitting of the semi-logarithmic plot of the drawdown data	Marechal et al (2004)

Figure 3.8 shows the occurrence of frequency of n in the entire database (not considering the duration of observation of n). The figure shows that there is a wide diversity of n values. In particular, the large clear bars of Figure 3.8 show that the linear, radial and spherical dimensions represent, respectively, 20%, 31% and 8% of the 121 flow dimensions analyzed. Non-integer n values are also significantly represented. The fractional n values in ranges 0 to 1, 1 to 2, 2 to 3 and >3 represent, respectively, 3%, 24%, 11%, and 1% of all n values, which together amount to a total of 38% of fractional flow dimension values.

Radial flow regimes are observed in 55% of the 69 pumping tests and represent 31% of the 121 flow regimes that were interpreted overall (large bars in Figure 3.8). These radial flow regime occurrences are observed systematically in a sequence of several flow regimes with non-radial flow dimensions. As a result: i) the unique radial flow conditions as stipulated by Theis are rarely observed in this database; ii) radial flow is observed only 31% of the overall reported flow regimes, while it is assumed in an overwhelming majority of existing interpretative models. In fact, most analytical models published in the petroleum literature since the 80's are variations on the radial theme. The fact that we are now able to observe predominantly non-radial flow dimensions emphasizes the need to develop interpretative models that represent the real dimension of flow more accurately than Theis and Theis-derived models, which remain commonly used.

It is interesting to note that the n values smaller than 2, equal to 2 and greater than 2 are associated with different flow behaviors: $0 < n \leq 2$ is related to an increase of the drawdown rate (thus, the head decline accelerates), while $n > 2$ expresses a decline of the drawdown rate (thus, the head decline decelerates). A summary of the hydrodynamics of each class is

given in Table 3.5. Based on the Barker relation (Equation (3.1)), the n values ranging between 0 and 1 are interpreted as a decrease of the cross-flow area as it expands radially. This can suggest a reduction of the transmissivity as the pressure-front pulse expands or, for $n = 0$, a depletion of the aquifer. The n values equal to 1 are associated with a cross-flow area that is constant (Equation (3.1)), suggesting that the pressure wave is diffusing through a channelized environment, as explained above. All the values of $n > 1$ express an increase of $A(r)$ (Table 3.3) that is induced by various geometries of boundaries, transmissivity configurations, fault-matrix relations, *etc.* (cf. section 3.3.2.2).

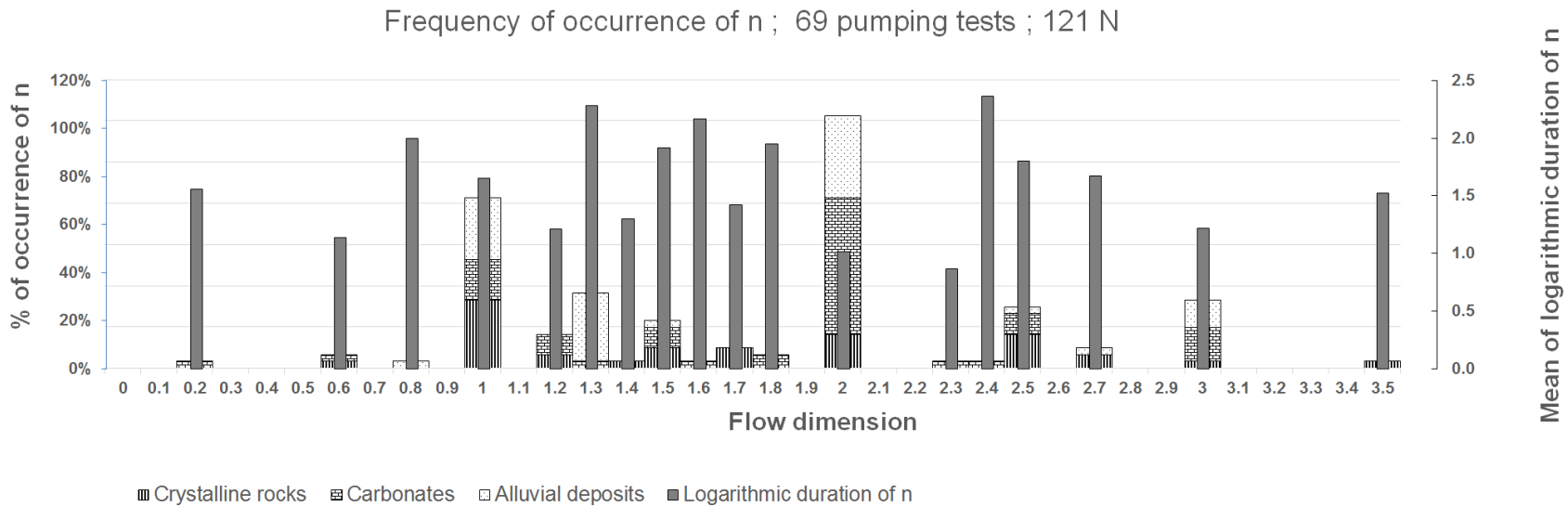


Figure 3.8: Statistical analysis of the flow dimension occurrence during 69 constant-rate pumping tests (including respectively 19, 22 and 28 pumping tests in fractured rocks, deposits and carbonate rocks), located in Canada, France and Tunisia. The database contains 121 distinct flow dimension values. The “N” in the graph titles represents the number of observed flow dimensions. The flow dimension is manually estimated from a sequential analysis. The large bars are read on the left y-axis, the thin-dark bars are read on the right y-axis.

Table 3-5: Summary of hydrodynamic interpretations of n and their graphical representations.

Flow dimension n	$n < 1$	$n = 1$	$1 < n < 2$	$n = 2$	$n > 2$
Cross-flow area $A(r)$	↘	→	↗	↗	↗
Rate of drawdown s	↗	↗	↗	↗	↘
Shape of s on a semi-log plot	convex curve	convex curve	convex curve	straight line	concave curve
Shape of $ds/d\log t$ on a log-log plot	rising slope	rising slope	rising slope	horizontal slope	declining slope

↗: increases when r ↗

↘: decreases when r ↗

→: is constant when r ↗

3.5.2.1.2 Flow regime duration

The duration of flow regimes is a critical point of the flow dimension analysis. This issue was addressed by computing the “mean of the logarithmic duration of n ”, calculated as follows: (the number of observation of n of a pumping test) * (\sum of the logarithmic duration of n of a pumping test) / (\sum of the logarithmic durations of n of the entire database).

The thin dark bars of Figure 3.8 represent the mean of the logarithmic duration of n (right axis) and the large bars of Figure 3.8 show the frequency of occurrence of n (left axis). Presenting these two types of information in combination shows that the most frequently observed flow dimensions are not necessarily the longer-lasting ones. In fact, the thin dark bars show that the most stable long-term flow dimensions are $n = 2.4$, $n = 1.3$ and $n = 1.6$, which are observed during respective averages of 2.36, 2.28 and 2.17 log-cycles. The sub-radial flow dimension ($n = 1.3$), which is almost exclusively observed in alluvial deposits, is observed during a long-lasting duration (2.3 log-cycles in average). The bilinear flow dimension ($n = 1.5$), mostly observed in fractured rocks, is observed during 1.9 log-cycle on average. On the contrary, the radial flow dimension $n = 2$ is one of the most frequent flow

dimensions of the database (31% of the 121 flow dimensions) but it is also one of the shortest-lasting flow dimensions. On average, $n = 2$ is observed during less than one log-cycle (0.97 log-cycle in average). In fact, in all the various geological settings, $n = 2$ has generally been observed at the beginning of the pumping tests and during a short time period. The linear flow dimension ($n = 1$) is also related to a long-lasting signal (1.7 log-cycles in average) and is observed in equal proportions between the alluvial deposits (7%), the carbonates (8%) and the crystalline rocks (5%). Insights on the conceptual interpretation of the observed flow dimensions are given in the following section by combining the values and the duration of n and the geological settings.

This figure also shows some relationships between the n values and the geological environments. For instance, $n = 1.3$ is exclusively observed in alluvial deposits, while $n = 1.5$ and $n = 2.5$ are almost exclusively observed in fractured rocks. The affinity of n to certain environments suggests that the geological facies influences the geometry of the pressure wave, and so the flow dimension. It may be thus a valuable tool to explore the properties of the aquifer that control the flow regimes.

3.5.2.1.3 Flow dimension sequences

The flow dimension values included the database are only those that are assumed to be representative of the properties of a volume of aquifer. However, the flow dimension sequence takes into account every slope of a signal. Thus, for certain signals, the wellbore effects, transitions and/or hydraulic boundaries are considered into the sequence.

Most signals exhibit several successive flow regimes marked by different n values: 88% of the pumping tests analyzed for this study were multi-stage, with 38%, 44% and 6%, presenting, respectively, 2, 3, and 4 sequences of flow dimensions (Figure 3.9). The n sequences express various geological facies that control the pressure wave and which are successively reached by this pressure wave.

Fractured media produce a major proportion of n -sequential signals: they represent, respectively, 85%, 100% and 96% of the pumping tests performed in faulted crystalline rocks, altered crystalline rocks and carbonate rocks. This suggests that fractured media are complex heterogeneous systems involving various flow regimes (Figure 3.9).

At early times, a change of derivative slope may signal the evolution from wellbore and skin effects to the aquifer response. At middle times and late times, as the pressure front pulse expands through the aquifer, variable slope sequences of $ds/d\log t$ can express changes in the hydraulic and/or geometrical conditions of the aquifer, transitions and/or eventually the attainment of hydraulic boundaries. Note that the derivative signatures that are related to skin effects, wellbore storage effects or hydraulic boundaries have not been included in the flow dimension database.

Sequences of flow regimes have often been reported in various field and numerical studies conducted in fractured rock aquifers (Ehlig-Economides, 1988; Escobar et al., 2005; Mattar, 1997; Rafini and Larocque, 2012; Renard et al., 2009). This study, based on an n -sequential analysis, further shows that, contrary to current opinion, alluvial deposits can also exhibit

complex flow behaviors with discontinuous flow regimes and fractional n values (primarily ranging from 1 to 2).

A wide array of n values was observed in the database, in different sequences, of various durations and with varying frequencies of occurrence. The following section describes the results obtained when comparing the flow regimes to the geological environments of wells in order to obtain insights on the physical interpretation of n .

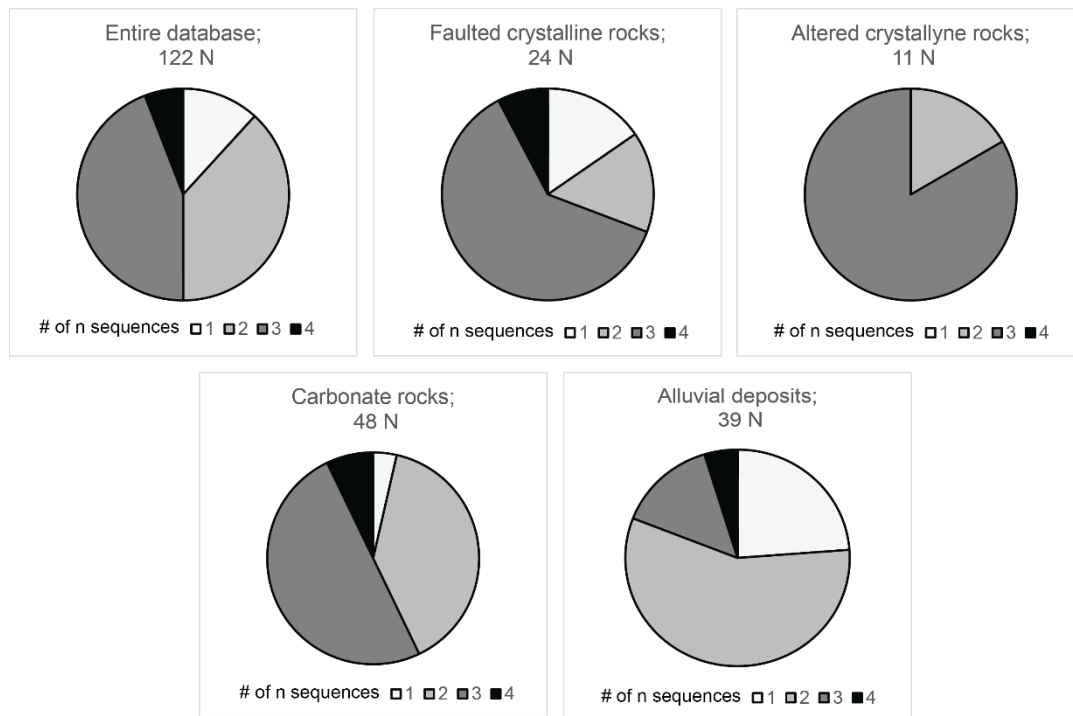


Figure 3.9: Proportional distribution of the 1, 2, 3 and 4 n sequences in the 69 pumping tests conducted for this study.

3.5.2.2 Analysis of the distribution of n in different geological environments

3.5.2.2.1 Crystalline rock aquifers

Based on 19 pumping tests, the frequency histogram of n in crystalline rock aquifers displays scattered and highly variable values. The faulted crystalline rocks (FCR) studied are located in Canada while the altered crystalline rocks (ACR) studied are located in France. Because the sequences and values of n are different between the 2 groups, they were analyzed separately.

The FCR group of pumping tests, which produced 24 distinct flow regimes with 13 pumping tests, showed various n values characteristic of long-lasting flow regimes. The most significant n values are 1 – 2.5 – 2 – 1.5, representing, respectively, 38%, 21%, 17% and 8% of the FCR n , and lasting, respectively, 1.6, 1.5, 0.9 and 2.7 log-cycles (Figure 3.10a).

The occurrence of linear ($n = 1$) and bilinear flow regimes ($n = 1.5$) in these environments corroborate their common conceptual interpretation as expressing the presence of conductive fractures: $n = 1$ has been attributed by Gringarten et al. (1974, 1975) to an infinite-conductivity fracture and by Cinco-Ley et al. (1978) and Cinco-Ley et Samaniego-V. (1981b) to a finite-conductive fracture (early pumping time). The first conceptual model assumes a matrix linear flow originating from the uniformly depressurized fault, which consequently acts as a planar source, while the second model stipulates a linear flow occurring into the fault before the embedding matrix is depressurized. The embedding environment is assumed to behave like a continuous porous media, which means that the fracture network is dense with a sufficiently high degree of connectivity. Obviously, any flow

model that produces a diffusion of the cross-flow area that does not change with distance will produce a linear flow regime. Linear flow regimes may also be produced in hard rock aquifers from one-dimensional flow conduits formed at the intersection of two fractures or faults (Equation (3.1)), in channels along the fault plane (Figueiredo et al. 2016) or when a fracture set controls the flow in one direction.

The value $n = 1.5$ has been associated with an aquifer composed of a vertical finite-conductive fault supplied by a continuous Theissian matrix with a hydraulic conductivity lower than the fault (Cinco-Ley et al., 1978; Cinco-Ley and Samaniego-V., 1981b; Rafini and Larocque, 2012).

The fractional values of n which range between 1 and 2 (e.g, $n = 1.2$ or $n = 1.7$) have not to this date been assigned a conceptual description (with the exception of $n = 1.5$). Some assumptions on the physical interpretation of sub-radial flow dimensions can however be made regarding the properties of faulted/fractured networks, the distribution of transmissivity around the well and the geometry of faults or boundaries. The only limitation is that the diffusion of the pressure disturbance must satisfy Equation (3.1). For instance, as stated by Bowman et al. (2012), n is influenced either by the geometry of flow conduits or by leakage effects into the conduits. According to Raghavan (2004), a decreasing permeability with distance from the wellbore leads to an increase of the $ds/d\log t$ signal ($0 < n < 2$). Several authors have associated fractional flow dimensions to the scale-invariant properties of fracture networks (Chang et Yortsos 1990, Bangoy et al. 1992, Acuna et Yortsos 1995, de Dreuzy et al. 2000, Doughty et Karasaki 2002, Walker et al. 2006). Following this principle, it has been shown that fractional flow responses represent to a diffusion slow-down into

fractal networks, and n is a function of the fractal dimension and the anomalous diffusion coefficient which likely indicates the presence of connectivity. More recently, Figueiredo et al. (2016) interpreted the sub-radial flow dimension values to be related to the density of channel intersections (or when a fracture is intersected by more than one inflow and one outflow fractures) and local heterogeneities as a function of distance from the pumping well.

The sub-spherical flow regime ($n = 2.5$) also occurs predominantly in our study. By analyzing both the lithostratigraphy of wellbore loggings and n , we observe that this flow regime is statistically correlated with fractured rocks that are supplied by an overlying granular horizon. Obviously, further field data and consistent numerical results are needed to establish any link between this flow dimension and possible leakage effects. However one author, Doe (2002), stated that for a planar conductor (a horizontal and tabular aquifer) generating a radial flow regime, « leakage over the conductor surface may lead to a dimension somewhat greater than 2 » (no proof was presented). This phenomenon will be investigated in future works.

Note that 23% of cases in the FCR group show negative unit slopes of the $ds/d\log t$ signal, which suggests that there are transitions to higher values of hydraulic properties (Rafini et al., 2017) or transitions to another flow dimension value (Rafini and Larocque, 2012) or transitions to constant-head boundary conditions (Walker and Roberts, 2003). Transitions in FCR aquifers reflect heterogeneity of the fractured media. When constant-head boundary effects are observed in the FCR aquifers, this reflects the existence of hydraulic relationships between the fractured media and lakes or rivers on the surface, or may reflect a significant

increase of the hydraulic conductivity or of the storage coefficient (for instance, a system of minor faults intersecting a major fault).

The ACR group, composed of 6 pumping tests and 10 n values, is represented by flow dimension values ranging from 0.6 to 3.5 (Figure 3.10b). The spherical and the radial flow dimensions are frequently observed and each represent 18 %, but the radial flow is only observed during a short period of time. The radial flow dimension is observed at early times or at late times, depending on the derivative signatures. The ACR group is composed of sub-linear ($n = 0.8$), linear ($n = 1$), sub-radial ($n = 1.4 - 1.5 - 1.6 - 1.7$), radial ($n = 2$), sub-spherical ($n = 2.7$), spherical ($n = 3$) and hyper-spherical-spherical ($n = 3.5$) flow dimensions. Comparatively to the FCR group, the ACR group demonstrates a lesser proportion of linear flow values and a greater proportion of n values higher than 2.7. The spherical flow dimension is observed in the ACR group, whereas it is not observed in the FCR group. These features may be expressions of the effects of chemical alterations on FCR aquifers. Indeed, chemical alteration increases the fracture density and the connectivity between fractures, leading to a thicker flow media in which the pressure front pulse can expand more easily. The altered rock aquifers are characterised by granitic sand overlaying a fractured-weathered layer, requiring the use of a screened borehole. Chemical alteration processes tend to increase the connectivity of existing fractures, leading to an enhancement of the permeability of hard rock aquifers (Lachassagne, 2008; Lachassagne et al., 2011; Worthington et al., 2016). According to these authors, chemical processes such as the swelling of certain minerals can widen fractures. As may be expected, such expansion of the volume and hydraulic activity of fractures is revealed by a statistical increase of the flow

dimension, as observed here, as well as a higher occurrence of the spherical flow regime. In this context, the spherical flow regime likely reflects conditions of a partially penetrating well, in other words, a situation in which a full volume aquifer which has a thickness much greater than the screened or open-borehole window (Escobar et al., 2012a; Ferroud et al., 2015a). This supposes that the density and connectivity of the fracture network are sufficiently high, presumably as a consequence of weathering, for the network to behave like a three-dimensional continuum. Conceptually, the well is associated with a point source involving a cross-flow area expansion in the form of concentric spheres. The value of n greater than 3 ($n = 3.5$), which is a long-term and low-noise signal (Figure 3.11), is enigmatic and requires more field and numerical investigations in order to be better understood. However, we provide some possible explanations in the general discussion section.

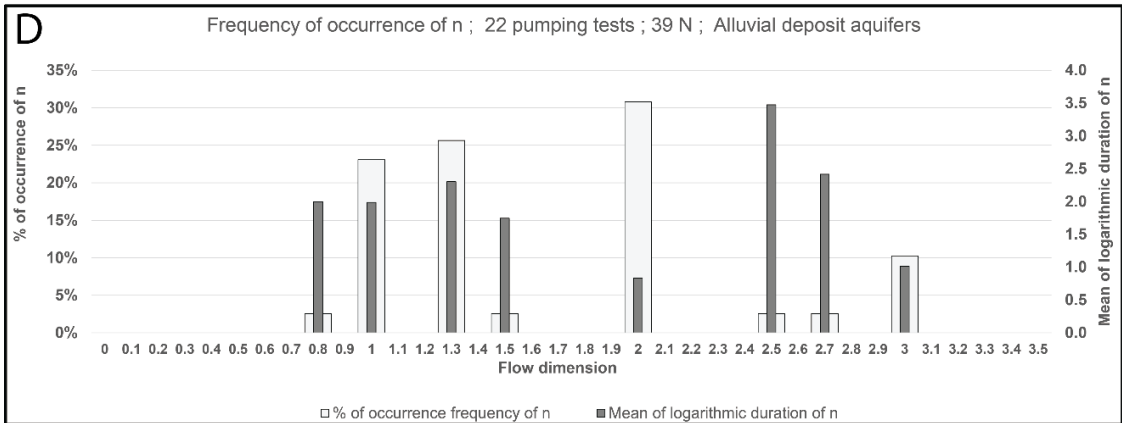
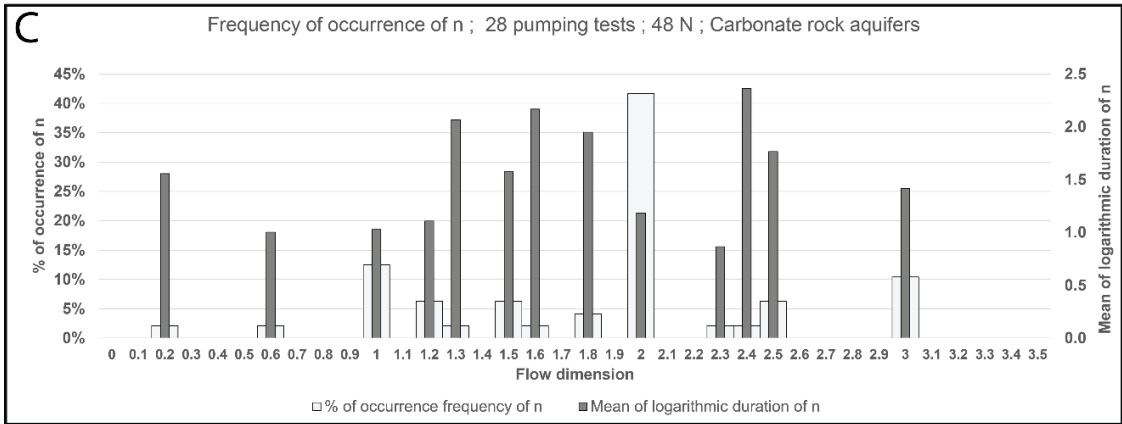
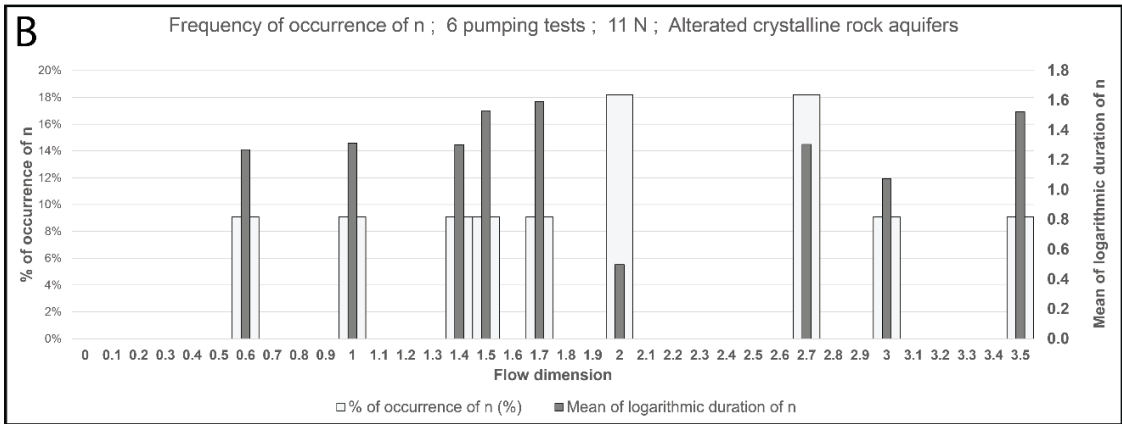
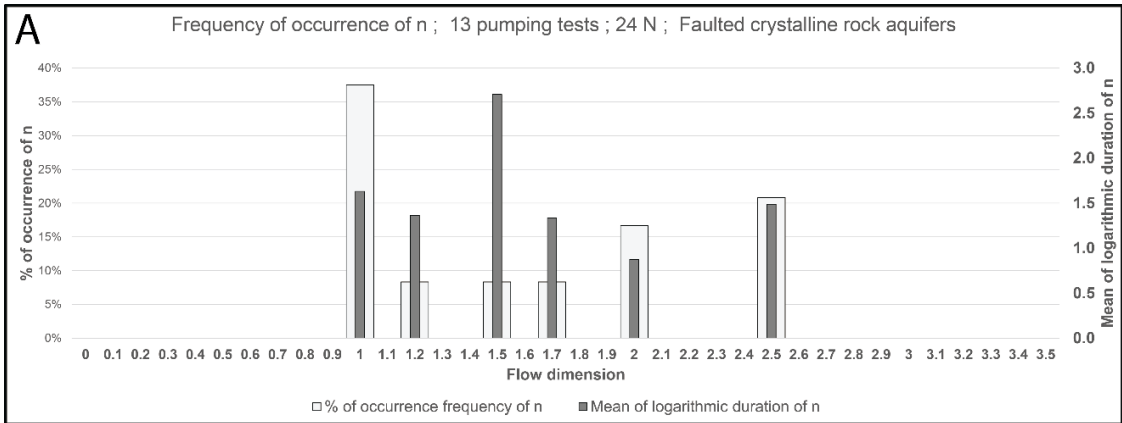


Figure 3.10: Statistical analysis of the flow dimension occurrence in 69 constant-rate pumping tests performed A) in altered crystalline rock aquifers, B) in faulted crystalline rock aquifers, C) in carbonate rock aquifers and D) in alluvial deposits. The flow dimension was manually estimated based on a sequential analysis. The large dark bars that represent the flow dimension occurrence are read on the left y-axis. The thin clear bars that represent the mean logarithmic duration of n are read on the right y-axis. The “N” in the graph titles represents the number of observed flow dimensions.

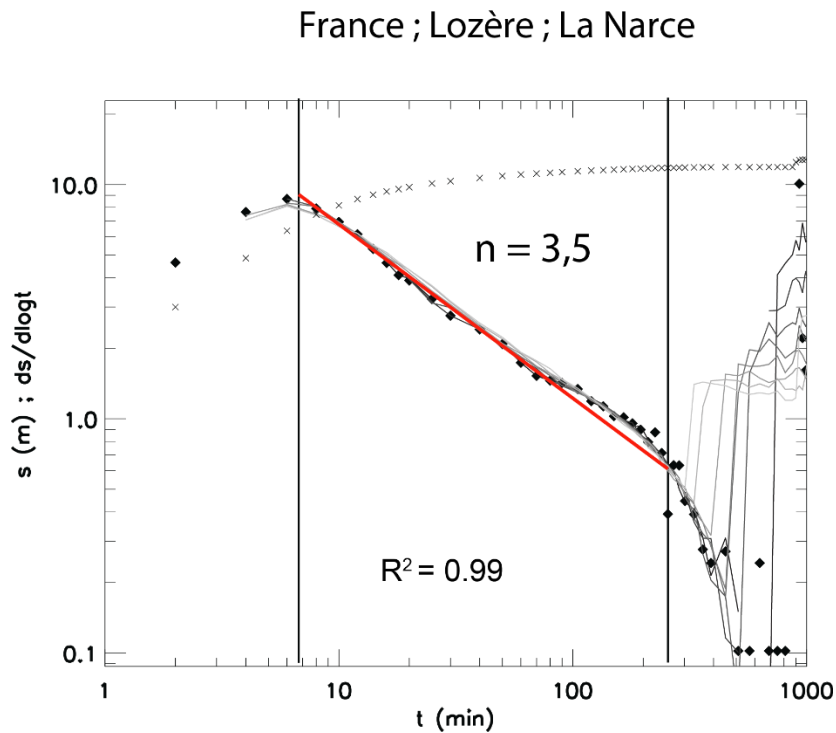


Figure 3.11: Example of a diagnostic plot with a flow dimension value greater than 3 ($n = 3.5$). The diamond shapes represent the drawdown log-derivative signal and the “x” shapes represent the drawdown signal. The well test was performed in a weathered crystalline rock located in France. The fit is performed using the SIREN code. The quality of the manual fit is evaluated using the determination coefficient R^2 between the regression line and the derivative data. The $n = 3.5$ is assumed to be induced by a partially penetrating/completed/screened well which is influenced by leakage.

3.5.2.2.2 Carbonate aquifers

The histogram of carbonate rock aquifers was established based on 29 pumping tests located in the regions of Mirabel, CHCN, SLSJ (Quebec), Nord-Pas-de-Calais, Midi-Pyrénées (France) and Kef (Tunisia). The most observed n values are: $n = 2 - 1 - 3 - 1.2 - 1.5 - 2.5$ representing, respectively, 42%, 13%, 10%, 6%, 6% and 6% of the carbonate group, lasting, respectively, 1.2, 1, 1.4, 1.1, 1.6, 1.8 log cycles (Figure 3.10c).

In terms of the ratio between the frequency of occurrence of n and its average log-duration, the radial flow regime is the most significant. (Rafini and Larocque, 2012) demonstrated that a radial flow regime can be generated by horizontal faults. Jourde et al. (2002) stipulated that a radial flow regime can be observed in an orthogonal discontinuity network when the fractures are well-connected. In general, when the pressure front-pulse is large enough, smaller occasional heterogeneities will exert only a negligible impact on the large-scale flow behavior. In such a case, the aquifer would be associated with an equivalent continuous media where a radial flow regime is feasible.

Furthermore, in fractured carbonate rocks, the flow is supposed to be mainly governed by horizontal plane fractures that are cross-connected by vertical fractures (Novakowski and Lapcevic, 1988; Zanini et al., 2000). Such a conceptual model is well-supported by the large proportion of $n = 2$ values reported in these environments. The early-time radial flow observed in our database may indicate that the bedding plane fractures are well-connected and contribute to the flow. Whereas the late-time radial flow may be associated with the continuous-like fracture network contribution at large scale. When the cross-flow area is large enough, the fractured dolomite, which generally presents a well-developed fracture

network that is cross-connected to a less-developed bedding plane fracture network, is also favorable to the development of a radial flow dimension. Finally, conceptual models with horizontal planes that exhibit only plane beddings, such as those composed of pure non-fractured limestones, are also favorable to the establishment of a radial flow dimension (Rafini and Larocque, 2012).

Figure 3.10c shows the presence of $n = 1$, implying the influence of a vertical fault or an intersection of faults. The size of the discontinuity may be understood based on the time-period during which the flow regime occurs: an early-time linear regime may be due to a submeter scale vertical fracture, while a late-time linear regime may reveal the presence of large-scale vertical faults. On the contrary, the value of $n = 1.5$ expresses the presence of a leaky-vertical fault supplied by a conductive matrix embedded in the fracture network, which is sufficiently transmissive and connected in order to significantly feed the fault.

The fractional values of flow dimension (non-integer n values) are commonly interpreted to be associated with the fractal properties of fractured rock systems (crystalline or carbonate aquifers). The fractal flow models assume that the fractured rock is composed of scale-invariant fracture geometries. When during a same pumping test a sequence of integer and non-integer values of n are observed, this compromises the fractal theory which is based on assumptions regarding the homogeneity and density of fractures. The mismatch between the fractal dimension and n has been reported (Rafini and Larocque, 2012; Verbovšek, 2009). Indeed, Verbovšek (2009), using a statistical approach, shows that the fractal dimension parameter (obtained by the classic box-counting method) and n (obtained by an automated type-curve matching of the drawdown log-derivative signal) are not correlated.

He interprets the fractional n values as being related to the degree of connectivity between the fractures.

Carbonate rocks are the context with the most variable flow dimension values. The values range between 0.2 and 3 with fractional sub-radial flow dimensions of $n = 1.2 - 1.3 - 1.5 - 1.6 - 1.8$ and sub-spherical flow dimensions of $n = 2.3 - 2.4 - 2.5$. This variability in flow dimension reflects an important variability of fracture and fault configurations. As shown by the thin dark bars of Figure 3.10c, these flow dimensions are generally stable and long-term. This variability in the n values reflects environments with a variability of fractures and/or fault configurations.

Some pumping tests performed in carbonate rock aquifers exhibit late times unit slopes. In the petroleum literature, such a flow regime is commonly associated with a reservoir that is depleted with no spatial diffusion of drawdown (among others, Ehlig-Economides and Vera (2013) and Mattar (1997)). In other words, the no-flow boundaries have been attained. This assumption is consistent with carbonate systems, where sealing faults are frequent due to self-forming calcite or clay seals. This late time unit slope may express the attainment of sealing faults or impermeable boundaries in every direction. Observing this signal in CFR aquifers suggests either that the productive zones are limited to specific fracture zones in the vicinity of the pumping well, or that sealed faults are frequently reached by the pressure wave.

Negative unit slopes are also observed between some flow dimensions and may reflect a transition period between two flow dimensions or may be related to a significant change in hydraulic conductivity. For instance, the dual-porosity model (Warren and Root, 1963) assumes a transitional flow period between two radial flow regimes which represents, firstly, the water supply from the fracture network and secondly, the water supply from the matrix. (Rafini and Larocque, 2012) show that when a finite-conductive vertical fault is not connected to the well, a transitional flow period is observed between the radial flow through the matrix and the bilinear flow through the leaky fault. The frequent occurrence of negative unit slopes thus expresses heterogeneous media with participation of several flow regimes.

3.5.2.2.3 Fluvial-glacial deposit aquifers

The fluvio-glacial-deposit (FGD) histogram generated in this study comprises 22 pumping tests conducted in the regions of CHCN and SLSJ (Quebec) and the eskers of the Abitibi region (Quebec). The most prominent flow dimensions, in terms of frequency of occurrence and duration, are represented by $n = 1.3$ and 1, representing, respectively, 20% and 17% of the FGD group (composed of 46 n values), lasting respectively 2.2 - 2.3 log-cycles (Figure 3.10d).

All the pumping tests performed in the eskers of the Abitibi region showed a long-term and single-stage pseudo-linear flow regime ($n = 1.3$). The linear flow regime in fluvioglacial deposits has until now seldom been investigated. Two studies interpreted the linear flow in granular aquifers to be related to two different contexts:

- i) a long and narrow system which channels the flow between two parallel impermeable hydraulic boundaries or low-permeability levees (Escobar et al., 2004b; Escobar and Montealegre-M, 2007). Such systems may be observed in channelized deposits such as glacial hollows filled by sediments or eskers.

- ii) Micro-cross flow within non-communicating layers. Indeed, by modelling pumping tests in fluvial deposits, Corbett et al. (2012) observed that the deposit systems, formed by the transport and deposition of sediments, exhibit characteristics of hydraulic conductivity distribution, anisotropy and geometry which strongly influence the hydraulic behavior of these systems. They showed that a decrease of lateral transmissivity and a poor lateral connectivity of facies favor the development of an increasing slope of the derivative signal (which implies a linear/pseudo-linear n), which they named the “ramp” effect.

As stated by Corbett et al. (2012), the internal properties of fluvial sediments are valuable assumptions which greatly contribute to the interpretation of such linear flow regimes. Being long and narrow systems, eskers are fluvio-glacial deposits whose geometry favors the establishment of linear flow regimes. However, the pseudo-linear flow regimes observed in the database are more enigmatic. More field and numerical studies are needed to determine the geological facies involved in such flow regimes.

A significant number (8 %) of spherical flow regimes are reported in this study, notably in thick deposit aquifers. These systems, characterized by a screen thickness significantly smaller than the aquifer thickness, favor the establishment of $n = 3$. In some cases, the

variable thickness aquifer is a more valuable conceptual model to explain this value of n . For instance, one of the pumping tests, showing a spherical flow, was performed in a topographic depression that had been carved and then filled by glaciers. The geometrical increase of the aquifer thickness associated with the depression favors the establishment of a spherical flow regime (Dal Soglio, 2012; Rafini and al., 2014).

The FGD group displays early unit negative slopes of the $ds/d\log t$ signal which may indicate a transition period between the wellbore effects and the aquifer's signal (Tiab, 1995). It is not surprising to observe wellbore effects more frequently in deposit aquifers than in fractured aquifers, because granular boreholes require a screen which may induce skin effects, while the borehole dug into fractured rock is a simple open hole without a screen.

As explained above, fractional n values are widely interpreted to reflect the fractal properties of the fractured rock media, an interpretation that is challenged by the observation of frequent non-integer values of n in granular aquifers, mostly in the range of 1 to 2.

It should be noted that no relationship between n and the confinement conditions of the aquifer (confined/unconfined) has been observed. The typical type-curve provided by Neuman's solution has not been observed either.

3.6 DISCUSSION

This study has collected and summarized the flow dimension values of several pumping tests and reviewed the current published assumptions used to interpret these flow dimension values. Any flow model where the transient flow area changes by a certain value of the power of the distance to the well corresponds to a specific flow dimension. This is the reason why the assumptions presented in the “Result and discussion” section are non-unique; it is possible for different hydraulic and geometrical configurations to yield a same value of flow dimension.

When conducting the n -sequential analysis, it is important to keep in mind that the propagation of the pressure front-pulse is a diffusive process, and that the drawdown behavior is governed by averaged conditions rather than by local heterogeneities (Horne, 1995). Furthermore, the flow dimension is not an integrative value that would represent a combination of all the flow regimes. Rather, it is an apparent value that reflects the dominant flow regime which influences the cross-flow area diffusion felt by the pressure-front pulse. For instance, as modelled by Rafini and Larocque (2012), a vertical leaky fault located in a homogeneous matrix generates the n -sequence 1.5 – 2, reflecting, firstly, the influence of the fault and secondly, the influence of the matrix. Under no circumstance will the second n express a mean value between the two flow regimes. Rather, it should be underlined that the second flow regime is a value that expresses the flow regime related to the most influential flow of the hydrogeological facies. The sequences of n can thus be interpreted independently and successively. Because each flow regime observed during a single pumping test exists independent from any other, it is conceivable to interpret an n -sequential

signal by successively matching various analytical solutions (as done by Hammond and Field (2014)).

The drawdown log-derivative signal and Barker's law help in better interpreting the flow regime occurring during a constant-rate pumping test. In order to use the flow dimension value as a diagnostic tool, it is important, however, to keep in mind that the cross-flow area is growing as the pressure wave is diffused through the aquifer. Due to the expansion of the cross-flow area, a variation in the observational scale must be considered. Hence, the sensitivity of the transient well test signal to small heterogeneities diminishes as the radius of investigation increases. Beauheim et al. (2004) highlighted the importance of considering the scale when analysing the flow dimensions of pumping tests in a heterogeneous aquifer. They stated that for a single pumping well, different estimated flow dimensions can be obtained, depending on the pumping test method used. Indeed, some of these pumping tests may not have the same radius of investigation, such as for instance slug test compared to pumping test. It is worth noting that the extent and the diffusion rate of the radius of investigation is independent of the pumping rate, because it is an intrinsic value only associated with the diffusive properties of the aquifer (transmissivity and storage).

The interpretation of flow regimes employs successive linear regressions on derivative data, into several time windows. The recognition of these time windows, and the confidence this provides for the interpretation of flow dimension, remains a sensitive aspect of the approach that may, in some cases, leave uncertainties. A manual interpretation is recommended rather than any automated process which optimizes regression coefficient sequences. Indeed, the quality of regressions is not the only component of a proper interpretation of flow

regimes: a manual analysis of derivative data makes it possible to identify pumping rate stops or changes, to award a lesser degree of significance to certain noisy sections that have a more obvious and greater degree of data instability – either instrumental, due to a temporary high diffuse heterogeneity field, or for other reasons. Furthermore, the practitioner conducting a manual interpretation may benefit from derivative differentiation without being misled by it, in other words, to “stick to raw data”. We finally submit that a simultaneous fit on both s and $ds/d\log t$ significantly contributes to reducing subjectivity issues regarding the interpretation of flow regimes.

A major issue of any derivative analysis remains the quality of the data. Even though derivative data are, advantageously, highly sensitive to hydrodynamic changes in the aquifer, they are also strongly impacted by noise sources, either natural or instrumental. It is not rare that noise impedes any confident and unique interpretation of derivative curves. As stated by Anderson et al. (2006), interpreting a pumping test without taking data quality into account can lead to the erroneous understanding of aquifer features. Various differentiation methods are proposed in the literature to improve the signal/noise ratio. The deconvolution techniques, initially proposed by Birsoy and Summers (1980) in hydrogeology and by von Schroeter et al. (2001) and Azi et al. (2008) in the petroleum industry, make it possible to assess the equivalent constant-rate drawdown of a variable-rate test. The practice is extremely popular in petroleum studies to process the transient tests before their interpretation (Azi et al., 2008, Gringarten 2010, Onur et Kuchuk 2012, Obeahon et al. 2014). These approaches require knowledge of the drawdown s , the time t and the pumping rate Q . It may be advantageous to adopt this data processing practice in hydrogeology studies

in order to improve the accuracy of interpretations. However, the deconvolution tools could not have been integrated in this study due to the lack of detailed pumping rate survey data.

Even though variations in pumping rate steps do not influence the estimation of the flow dimension (because single variations do not change the general trend of the derivative signal and may, thus, be disregarded in the analysis), each pumping rate adjustment strongly affects the derivative signal by generating significant noise. Thus, analysing the recovery data appears to be a favorable option. Practitioners must, however, be aware that drawdown and recovery signals are not necessarily similar. As stated by Mattar (1997, 1999), the differences between the drawdown and the buildup data appear when the test is affected by aquifer heterogeneities or boundaries. Because the analytical type curves are mostly configured for drawdown, the drawdown data are needed to estimate the hydraulic properties. The buildup signal should be interpreted qualitatively, in addition to the drawdown data (because it is not subject to disturbances caused by changes in pumping rate). The buildup signal should indeed be analyzed in order to help with the diagnostics rather than for quantitative analysis.

When using the derivative signal in order to estimate the hydraulic properties of the aquifer, it is important to keep in mind that i) the flow dimension value can reflect the geometry of the aquifer and/or the geometry of the well and/or the geometry of the flow and/or the geometry and connectivity of fractures (in fractured media); and ii) certain mechanisms can disrupt the signal of the aquifer. In early times, the signal of the aquifer can be masked or disrupted by wellbore effects. At middle times, the aquifer's signal can be influenced by rain infiltration or leakage. At late times, the signal of the aquifer can be masked by boundary

conditions. When interpreting flow regimes, it is therefore important to have good knowledge of the environment surrounding the well and the conditions of the pumping tests. Further numerical simulations are needed to i) distinguish such effects from the aquifer's signal and ii) develop analytical equations for non-radial flow regimes.

The spherical flow dimensions of the entire database were analysed, in order to correlate the well conditions of a partial penetrating/completed/screened pumping well with the frequency of occurrence of the spherical flow dimension. The spherical flow dimension is observable in 10 pumping tests, four of which were performed in alluvial deposits, two in weathered crystalline rock aquifers, three in carbonate rocks and one with a screen intercepting both a carbonate rock and a moraine (Table 3.6). According to Escobar et al. (2012), the early-times flow dimension is significantly influenced by the penetration ratio of the pumping well. Moncada et al. (2005) explained that the typical -0.5 slope of the $ds/d\log t$ signal, which is characteristic of the spherical flow dimension, is absent for penetration ratios greater than 40%. Based on this knowledge, we interpret three pumping tests to be related to partial penetration effects because the penetration ratios are lower than 29% (Table 3.6). The pumping well of La Narce shows a long-term and weakly noisy signal with $n = 3.5$ (Figure 3.11). We suggest that this hyper-spherical flow dimension may reflect a partial penetrating well effect combined with leakage effects. We will discuss this assumption in the next paragraph. Unfortunately, three pumping tests with $n = 3$ are not interpretable due to a lack of data or poor conditions (the static level is 0.77 m above the top of the screen and the dynamic level is below the top of the screen). Finally, three of the signatures show a spherical flow dimension but cannot be interpreted with the partially penetrating well effects,

suggesting that other conditions may produce such a spherical flow dimension. The non-unicity of the derivative signal has already been reported in the literature and will be discussed in the next sections. More field and numerical analyses are thus needed to interpret these pumping tests.

This paragraph aims at providing some thoughts about Barker's model and widening the concepts of the flow dimension parameter that may be related to leakage effects. Since the initial development of the GRF model by Barker (1988), the interpretation of the flow dimension has been extended. As previously explained in section 1.2.2, the fractal interpretation of fractional values has been open to non-space filling (Doe, 1991), non-fractal fractured media settings (Giese et al., 2017; Jourde et al., 1998; Maréchal et al., 2008) and non-homogeneous systems (Rafini and Larocque, 2009). Rafini and Larocque (2009, 2012) explained that a vertical fault, which is expected to induce a linear flow dimension ($n = 1$), actually produces a bilinear flow dimension ($n = 1.5$), because the flow from the matrix supplies the fault. Furthermore, we observed a statistical correlation between the sub-spherical flow dimension ($n = 2.5$) and the fractured rocks that are supplied by an overlying granular horizon. In addition, Doe (2002) explained that a media inducing a radial flow dimension, which is supplied by leakage, "may lead to a dimension somewhat greater than 2". These observations lead us to suppose that the sub-radial flow dimensions ($2 < n < 3$) may reflect a system that induces a radial flow dimension which is supplied by leakage. Also, we observed a sub-radial flow dimension ($n = 1.3$) in eskers that are highly transmissive flow conduits supplied by surrounding alluvial deposits. In the same line of thought, the esker flow system is expected to induce a linear flow dimension. But leakage around eskers results

in increasing linear flow dimension to reach sub-radial flow dimension. Thus, a system supplied by leakage seems to induce a flow dimension somewhat greater than expected. Based on this observation, a point source system or a partially penetrating well (that produces $n = 3$), which is supplied by leakage, may induce a hyper-spherical flow dimension. Indeed, we observe a hyper-spherical flow dimension ($n = 3.5$) in the La Nacre weathered crystalline rock (fourth line of Table 3.6 and Figure 3.11). We assume that this value reflects the signal of a partially penetrating well (expected to induce $n = 3$) that is supplied by leakage. This assumption is in line with the conceptual models of weathered crystalline rock aquifers (Lachassagne, 2008; Lachassagne et al., 2011; Worthington et al., 2016).

Table 3-6: Summary of the pumping tests that show a spherical or a hyper-spherical flow dimension (highlighted in bold in the n -sequence column) with their intercepted aquifer thickness, their screen thickness and the ratio between both thickness and our interpretation of the spherical flow dimension. In the “location” column, the abbreviations CHCN, SLSJ and Qc designate, respectively, Charlevoix-Haute-Côte-Nord, Saguenay-Lac-Saint-Jean and Quebec. In the “ n -sequence” column, the abbreviations MG, G and VG represent the appreciation of the quality of the $ds/dlogt$ signal and signify, respectively, mediocre-good, good and very good. The letter (U) indicates either an undefinable slope of the $ds/dlogt$ signal or a slope that has not been considered as a flow dimension, but rather as a transition or a boundary effect.

Location	Pumping well name	Simplified geology	Confinement condition	n -sequence	Intercepted aquifer thickness (m)	Screen thickness (m)	Penetration ratio	Remarks and interpretations of $n = 3$
Baie-Saint-Paul (CHCN, Qc)	P-1	Alluvial deposits	Confined	2 (MG); 3 (VG) ;	27.3	8	29%	Partial penetration
Saint Siméon (CHCN, Qc)	P-1	Alluvial deposits	Confined	2 (M); (U); 3 (MG) ; 2 (MG); 1 (G);	39.32	0.99	3%	Partial penetration
Saint-Félicien (SLSJ, Qc)	PE-3	Carbonate rocks+ Alluvial deposits	Confined	2 (MG); (U); 3 (G) ;	10.5	3.05	29%	Partial penetration
Lozère (France)	LaNarce	Weathered crystalline rocks	N/A	2 (M); 3.5 (VG) ; (U);	116	18	16%	Partial penetration + leakage
Longue-Rive (CHCN, Qc)	P-1	Alluvial deposits	Confined	1.3 (M); 3 (VG) ; 2.7 (MG);	9.75	5.56	57%	Other conditions
Pays de la Loire (France)	Mout_3	Weathered crystalline rocks	N/A	(U); 3 (VG) ; (U);	74.36	40	53%	Other conditions
Mirabel (Qc)	StJanvHamel	Carbonate rocks	N/A	1 (MG); 3 (MG) ; 1 (MG);	N/A	0	N/A	The pumping well is located in a fracture; $n = 3$ may represent a transition between the two linear flow dimensions.
La Malbaie; Joyeuse (CHCN, Qc)	PP-5D	Alluvial deposits	Unconfined	1 (MG); 3 (G) ; 2 (MG);(U);	4.04	3.05	75%	The static level is 0.77 m above the top of the screen
Midi-Pyrenees (France)	Faha	Carbonate rocks	Partially-confined	(U); 3 (MG) ; 2 (MG);	N/A	30	N/A	Lack of data
Mirabel (Qc)	MT2	Carbonate rocks	N/A	(U); 3 (MG) ;	N/A	0	N/A	Lack of data

3.7 CONCLUSION

Based on 69 constant-rate pumping tests, this study presents an overview of the occurrence in nature of the flow dimension parameter in fractured/altered crystalline rock aquifers, carbonate aquifers and fluvio-glacial deposit aquifers. The database is provided in Appendix 1 - Table 3.7.

The real flow dimension statistics obtained in this study emphasize the generally major prevalence of non-radial flow regimes in nature, expressed by a wide diversity of n values. Indeed, the flow dimension values obtained in this study range between 0 and 3.5 with 69% of the 121 interpreted flow dimensions producing a value for n that is different from 2.

A key element of information obtained in this study is that the flow dimension analysis delivers results that are significantly different from one geological setting to another in terms of n values, variability of the duration of n and n sequences. More particularly, the most statistically significant flow dimensions (in terms of duration and frequency of occurrence) display a higher degree of correlation with the geological conditions around the well. This shows that the hydrodynamic interpretation of these flow dimensions has a physical expression that may relate to the geological framework. This confirms the positive association between conceptual models and flow dimension analysis. For instance, faulted hard-rock aquifers exhibit a high proportion of linear flow regimes, which may express drawdown diffusion through inclined or vertical faults embedded into no-flow boundaries, or one-dimensional flow conduits formed by an intersection of faults. Pumping tests performed in altered crystalline rocks and thick alluvial aquifers preferentially produce spherical and

pseudo-spherical flow regimes. These can be related to partial completion/penetration of wells or partial screening effects, which produce point sources generating spherical equipotential surfaces or any aquifer's configurations that may lead to a proportional relation of the cross-flow area $A(r)$ and r^2 . Fluvio-glacial aquifers exhibit a high frequency of single-stage linear or pseudo-linear responses. These were related to channelized shapes typical of fluvio-glacial environments, such as eskers or micro-cross flows which result from internal heterogeneities within the granular layers. It is interesting to note that, contrary to common opinion, the radial flow assumption is in many cases not suitable to model granular aquifers of the database. Finally, carbonate-rock aquifers exhibit a high proportion of radial flow regimes, interpreted either as the influence of conductive horizontal strata or of large-scale equivalent continuous media.

The use of derivative data allows for a much greater degree of uniqueness of the interpretative type-curves as compared to drawdown-only. Observing similar flow dimensions in different geological facies raises the issue of non-uniqueness of the log-derivative signal. For instance, linear flow regimes have been observed in both fractured rock and fluvio-glacial-deposit aquifers. As stated by Mattar (1997), several conceptual models predict identical $ds/d\log t$ type-curves, but the estimated aquifer parameters (geometry, hydraulic properties) will be very different from one model to the other. Massonnat and Bandiziol (1991) and Liang et al. (2012) point out the critical insights regarding the geological context to take into account when choosing the adequate analytical model. An interesting continuity of this paper would be to review all the sequences of n that are observed in nature and analytically modelled, in order to assess the potential

advantages of using the n -sequential approach to improve the uniqueness of $ds/d\log t$ interpretations.

Finally, our compilation revealed that in natural aquifers, radial flow regimes occur quite infrequently, representing, overall, 31% of the flow regimes that were interpreted for this study. Most of the radial flow dimensions were generally observed at early times and were mostly related to a short and noisy signal. In view of these results, it is remarkable that most interpretative models available in the literature describe various types of combined or modified but still radial behaviours, within the radial interpretative framework. This demonstrates that current and common interpretations, using either Theis or Theis-derived models, are in fact hydraulic approximations as they do not account for the real dimension of flow in aquifers. This calls in question the reliability of any interpretative model that does not integrate a flow dimension analysis. New knowledge about occurrences of n in nature may provide impetus to the development of new non-radial flow conceptual models more representative of observed real situations and, more globally, to further research on the flow dimension parameter. The analysis and interpretation of aquifers based on the results of pumping tests might in fact be in its infancy.

A common, yet non-consensual, conceptual interpretation of fractional flow dimension consists in relating it to a gain or a loss of connections in fractures networks with increasing investigation scale (e.g. Leveinen 2000). However, our compilation of n -values occurrences in various geological contexts indicate that such fractional flow dimensions do not occur more likely in hard-rock than in granular settings (Figure 3.10). This leads to consider other avenues than fractured networks for the conceptual interpretation of fractional flow regimes.

Furthermore, the databased highlighted correlations between some fractional n values and leakage. In fact, some sub-radial (e.g. $n = 1.3$), sub-spherical (e.g. $n = 2.5$) and hyper-spherical (e.g. $n = 3.5$) flow dimensions seem to be related to conceptual models, which are influenced by leakage and which were expected to produce respectively, a linear, a radial and a spherical flow dimension. It has already been established that a vertical fault (expected to induce a linear flow dimension) which is supplied by the matrix produces a bilinear flow dimension ($n = 1.5$) (Rafini and Larocque, 2009). We planned to numerically investigate the issue of leakage in order to confirm our assumptions based on field observations.

From a more practical viewpoint, we now know with more certainty that automatically assuming that a flow regime is radial may lead practitioners to over- or under-estimate the hydraulic properties of the aquifers they are studying. Non-radial flow regimes will typically generate investigation areas whose shape is different from that of a regular circle produced by a cylindrical-radial flow. Consequently, in most real-life cases, WHPA delineation may be significantly biased because of erroneous postulates regarding flow dimension regimes. When a radial flow is observable on a log-log plot of $ds/dlogt$, the hydraulic conductivity of the aquifer is accurately estimated when using the radial derivative analysis (Equation (3.14)). Aquifer evaluation may be improved by analysing the duration and sequences of the flow dimension as it directly relates to the geometrical diffusion of the pressure front-pulse. Further research work is needed in order to develop equations that estimate the hydraulic properties of a non-radial flow regime aquifer and to better understand the physical meaning of fractional flow dimensions. Finally, we recommend improving hydrogeological pumping test practices through the inclusion of the flow dimension analysis in the pumping test

interpretation. In particular, both the head and the pumping rate should be accurately measured using a logarithmic time step. It should be remembered that the derivative signal is very sensitive to small variations of the drawdown and the pumping rate. Pumping rate adjustments will generate noise in the derivative signal and pumping rate drifts can induce an apparent flow dimension, which is different from the equivalent constant-rate flow dimension.

3.8 ACKNOWLEDGMENTS

The authors acknowledge the financial support of the Natural Sciences and Engineering Research Council (NSERC – federal funding) of Canada in the framework of the Individual Discovery Grant Program as well as the “Fonds de Recherche du Québec Nature et Technologies (FRQNT – provincial funding)” in the framework of the individual grant “Nouveaux-chercheurs” held by Prof. Romain Chesnaux. We also thank the municipalities of Charlevoix-Haute-Côte-Nord (Quebec) and the environmental government of Quebec (MDDELCC, Développement durable, Environnement et Lutte contre les changements climatiques) for their financial support. Ms. Josée Kaufmann is thanked for editorial collaboration. Data were supplied by Geological Survey of Canada (GSC), the French Board of Geological and Mining Research (BRGM) and the Ministry of the environment of Quebec (MDDELCC). We also thank the anonymous reviewers and Dr. Doe for their valuable comments that have greatly improved the quality of this manuscript.

3.9 REFERENCES

- Abbaszadeh M, Cinco-Ley H (1995) Pressure-transient behavior in a reservoir with a finite-conductivity fault. *SPE Form Eval* 10:26–32 . doi: 10.2118/24704-PA
- Acuna JA, Yortsos YC (1995) Application of fractal geometry to the study of networks of fractures and their pressure transient. *Water Resour Res* 31:527–540 . doi: 10.1029/94WR02260
- Anderson D., Scotts GW., Mattar L, et al (2006) *Production Data Analysis--Challenges, Pitfalls, Diagnostics*. Society of Petroleum Engineers
- Audouin O, Bodin J (2008) Cross-borehole slug test analysis in a fractured limestone aquifer. *J Hydrol* 348:510–523 . doi: 10.1016/j.jhydrol.2007.10.021
- Azi AC, Gbo A, Whittle T, Gringarten AC (2008) Evaluation of confidence intervals in well test interpretation results. In: Society of Petroleum Engineers paper No. 113888, Europec/EAGE Conference and Exhibition, 9-12 June 2008, Rome, Italy
- Bangoy LM, Bidaux P, Drogue C, et al (1992) A new method of characterizing fissured media by pumping tests with observation wells. *J Hydrol* 138:77–88 . doi: 10.1016/0022-1694(92)90156-P
- Barker J (2007) Diffusion in Hydrogeology. *Diffus Fundam* 6:50.1-50.18
- Barker JA (1988) A generalized radial flow model for hydraulic tests in fractured rock. *Water Resour Res* 24:1796–1804 . doi: 10.1029/WR024i010p01796
- Barlow JRB, Coupe RH (2012) Groundwater and surface-water exchange and resulting nitrate dynamics in the Bogue Phalia basin in northwestern Mississippi. *J Environ Qual* 41:155–169 . doi: 10.2134/jeq2011.0087
- Barry F, Ophori D, Hoffman J, Canace R (2009) Groundwater flow and capture zone analysis of the Central Passaic River Basin, New Jersey. *Environ Geol* 56:1593–1603 . doi: 10.1007/s00254-008-1257-5
- Bear J, Jacobs M (1965) On the movement of water bodies injected into aquifers. *J Hydrol* 3:37–57 . doi: 10.1016/0022-1694(65)90065-X
- Beauheim RL, Roberts RM (1998) Flow-dimension analysis of hydraulic tests to characterize water-conducting features. In: *Water-conducting Features in Radionuclide Migration, GEOTRAP Project Workshop Proceedings, Barcelona, Spain, June 10-12, 1998*. Paris, France: OECD NEA. 287-294. ISBN 92-64-17124-X
- Beauheim RL, Roberts RM (2002) Hydrology and hydraulic properties of a bedded evaporite formation. *J Hydrol* 259:66–88 . doi: 10.1016/S0022-1694(01)00586-8
- Beauheim RL, Roberts RM, Avis JD (2004) Well testing in fractured media: flow dimensions and diagnostic plots. *J Hydraul Res* 42:69–76 . doi: 10.1080/00221680409500049

- Bhatt K (1993) Uncertainty in wellhead protection area delineation due to uncertainty in aquifer parameter values. *J Hydrol* 149:1–8 . doi: 10.1016/0022-1694(93)90095-Q
- Billaux D, Gentier S (1990) Numerical and Laboratory Studies of Flow in a Fracture. A a Balkema, Rotterdam
- Birsoy YK, Summers WK (1980) Determination of Aquifer Parameters from Step Tests and Intermittent Pumping Data. *Ground Water* 18:137–146 . doi: 10.1111/j.1745-6584.1980.tb03382.x
- Black JH (1994) Hydrogeology Of Fractured Rocks – A Question Of Uncertainty About Geometry. *Appl Hydrogeol* 2:56–70 . doi: 10.1007/s100400050049
- Bourdet D, Ayoub JA, Pirard YM (1989) Use of pressure derivative in well test interpretation. *SPE Form Eval* 4:293–302 . doi: 10.2118/12777-PA
- Bourdet D, Whittle T., Douglas A., Picard Y. (1983) A new set of types curves simplifies well test analysis. *World Oil* 196:95–106
- Bowman DO, Roberts RM, Holt RM (2012) Generalized radial flow in synthetic flow systems. *Groundwater* 51:768–774 . doi: 10.1111/j.1745-6584.2012.01014.x
- Carrera J (1993) An overview of uncertainties in modelling groundwater solute transport. *J Contam Hydrol* 13:23–48 . doi: 10.1016/0169-7722(93)90049-X
- Cello PA, Walker DD, Valocchi AJ, Loftis B (2009) Flow Dimension and Anomalous Diffusion of Aquifer Tests in Fracture Networks. *Vadose Zone J* 8:258–268 . doi: 10.2136/vzj2008.0040
- Chang J, Yortsos YC (1990) Pressure-transient analysis of fractal reservoirs. *SPE Form Eval* 5:31–38 . doi: 10.2118/18170-PA
- Chesnaux R, Lambert M, Walter J, et al (2011) Building a geodatabase for mapping hydrogeological features and 3D modeling of groundwater systems: Application to the Saguenay–Lac-St.-Jean region, Canada. *Comput Geosci* 37:1870–1882 . doi: 10.1016/j.cageo.2011.04.013
- Cinco-Ley H, Samaniego V. F, Dominguez A. N (1978) Transient Pressure Behavior for a Well With a Finite-Conductivity Vertical Fracture. *Soc Pet Eng J* 18:253–264 . doi: 10.2118/6014-PA
- Cinco-Ley H, Samaniego-V. F (1981) Transient pressure analysis: finite conductivity fracture case versus damaged fracture case. In: *SPE Annual Technical Conference and Exhibition*, 4-7 October, 1981, San Antonio, Texas, USA, SPE-10179-MS
- Cooper HH Jr, Jacob CE (1946) A generalized graphical method for evaluating formation constants and summarizing well-field history. *Trans Am Geophys Union* 27:526–534 . doi: 10.1029/TR027i004p00526
- Corbett PWM, Hamdi H, Gurav H (2012) Layered fluvial reservoirs with internal fluid cross flow: a well-connected family of well test pressure transient responses. *Pet Geosci* 18:219–229 . doi: 10.1144/1354-079311-008

- Culham WE (1974) Pressure Buildup Equations for Spherical Flow Regime Problems. Soc Pet Eng J 14:545–555 . doi: 10.2118/4053-PA
- Dal Soglio L (2012) Simulation numérique d'essai de pompage pour le diagnostic des discontinuités structurales et des hétérogénéités des aquifères de dépôts
- de Dreuzy J-R, Davy P, Bour O (2000) Percolation parameter and percolation-threshold estimates for three-dimensional random ellipses with widely scattered distributions of eccentricity and size. Phys Rev E 62:5948–5952 . doi: 10.1103/PhysRevE.62.5948
- Dewandel B, Lachassagne P, Zaidi FK, Chandra S (2011) A conceptual hydrodynamic model of a geological discontinuity in hard rock aquifers: Example of a quartz reef in granitic terrain in South India. J Hydrol 405:474–487 . doi: 10.1016/j.jhydrol.2011.05.050
- Doe T (2002) Generalized dimension analysis of build-up and pressure interference tests. Stockholm Suède
- Doe TW (1991) Fractional dimension analysis of constant-pressure well tests. In: Society of Petroleum Engineers paper No. 22702, SPE Annual Technical Conference and Exhibition, 6-9 October, 1991, Dallas, Texas, USA. pp 461–467
- Doughty C, Karasaki K (2002) Flow and transport in hierarchically fractured rock. J Hydrol 263:1–22 . doi: 10.1016/S0022-1694(02)00032-X
- Ehlig-Economides C (1988) Use of the pressure derivative for diagnosing pressure-transient behavior. J Pet Technol 40:1280–1282 . doi: 10.2118/18594-PA
- Ehlig-Economides CA, Vera FE (2013) Diagnosing Pressure-Dependent-Permeability in Long-Term Shale Gas Pressure and Production Transient Analysis. In: Society of Petroleum Engineers paper No. 168698, Unconventional Resources Technology Conference, 12-14 August, Denver, Colorado, USA. Society of Exploration Geophysicists, American Association of Petroleum Geologists, Society of Petroleum Engineers, pp 569–578
- Escobar F., Montealegre-M M (2007) A complementary conventional analysis for channelized reservoirs. CTF - Cienc Tecnol Futuro 3:137–146
- Escobar F, Saavedra N, Hernandez C, et al (2004a) Pressure and Pressure Derivative Analysis for Linear Homogeneous Reservoirs Without Using Type-Curve Matching. Society of Petroleum Engineers
- Escobar F-H, Corredor C-M, Gomez B-E, et al (2012a) Pressure and pressure derivative analysis for slanted and partially penetrating wells. Asian Res Publ Netw ARPN 7:932–938
- Escobar FH, Hernández DP, Saavedra JA (2010) Pressure and pressure derivative analysis for long naturally fractured reservoirs using the TDS technique. DYNA 77:102–114

- Escobar FH, Hernández YA, Hernández CM (2007) Pressure transient analysis for long homogeneous reservoirs using TDS technique. *J Pet Sci Eng* 58:68–82 . doi: 10.1016/j.petrol.2006.11.010
- Escobar F-H, Muñoz O, Sepúlveda J, Montealegre M (2005) New finding on pressure response in long, narrow reservoirs. *CTF - Cienc Tecnol Futuro* 3:151–160
- Escobar FH, Navarrete JM, Losada HD (2004b) Evaluation of Pressure Derivative Algorithms for Well-Test Analysis. Society of Petroleum Engineers
- Escobar FH, Rojas MM, Bonilla LF (2012b) Transient-rate analysis for long homogeneous and naturally fractured reservoir by the TDS technique. *J Eng Appl Sci* 7:353–370
- Fadlilmawla AA, Dawoud MA (2006) An approach for delineating drinking water wellhead protection areas at the Nile Delta, Egypt. *J Environ Manage* 79:140–149 . doi: 10.1016/j.jenvman.2005.06.001
- Ferris J. (1949) Ground Water. In: *Hydrology*. John Wiley & Sons Inc, New York, United-States, pp 198–272
- Ferroud A, Chesnaux R, Rafini S (2015) Pumping test diagnostic plots for the investigation of flow patterns in complex aquifers: numerical results. In: 42nd IAH International Congress “Hydrogeology: Back to the future”, September 13-18, 2015, Rome, Italy
- Figueiredo B, Tsang C-F, Niemi A, Lindgren G (2016) Review: The state-of-art of sparse channel models and their applicability to performance assessment of radioactive waste repositories in fractured crystalline formations. *Hydrogeol J* 1–16 . doi: 10.1007/s10040-016-1415-x
- Forster CB, Lachmar TE, Oliver DS (1997) Comparison of models for delineating wellhead Protection areas in confined to semiconfined aquifers in alluvial basins. *Ground Water* 35:689–697 . doi: 10.1111/j.1745-6584.1997.tb00135.x
- Geier JE, Doe TW, Benabderrahman A, Hassler L (1996) Generalized radial flow interpretation of well tests for the site-94 project
- Giese M, Reimann T, Liedl R, et al (2017) Application of the flow dimension concept for numerical drawdown data analyses in mixed-flow karst systems. *Hydrogeol J* 25:799–811 . doi: 10.1007/s10040-016-1523-7
- Gringarten A., Witherspoon P. (1972) A method of analyzing pump test data from fractured aquifers. In: *Int. Soc. Rock Mechanics and Int. Ass. Eng. Geol.* Stuttgart, pp 1–9
- Gringarten AC (2010) Practical use of well-test deconvolution. In: Society of Petroleum Engineers paper No. 134534, SPE Annual Technical Conference and Exhibition, 19-22 September, Florence, Italy
- Gringarten AC, Ramey HJ, Raghavan R (1975) Applied Pressure Analysis for Fractured Wells. *J Pet Technol* 27:887–892 . doi: 10.2118/5496-PA

- Gringarten AC, Ramey HJ, Raghavan R (1974) Unsteady-state pressure distributions created by a well with a single infinite-conductivity vertical fracture. *Soc Pet Eng J* 14:347–360 . doi: 10.2118/4051-PA
- Grubb S (1993) Analytical model for estimation of steady-state capture zones of pumping wells in confined and unconfined aquifers. *Ground Water* 31:27–32 . doi: 10.1111/j.1745-6584.1993.tb00824.x
- Hamm, S., 1995. Hydraulic Characteristics of Fractured Aquifers in South Korea Applying Fractal Models. *Jour Geol Soc Korea* 4, 467.
- Hammond PA, Field MS (2014) A reinterpretation of historic aquifer tests of two hydraulically fractured wells by application of inverse analysis, derivative analysis, and diagnostic plots. *J Water Resour Prot* 06:481–506 . doi: 10.4236/jwarp.2014.65048
- Hantush MS (1956) Analysis of data from pumping tests in leaky aquifers. *Trans Am Geophys Union* 37:702 . doi: 10.1029/TR037i006p00702
- Hantush MS (1960) Modification of the theory of leaky aquifers. *J Geophys Res* 65:3713–3725 . doi: 10.1029/JZ065i011p03713
- Horne RN (1995) Modern well test analysis: a computer-aided approach. *Petroway*
- Jourde H, Bidaux P, Pistre S (1998) Fluid flow modelling in orthogonal fracture networks: influence of pumping well location on the hydrodynamic response of the modelled aquifer. *Bull Soc Geol Fr* 169:635–644
- Jourde H, Cornaton F, Pistre S, Bidaux P (2002a) Flow behavior in a dual fracture network. *J Hydrol* 266:99–119 . doi: 10.1016/S0022-1694(02)00120-8
- Jourde H, Pistre S, Perrochet P, Drogue C (2002b) Origin of fractional flow dimension to a partially penetrating well in stratified fractured reservoirs. New results based on the study of synthetic fracture networks. *Adv Water Resour* 25:371–387 . doi: 10.1016/S0309-1708(02)00010-6
- Kruseman GP, Ridder NA de (1994) Analysis and evaluation of pumping test data, 2. ed. (compl. rev.), repr. International Institute for Land Reclamation and Improvement, Wageningen
- Kuusela-Lahtinen A, Niemi A, Luukkonen A (2003) Flow dimension as an indicator of hydraulic behavior in site characterization of fractured rock. *Ground Water* 41:333–341 . doi: 10.1111/j.1745-6584.2003.tb02602.x
- Lachassagne P (2008) Overview of the Hydrogeology of Hard Rock Aquifers: Applications for their Survey, Management, Modelling and Protection. In: Ahmed S, Jayakumar R, Salih A (eds) *Groundwater Dynamics in Hard Rock Aquifers*. Springer Netherlands, pp 40–63
- Lachassagne P, Wyns R, Dewandel B (2011) The fracture permeability of Hard Rock Aquifers is due neither to tectonics, nor to unloading, but to weathering processes. *Terra Nova* 23:145–161 . doi: 10.1111/j.1365-3121.2011.00998.x

- Le Borgne T, Bour O, de Dreuzy JR, et al (2004) Equivalent mean flow models for fractured aquifers: Insights from a pumping tests scaling interpretation. *Water Resour Res* 40:W03512 . doi: 10.1029/2003WR002436
- Lemieux J-M, Therrien R, Kirkwood D (2006) Small scale study of groundwater flow in a fractured carbonate-rock aquifer at the St-Eustache quarry, Québec, Canada. *Hydrogeol J* 14:603–612 . doi: 10.1007/s10040-005-0457-2
- Lemieux Y, Tremblay A, Lavoie D (2003) Structural analysis of supracrustal faults in the Charlevoix area, Quebec: relation to impact cratering and the St-Laurent fault system. *Can J Earth Sci* 40:221–235
- Levasseur D (1995) *Les eskers : essai de synthèse bibliographique*
- Leveinen J (2000) Composite model with fractional flow dimensions for well test analysis in fractured rocks. *J Hydrol* 234:116–141 . doi: 10.1016/S0022-1694(00)00254-7
- Leveinen J, Rönkä E, Tikkanen J, Karro E (1998) Fractional flow dimensions and hydraulic properties of a fracture-zone aquifer, Leppavirta, Finland. *Hydrogeol J* 6:327–340 . doi: 10.1007/s100400050156
- Liang H., Lin S., Huang T., et al (2012) Identifying the flow dimension in fractured rock using an interference test. *J Pet Gas Eng* 3:114–123
- Lods G, Gouze P (2004) WTFM, Software for Well Test Analysis in Fractured Media Combining Fractional Flow with Double Porosity and Leakance Approaches. *Comput Geosci* 30:937–947 . doi: 10.1016/j.cageo.2004.06.003
- Maréchal JC, Dewandel B, Subrahmanyam K (2004) Use of hydraulic tests at different scales to characterize fracture network properties in the weathered-fractured layer of a hard rock aquifer. *Water Resour Res* 40:W11508 . doi: 10.1029/2004WR003137
- Maréchal J-C, Ladouche B, Dörfli N, Lachassagne P (2008) Interpretation of pumping tests in a mixed flow karst system. *Water Resour Res* 44:W05401 . doi: 10.1029/2007WR006288
- Massonnat GJ, Bandiziol D (1991) *Interdependence Between Geology and Well Test Interpretation*. Society of Petroleum Engineers
- Mattar L (1997) *Derivative Analysis Without Type Curves*. Society of Petroleum Engineers
- Mattar L (1999) Derivative analysis without type curves. *J Can Pet Technol* 38: . doi: 10.2118/99-13-63
- Meier PM, Carrera J, Sánchez-Vila X (1998) An evaluation of Jacob's method for the interpretation of pumping tests in heterogeneous formations. *Water Resour Res* 34:1011–1025 . doi: 10.1029/98WR00008
- Moncada K, Tiab D, Escobar F-H, et al (2005) Determination of vertical and horizontal permeabilities for vertical oil and gas wells with partial completion and partial penetration using pressure and pressure derivative plots without type-curve matching. *CTF - Cienc Tecnol Futuro* 3:77–94

- Nadeau S, Rosa E, Cloutier V, et al (2015) A GIS-based approach for supporting groundwater protection in eskers: Application to sand and gravel extraction activities in Abitibi-Témiscamingue, Quebec, Canada. *J Hydrol Reg Stud* 4, Part B:535–549 . doi: 10.1016/j.ejrh.2015.05.015
- Nastev M, Savard MM, Lapcevic P, et al (2004) Hydraulic properties and scale effects investigation in regional rock aquifers, south-western Quebec, Canada. *Hydrogeol J* 12:257–269 . doi: 10.1007/s10040-004-0340-6
- Neuman SP, Witherspoon PA (1969) Theory of flow in a confined two aquifer system. *Water Resour Res* 5:803–816 . doi: 10.1029/WR005i004p00803
- Novakowski KS, Lapcevic PA (1988) Regional hydrogeology of the Silurian and Ordovician sedimentary rock underlying Niagara Falls, Ontario, Canada. *J Hydrol* 104:211–236 . doi: 10.1016/0022-1694(88)90166-7
- Obeahon PP, Sedgwick A, Okereke O (2014) Practical application of multi rate deconvolution. In: Society of Petroleum Engineers paper No. 172446, SPE Nigeria Annual International Conference and Exhibition, 5-7 August, Lagos, Nigeria
- Odling, N.E., West, L.J., Hartmann, S., Kilpatrick, A., 2013. Fractional flow in fractured chalk; a flow and tracer test revisited. *J. Contam. Hydrol.* 147, 96–111. <https://doi.org/10.1016/j.jconhyd.2013.02.003>
- Onur M, Kuchuk F (2012) A New Deconvolution Technique Based on Pressure-Derivative Data for Pressure-Transient-Test Interpretation. *SPE J* 17: . doi: 10.2118/134315-PA
- Paradis D, Martel R, Karanta G, et al (2007) Comparative study of methods for WHPA delineation. *Ground Water* 45:158–167 . doi: 10.1111/j.1745-6584.2006.00271.x
- Pechstein A, Attinger S, Krieg R, Copty NK (2016) Estimating transmissivity from single-well pumping tests in heterogeneous aquifers. *Water Resour Res* 52:495–510 . doi: 10.1002/2015WR017845
- Polek, J, Karasaki K, Long JCS, Barker J (1989) Flow to wells in fractured rock with fractal structure. In: *Fractal Aspects of Materials*, Materials Research Society
- Rafini S (2008) Comportement hydraulique des milieux faillés [The hydraulic behaviour of faulted environments]. PhD, Université du Québec à Montréal
- Rafini S (2004) Contrôle structural des écoulements en milieux fractures contribution de l'approche combinée simulation de flux – analyse de la déformation. Université du Québec à Montréal
- Rafini S, Chesnaux R, Dal Soglio L (2014) A numerical analysis to illustrate the usefulness of drawdown log-derivative diagnostic plots in characterizing the heterogeneity of non-Theis aquifers. In: 2014 GSA Annual Meeting, October 19-22, 2014 Vancouver, British Columbia, Canada

- Rafini S, Chesnaux R, Ferroud A (2017) A numerical investigation of pumping-test responses from contiguous aquifers. *Hydrogeol J* 3:877–894 . doi: 10.1007/s10040-017-1560-x
- Rafini S, Larocque M (2009) Insights from numerical modeling on the hydrodynamics of non-radial flow in faulted media. *Adv Water Resour* 32:1170–1179 . doi: 10.1016/j.advwatres.2009.03.009
- Rafini S, Larocque M (2012) Numerical modeling of the hydraulic signatures of horizontal and inclined faults. *Hydrogeol J* 20:337–350 . doi: 10.1007/s10040-011-0812-4
- Raghavan R (2004) A review of applications to constrain pumping test responses to improve on geological description and uncertainty. *Rev Geophys* 42:RG4001 . doi: 10.1029/2003RG000142
- Renard P, Glenz D, Mejias M (2009) Understanding diagnostic plots for well-test interpretation. *Hydrogeol J* 17:589–600 . doi: 10.1007/s10040-008-0392-0
- Rondot J (1989) Géologie de Charlevoix. Série de manuscrits bruts. Rapport MB 89-21, Ministère de l'Énergie et des Ressources du Québec
- Rozemeijer JC, van der Velde Y, McLaren RG, et al (2010) Integrated modeling of groundwater–surface water interactions in a tile-drained agricultural field: The importance of directly measured flow route contributions. *Water Resour Res* 46:W11537 . doi: 10.1029/2010WR009155
- Sánchez-Vila X, Meier PM, Carrera J (1999) Pumping tests in heterogeneous aquifers: An analytical study of what can be obtained from their interpretation using Jacob's Method. *Water Resour Res* 35:943–952 . doi: 10.1029/1999WR900007
- Theis CV (1935) The relation between the lowering of the piezometric surface and the rate and duration of discharge of a well using ground-water storage. *Trans Am Geophys Union* 16:519–524 . doi: 10.1029/TR016i002p00519
- Therrien R, McLaren R., Sudicky E., Panday S. (2010) HydroGeoSphere, A three-dimensional numerical model describing fully integrated subsurface and surface flow and solute transport. DRAFT, Univ. of Waterloo, Waterloo, Ont., Canada
- Tiab D (1994) Analysis of pressure and pressure derivative without type-curve matching: Vertically fractured wells in closed systems. *J Pet Sci Eng* 11:323–333 . doi: 10.1016/0920-4105(94)90050-7
- Tiab D (1995) Analysis of pressure and pressure derivative without type-curve matching — Skin and wellbore storage. *J Pet Sci Eng* 12:171–181 . doi: 10.1016/0920-4105(94)00040-B
- Tiab D (2005) Analysis of pressure derivative data of hydraulically fractured wells by the Tiab's Direct Synthesis technique. *J Pet Sci Eng* 49:1–21 . doi: 10.1016/j.petrol.2005.07.001
- Tiab D (1993) Analysis of pressure and pressure derivatives without type-curve matching - I. Skin and Wellbore Storage. Society of Petroleum Engineers

- Todd DK (1980) *Groundwater hydrology*, 2nd ed. JWiley, New York ; Toronto
- Tremblay, A., Lemieux, Y., 2001. Supracrustal faults of the St. Lawrence rift system between Cap-Tourmente and Baie-Saint-Paul, Quebec. *Curr. Res. Part Geol Surv Can.*
- Tremblay, A., Long, B., Massé, M., 2003. Supracrustal faults of the St. Lawrence rift system, Québec: kinematics and geometry as revealed by field mapping and marine seismic reflection data. *Tectonophysics* 369, 231–252.
- Tsang C-F, Neretnieks I (1998) Flow channeling in heterogeneous fractured rocks. *Rev Geophys* 36:275–298 . doi: 10.1029/97RG03319
- Verbovšek T (2009) Influences of Aquifer Properties on Flow Dimensions in Dolomites. *Ground Water* 47:660–668 . doi: 10.1111/j.1745-6584.2009.00577.x
- Verbovšek T (2011) Hydrogeology and Geochemistry of Fractured Dolomites—A case study of Slovenia. In: *Aquifers: formation, transport, and pollution*. Nova Science Publishers, Hauppauge, N.Y., pp 87–147
- von Schroeter T, Hollaender F, Gringarten AC (2001) Deconvolution of well test data as a nonlinear total least squares problem. In: *Society of Petroleum Engineers paper No. 71574, SPE Annual Technical Conference and Exhibition, 30 September-3 October, 2001, New Orleans, Louisiana, USA*
- Walker DD, Cello PA, Valocchi AJ, Loftis B (2006) Flow dimensions corresponding to stochastic models of heterogeneous transmissivity. *Geophys Res Lett* 33:L07407 . doi: 10.1029/2006GL025695
- Walker DD, Roberts RM (2003) Flow dimensions corresponding to hydrogeologic conditions. *Water Resour Res* 39:1349
- Warren JE, Root PJ (1963) The behavior of naturally fractured reservoirs. *Soc Pet Eng J* 3:245–255 . doi: 10.2118/426-PA
- Winberg A (2000) Äspö Hard Rock Laboratory: final report of the first stage of the tracer retention understanding experiments. Svensk kärnbränslehantering AB/Swedish Nuclear Fuel and Waste Management, Stockholm
- Worthington SRH, Davies GJ, Alexander Jr. EC (2016) Enhancement of bedrock permeability by weathering. *Earth-Sci Rev* 160:188–202 . doi: 10.1016/j.earscirev.2016.07.002
- Wyssling L (1979) Eine neue formel zur Berechnung der Zuströmungsdauer (Laufzeit) des grundwassers zu einem grundwasser pumpwerk. *Eclogae Geol Helvetiae* 72:401–406
- Zanini L, Novakowski K s., Lapcevie P, et al (2000) Ground Water Flow in a Fractured Carbonate Aquifer Inferred from Combined Hydrogeological and Geochemical

Measurements. Ground Water 38:350–360 . doi: 10.1111/j.1745-6584.2000.tb00220.x

CHAPITRE 4

Le travail présenté dans ce chapitre 4 est également rédigé sous forme d'article. Il vise à conceptualiser le fonctionnement hydrodynamique d'un aquifère à substratum incliné (SI) (augmentation constante de l'épaisseur dans une direction) à partir d'une analyse numérique. Ce contexte géologique a été identifié grâce à l'analyse de la base de données de n (Ferroud et al., 2018). En effet, cette base de données a mis en avant un régime d'écoulement sphérique dans des dépôts granulaires. Étant donné que le puits interceptait la plupart de l'épaisseur de l'aquifère, le régime sphérique ne pouvait être interprété à partir du modèle à pénétration partielle. Les résultats montrent qu'un aquifère à SI induit également un régime sphérique. Plus particulièrement, les aquifères à SI peuvent être détectés à partir de la séquence diagnostique $n = (2) - 2 - 3$. Cette étude permet également de mieux comprendre comment s'exprime la dimension d'écoulement. En d'autres termes, nous avons observé que dans un milieu tel qu'un aquifère à SI, le front de pression peut se décomposer en portions ayant des comportements hydrauliques différents. Dans le cas de cette étude, l'onde de pression a une partie évoluant radialement (cylindre) et une autre portion évoluant sphériquement (portion de sphère). La dimension d'écoulement exprime le comportement hydraulique de la portion de l'onde de pression ayant la plus grande surface. Enfin, l'analyse de sensibilité a permis de proposer des équations afin d'estimer plus précisément les propriétés hydrauliques de ce type d'aquifère. Cet article a été soumis à la revue *Journal of Hydrology* en décembre 2017.

**DRAWDOWN LOG-DERIVATIVE ANALYSIS FOR INTERPRETING
CONSTANT-RATE PUMPING-TESTS IN INCLINED SUBSTRATUM
AQUIFERS**

Anouck Ferroud*, Romain Chesnaux and Silvain Rafini

Research Group R2Eau, Centre d'études sur les ressources minérales, Université du Québec à Chicoutimi, 555, boulevard de l'Université, Chicoutimi (Québec), Canada G7H 2B1

Article soumis à *Journal of Hydrology* en décembre 2017.

4.1 ABSTRACT

Constant-rate pumping tests (CRPT) performed in aquifers having an inclined substratum (IS) cannot be interpreted using Theis-like models, due to an increasing thickness that is beyond conventional hydraulic assumptions. Using an empirical process based on numerical modelling, this study submits original tools for the detection of IS aquifers and the interpretation of their hydrodynamic responses to CRPT, using derivative ($ds/d\log t$) and flow dimension (n) analyses. It is shown that IS aquifers produce a drawdown log-derivative signal composed of two radial regimes and one spherical flow regime ($n = (2) - 2 - 3$). Comprehensive sensitivity analyses make it possible to constrain relationships between, on one hand, characteristic derivative responses and on the other hand, hydraulic conditions such as: pumping rate, distance from the well to the corner, substratum inclination and aquifer properties, including anisotropic hydraulic conductivity. Empirical formulas were developed to reliably and accurately estimate the hydraulic properties of an IS aquifer and to avoid common misinterpretations in CRPT practices. This study contributes to widening the array of tools available for the interpretation of pumping tests, by implementing a novel conceptual model for a specific type of non-uniform aquifer that has remained unaddressed; further, it provides another interpretation of the spherical flow regime, which has been interpreted in the petroleum literature to reflect partially penetrating/completing wells. Finally, a field application of the submitted interpretative tools to a CRPT into an IS aquifer is presented.

Keywords: radial and spherical flow dimensions, drawdown log-derivative $ds/d\log t$ signal, inclined substratum aquifer, numerical modeling, field data, empirical solutions

4.2 NOMENCLATURE

α : angle of inclination of the substratum (radians)

d : distance from the well to the corner formed by the intersection of the inclined substratum and the top of the confined aquifer [L]

K : hydraulic conductivity of the confined aquifer [$L.T^{-1}$]

m_{2-BC} : Y-intercept of the radial flow dimension ($n = 2$) before the pressure front pulse reaches the corner [L]

m_{2-AC} : Y-intercept of the radial flow dimension ($n = 2$) after the pressure front pulse has reached the corner [L]

m_3 : Y-intercept of the spherical flow dimension ($n = 3$)

L_w : length of the well intercepting the aquifer [L]

Q : pumping rate [$L^3.T^{-1}$]

S_s : specific storage of the confined aquifer [L^{-1}]

t_{AC} : time corresponding to the intersect between the predominant radial flow dimension (second plateau, $n = 2$) and the spherical flow dimension ($n = 3$) on a log-log plot of $ds/d\log t$ versus t [T]

t_c : time corresponding to the end of the compensated radial flow dimension (first plateau, $n = 2$) on a log-log plot of $ds/d\log t$ versus t [T]

4.3 INTRODUCTION

The configuration of real aquifers can be very different from the assumptions of conventional Theis-like flow models. This may pose a challenge when interpreting pumping tests, rendering inaccurate or imprecise estimations of an aquifer's hydraulic properties. The complexity of real aquifers has been highlighted in a previous study which analyzed the flow dimension parameter of 69 constant-rate pumping tests (Ferroud et al. 2018). The flow dimension is a parameter that reflects the flow geometry and/or the hydraulic properties of an aquifer. A total of 121 flow dimensions were estimated from the drawdown log-derivative signal of various aquifers composed of fluvio-glacial deposits, crystalline and carbonate rocks (Ferroud et al. 2018). That study revealed that 80% of the 75 long-lasting (lasting over 1 logarithmic interval) flow dimensions had an n value different from 2, which did not satisfy the cylindrical-radial Theis assumptions. Despite the fact that the Theis model is still largely used by hydrogeologists, our verification of the occurrences of the Theis assumptions in nature indicates that it is rarely representative of reality. It would thus be necessary to develop more accurate diagnostic tools which render more accurate representations based on pumping well tests, in order to enhance the suitability of the hydrodynamic interpretation of well tests. A better understanding of the conceptual models associated with the value and sequence of the flow dimension will improve the suitability of the hydrodynamic

interpretations of transient well tests and the accuracy of the estimation of the hydraulic properties of aquifers. The relevance of this last objective needs no further justification beyond reminding the reader of its implications in several domains in hydrogeology. Hydraulic conductivity is a crucial parameter used to estimate wellhead protection areas (Bear and Jacobs 1965; Wyssling 1979; Todd 1980; Grubb 1993), to characterize flow fields and to predict contaminant transport (Carrera 1993; Rozemeijer et al. 2010; Barlow and Coupe 2012).

Our previous flow dimension analysis (Ferroud et al. 2018) identified that 21% of the 121 n observations were greater than 2. Spherical $n = 3$ values, which represent 8% of the 121 flow regimes analysed in our database, were mainly observed in thick fluvio-glacial deposits, in thick dolomite rocks, in intensively fractured limestones and in weathered crystalline granitic sands. The literature currently interprets the spherical flow dimension ($n = 3$) to be the signal of a partially penetrating well or a partially screened well (Moncada et al. 2005; Escobar et al. 2012). More particularly, Moncada et al. (2005) showed that the spherical flow dimension induced by a partially penetrating well is visible on a derivative signal only if the penetration ratio is less than 40%. Our database showed that 10 out of 69 pumping tests identified a spherical flow dimension, of which 4 were induced by partially penetrating wells, confirming the work of Moncada et al. (2005). However, 6 of these 10 pumping tests indicated a spherical flow dimension even though the penetration ratio was greater than 40%. The interpretation of these 6 pumping tests required conditions other than a partial penetration, and/or more field data. Unfortunately, the understanding of the spherical flow dimension was not possible for 5 of the 6 pumping tests because of a lack of geological

data. However, 1 of the 6 pumping tests was known to be conducted in an aquifer presenting an inclined substratum (i.e., of variable thickness). This specific pumping test yielded a spherical flow dimension that could not be interpreted solely based on the assumption of a partially penetrating well, because that particular well is known to totally penetrate the confined granular aquifer and to reach the underlying rock. Consequently, an increasing thickness of the aquifer could be one cause of the observation of a spherical flow dimension. The non-uniqueness of the drawdown log-derivative signal (in the petroleum literature, this is called a pressure derivative signal) has been previously mentioned by Mattar (1997). Also, Rafini et al. (2013) have suggested that an increase of the thickness of the aquifer due to an inclined no-flow substratum may yield the spherical flow dimension during a pumping test. The conceptual model of granular aquifers having an increasing thickness has received little attention so far. Only Hantush (1962) proposed a transient analytical solution describing the flow towards a well in granular aquifers of non-uniform thickness where the thickness increases exponentially in the direction of flow. The $ds/d\log t$ signal of a pumping test in an inclined substratum (IS) aquifer has not yet been investigated and a solution for assessing the hydraulic properties of such an aquifer has yet to be proposed.

This study further expands on Rafini et al.'s (2013) observation by characterizing the drawdown log-derivative signal of an aquifer having an inclined substratum. Indeed, this conceptual model of increasing thickness is expected to be observed in nature, namely in geological settings such as glacial or alluvial valleys.

The focus of this current study consists in developing new diagnostic tools based on the $ds/d\log t$ signal and the flow dimension parameter, with the objective of improving the

qualitative and quantitative interpretation of constant-rate pumping tests performed in IS aquifers. Our study not only provides insights on the hydrodynamic behaviors that yield radial and spherical flow regimes, but it also proposes a series of empirical equations that make it possible to more accurately estimate the hydraulic properties and the inclination of IS aquifers. We will take advantage of the numerical tool to reach these goals. The modeled IS aquifer, being homogeneous and isotropic, may represent a granular aquifer that overlies an inclined aquitard layer (ex: fractured rock or clay horizon). A field case study of an inclined substratum is also presented, which shows that the flow model presented in this study is observable in nature, underlining the relevance of our approach and assumptions. The presented case shows how to apply the diagnostic tools developed in this study to improve the interpretation of a constant-rate pumping test performed in an IS aquifer. The new tools and equations hereby developed are intended to expand the hydrogeologist's tool box for the interpretation of pumping tests in aquifers having an inclined substratum configuration.

For reasons of brevity in this text, the new diagnostic tools and the empirical formula developed in this study will be referred to as the Method.

4.4 THE THEORY OF FLOW DIMENSION

The drawdown log-derivative signal $ds/d\log t$, which in the petroleum literature is named the pressure derivative signal, significantly improves the sensitivity of the signal to small variations of drawdown rate (Bourdet et al. 1989). This gain in sensitivity of the drawdown makes the signal more unique and more sensitive to the hydraulic properties of the pumped

aquifer and its boundary conditions. For decades, the $ds/d\log t$ signal has been interpreted by recognising the slopes that were generated with numerical modelling in specific conceptual models. The flow dimension is still only moderately used in the literature, despite the fact that it is a powerful tool which makes it possible to follow the evolution of the cross-flow area, greatly contributing to evaluating the flow geometry around the pumped well. The flow dimension brings a hydrodynamic interpretation of the pumping test instead of only comparing the modeled and the real signatures.

The flow dimension n is a parameter introduced in the Generalized Radial Flow (*GRF*) model by Barker (1988) in order to improve the interpretation of constant-rate pumping tests in aquifers that cannot be represented adequately using the conventional Theis (1935) or Cooper and Jacob (1946) methods. More particularly, the n parameter is defined as being related to the cross-flow area $A(r)$ and the radial distance r from the pumping well, following the relationship given in Equation (4.1).

$$A(r)_n = b^{3-n} \alpha_n r^{n-1} \quad (4.1)$$

With b the extent of the flow zone [L], r the radius of the pressure front pulse [L] and α_n (Equation (4.2))

$$\alpha_n = \frac{2\pi^{\frac{n}{2}}}{\Gamma\left(\frac{n}{2}\right)} \quad (4.2)$$

with, $\Gamma(x)$ the gamma function.

Barker (1988) introduced the n parameter in the continuity equation as follows (Equation (4.3))

$$\frac{K}{r^{n-1}} \frac{\partial}{\partial r} \left(r^{n-1} \frac{\partial h}{\partial r} \right) = S_s \frac{\partial h}{\partial t} \quad (4.3)$$

where K [LT^{-1}] is the hydraulic conductivity, r [L] is the radial distance from the borehole at time t [T], n is the flow dimension, S_s [L^{-1}] is the specific storage and h [L] is the hydraulic head.

During a constant-rate pumping test, the pressure front pulse expands outwards from the borehole throughout the aquifer; it is influenced by the hydraulic properties and the geometry of the aquifer. As the pressure wave is deformed, the relationship between its equipotential surface area and its radial distance from the pumping well evolves according to Equation (4.1). The flow dimension is thus a parameter that reflects the geometrical evolution of the pressure front pulse as it is diffused throughout the aquifer. In other words, the n value reflects the power by which the cross-flow area and/or the reservoir properties change according to the radial distance from the well (Equation (4.3)). If the hydraulic properties (hydraulic conductivity and specific storage) are constant, the flow dimension n reflects the geometry of the flow media.

According to Barker (2007), the parameter n is a value “that must be determined empirically and which may not have an integer value”. The estimation of the flow dimension parameter of a constant-rate pumping test is rapidly determined by conducting a graphical analysis of $ds/d\log t$ with respect to time on a log-log plot. The n parameter is obtained from the

asymptotic portions of the $ds/d\log t$ curve. This asymptotic assumption is valid when the parameter $u = (S_s r^2)/(4Kt)$ is small enough, which implies that the specific storage S_s and the hydraulic conductivity K are uniform, the radial distance r is small (*i.e.* the head is measured in the pumping well) or the time t is long. In other words, when the drawdown log-derivative time series maintains a constant slope ν on a log-log plot, the associated n parameter is determined using the relationship given in Equation (4.2). The term “flow regime” will be used in this paper to define a lasting and stable flow period during which Equation (4.1) is valid.

$$n = 2(1 - \nu) \quad (4.4)$$

For further details, the reader is directed to read the development of Equation (4.4) in the papers (among others) of: Barker (1988), Ehlig-Economides et al. (1990), Walker and Roberts (2003) and Rafini and Larocque (2009).

The physical interpretation of n remains unexplained for most n values, in particular for non-integer n values. Does n reflect the intrinsic or non-intrinsic properties of the aquifer? The GRF model is based on the assumption that the transmissivity and the storage of the aquifer are constant. Therefore, non-integer values of n were initially interpreted to reflect the fractal properties of the flow media (Barker 1988). During the last decades, much work was conducted on the use of fractal models to interpret fractional n values. Some fractal models are based on a scaling dependence of the geometry structure or a scaling dependence of the permeability structure, or both. Particularly, by analysing geometrical scaling structures, de Dreuzy et al. (2004) and de Dreuzy and Davy (2007) have shown that non-integer n

values can be observed in flow models with local scaling of transmissivity in non-stationary multifractal correlation patterns (such as Sierpinski- and percolation-like fractal media). In 1991, Doe (1991) extended the interpretation of fractional n values to non-fractal geometries which are not space-filling. In other words, Euclidian configurations, with heterogeneity either in hydraulic conductivity or geometry or a combination of both, can produce non-integer values of n . Some conceptual models have been proposed to interpret the integer values of n ($n = 1, 2$ or 3) and for $n = 1.5$. A value of n equal to 1 (a linear flow regime) reflects a system where the cross-flow area $A(r)$ remains constant as the pressure-front pulse expands throughout the aquifer. Such conditions can occur in systems that induce a flow corridor, such as an intersection of faults, a vertical fault with infinite conductivity (Gringarten and Witherspoon 1972; Gringarten et al. 1974) or a long and narrow aquifer, such as fluvial and deep sea fans (Escobar et al. 2004a; Escobar and Montealegre-M 2007; Corbett et al. 2012). A value of $n = 1.5$ is interpreted as being a bilinear flow regime which is induced by a vertical leaky fault. A value of $n = 2$ is interpreted to reflect a cylindrical-radial cross-flow area ($A(r)$ evolves proportionally to the radial distance), as it is assumed in Theis-like models. A value of $n = 3$ (spherical flow regime) suggests that $A(r)$ increases proportionally to r^2 . Such spherical conditions have so far been interpreted as reflecting a non-intrinsic parameter of the aquifer: a partially screened well, a well with a short screen relative to the aquifer or a partially penetrating well (Moncada et al. 2005; Escobar et al. 2012; Ferroud et al. 2015). This study presents a different spherical flow model which is associated with a non-stationary geometry: a linear increase of the transmissivity induced by an inclined substratum. It is known that the proposed conceptual models are non-unique. Other

configurations that induce a flow behavior that verifies Equation (4.1) may be proposed to interpret n .

Despite being a suitable tool to interpret the sequences of flow regimes during a transient well test, the physical interpretation of n values remains in most cases enigmatic. In particular, the fractional values of n are still often misunderstood. This study does not seek to resolve the issue of the physical interpretation of n values; rather, it proposes another conceptual model –in addition to the Theis-like models –to interpret the radial flow dimension ($n = 2$), and another conceptual model - in addition to the partially penetrating well model – to interpret the spherical flow dimension ($n = 3$).

4.5 MATERIALS AND METHODS

The approach of this study consists in characterizing the hydrodynamic behavior of an aquifer with an inclined substratum. The interpretation is based on the analysis of the $ds/d\log t$ signal of a constant-rate pumping test. We took advantage of numerical modelling technology to analyse the shape of the cross-flow area as it expands through the aquifer and to compare this behavior against the n -sequence. The behavior of the cross-flow area is investigated by tracking the pressure front pulse. In other words, the pressure front pulse and the 3D shape of the cross-flow area $A(r)$ are combined with the $ds/d\log t$ signature and the flow dimension n -sequence to draw a more accurate representation of the aquifer. Figure 4.1 depicts an illustration of our approach for a Theis-like flow model that induces a

cylindrical-radial diffusion of the pressure front pulse's equipotential surface associated with a cylindrical radial flow dimension ($n = 2$).

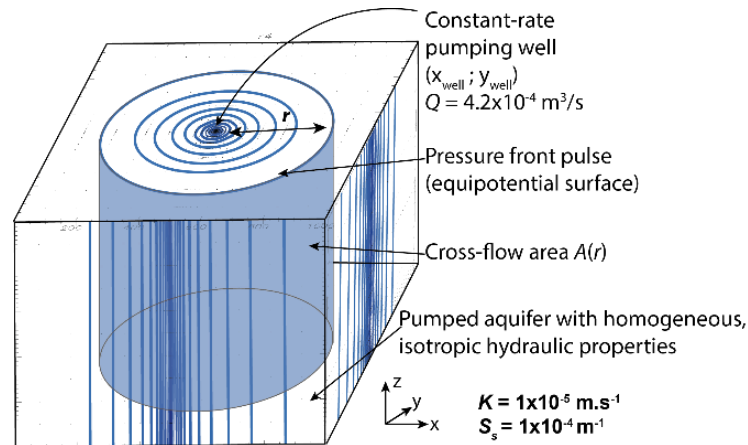


Figure 4.1: Example of the behavior of the cross-flow area in a 3D cylindrical-radial flow dimension conceptual model (A Theissian flow occurs before reaching the hydraulic boundaries).

The numerical simulations are performed using the HydroGeoSphere (HGS) code (Therrien et al. 2010; Brunner and Simmons 2012). The HGS code makes it possible to solve three-dimensional, fully-integrated surface/subsurface water flow, solute and heat transport models. This code discretizes the flow equation in 3-D using the control volume element method (Baliga and Patankar 1980). This approach divides the domain into non-overlapping control volumes. Each node is associated with one surrounding control volume in which the governing equations are integrated into each control volume. This method leads to discrete equations that conserve each quantity on a control-volume basis, as the differential

equations express the variation of a parameter for an infinitesimal control volume. This method has the advantage of providing good stability over a wide range of values of time and space and also of sampling sizes. We have selected this code because several studies have shown that it is a fast, robust and stable code and because it has the capability of generating various and complex 3-D geometries of aquifers. Simulation results are visualized by means of an original code in Interactive Data Language (IDL) reading HGS output ASCII files.

The conceptual model is composed of a saturated, homogeneous and isotropic porous media bounded by no-flow boundary conditions. The pumping rate is arbitrarily set at $4.2 \times 10^{-4} \text{ m}^3/\text{s}$. Note that the value of the constant pumping rate will not influence the characteristics of the $ds/d\log t$ signal because this signal reflects the diffusion of the pressure front-pulse, which is controlled only by the intrinsic properties of the aquifer (the hydraulic conductivity K and the specific storage S_s , the ratio of which expresses the diffusivity of the aquifer). The flow domain is set intentionally and sufficiently large in order to observe the entire n -sequence. The dimensions of the flow domain are 10 km along the x-axis and 20 km along the y-axis. The IS aquifer is composed of a no-flow inclined plane sloping from the west side to the east side of the conceptual model (Figure 4.2). The angle of inclination of the substratum ranges between 5 and 65°. In most simulations, the pumping well is fully screened, has a length L_w of 4 meters and fully penetrates the aquifer, reaching the IS. The well is centered in the z-axis and is located close to the corner formed by the angle between the inclined substratum and the top of the confined aquifer in the x-axis (Figure 4.2).

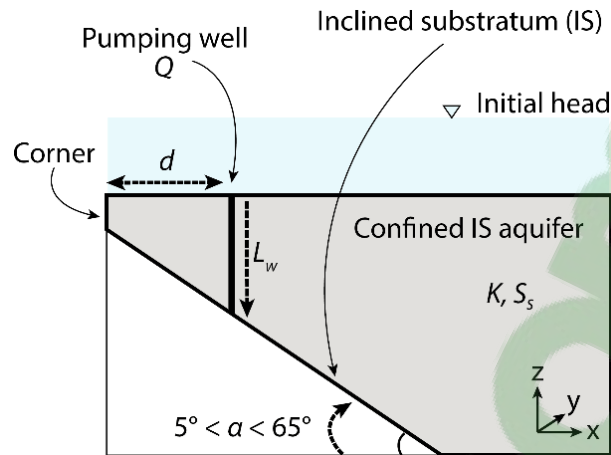


Figure 4.2: Conceptual model of an aquifer having an inclined substratum. The arrows represent the geometrical parameters that were varied in the sensitivity analysis, such as the distance from the pumping well to the corner d , the length of the well L_w , the inclination of the substratum α .

The spatial discretization is generated by quadrilateral elements of variable size ranging from 0.05 in the vicinity of the well, to 200 m close to the boundaries. Time intervals increase exponentially in order to obtain a suitable distribution of points in a time-logarithmic axis.

A sensitivity analysis was performed in order to establish relationships between the physical parameters of the IS aquifer (hydraulic conductivity K [$L \cdot T^{-1}$], specific storage S_s [L^{-1}], distance from the well to the corner d [L], well length L_w [L] and inclination of the substratum α [radians]) and the specific key points of the derivative signal. Each section of the sensitivity analysis briefly presents the tested parameters of the model. Only one parameter is tested at a time. For each section, a log-log plot of the tested variable parameter (K , S_s , α , L_w , d) and the $ds/d\log t$ is presented. For each log-log plot, a regression equation is estimated.

Empirical equations are developed by combining all the regression equations of the relationships between the aquifer's parameters and the characteristic points of the derivative signal. Two methods were used to estimate the coefficients of the developed equations: these were calculated from the developed equations and estimated by minimizing the relative error between the modeled values and the equation-based estimated values. The equations make it possible to estimate K , S_s , α from the graphic read of m_{2-BC} and m_3 on a log-log plot of $ds/dlogt$.

4.6 NUMERICAL RESULTS AND INTERPRETATIONS

4.6.1 BASE CASE ANALYSIS AND HYDRODYNAMIC INTERPRETATIONS

This section presents a base case study to illustrate the numerical approach and the diagnostic tools of this study used to represent the hydrodynamic flow behavior of an IS conceptual model. The next section will present the results of the sensitivity analysis and an illustration of the cross-flow area. The example model is composed of an aquifer featuring a 65° inclined substratum; the well is located close to the corner (Figure 4.3). Examples of the cross-sections of the pressure front pulse (Figure 4.3), the diagnostic plots (Figure 4.4) and the main hydrodynamic interpretations (Figure 4.5) are presented. Furthermore, this section presents the benefits of a qualitative interpretation of the constant-rate pumping test when analysing both the log-log plot of the drawdown log-derivative signal and the semi-logarithmic plot of the drawdown.

The flow dimension sequence is hydrodynamically interpreted by tracking the equipotential surface of the pressure front pulse through the aquifer as a function of space and time (Figure 4.3). The cross-flow area is composed of a truncated cylinder (whose length is the same as the length of the pumping well) and a truncated hemisphere. Both cross-flow areas are truncated by the inclined substratum (Figure 4.3-D).

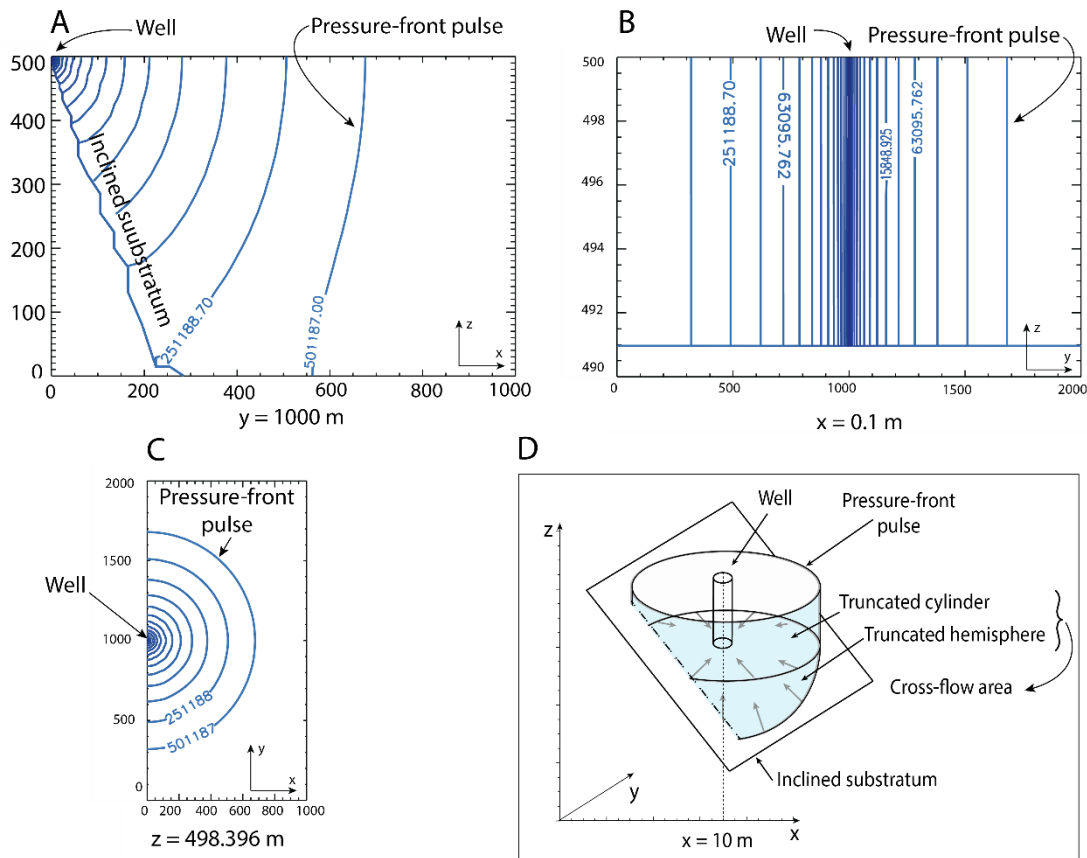


Figure 4.3: Examples of cross-flow area shapes throughout the aquifer in a X-cross section (A), a Y-cross section (B) and a plan view (C) for an aquifer having a 65° inclined substratum. The pumping well is located at $x = 10$ m and reaches the inclined substratum. (D) 3D conceptual model of a cross-flow area produced by a well located in an IS aquifer.

Figure 4.4 depicts the semi-logarithmic plot of the drawdown and the log-log plot of the drawdown log-derivative signal of a pumping test located at $x = 10$ m (Figure 4.3-A). The drawdown signal is composed of two slopes (Figure 4.4-A). A conventional interpretation would have interpreted the first slope as being a reflection of the signal of a Theis-like model. The second slope, showing a slowdown of the drawdown, would have been interpreted as the attainment of constant-head boundaries (Figure 4.4-A). It now appears evident that these two interpretations would be erroneous: the model is actually composed of an IS aquifer bounded by no-flow boundaries. The interpretation of the drawdown log-derivative signal (Figure 4.4-B) will make it possible in future to avoid these erroneous interpretations and furthermore to appropriately diagnose the geometry of flow and the boundaries of the aquifer, as well as to more accurately estimate the aquifer's hydraulic parameters. The following section will develop the proposed methodology to improve the diagnosis of the transient test. The $ds/d\log t$ signal is composed of two plateaus of zero slope (radial flow dimension, $n = 2$) followed by a -0.5 slope (spherical flow dimension, $n = 3$) (Figure 4.4-B). The constant-head boundaries which would classically have been interpreted using the Cooper-Jacob plot are in fact the signal of an increase in transmissivity due to the IS which induces $n = 3$.

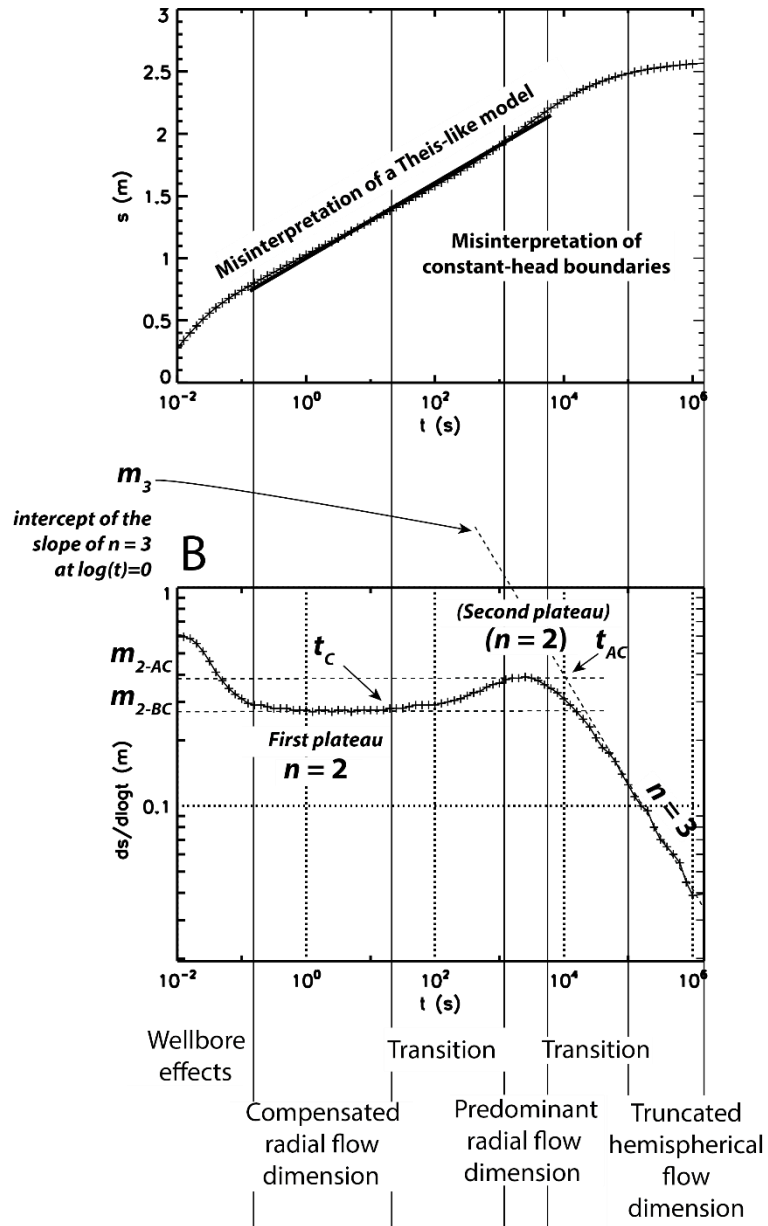


Figure 4.4: A) Semi-logarithmic plot of the drawdown signal (s) as a function of time (t), B) Log-log plot of the drawdown log-derivative signal ($ds/d\log t$) as a function of time (t) of an aquifer with a sharply inclined substratum (65°).

Figure 4.5 illustrates the cross-flow area which is induced by a pumping test performed in an IS aquifer. The first plateau of Figure 4.4-B reflects the cylindrical expansion of the pressure front pulse before it reaches the corner. This first radial flow dimension reflects the diffusion of the smallest cross-flow area of Figure 4.5 and is named the “compensated radial flow dimension”. t_c represents the time when the pressure front pulse reaches the corner. Before reaching the corner (when the radius is smaller than the distance well-to-corner), the cross-flow area has the shape of a truncated cylinder in which a portion is lost (lost cylindrical surface A''_{C-loss} in Figure 4.5) in the west direction (direction of the corner) and another portion is gained (truncated hemisphere inducing a spherical surface A'_s in Figure 4.5) in the east direction (direction opposite of the corner). Because the surfaces A''_{C-loss} and A'_s are comparable, the gain in transmissive surface to the east is compensated by the loss of surface to the west. As a result, the surface of the IS cross-flow area grows as though it were a whole cylinder: $A(r) \sim 2\pi r(t)L_w$, with L_w the length of the pumping well. The Y-intercept of the plateau which represents the compensated radial flow dimension is named m_{2-BC} (before the pressure front pulse has reached the corner). The second plateau, which is twice the Y-value of the first plateau, appears when the pressure front pulse reaches the west corner (located in $x = 0$ m) (Figure 4.5). The Y-intercept of the second plateau is named m_{2-AC} (after the pressure front pulse has reached the corner). This second radial flow dimension reflects the diffusion of the greatest cross-flow area of Figure 4.5 and is named the “predominant radial flow dimension”. Once the pressure front pulse has reached the corner and during the remainder of the pumping test (when the radius is greater than the distance between the well and the corner), the cross-flow area is only composed of a truncated cylinder (A'_c in Figure 4.5) and a truncated hemisphere (A'_s in Figure 4.5). As the

pressure front pulse expands, the surfaces of both the truncated cylinder $A'_C \sim \pi r(t)L_w$ and the truncated hemisphere $A'_S \sim 2\alpha r(t)^2$ will increase when the angle α of the inclined substratum increases. Note that when $\alpha = 2\pi$, the result of the previous equation of A'_S is equivalent to the surface of a sphere. As long as the surface A'_C is greater than the surface A'_S , the predominant radial flow dimension is rendered. Because the $ds/d\log t$ signal reflects the flow dimension of the largest geometrical surface of the equipotential surface of the pressure front pulse, the signal will express a radial flow dimension (plateau) when $A'_C > A'_S$ and it will express a spherical flow dimension (a straight line with a slope of 0.5), when $A'_S > A'_C$. Note that, if the distance from the well to the corner is very short, the compensated radial flow regime does not occur. Thus, only one plateau (the predominant radial flow regime) is observed before the spherical flow regime, as observed in Figures 4.6 and 4.11. The time that represents the intersection point between the predominant radial flow dimension and the spherical flow dimension is named t_{AC} (time after the pressure front pulse has reached the corner). This point can be found (Equation (4.7)) when equalizing the power law regression of the predominant radial flow dimension (Equation (4.5)) and that of the spherical flow dimension (Equation (4.6)).

$$ds/d\log(t_{AC}) = m_{2-AC} \times (t_{AC})^0 \quad (4.5)$$

$$ds/d\log(t_{AC}) = m_3 \times (t_{AC})^{-0.5} \quad (4.6)$$

From graphical constraints, the time t_{AC} is estimated as Equation (4.7):

$$t_{AC} = \left(\frac{m_3}{m_{2-AC}} \right)^2 \quad (4.7)$$

with m_3 the Y-intercept of the spherical flow dimension and m_{2-AC} the Y-intercept of the second plateau. Note that t_{AC} is different from the time required for the pressure front pulse to reach the corner t_C with $t_C < t_{AC}$ (Figure 4.4-B). Note also that when the pressure front pulse reaches all the no-flow boundaries, the $ds/d\log t$ signal will show a late-time unit slope reflecting the depletion of the aquifer.

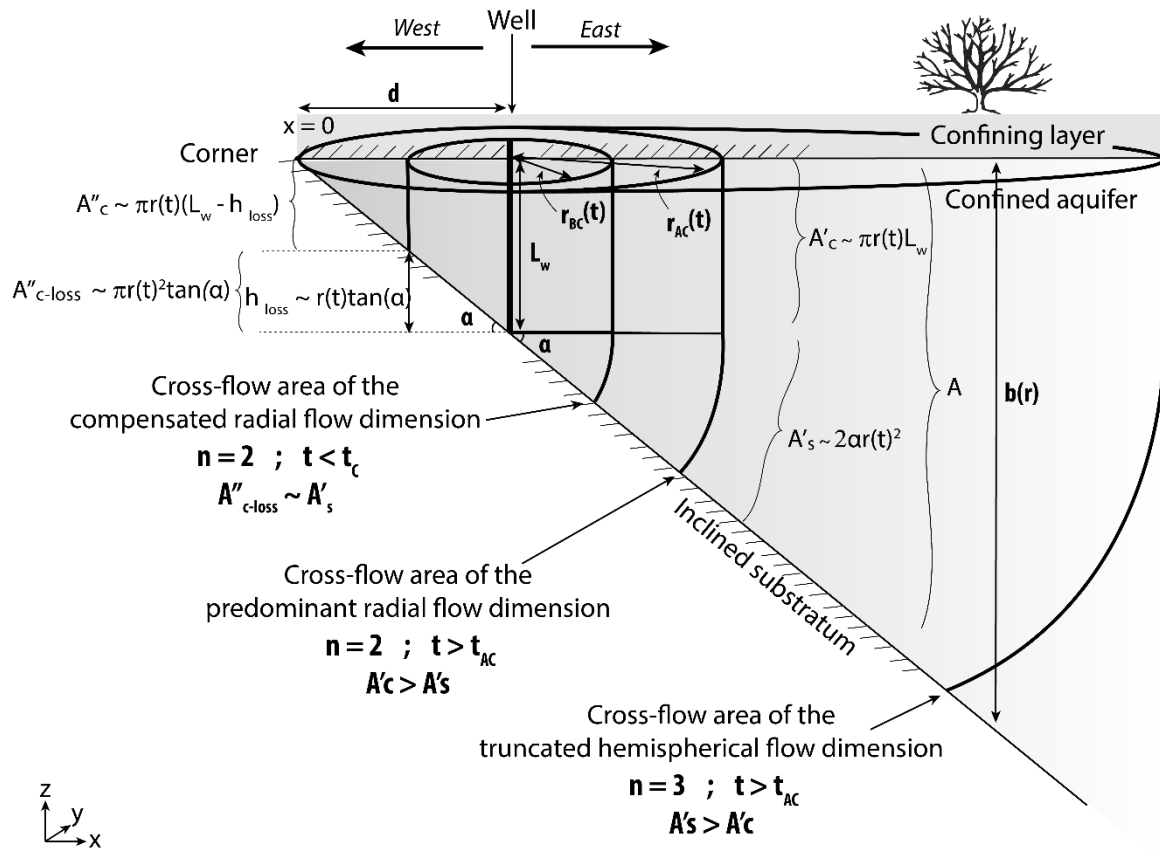


Figure 4.5: Conceptual models of the diffusion of the cross-flow area before and after reaching the corner in $x = 0$. The notations with A_c (A''_c , A''_c-loss and A'_c) represent the different portions of surfaces of the truncated cylinder as visualized on the figure; the notation A_s represents the surface of the truncated hemisphere. The single apostrophe (for A'_c and A'_s) indicates the surface in the east direction, whereas the double apostrophe (A''_c and A''_c-loss) indicates the surfaces in the west direction (direction of the corner).

4.6.2 $ds/d\log(t)$ PLOTS AND SENSITIVITY ANALYSIS: ESTABLISHING EMPIRICAL FORMULAS FOR ASSESSING THE HYDRAULIC PROPERTIES OF THE AQUIFER

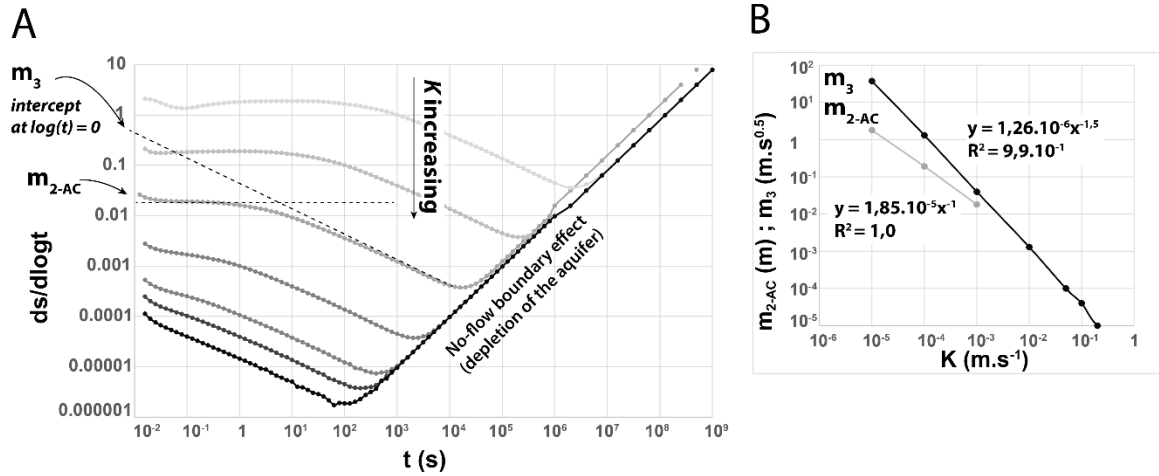
This sensitivity analysis conducted using numerical modeling aims at determining the influence of the physical parameters of the aquifer on the $ds/d\log t$ signal. More particularly, the focus of this section is to analyse how and to what extent the derivative signature reflects the hydraulic properties (K , S_s), the pumping rate (Q), the well location (d), the inclination of the no-flow substratum (α) and the length of the well (L_w). This sensitivity analysis makes it possible, in the following section, to develop an empirical equation for estimating the hydraulic properties of an IS aquifer more accurately than the conventional Theis (1935) and Cooper and Jacob (1946) methods. Note that, depending only on the intrinsic properties of the aquifer (Diffusivity K/S_s), the rate of the diffusion of the pressure wave is independent of the rate of pumping. Therefore, hydraulic boundaries of the aquifer will not be reached sooner for higher pumping rates. Changes of pumping rate will only translate the derivative signal vertically resulting from the proportional relationships $m_{2-AC} \sim Q$, $m_{2-BC} \sim Q$ and $m_3 \sim Q$.

4.6.2.1 *Influence of the hydraulic conductivity K [$L.T^{-1}$]*

Figure 4.6-A depicts $ds/d\log t$ signatures where various K values are tested: $K = 10^{-5}$; 10^{-4} ; 10^{-3} ; 10^{-2} ; 5×10^{-2} and 10^{-1} m/s. In Figure 4.6-A, K increases from up to down. Thus, K changes the Y-intercept of the derivative signal of the predominant radial flow dimension (m_{2-AC}) and the spherical flow dimension (m_3). Figure 4.6-B shows that the relationships

between K and m_{2-AC} and m_3 are different. Both m_{2-AC} and m_3 are decreasing as K is increasing; the relationships are, respectively: $m_{2-AC} \sim K^1$ and $m_3 \sim K^{1.5}$ (Figure 4.6-B).

Figure 4.6-A also shows that when K is low, the derivative signal is composed of $n = 2$ followed by $n = 3$, whereas when K is high, the derivative signal shows a single-stage $n = 3$. In fact, the higher the hydraulic conductivity, the shorter the predominant radial flow dimension. For transmissive IS aquifers, the pressure front pulse spreads rapidly (due to a high diffusivity value); thus the area of the portion of sphere A'_s becomes quickly greater than the area of the half cylinder A'_c . Therefore, the spherical flow dimension is masking the predominant radial flow dimension at an earlier time. Note that for highly transmissive aquifers, the predominant radial flow dimension does not have enough time to occur (see $ds/d\log t$ curves at the bottom of Figure 4.6-A). Thus, the derivative signal of the aquifer is only represented by a single-stage spherical flow dimension. It should also be noted that because the well is located close to the aquifer's corner, the compensated radial flow dimension is not visible.



Parameters of the model:

$S_s = 10^{-4} m^{-1}$ $y_{well} = 1000 m$
 $Q = 4.2 \times 10^{-4} m^3 \cdot s^{-1}$ $\alpha = 65^\circ$
 $d (= x_{well}) = 0.1 m$ $L_w = 8 m$

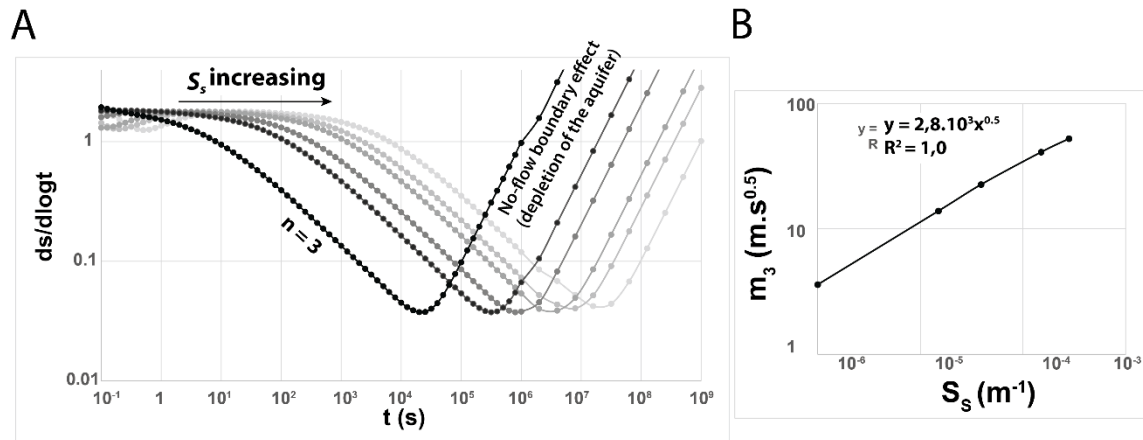
Tested parameters:

$K = 10^{-5}, 10^{-4}, 10^{-3}, 10^{-2}, 5 \cdot 10^{-2}, 10^{-1} m \cdot s^{-1}$

Figure 4.6: A) Log-log plot of the drawdown log-derivative signal versus time in a sensitivity analysis of the hydraulic conductivity K . B) depicts the Y-intercept of the radial flow dimension m_{2-AC} and the Y-intercept of the spherical flow dimension m_3 versus K .

4.6.2.2 Influence of the specific storage S_s [L^{-1}]

Figure 4.7-A depicts $ds/d\log t$ signatures where various S_s values are tested: $S_s = 7.8 \times 10^{-4}$; 2.8×10^{-4} ; 1.5×10^{-4} ; 3.9×10^{-5} ; 1.5×10^{-5} and $1 \times 10^{-6} m^{-1}$. The decrease of the specific storage shifts the derivative curve with respect to time but it does not change the shape of the curve. An increase of the specific storage S_s induces an increase of the Y-intercept of the spherical flow dimension m_3 as: $m_3 \sim S_s^{0.5}$ (Figure 4.7-B).



Parameters of the model: $K = 10^{-5} \text{ m}^{-1}$, $d (= x_{\text{well}}) = 1 \text{ m}$, $Q = 4.2 \times 10^{-4} \text{ m}^3 \cdot \text{s}^{-1}$, $y_{\text{well}} = 1000 \text{ m}$, $L_w = 8.2 \text{ m}$, $\alpha = 65^\circ$

Tested parameters: $S_s = 7.8 \times 10^{-4}; 2.8 \times 10^{-4}; 1.5 \times 10^{-4}; 3.9 \times 10^{-5}; 1.5 \times 10^{-5}; 1 \times 10^{-6} \text{ m}^{-1}$

Figure 4.7: A) Log-log plot of the drawdown log-derivative signal versus time in a sensitivity analysis of the specific storage S_s . B) depicts the Y-intercept of the spherical flow dimension m_3 versus the specific storage S_s .

4.6.2.3 Influence of the distance from the well to the corner d [L]

Figure 4.8-A displays the $ds/d\log t$ signatures where various well positions are tested: $d = 0, 1, 10, 100, 200, 500, 800 \text{ m}$. Figure 4.8-A shows that the longer the distance d separating the corner from the well, the longer the first plateau. In other words, as long as the pressure front pulse has not reached the corner, the compensated radial flow dimension occurs. The time of the end of the compensated radial flow dimension t_c increases with d (Figure 4.8-B) with the linear regression: $t_c \sim d^2$.

When the well is located at 0,1 m from the corner, the effect of the corner is immediately felt. Thus, the derivative curve displays a single predominant radial flow dimension before the spherical flow dimension. If the well is located in the center of the flow model ($d = 500$, the lowest signal of Figure 4.8-A), the derivative shows a single plateau. In this case, the compensated radial flow dimension is the only visible flow dimension because the corner and the other no-flow boundaries are equidistant. Thus, despite the fact that the thickness of the aquifer is increasing (IS aquifer), the spherical flow dimension is masked by the compensated radial flow dimension (lower $ds/d\log t$ signal of Figure 4.8-A).

Because the scope of this paper is limited to analysing the signal of an IS aquifer, which does not present any partially penetrating well effects, if d increases, therefore L_w increases as well, so that the well is fully penetrating the IS aquifer. As a result, the derivative signal is offset downward (Figure 4.8-A). Figure 4.8-C expresses this relationship by showing the Y-intercept of the first plateau of the derivative signal m_{2-BC} as a function of the length of the well L_w . The regression equation is:

$$m_{2-BC} \sim L_w^{-1}.$$

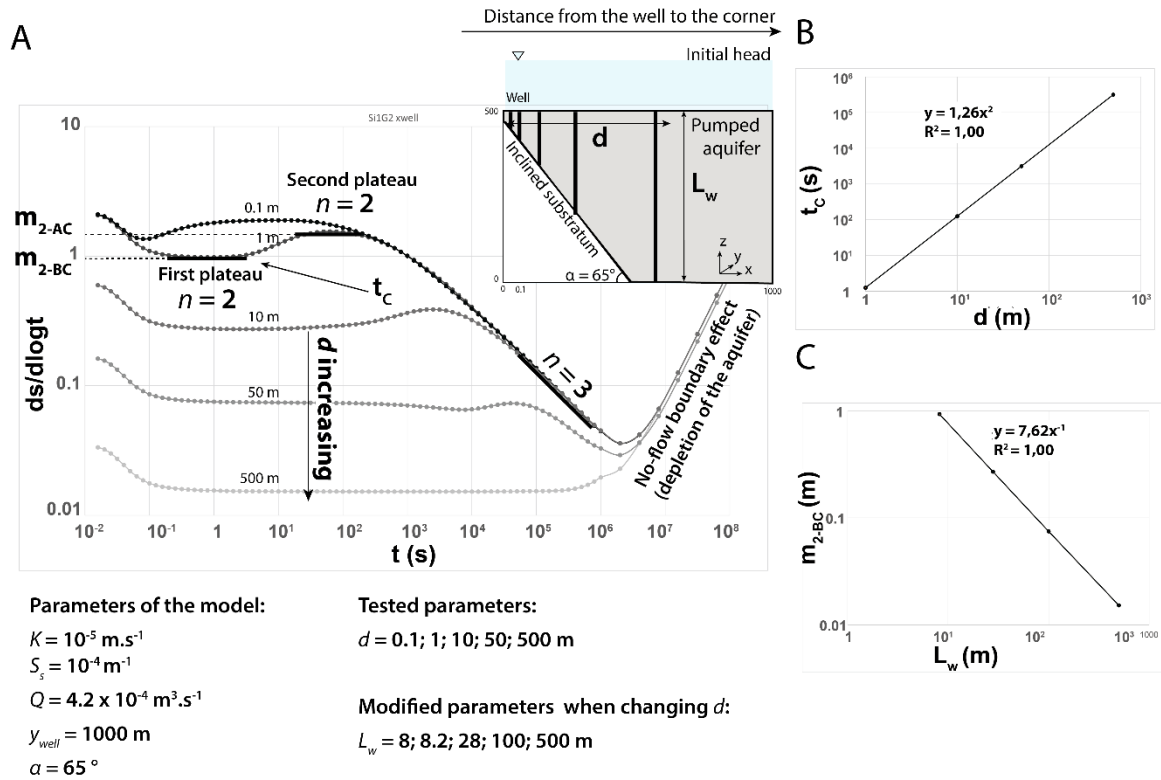


Figure 4.8: A) shows the log-log plot of the drawdown log-derivative signal of an aquifer having a 65° inclined substratum versus time in a sensitivity analysis of the distance from the well to the corner d . B) depicts the time of the end of the early radial flow dimension (first plateau in A1)) versus d . This first plateau represents the cylindrical-radial flow diffusion of the pressure front pulse before it reaches any flow boundary (compensated radial flow dimension). C) depicts the Y-intercept of the first plateau m_{2-BC} versus the length of the well L_w .

4.6.2.4 Influence of the length of the well L_w [L]

Figure 4.9-A displays $ds/d\log t$ signatures where various well lengths are tested: $L_w = 8, 41$ and 150 m . The thickness above the inclined substratum is increased in order to elongate the length of the well but the inclination of the substratum and the well position are maintained (see conceptual models in Figure 4.9-A).

On Figure 4.9-A, the length of the well increases, going from the uppermost to the lowermost curve. The greater the well length, the longer the predominant radial flow dimension. The greater L_w , the higher the transmissivity of the truncated cylinder. Therefore, the Y-intercept of the predominant radial flow dimension m_{2-AC} is inversely proportional to the length of the well, with the relationship $m_{2-AC} \sim L_w^{-1}$ (Figure 4.9-C). Note that because the well is close to the corner, the first plateau (m_{2-BC}) is not visible.

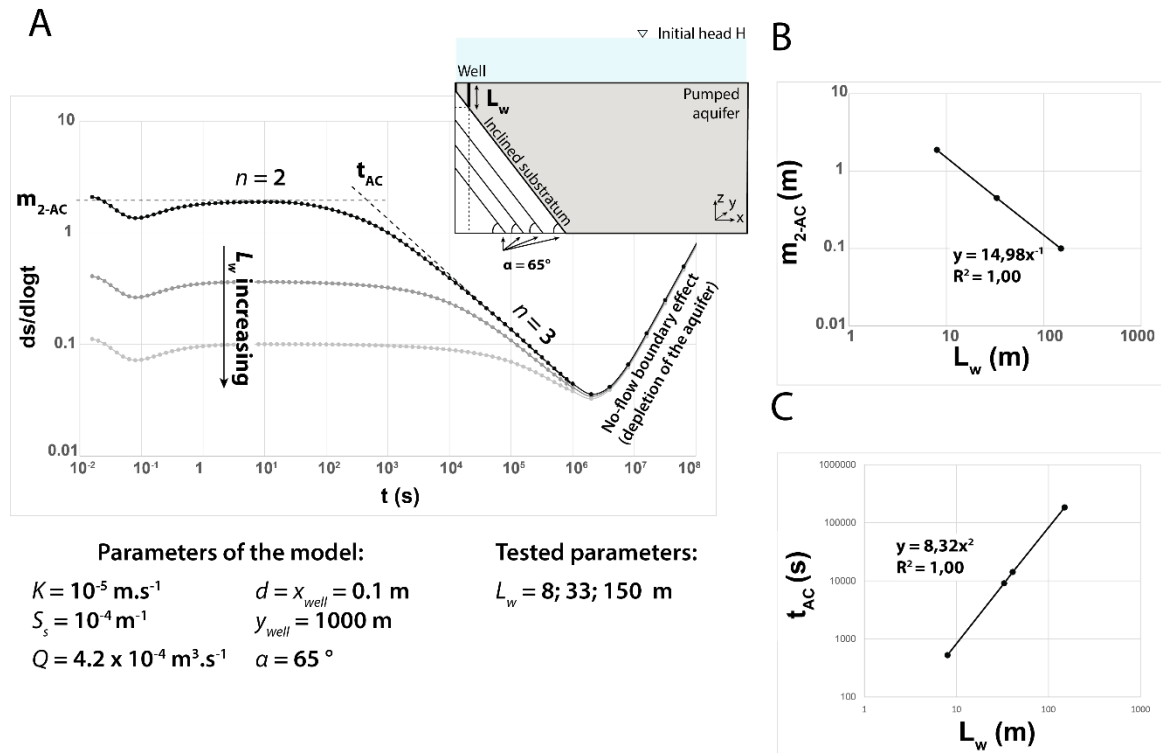


Figure 4.9: A) shows the log-log plot of the drawdown log-derivative signal versus time in an aquifer having a 65° inclined substratum in a sensitivity analysis of the length of the well L_w . B) depicts the Y-intercept of the predominant radial flow dimension m_{2-AC} versus L_w .

4.6.2.5 Influence of the inclination of the substratum α

Figure 4.10-A displays the $ds/d\log t$ signatures where various inclinations of the substratum are tested: $\alpha = 5, 10, 20, 50^\circ$. On Figure 4.10-A, the inclination of the substratum increases from up to down. Figure 4.10-A also shows that the lesser the inclination of the substratum, the longer the predominant radial flow dimension masks the spherical flow dimension. Indeed, because the surface of the truncated cylinder $A'c$ evolves proportionally to $r.L_w$ and because the surface of the truncated hemisphere $A's$ evolves proportionally to $\alpha.r(t)^2$ (Figure 4.5), when α is small, $A's$ increases slowly and becomes greater than $A'c$ at a later time than when α is large. Thus, the predominant radial flow dimension is of longer duration when the substratum is less inclined.

Figure 4.10-A also shows that the lesser the inclination of the substratum, the higher the Y-intercept of the spherical flow dimension m_3 . In other words, the higher the inclination of the substratum, the higher the transmissivity of the IS aquifer and therefore the lower m_3 : $m_3 \sim \alpha^{-1}$ (Figure 4.10-C).

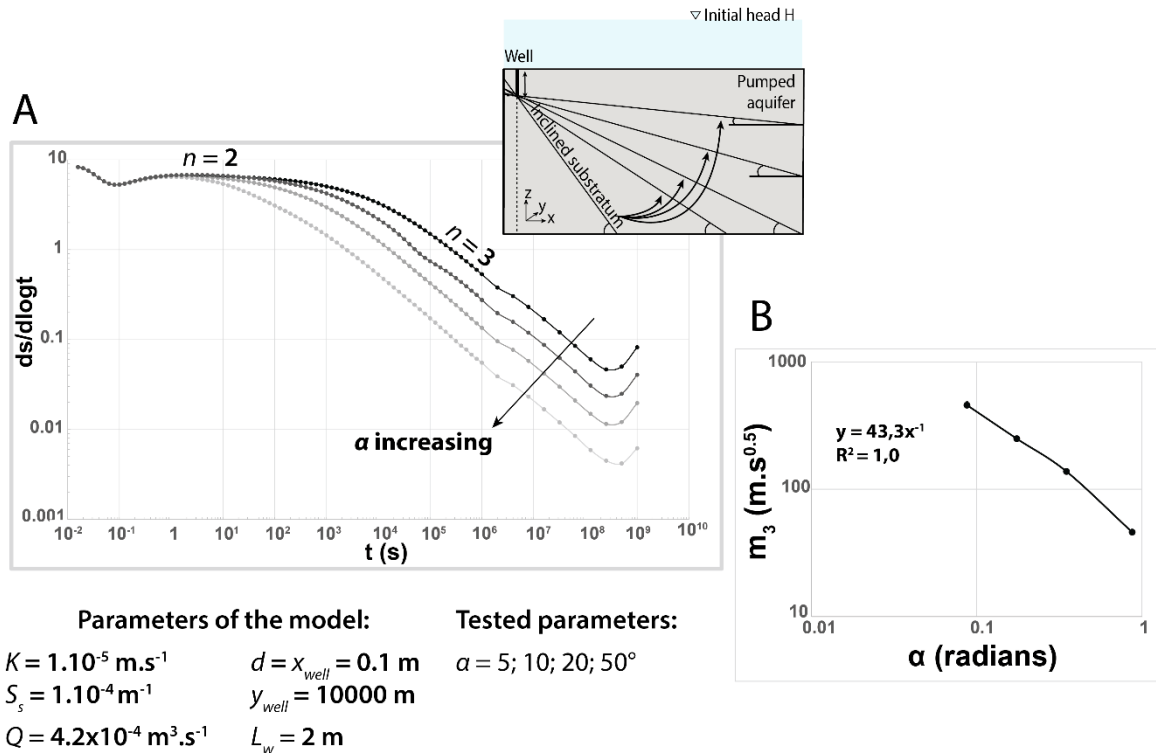


Figure 4.10: A) shows the log-log plot of the drawdown log-derivative signal of four conceptual models having, respectively, $\alpha = 5, 10, 20$ and 50° of inclination of the substratum, from dark to light-gray. B) depicts the Y-intercept of the spherical flow dimension m_3 versus α .

4.6.2.6 Influence of the anisotropy of the hydraulic conductivity

Figures 4.12-A and B display the $ds/d\log t$ signatures of two IS conceptual models: one with a deep inclination (65°) and another with a weak inclination (5°) of the substratum. For each conceptual model, four case studies are analysed. Respectively, case 1, case 2, case 3 and case 4 represent flow models with isotropic K values, anisotropic K values where the highest K is in the Z-direction, anisotropic K values where the highest K is in the Y-direction and

anisotropic K values where the highest K is in the X-direction. Figures 4.12-A and B show that the derivative curves associated with case 1 and case 2 (Figure 4.11-A) or superimposed (Figure 4.11-B) and the plan view of the pressure wave of both models are identical (Figures 4.11 C and D). This suggests that there is no vertical flow (or that vertical flow is negligible).

As shown in Figure 4.6-B, the hydraulic conductivity is inversely proportional to the Y-intercept of the derivative signal m . The $ds/dlogt$ signal of case 3 and case 4 are shifted downward relative to the curves of case 1 and case 2 because the hydraulic conductivity in which the pressure front pulse diffuses (in the X or Y direction) is increased. Figure 4.11-B shows that depending on whether the anisotropy is parallel (in the X-direction, Figure 4.11-F, case 4) or perpendicular (in the Y-direction, Figure 4.11-E, case 3) to the direction of the substratum's inclination, the spherical signal is accentuated or masked. In fact, the spherical flow dimension ($n = 3$) is seen earlier for the case 4 model (highest K in the X-direction) whereas the predominant cylindrical radial flow is longer for the case 3 model (higher K in the Y-direction). For the case 4 model, the pressure front pulse is diffused faster in the X-direction (Figure 4.11-F); thus, the surface of A_s' (Figure 4.5-B) increases faster and becomes earlier superior to A_c' . For case 3, the diffusion of the pressure front pulse is faster in the Y-direction. Because the diffusion of the pressure front pulse is faster and there is no variation of the thickness of the aquifer in the Y-direction, A_c' is longer and greater to A_s' . Thus, the predominant radial flow dimension is longer.

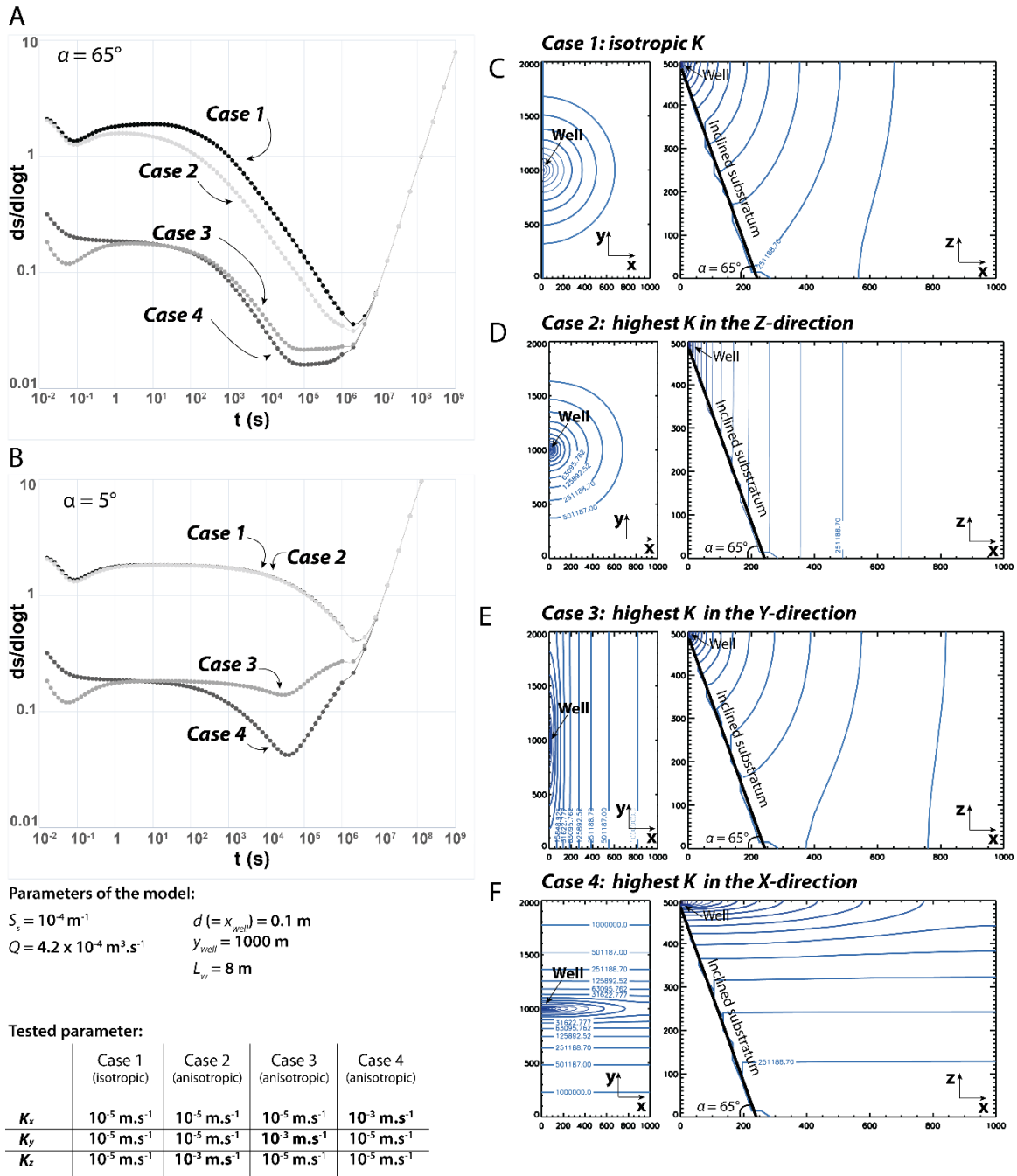


Figure 4.11: A) Log-log plot of the drawdown log-derivative signal *versus* time in an IS aquifer having $\alpha = 65^\circ$. B) Same flow model as A) with $\alpha = 5^\circ$. Respectively, the black, the light grey, the grey and the dark grey curves are respectively associated

with case 1 (isotropy of K), case 2 (anisotropy of K with highest K in the Z-direction), case 3 (anisotropy of K with highest K in the Y-direction) and case 4 (anisotropy of K with highest K in the X-direction). C), D), E), F) represent a plan and a transversal view of the equipotential surfaces of the pressure front pulse as it diffuses through aquifers of cases 1, 2, 3 and 4.

4.6.3 ESTIMATION OF HYDRAULIC PROPERTIES

4.6.3.1 Analytical solution for an inclined substratum aquifer

The previous sensitivity analysis has made it possible to establish relationships between the characteristic points and lines of the log-log plot of the $ds/d\log t$ signal (*i.e.*, m_{2-BC} , m_{2-AC} and m_3) and the various parameters of the inclined substratum model (*i.e.*, K , S_s , Q , d , L_w , α). The following equations are valid for a confined, homogeneous, isotropic and totally screened aquifer. Table 4.1 summarizes the relationships obtained in the sensitivity analysis section of the numerical modeling. Based on these relationships, two equations (Equations (4.8) and (14)) are developed to estimate the hydraulic properties of the IS conceptual model. Two distinct methods were used to estimate the constant values in equations (4.8) and (4.9): i) because the numerical modeling makes it possible to precisely determine all the parameters of the model, the coefficients were calculated from equations (4.8) or (4.9) for several IS models with various configurations (various substratum inclinations, well positions, hydraulic properties, pumping rates), ii) the coefficients were also adjusted in order to minimize the relative error between the simulated and the estimated values of α , K , L_w , Q or S_s using equations (4.8) and (4.9). Then, for each equation, the values of the coefficient (using both methods) were averaged.

$$m_{2-BC} = 0.183 \cdot \frac{Q}{K \cdot L_w} \quad (4.8)$$

$$m_3 = 0.4 \cdot \frac{Q \cdot S_s^{0.5}}{K^{1.5} \cdot \alpha} \quad (4.9)$$

Note that if the well is close to the corner, the first plateau may not be visible. In this case, the term m_{2-BC} of Equation (4.8) can be replaced by $\frac{m_{2-AC}}{2}$. Indeed, according to the theory of image wells, when a no-flow boundary is reached, the drawdown rate is doubled. Thus, the Y-intercept of the radial flow dimension of the derivative signal is also doubled.

Note that the solution of Theis expressed with the $ds/dlogt$ signal characteristics is written as Equation (4.10):

$$K = \frac{2.3 \cdot Q}{m_2 \cdot 4 \cdot \pi \cdot b} \quad (4.10)$$

With m_2 the Y-intercept of the cylindrical radial flow dimension and b the thickness of the constant thickness aquifer. Equation (4.8), which is an empirical formula developed from the numerical analyses conducted in this study, is quasi identical to Equation (4.10), which is an analytical formula. The only differences are the denominators L_w and b . In the case of the inclined substratum, the thickness of the IS aquifer is not constant; hence it cannot be used in Equation (4.10). However, this study shows that if the early radial flow dimension is observed on a $ds/dlogt$ signal. The length of the well L_w must be used to determine the hydraulic conductivity, regardless of the thickness of the aquifer. This result can be

understood when observing Figure 4.5: the cylindrical portion of the cross-flow area expands radially by the same length as the length of the well. This result can also be demonstrated by comparing the $ds/d\log t$ signals of a Theissian conceptual model having a constant thickness (left sketch in Figure 4.12 A and B) against those of a conceptual model having an inclined substratum (right sketch in Figure 4.12 A and B). Each model has the same well position d and the same well length L_w . Figures 4.12 A and B represent, respectively, the comparison of the $ds/d\log t$ between a Theissian and an IS aquifer when the well is close to the corner and when the well is centered in the model. In Figure 4.12-A, both signals are superimposed until the spherical flow dimension becomes dominant in the IS aquifer. Hence, the same Y-intercept of both models, the Theissian and the IS aquifer, will be used to estimate the hydraulic properties in Equations (4.8) and (4.10). In Figure 4.12-B, the compensated radial flow dimension of the IS aquifer and the cylindrical radial flow dimension of the Theissian aquifer are entirely superimposed. It is therefore impossible to differentiate between the IS aquifer model and the Theis-like model when the pumping well is centered in the model. These simulations confirm that when a radial flow dimension is observable in an IS aquifer, then Equation (4.10) can be reformulated as Equation (4.8), by replacing m_2 by m_{2-BC} and b (the length of the aquifer) by L_w (the length of the well).

Table 4-1: Synthesis of the Y-intercept of the radials and the spherical flow dimension m_{2-BC} , m_{2-AC} and m_3 and the parameters of the conceptual model such as K , S_s , Q , d , L_w and α .

	Y-intercept of the $ds/d\log t$ signal
	m_{2-AC} or m_3
Hydraulic conductivity K ($m \cdot s^{-1}$)	$m_{2-AC} \sim K^{-1}$ $m_3 \sim K^{-1.5}$
Specific storage S_s (m^{-1})	$m_3 \sim S_s^{0.5}$
Constant-rate pumping test Q ($m^3 \cdot s^{-1}$)	$m_{2-AC} \sim Q$ $m_3 \sim Q$
Distance from the well to the corner d (m)	$m_{2-AC} \sim L_w^{-1}$
Length of the well L_w (m)	$m_{2-AC} \sim L_w^{-1}$
Inclination of the substratum α (radians)	$m_3 \sim \alpha^{-1}$

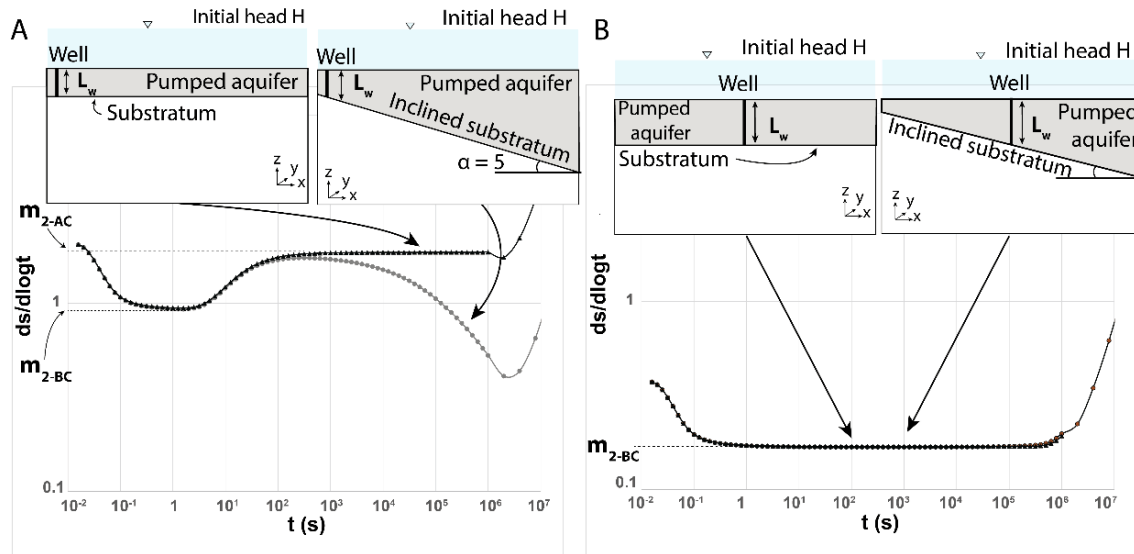


Figure 4.12: Log-log plot of the drawdown log-derivative signal versus time in a Theis-like conceptual model and an inclined substratum conceptual model when the well is located in the corner A) or in the center B) of the model.

4.6.3.2 Comparison between the Theis solution and the proposed method for assessing hydraulic properties

This section compares the values for hydraulic properties that are estimated using conventional Theis approaches (the Theis model and the Cooper-Jacob model) and the values obtained using the equations developed empirically in this study. A confined conceptual model having an inclined substratum of 20° was selected. The hydraulic conductivity and the storage coefficient were estimated from the three models (the Theis model, the Cooper-Jacob model and the empirical equations developed in this study). The results are summarized in Table 4.2. The log-log plot of s , the semi-log plot of s and the log-log plot of $ds/dlogt$ versus time are given in Figure 4.13.

Table 4.2 shows that the relative error when estimating K and S_s is systematically lesser when using the equation developed in this study than when using the conventional Theis and Cooper-Jacob models. The relative errors of K and S_s are, respectively, -1% and 0% using the empirical solutions of this study against 731% and 607% using the Theis model and -6% and -100% using the Cooper-Jacob model (Table 4.2). This comparison between calculated hydraulic properties demonstrates that the equations developed in this study are able to more accurately estimate the hydraulic properties of an IS aquifer than are the conventional Theis-like models. Furthermore, the Cooper-Jacob method may lead to the false interpretation of a constant head boundary because the semi-log plot of s versus t shows a stabilisation of the drawdown (Figure 4.13). In this case, however, it is known that the decrease of the drawdown rate is in reality related to the transmissivity increase of the pressure front pulse as it expands through the IS aquifer.

Table 4-2: Comparative summary of the accuracy of the hydraulic properties estimated by means of the Theis model, the Cooper-Jacob model and the equations developed in this study.

	K (m/s)	Relative error	S	Relative error	α (°)	Relative error
Parameters of the model	1.0E-05		1.0E-04		20	
Theis model	8.31.E-05	731%	7.1E-04	607%	-	
Cooper-Jacob model	9.42.E-06	-6%	8.9E-09	-100%	-	
This study	9.92.E-06	-1%	1.0E-04	0%	20	0%

We have thus shown that interpreting the drawdown log-derivative signal makes it possible to more accurately estimate the hydraulic properties of a confined aquifer having an inclined substratum. This method also helps to better characterize the hydrodynamic behavior (n -sequence = (2) - 2 - 3) around the well and helps to better determine the aquifer's boundary conditions. Note that the estimation of S_s by means of Equation (4.9) does require knowledge of the inclination of the substratum; this value must be estimated from field data, based on a cross-section and well logs or based on geophysical methods. If S_s is already known (if using Equation (4.11), proposed by Freeze and Chery (1979)), the inclination of the substratum can be estimated from Equation (4.9).

$$S_s = \rho g((1 - n).m_v + n\beta) \quad (4.11)$$

With, ρ the density of water [$M.V^{-3}$], g the gravitational constant [$L.T^{-2}$], n the porosity, m_v the volumetric compressibility of the porous matrix [$L.M^{-1}.T^2$] and β the coefficient of compressibility of water [$L.M^{-1}.T^2$].

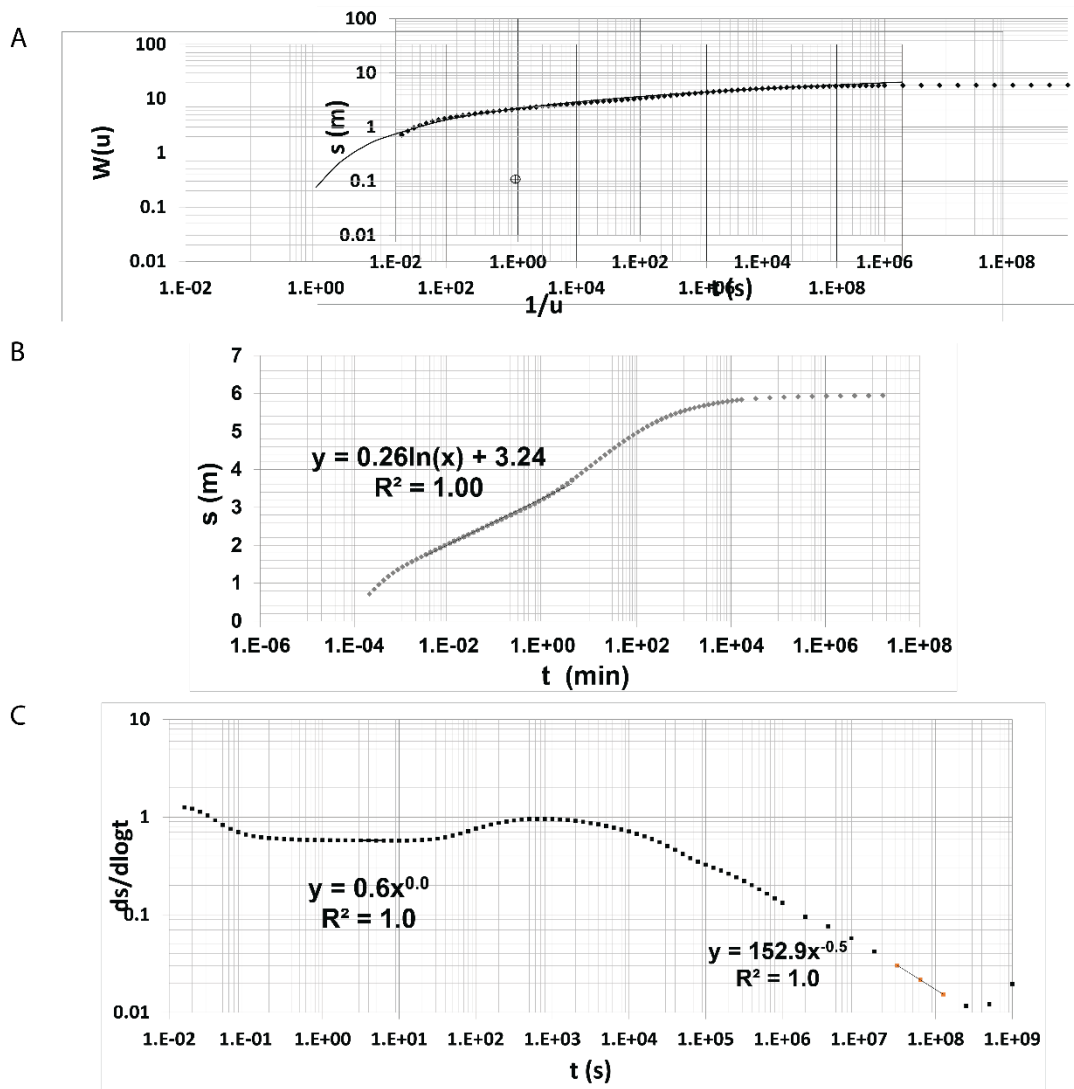


Figure 4.13: A) Log-log plot of the drawdown versus time, This model; B) semi-log plot of the drawdown versus time, Cooper-Jacob model; and C) log-log plot of the drawdown log-derivative signal, i.e the conceptual model developed in this study with substratum having an inclination of 50° , $K = 1 \times 10^{-5}$ m/s, $S_s = 1 \times 10^{-4}$ m $^{-1}$, $lw = 2$ m.

4.7 FIELD EXAMPLES

This section applies the diagnostic tools developed in this study to field data. Two derivative signatures are analysed: one of a partially penetrated (PP) aquifer and another of an aquifer having an inclined substratum (IS). Both curves are presented in order to alert practitioners to the fact that the derivative signal is not unique and that a minimum of geological information is required to accurately interpret a pumping test.

Because the drawdown log-derivative of field data is typically very noisy, the field case study example of section 5 presents a $ds/d\log t$ signal that has been smoothed using the algorithm of Bourdet et al. (1989). This algorithm has proven to be one of the most efficient in filtering noise without deteriorating the hydraulic signature (Escobar et al. 2004b). The noise or the spreading of data may be due to datalogger or operator complications, pumping rate variations, random diffuse heterogeneity fields and tidal or recharge effects. The field example presented in Figure 4.14-A shows three pumping rate adjustments (vertical dashed line). The differentiation equation is:

$$\frac{ds_i}{dX_i} = \frac{\left(\frac{\Delta s_1}{\Delta X_1} \Delta X_2 + \frac{\Delta s_2}{\Delta X_2} \Delta X_1 \right)}{(\Delta X_1 + \Delta X_2)} \quad (15)$$

with: $\Delta s_1 = s_i - s_1$; $\Delta s_2 = s_i - s_2$; $\Delta X_1 = X_i - X_1$; $\Delta X_2 = X_i - X_2$ and $X = \log(t)$.

Equation (15) uses 3 points: the next and previous points (1 and 2) of point i which are the first to be separated by a minimum length of L . This length can be adjusted until the noise is attenuated and the signal is no longer distorted. The drawing of straight lines on the log-log plot of $ds/dlogt$ signal is performed manually by considering the differentiation curve for a specific L value that smooths the derivative data without changing the trend of the signal (Equation (15)).

The selected site is that of Longue-Rive. It is located north of the Saint-Lawrence River in the Haute-Côte-Nord region of the province of Quebec, Canada. The Precambrian substratum has been eroded by glaciers and scours were then filled by the fluvio-glacial outwash during Quaternary deglaciation, creating granular aquifers located in a glacial valley. When the ice cap farther retreated, sea water invaded the lowlands (whose surfaces were then below sea level). These became part of the Goldthwait Sea and a thick layer of clay (approximately 35 m) was deposited and covered the previously deposited granular aquifer, thus confining it. The stratigraphic-log of P-1 depicts from top to depth: 2.1 m of fine sand, 34.4 m of clayey silt, 4.6 m of sand, 1.5 m of fine gravel and 3.4 m of sand and gravel. In the study site of Longue-Rive, all the drilling logs reach the granitic basement rock, making it possible to construct a stratigraphic section and to model the topography of the rock and the thickness of the granular deposits (Figure 4.14). The stratigraphic sections 1 and 2 emphasize a North-South glacial valley. Thus, in the North-South direction, the substratum has an inclination of 5° and in the East-West the substratum has an inclination of 4.2° . In the framework of a water supply study, a constant-rate pumping test study was performed in the well P-1 (Figure 4.14). The drawdown log-derivative signal shows a single-stage and long-

term spherical flow dimension (Figure 4.14-A). Unfortunately, the signal is disturbed by pumping rate adjustments at 55, 243 and 3390 min that cause an upward translation of the spherical signal. It appears evident that the spherical flow dimension cannot be interpreted using the partial penetration assumption, because the pumping well and the piezometers are known to reach the substratum. The assumption of a partially screened well is also invalid in this case study, because the screen thickness of P-1 represents 57% of the thickness of the granular aquifer, which is above the 40% penetration ratio suggested by Moncada et al. (2005) to observe a spherical flow dimension. The spherical flow dimension is better interpreted using the IS aquifer model rather than the PP aquifer model.

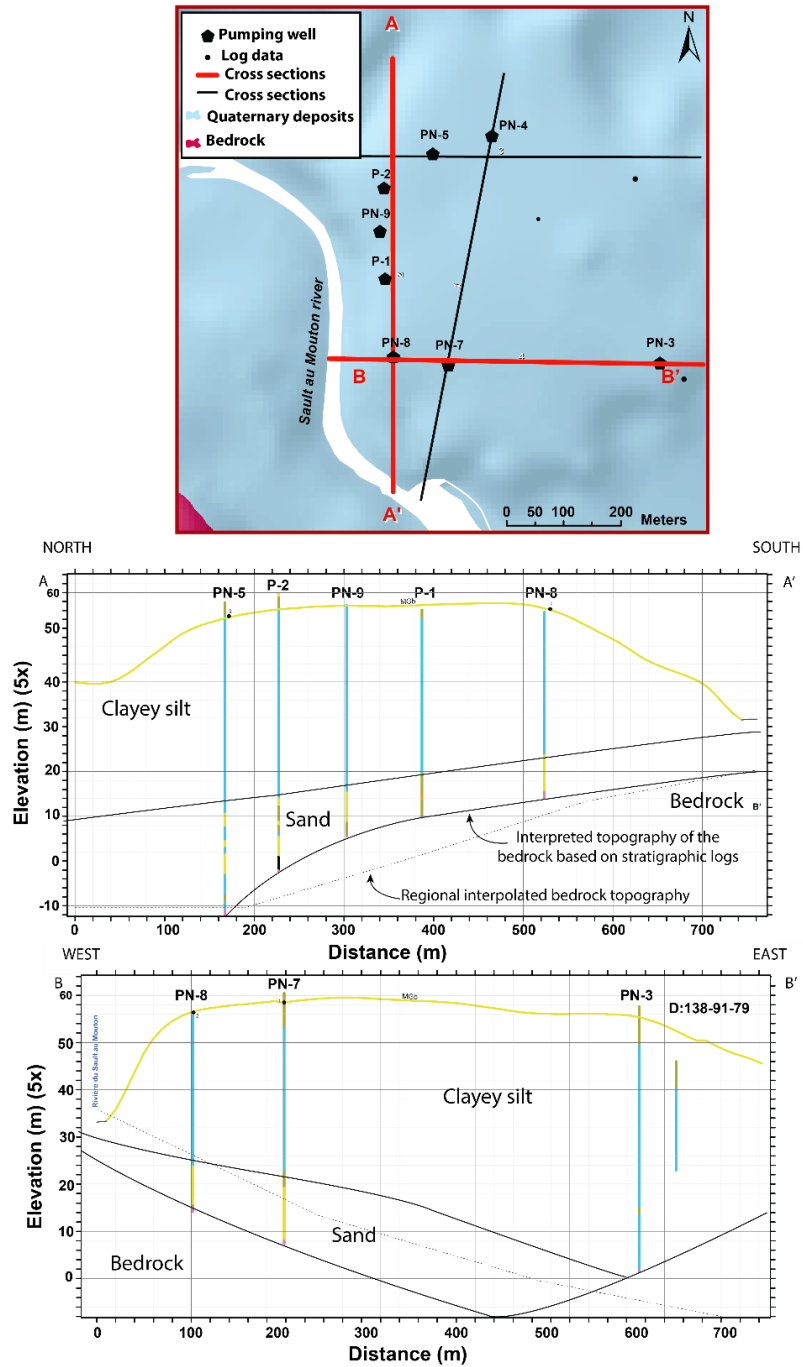


Figure 4.14: North-south (A-A') and east-west (B-B') stratigraphic sections of the Longue-Rive region illustrating the inclined substratum aquifer conceptual model.

A long-term spherical flow dimension has also been observed in the Philipon well located in Mirabel (southern Quebec) (Figure 4.14B). The stratigraphic log shows, from top to bottom, 4.6 m of clay that confines the underlying aquifer, 1.5 m of weathered rock (loose, oxidized, highly permeable breccia induced by a diagenetic alteration) and 17.1 m of fractured sandstone (coarse sandstone, poorly graded and poorly cemented) of the Covey Hill Formation (Nastev et al. 2004). The sandstone aquifer is confined by the clay formation (piezometric level at a depth of 1.8 m). The screen has a length of 18.6 m and collects the water from the fractured sandstone. The derivative signal depicts a short early times radial flow dimension (until around 160 s) followed by a long-term spherical flow dimension (from 160 s until 18,000 s). Geological field observations indicate that the thickness of the Covey Hill generally exceeds 500 m in the St. Lawrence Lowlands of south-western Quebec (Nastev et al. 2004). Thus, the spherical flow dimension observed in the Philipon well may be interpreted using the partially penetrating well model. The late radial flow dimension (as described in the simulations of Moncada et al. (2005) is not observed on the signal, probably because the sandstone formation is very thick. Therefore, the cross-flow area has not yet reached the bottom of the sandstone aquifer during the pumping test time period.

These two case studies have both shown a spherical flow dimension, but their hydrodynamic interpretation is different. The selection is made to use either the IS aquifer conceptual model or the partially penetrating (PP) well conceptual model, by analysing the main geological settings. The Longue-Rive pumping test (Figure 4.14-A) shows a spherical flow dimension that is interpreted using the IS aquifer model, whilst the Mirabel pumping test (Figure 4.14-B) is interpreted using the PP flow model.

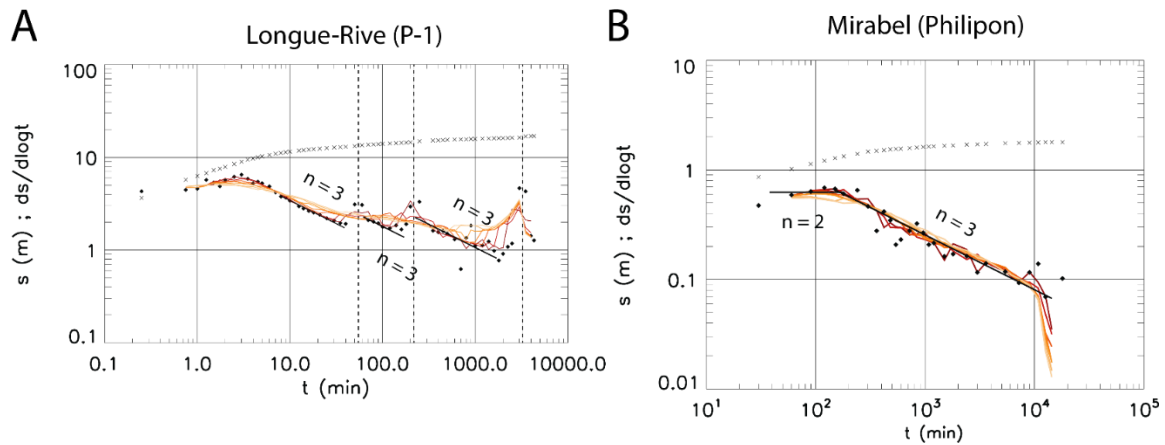


Figure 4.15: Log-log plot of the drawdown data *versus* time (cross data) and the drawdown log-derivative data *versus* time (black diamond data) of two constant-rate pumping tests, one performed in A) Longue-Rive (Haute-Côte-Nord region) and the other in B) Mirabel (St. Lawrence Lowlands of south-western Quebec). The P-1 well (Longue-Rive) is installed in glacial sands in a confined sand aquifer that fills a glacial valley. It produces the signal of an aquifer having an inclined substratum A). The Philipon well is installed in thick sandstone (generally exceeding 500 m). It produces the signal of a partially penetrated aquifer B).

4.8 DISCUSSION

In this study, we observed that various cross-flow area shapes can produce the same flow dimension value. For instance, the radial flow dimension has been observed in an inclined substratum aquifer with both an isotropic hydraulic conductivity (Figure 4.11-D) and an anisotropic hydraulic conductivity in the X-direction (Figure 4.11-F), Y-direction (Figure 4.11-E) and Z-direction (Figure 4.11-D). Evidently, the shape of the cross-flow area is different for the isotropic and the anisotropic media, because the pressure-front pulse diffuses faster

in the direction of the highest K value (Figures 4.11-C-D-E-F). These results confirm the validity of Barker's theory (1988) stipulating that the flow dimension value, and therefore the type-curves of the drawdown log-derivative signal, reflect only the relationship between the surface of the cross-flow area $A(r)$ and the radial distance from the well r , presented in Equation (4.1). Thus an important point raised in this study is that the drawdown log-derivative signal is more a reflection of the behavior of the cross-flow area rather than a specific conceptual model or a specific flow geometry, as it has often been interpreted in the petroleum literature.

Another important issue regarding the interpretation of n is that the cross-flow area induced by a constant-rate pumping test can be subdivided into several specific portions of cross-flow areas, each having a different geometry; among these, it is the evolution of the most sizeable cross-flow area portion that will be expressed by the n value. This study has shown that in an IS flow model, the cross-flow area is composed of a truncated cylinder having a surface $A'c$ and a truncated hemisphere having a surface $A's$. Either the predominant radial flow dimension ($n = 2$) or the spherical flow dimension ($n = 3$) are observed, depending on the ratio of $A'c/A's$ surfaces.

The evolution in time of the sequence of n during a single constant-rate pumping test is generally interpreted to reflect changes in the flow geometry and/or changes in the configuration of the hydraulic properties of the aquifer (Equation (4.1)). For instance, the numerical investigation of Rafini and Larocque (2012) in a flow media with a vertical and finite-conductivity fault emphasized a n -sequence representing the flow conditions as the pressure front pulse is diffused through the matrix ($n = 2$) and then through the fault ($n =$

1.5). This study illustrates that it is possible for one isotropic and homogeneous conceptual model of invariable flow geometry to produce a n -sequence. The progression of the predominant radial flow dimension towards the spherical flow dimension does not reflect a change in the intrinsic properties of the aquifer or in its flow geometry, but rather, it reflects the ratio between the cross-flow area portions of the pressure front pulse (truncated cylindrical area *versus* truncated hemispherical cross-flow area).

This article has also addressed the issue of the non-uniqueness of the $ds/dlogt$ signal produced by a transient pumping test. This issue has been previously stated by Doe (1991) and Mattar (1999) but these authors did not provide specific examples. Certainly, the drawdown log-derivative data confers more uniqueness to the signal than does the drawdown data, but the problem of non-uniqueness still persists. Moncada et al. (2005) and Escobar et al. (2012) numerically showed that the derivative curve of a partially penetrating well or a partially screened aquifer shows an early times radial flow followed by spherical flow. They developed an equation using the Tiab's Direct Synthesis (TDS) technique (Tiab 2005) to estimate the permeability, the skin and the wellbore storage. In this study, the field data analysis emphasised the problem of non-uniqueness of the flow dimension parameter: the n -sequences of the IS substratum and the partially penetrated aquifer are similar ($n = 2 - 3$). Traditionally, the radial flow dimension has been interpreted as being representative of a cylindrical radial flow dimension in a constant thickness and a totally screened aquifer. In this study, we presented two radial flow dimensions: the compensated radial flow dimension and the predominant radial flow dimension; both are induced by an increasing thickness of an aquifer. This study thus presents a conceptual model that is not a Theis-like conceptual

model, but rather one that produces a radial flow dimension. Further analysis has shown that the anisotropy of K does not change the flow dimension value; rather, it affects the duration of the radial flow dimension and the duration of the transition (demonstrating the influence of the diffusivity on the propagation of the pressure front pulse). Selecting the most appropriate model to interpret the $ds/d\log t$ signal is a challenge. For instance, a sharply inclined substratum presenting an anisotropy in the horizontal plan of the substratum ($K_y > K_x$) may be interpreted as being an isotropic and gently inclined substratum. When interpreting the derivative signal of a constant-rate pumping test, a minimal quantity of information about the geometry and/or the geology of the aquifer is absolutely necessary.

Analysis of the n -sequence may help to distinguish between the partially penetrating well model and the IS aquifer conceptual model. For instance, the n -sequence $n = 2 - 3 - 2$ may indicate a partially penetrating well aquifer. The first radial flow dimension reflects the cylindrical diffusion of the cross-flow area around the well. The second radial flow dimension reflects the attainment of both the top and the bottom of the aquifer. As explained in this study, the n -sequence $n = 2 - 2 - 3$ may reflect an IS aquifer in which the pumping well is located at a significant distance from the corner. Both radial flow dimensions indicate, respectively, the compensated and the predominant radial flow dimension. It cannot be overstated that both geological information and field data are required for the interpretation of a pumping test.

However, when the well is far from the corner and penetrates a major portion of the thickness of the IS aquifer, the spherical flow dimension may not be observable. Instead, the derivative signal will show a single-stage radial flow regime. In such conditions, it is not possible to

differentiate between the conventional Theis-like models or an IS aquifer. Equation (4.8) makes it possible to estimate the hydraulic properties of both theisian and IS aquifers. However, it may be important to differentiate between both conceptual models when delineating wellhead protection areas. Certain types of field data, such as well-logging observations in several piezometers, surface geophysical cross-sections and groundwater age data, will help to select the appropriate conceptual model. Electromagnetic methods (Chandra et al. 2008) and seismic methods may be particularly relevant to investigate the geometry and the thickness of sediments. The distribution of residence times may also help in detecting sloping aquifers (Leray et al. 2012). Leray et al. (2012) observed that in an IS aquifer, when the natural hydraulic gradient induces a groundwater flow in the same direction as the increase of thickness, the flow velocity is slower and the residence time is longer. Alternatively, when the groundwater flows in the same direction as the decrease of thickness, the wedge shape induces a shorter circulation path and a shorter residence time distribution.

One interesting outcome of this study is that the spherical flow regime is observable even in cases where the substratum is only slightly inclined (e.g. $\alpha = 5^\circ$). It should be noted, however, that the lesser the inclination of the substratum, the longer the time required for the spherical flow to be observable. For a substratum presenting an inclination of 5° , $K = 10^{-5}$ m/s and $S_s = 10^{-4}$ m⁻¹, the spherical flow dimension has been observed at $1,6 \times 10^7$ s, which represents approximately 6 months. From the perspective of aiming to improve hydraulic diagnostics based on interpretations of the derivative signal, it should be noted that, depending on the properties of the aquifer, the transition between two flow dimensions can be long. For

instance, in Figure 4.10, the transition time period between $n = 2$ and $n = 3$ may last 4 log cycles. When interpreting the derivative signal, therefore, it is important to detect these transition time periods so as to exclude them when determining a flow dimension value. In the same manner, the practitioner should keep in mind that the duration of a pumping test, which is usually of 72 h, may not be sufficient to allow a spherical flow dimension to establish itself; in these cases, the derivative signal would show only the radial flow dimensions followed by a transition period.

4.9 CONCLUSION

Adapting interpretative tools to the complexity of aquifers is crucial to improve the hydrodynamic interpretation of pumping tests and to more accurately estimate the hydraulic properties of aquifers. Interpreting the $ds/d\log t$ signal by performing a flow dimension analysis is a suitable method for understanding flow behavior around the pumped well. The comparison between the s and the $ds/d\log t$ signal has shown that the $ds/d\log t$ signal provides a significantly greater accuracy than the s signal, reducing the margin of error when interpreting pumping tests and determining hydraulic boundaries.

One of the pumping tests contained in our n -database (Ferroud et al. 2018) showed a spherical flow dimension that could not be interpreted by assuming a partially penetrating well model, leading to the conclusion that a spherical flow dimension could be produced by means of a different conceptual model. This paper analyses the transient hydraulic behavior of an aquifer having an inclined substratum. By analysing the sensitivity of the drawdown

log-derivative signal to various parameters such as K , K_x , K_y , K_z , S_s , Q , d , L_w , and α , this study provides a method for identifying an IS aquifer during a constant-rate pumping test, along with tools for the qualitative interpretation of the transient pumping tests for such a model. A hydrodynamic flow model is proposed. This study also improves on the quantitative interpretation of constant-rate pumping tests, by developing empirical equations to estimate the hydraulic properties of the IS aquifer. Our numerical study widens the field of physical interpretations of the radial-spherical flow dimension. It is shown that both the totally penetrated aquifer having an inclined substratum and the partially penetrating well conceptual model can produce a n -sequence $n = 2 - 3$.

The HGS code was used to analyse the transient diffusion of the pressure front pulse through the aquifer and to obtain the $ds/d\log t$ signal at the pumping well. The numerical simulations showed that when the well is located at an appropriate distance d from the corner, the derivative signal depicts two plateaus ($n = 2$). The first plateau represents the “compensated radial flow dimension” and the second plateau represents the “predominant radial flow dimension”. The duration in time of the compensated radial flow dimension is variable (and is occasionally imperceptible), depending on d . The duration in time of the predominant radial flow dimension is also variable, depending on 3 factors: well length L_w , inclination of the substratum α and hydraulic conductivity of the aquifer K .

In this study, two empirical formulas to calculate the hydraulic conductivity and the specific storage (or the inclination of the substratum) were developed. These formulas are based on the $ds/d\log t$ signal (m_{2-BC} , m_{2-AC} and m_3) and were developed for a transient constant-rate pumping test, which is performed in a confined aquifer having an inclined substratum. The

Oil and Gas industry literature has proposed solutions based on graphical analysis of the pressure derivative signal to interpret a spherical flow dimension produced in a partially penetrated reservoir. The conceptual model proposed in our study may represent, for example, a glacial valley filled by granular deposits. The proposed solutions achieve more accurate estimations of the hydraulic properties than do the conventional models of Theis and Cooper-Jacob. Furthermore, analysing the $ds/dlogt$ signal makes it possible to more accurately identify the aquifer's hydraulic boundaries. The solutions proposed in this study should make it possible for practitioners to improve the accuracy of results when characterizing the hydraulic properties of aquifers featuring an inclined substratum. The flow model that we propose in this study helps to better understand the hydrodynamic behavior of aquifers that present a transmissivity that increases in a linear fashion.

4.10 ACKNOWLEDGMENTS

The authors acknowledge the financial support of the Natural Sciences and Engineering Research Council (NSERC – federal funding) of Canada in the framework of the Individual Discovery Grant Program as well as the “Fonds de Recherche du Québec Nature et Technologies (FRQNT – provincial funding)” in the framework of the individual grant “Nouveaux-chercheurs” held by Prof. Romain Chesnaux. We also thank the municipalities of Charlevoix-Haute-Côte-Nord (Quebec) and the environmental government of Quebec (MDDELCC, Développement durable, Environnement et Lutte contre les changements climatiques) for their financial support. We thank Dr. Therrien and Aquanty for providing the

HGS code in the framework of collaborations between universities. Ms. Josée Kaufmann is thanked for editorial collaboration. We also thank the 3 anonymous reviewers and Dr. de Dreuzy for their initial review of this manuscript.

4.11 REFERENCES

- Baliga BR, Patankar SV (1980) A New Finite-Element Formulation for Convection-Diffusion Problems. *Numer Heat Transf* 3:393–409. doi: 10.1080/01495728008961767
- Barker J (2007) Diffusion in Hydrogeology. *Diffus Fundam* 6:50.1-50.18
- Barker JA (1988) A generalized radial flow model for hydraulic tests in fractured rock. *Water Resour Res* 24:1796–1804 . doi: 10.1029/WR024i010p01796
- Barlow JRB, Coupe RH (2012) Groundwater and surface-water exchange and resulting nitrate dynamics in the Bogue Phalia basin in northwestern Mississippi. *J Environ Qual* 41:155–169 . doi: 10.2134/jeq2011.0087
- Bear J, Jacobs M (1965) On the movement of water bodies injected into aquifers. *J Hydrol* 3:37–57 . doi: 10.1016/0022-1694(65)90065-X
- Bourdet D, Ayoub JA, Pirard YM (1989) Use of pressure derivative in well test interpretation. *SPE Form Eval* 4:293–302 . doi: 10.2118/12777-PA
- Brunner P, Simmons CT (2012) HydroGeoSphere: A Fully Integrated, Physically Based Hydrological Model. *Ground Water* 50:170–176 . doi: 10.1111/j.1745-6584.2011.00882.x
- Carrera J (1993) An overview of uncertainties in modelling groundwater solute transport. *J Contam Hydrol* 13:23–48 . doi: 10.1016/0169-7722(93)90049-X
- Chandra, S., Dewandel, B., Dutta, S., Ahmed, S., 2010. Geophysical model of geological discontinuities in a granitic aquifer: Analyzing small scale variability of electrical resistivity for groundwater occurrences. *J. Appl. Geophys.* 71, 137–148. <https://doi.org/10.1016/j.jappgeo.2010.06.003>
- Cooper HH Jr, Jacob CE (1946) A generalized graphical method for evaluating formation constants and summarizing well-field history. *Trans Am Geophys Union* 27:526–534 . doi: 10.1029/TR027i004p00526
- Corbett PWM, Hamdi H, Gurav H (2012) Layered fluvial reservoirs with internal fluid cross flow: a well-connected family of well test pressure transient responses. *Pet Geosci* 18:219–229 . doi: 10.1144/1354-079311-008

- de Dreuzy, J.-R., Davy, P., 2007. Relation between fractional flow models and fractal or long-range 2-D permeability fields. *Water Resour. Res.* 43. <https://doi.org/10.1029/2006WR005236>
- de Dreuzy, J.-R., Davy, P., Erhel, J., de Brémond d'Ars, J., 2004. Anomalous diffusion exponents in continuous two-dimensional multifractal media. *Phys. Rev. E* 70. <https://doi.org/10.1103/PhysRevE.70.016306>
- Doe TW (1991) Fractional dimension analysis of constant-pressure well tests. In: Society of Petroleum Engineers paper No. 22702, SPE Annual Technical Conference and Exhibition, 6-9 October, 1991, Dallas, Texas, USA. pp 461–467
- Ehlig-Economides CA, Joseph JA, Ambrose RW, Norwood C (1990) A Modern Approach to Reservoir Testing (includes associated papers 22220 and 22327). *J Pet Technol* 42:1554–1563 . doi: 10.2118/19814-PA
- Escobar F., Montealegre-M M (2007) A complementary conventional analysis for channelized reservoirs. *CTF - Cienc Tecnol Futuro* 3:137–146
- Escobar F, Saavedra N, Hernandez C, et al (2004a) Pressure and Pressure Derivative Analysis for Linear Homogeneous Reservoirs Without Using Type-Curve Matching. Society of Petroleum Engineers
- Escobar F-H, Corredor C-M, Gomez B-E, et al (2012) Pressure and pressure derivative analysis for slanted and partially penetrating wells. *Asian Res Publ Netw ARPN* 7:932–938
- Escobar FH, Navarrete JM, Losada HD (2004b) Evaluation of Pressure Derivative Algorithms for Well-Test Analysis. Society of Petroleum Engineers
- Ferroud A, Chesnaux R, Rafini S (2018) Insights on pumping well interpretation from flow dimension analysis: The learnings of a multi-context field database. *J Hydrol* 556:449–474 . doi: 10.1016/j.jhydrol.2017.10.008
- Ferroud A, Chesnaux R, Rafini S (2015) Pumping test diagnostic plots for the investigation of flow patterns in complex aquifers: numerical results. In: 42nd IAH International Congress "Hydrogeology: Back to the future", September 13-18, 2015, Rome, Italy
- Gringarten A., Witherspoon P. (1972) A method of analyzing pump test data from fractured aquifers. In: *Int. Soc. Rock Mechanics and Int. Ass. Eng. Geol.* Stuttgart, pp 1–9
- Gringarten AC, Ramey HJ, Raghavan R (1974) Unsteady-state pressure distributions created by a well with a single infinite-conductivity vertical fracture. *Soc Pet Eng J* 14:347–360 . doi: 10.2118/4051-PA
- Grubb S (1993) Analytical model for estimation of steady-state capture zones of pumping wells in confined and unconfined aquifers. *Ground Water* 31:27–32 . doi: 10.1111/j.1745-6584.1993.tb00824.x
- Hantush MS (1962) Flow of ground water in sands of nonuniform thickness: 3. Flow to wells. *J Geophys Res* 67:1527–1534 . doi: 10.1029/JZ067i004p01527

- Leray, S., de Dreuzy, J.-R., Bour, O., Labasque, T., Aquilina, L., 2012. Contribution of age data to the characterization of complex aquifers. *J. Hydrol.* 464–465, 54–68. <https://doi.org/10.1016/j.jhydrol.2012.06.052>
- Mattar L (1997) Derivative Analysis Without Type Curves. Society of Petroleum Engineers
- Mattar L (1999) Derivative analysis without type curves. *J Can Pet Technol* 38: . doi: 10.2118/99-13-63
- Moncada K, Tiab D, Escobar F-H, et al (2005) Determination of vertical and horizontal permeabilities for vertical oil and gas wells with partial completion and partial penetration using pressure and pressure derivative plots without type-curve matching. *CTF - Cienc Tecnol Futuro* 3:77–94
- Nastev M, Savard MM, Lapcevic P, et al (2004) Hydraulic properties and scale effects investigation in regional rock aquifers, south-western Quebec, Canada. *Hydrogeol J* 12:257–269 . doi: 10.1007/s10040-004-0340-6
- Rafini S, Chesnaux R, Dal Soglio L (2013) A numerical analysis to illustrate the usefulness of drawdown log-derivative diagnostic plots in characterizing the heterogeneity of non-Theis aquifers. In: *GeoMontreal 2013, the 66th Canadian Geotechnical Conference and the 11th Joint CGS/IAH-CNC Groundwater Conference, September 29-October 3, 2013, Montreal, Quebec, Canada*
- Rafini S, Larocque M (2009) Insights from numerical modeling on the hydrodynamics of non-radial flow in faulted media. *Adv Water Resour* 32:1170–1179 . doi: 10.1016/j.advwatres.2009.03.009
- Rafini S, Larocque M (2012) Numerical modeling of the hydraulic signatures of horizontal and inclined faults. *Hydrogeol J* 20:337–350 . doi: 10.1007/s10040-011-0812-4
- Rozemeijer JC, van der Velde Y, McLaren RG, et al (2010) Integrated modeling of groundwater–surface water interactions in a tile-drained agricultural field: The importance of directly measured flow route contributions. *Water Resour Res* 46:W11537 . doi: 10.1029/2010WR009155
- Theis CV (1935) The relation between the lowering of the piezometric surface and the rate and duration of discharge of a well using ground-water storage. *Trans Am Geophys Union* 16:519–524 . doi: 10.1029/TR016i002p00519
- Therrien R, McLaren R., Sudicky E., Panday S. (2010) *HydroGeoSphere, A three-dimensional numerical model describing fully integrated subsurface and surface flow and solute transport. DRAFT, Univ. of Waterloo, Waterloo, Ont., Canada*
- Tiab D (2005) Analysis of pressure derivative data of hydraulically fractured wells by the Tiab's Direct Synthesis technique. *J Pet Sci Eng* 49:1–21 . doi: 10.1016/j.petrol.2005.07.001
- Todd DK (1980) *Groundwater hydrology*, 2nd ed. JWiley, New York ; Toronto
- Walker DD, Roberts RM (2003) Flow dimensions corresponding to hydrogeologic conditions. *Water Resour Res* 39:1349

Wyssling L (1979) Eine neue formel zur Berechnung der Zuströmungsdauer (Laufzeit) des grundwassers zu einem grundwasser pumpwerk. *Eclogae Geol Helvetiae* 72:401–406

CHAPITRE 5

DISCUSSIONS, RECOMMANDATIONS ET CONCLUSIONS

Cette section présente à la fois une discussion générale de l'ensemble des résultats de recherche ainsi que des recommandations par rapport à l'application des outils de la dérivée-log du rabattement et de la dimension d'écoulement dans les analyses d'essais de pompage.

5.1 LA DIMENSION D'ÉCOULEMENT DANS LA NATURE

La base de données de n a mis en évidence une grande variété de valeurs de dimension d'écoulement ainsi qu'une majorité de signatures manifestant une séquence de n et non une seule valeur de n . Ces résultats mettent en avant l'inadéquation entre la complexité des signatures et l'applicabilité du modèle de Theis. Comme le met en avant la Figure 3.8, la base de données montre que 31 % des 121 valeurs de dimension d'écoulement observées dans l'ensemble de la base de données représente des régimes d'écoulement radiaux ($n = 2$). Ce sont seulement ces 31 % des valeurs de n qui satisfont au modèle de Theis. Un rapide test numérique, présenté dans le chapitre 2, quantifie l'erreur d'estimation des propriétés hydrauliques lorsque le modèle de Theis est appliqué dans des contextes avec des régimes d'écoulement non-radiaux ($n \neq 2$). L'estimation des propriétés hydrauliques a

été réalisée dans différents modèles conceptuels, chacun étant associé à un régime d'écoulement différent. La comparaison entre la conductivité hydraulique K considérée dans la simulation d'écoulement des modèles numériques et la valeur de K estimée avec le modèle de Theis a montré que l'application du modèle de Theis : i) surestime la valeur de K de 89 % pour un modèle linéaire (aquifère ayant la forme d'un conduit), ii) sous-estime la valeur de K dans la matrice de 847 % pour un modèle bilinéaire (faille verticale de conductivité hydraulique finie et alimentée par la matrice) et iii) sous-estime la valeur de K de 100 % pour un modèle sphérique (pénétration partielle de l'aquifère). Il est intéressant de noter que lorsqu'un plateau radial de la dérivée-log est observé aux temps courts, l'application du modèle de Theis uniquement sur cette courte portion radiale permet une bonne estimation des propriétés hydrauliques de l'aquifère autour du puits.

La base de données de n met également en avant l'importance des valeurs de n fractionnaires (Figure 3.8) : les valeurs non-entières représentent 39 % des valeurs de n observées dans la base de données. Pour la plupart des valeurs de n non-entières, il n'existe pas encore d'interprétation conceptuelle des écoulements pour comprendre de telles valeurs. Tel que présenté dans le chapitre 2, il existe, jusqu'à présent, seulement deux modèles conceptuels permettant d'interpréter certaines dimensions d'écoulement fractionnaires : i) le modèle bilinéaire (*bilinear flow model*) à faille verticale ayant une conductivité hydraulique finie et étant alimentée par la matrice ($n = 2.5$) et ii) le modèle « trilinéaire » (*trilinear flow model*) représentant les écoulements à travers une faille verticale de conductivité hydraulique finie, alimentée par la matrice et influencée par une frontière à charge imposée (Lee et Brockenbrough 1986, Azari et al. 1990). Beaucoup d'autres valeurs

de n non-entières ont été observées, autant dans les milieux fracturés que dans les dépôts granulaires, ce qui suggère la nécessité de continuer à développer de nouveaux modèles conceptuels et de permettre la représentation des aquifères de plus grande complexité.

Enfin, la base de données de n a permis de corrélérer certaines valeurs de n à des contextes géologiques spécifiques (Figure 3.10). Cette observation met en lumière le potentiel diagnostique des observations de n dans la caractérisation hydrodynamique des aquifères, notamment dans la conceptualisation des écoulements souterrains complexes (non theissiens). Certaines valeurs observées reflètent des modèles conceptuels connus. Par exemple, les aquifères cristallins faillés ont montré une prédominance des $n = 1$ et quelques $n = 1.5$ ce qui confirme les interprétations conceptuelles présentées dans la littérature. En effet, le régime linéaire ($n = 1$) est conceptualisé par une faille verticale de conductivité hydraulique infinie (Gringarten et al. 1974, Gringarten et Ramey 1975) et finie (Cinco-Ley et al. 1978, Cinco-Ley et Samaniego-V. 1981b). Par ailleurs, le régime bilinéaire ($n = 1.5$) est conceptualisé par une faille verticale ou inclinée, de conductivité hydraulique finie et alimentée par la matrice (Cinco-Ley et al. 1978, Rafini et Larocque 2012). La dimension d'écoulement radiale ($n = 2$) qui est observée dans les milieux rocheux carbonatés peut refléter i) des écoulements à travers les fractures horizontales au niveau des inter-bancs de calcaire, ii) des écoulements à travers un réseau de fractures orthogonales et connectées une fois que l'extension de l'onde de pression est suffisamment importante pour ne plus sentir les petites hétérogénéités associées aux fractures. Ce point sur la relation entre sensibilité du front de pression aux hétérogénéités et l'échelle d'observation sera développé plus précisément dans la section suivante qui traite des limites de l'outil diagnostique. La

dimension d'écoulement sphérique ($n = 3$) observée dans les arènes granitiques, reflèterait l'importance de l'épaisseur des aquifères pompés par rapport à la longueur du puits, induisant un écoulement sphérique associé à la pénétration partielle du puits. Enfin, les dépôts fluvio-glaciaires ont montré une dimension d'écoulement linéaire ($n = 1$) qui peut être associée i) à la forme allongée et étroite d'un aquifère (de type « conduit ») limité latéralement par des limites imperméables, tels que des eskers (Escobar et al. 2004b, Escobar et Montealegre-M 2007), ii) à des micros écoulements à travers des couches de dépôts ayant une faible conductivité hydraulique verticale ainsi qu'une faible connectivité ou une transmissivité latérale, tels que des systèmes fluvio-glaciaires (Corbett et al. 2012) formés par le transport et le dépôt de sédiments.

L'analyse des séquences de n a remis en question la validité du modèle à double porosité et du modèle fractal à représenter les écoulements dans les milieux fracturés. En effet, les signatures hydrauliques associées à ces modèles n'ont jamais été observées dans la base de données de n . Le modèle à double porosité se reconnaît par un signal de $ds/d\log t$ composé de deux plateaux (représentant d'abord le régime radial à travers le réseau de fractures conductrices puis à travers la matrice emmagasinante) qui sont séparés par un creux (chute transitoire de la dérivée log du rabattement). Cette remarque a également été formulée par Biryukov et Kuchuk (2012) qui affirment que le modèle à double porosité proposé par Warren et Root (1963) est « inapproprié et fondamentalement incomplet pour interpréter les essais de pompage ». Le modèle fractal en milieu fracturé suppose que les objets fractaux sont représentés avec une ou plusieurs caractéristiques, par exemple le nombre de fracture par unité de surface (*box-counting*), la longueur des fractures, leur

ouverture, etc., présentant une invariance d'échelle et suivant une loi de puissance. Une telle configuration du réseau de fractures conduit à une homogénéité statistique de l'aquifère fracturé. Basés sur ces propriétés géométriques, des modèles hydrauliques ont été proposés, notamment ceux de Chang et Yortsos (1990), Acuna et Yortsos (1995). Ces modèles prédisent une stabilisation du signal de la dérivée log du rabattement sur une valeur non-entière de n . Cependant, observer des valeurs fractionnaires de n dans des milieux fracturés ne permet pas de reconnaître un réseau fracturé car i) d'autres modèles hydrauliques prédisent une stabilisation fractionnaire de la dimension d'écoulement, comme par exemple le modèle bilinéaire ($n = 1.5$) à faille verticale alimentée par la matrice, ii) des études de terrain en milieux fracturés ont mis en avant des signatures hydrauliques composées de plusieurs valeurs non-entières ou de plusieurs valeurs entières et non-entières révoquant ainsi la validité de l'hypothèse du continuum fractal car il impliquerait la superposition de deux continua dans l'espace ce qui est incompatible avec le concept d'invariance d'échelle et enfin iii) de nombreuses études sur le milieu fracturé remettent en cause la pertinence des réseaux fractals dans la nature. En effet, le contexte géologique permettant la mise en place de la fracturation est complètement différent selon l'échelle d'observation (Rafini, 2008). Par exemple, la mise en place des micro-fractures est plutôt contrôlée par l'arrangement cristallin alors que les fractures (mésomètre) et les failles (macromètre) sont plutôt associées à la stratification géologique ainsi que les contraintes de structures avoisinantes, tels que les plissements. De plus, en analysant 72 essais de pompage, réalisés dans des aquifères dolomitiques en Slovénie, à partir du modèles GRF et du logiciel AQTESOLV, Verbovšek (2009, 2011) montra qu'il n'y avait pas de corrélation entre les valeurs de dimension d'écoulement et les dimensions fractales. Enfin, le deuxième

article de cette thèse (Ferroud et al. 2018) a montré que des valeurs fractionnaires sont observées dans les milieux granulaires. Ces milieux ne peuvent évidemment pas être interprétés à partir de modèles d'écoulement stipulant un réseau fractal de fractures, ce qui laisse penser que d'autres modèles d'écoulement sont nécessaires afin de conceptualiser les valeurs fractionnaires de n . De nouvelles modélisations analytiques et numériques sont nécessaires afin de comprendre ces valeurs de n non-entières.

Il est cependant important de considérer les limites de cette étude qui sont essentiellement associées à la subjectivité de l'estimation de n . En effet, le signal de la dérivée logarithmique du rabattement est un signal souvent très bruité dû à sa forte sensibilité aux faibles variations de s . Les valeurs de n s'estimant à partir des pentes de la dérivée log du rabattement (en échelle log-log), son estimation peut s'avérer délicate lorsque les signaux sont bruités (nuages de points, pics de données dus à des ajustements de débit). Afin d'atténuer le problème de subjectivité associé à la détermination graphique de n , un grand nombre de données a été analysé (approche statistique) et le logiciel SIREN a été utilisé. Ce logiciel permet de déterminer les séquences de n d'un essai de pompage en calant simultanément s en échelle semi-log et $ds/d\log t$ en échelle log-log. Cette approche permet de combiner les avantages de deux représentations graphiques. Le premier graphique (s versus t) est peu sensible aux petites variations de s dues aux changements et/ou ajustements du débit de pompage, mais ne permet pas en revanche d'observer les régimes d'écoulement. Le second graphique quant à lui ($ds/d\log t$ versus t) retranscrit clairement les régimes d'écoulement mais est sujet à un bruit important, induit, entre autres par les

changements de débit de la pompe et de l'hétérogénéité du milieu pourraient également induire une dispersion des données).

5.2 ANALYSE SÉQUENTIELLE DE LA DIMENSION D'ÉCOULEMENT : POTENTIEL DIAGNOSTIQUE ET LIMITES

L'analyse séquentielle de la dimension d'écoulement est un outil très pertinent pour interpréter les essais de pompage car elle fournit un cadre universel pour caractériser les régimes d'écoulement. En d'autres termes l'analyse séquentielle permet de retranscrire l'évolution géométrique de l'onde de pression à travers l'aquifère pompé, à partir des variations du taux de rabattement observées dans le puits de pompage. Le chapitre 2 met d'ailleurs en évidence que l'observation du signal de la dérivée logarithmique et des séquences de dimension d'écoulement aide grandement à choisir un modèle analytique afin de conceptualiser la géométrie des écoulements et de l'aquifère et d'estimer les propriétés hydrauliques de l'aquifère avec le plus de justesse possible. Il convient de noter que le présent travail s'est consacré à l'analyse du signal de la dérivée-log induite par un essai de pompage dans un puits vertical et que des puits inclinés ou horizontaux donneront d'autres signaux hydrodynamiques. Le signal hydrodynamique induit par un puits incliné a été analysé, entre autres, par Cinco et al. (1975), Escobar et al. (2012), Sousa et Moreno (2015) et Jia et al. (2016). Ces auteurs montrent qu'un puits incliné peut induire un signal de la dérivée-log composé de 2 plateaux radiaux, dont le deuxième plateau est supérieur au premier.

Avant d'employer l'analyse séquentielle de n comme un outil diagnostique pour caractériser les écoulements au sein d'aquifères complexes (non theissiens), il convient d'appréhender ses limites. Voici donc un résumé des limites de cet outil, tiré à la fois, de l'étude bibliographique, des observations de terrain et de l'analyse numérique réalisée dans le cadre de cette thèse :

- ✓ tel que montré numériquement dans le chapitre 2, des variations linéaires du débit de pompage peuvent influencer linéairement le signal de la dérivée log du rabattement et induire une dimension d'écoulement apparente très différente de la dimension d'écoulement qui reflète le comportement hydraulique de l'aquifère. Afin de s'affranchir de toute incertitude associée aux variations du débit de pompage (tel que des ajustements du débit, ou une variation linéaire du débit), il convient d'appliquer des algorithmes de déconvolution et/ou de convolution et/ou de lissage. Dans la plupart des cas, ces algorithmes nécessitent des mesures précises des séries temporelles, à la fois, du rabattement et des débits de pompage. Lors d'un essai de pompage, il est donc essentiel de mesurer rigoureusement et régulièrement le rabattement et le débit de pompage à chaque pas de temps. Une synthèse de ces algorithmes est présentée dans le deuxième chapitre.
- ✓ Étant donné que la variation de pression dans l'aquifère obéit à un processus diffusif, les variations de rabattement observées dans le puits et l'évolution de la pression à travers l'aquifère sont gouvernées par des conditions moyennées au niveau du front de pression, plutôt que contrôlées par des hétérogénéités locales de direction d'écoulement et/ou de propriétés hydrauliques. La dimension d'écoulement est donc une valeur apparente qui reflète le régime d'écoulement dominant, plutôt qu'une combinaison des régimes

d'écoulement ressentis par l'onde de pression. Par exemple, les simulations numériques de Rafini et Larocque (2012) ont montré qu'à partir d'un certain volume d'aquifère faille/matrice investigué, le signal bilinéaire ($n = 1.5$) de la faille verticale alimentée par la matrice est masqué par le régime d'écoulement radial ($n = 2$) de la matrice.

- ✓ Étant donné que l'onde de pression grandit au fur et à mesure de son expansion (lorsque $n > 1$), la sensibilité du signal transitoire de $ds/d\log t$ aux petites hétérogénéités (associées à une hétérogénéité des directions d'écoulement et/ou des propriétés hydrauliques) diminue avec l'augmentation du rayon d'investigation. De cette manière, Chang et al. (2011) ont observé une augmentation de la dimension d'écoulement avec l'augmentation de la distance radiale au puits en analysant quatre essais de pompage d'une durée de 11 jours.
- ✓ De plus, le ratio entre la sensibilité du signal et l'échelle d'observation est probablement influencé par la dimension d'écoulement, puisque le taux d'augmentation de $A(r)$, l'aire traversée par les écoulements, est fonction de n . En d'autres termes, plus la surface de l'onde de pression augmente rapidement, plus les hétérogénéités du système d'écoulement seront « diluées » rapidement dans le signal.
- ✓ Les pentes de la dérivée log du rabattement ont traditionnellement été interprétées par les pétroliers en termes de géométrie d'écoulement ou associées à un modèle conceptuel particulier. Les simulations numériques présentées dans le quatrième chapitre ont montré qu'un régime radial pouvait être observé à la fois dans un milieu isotrope et anisotrope, ce qui rejoint les travaux de Hantush (1966). Dans le milieu isotrope, le front de pression se développe par des cercles concentriques autour du puits alors que dans un milieu anisotrope, il se développe selon des ellipsoïdes centrés sur le puits. Dans les deux cas, la forme de l'onde de pression est très différente, mais le régime d'écoulement ressenti au

puits est le même. L'interprétation conceptuelle de la dimension d'écoulement n'est donc pas uniquement associée à un modèle conceptuel particulier (en effet, la littérature pétrolière a souvent associé les régimes d'écoulement à des modèles conceptuels particuliers), ni à une géométrie spécifique de l'onde de pression, mais plutôt à la relation entre la variation de l'aire traversée par les écoulements et la distance radiale au puits. Le paramètre n reflète ainsi le comportement hydraulique de l'aquifère. C'est donc un outil particulièrement pertinent à la fois parce qu'il offre un cadre qui permet de façon universelle, d'interpréter toutes les pentes de $ds/d\log t$ et il permet de conceptualiser le front de pression pour un même régime d'écoulement dans deux contextes différents.

- ✓ L'onde de pression peut être constituée de plusieurs portions d'aire traversées par les écoulements ayant des comportements différents. La valeur de n apparente exprime l'évolution géométrique de la plus importante des portions. Par exemple, le modèle d'aquifère à substratum incliné, présenté dans le chapitre 4, induit une onde de pression composée d'un cylindre tronqué (A^c , *truncated cylinder cross-flow area*) et d'un hémisphère tronquée (A^s , *truncated hemisphere cross-flow area*). Lorsque $A^c > A^s$, alors $n = 2$, ce qui exprime le régime d'écoulement radial associé à l'évolution cylindrique de A^c . Lorsque $A^s > A^c$, alors $n = 3$, ce qui exprime le régime d'écoulement sphérique associé à l'évolution sphérique de A^s .
- ✓ Contre toute attente, le changement de n ne retranscrit pas forcément une hétérogénéité (par exemple, une faille ou des limites) ou un changement de géométrie d'écoulement. En effet, les simulations numériques présentées au quatrième chapitre montrent qu'un aquifère à substratum incliné induit une séquence $n = 2 - 2 - 3$ et que le dernier changement de n (du régime radial ($n = 2$) au régime sphérique ($n = 3$)) reflète un changement de ratio entre les

surfaces qui constituent les « portions géométriques » de l'onde de pression. Ainsi l'évolution du signal du régime radial au régime sphérique ($n = 2 - 3$), exprime l'augmentation de la surface de la portion sphérique de l'onde de pression ($A's$) qui est associée à l'augmentation d'épaisseur aquifère induite par l'inclinaison du le substratum. Lorsque $A's$ devient supérieure à $A'c$, le régime sphérique masque le régime radial.

- ✓ Bien que le signal de la dérivée log du rabattement aide à réduire la non-unicité des séries temporelles du rabattement, le problème de non-unicité persiste. Dans chacun des trois articles présentés dans cette thèse, le problème de non-unicité est abordé. En effet, la base de données sur l'occurrence des dimensions d'écoulement qui sont observées dans la nature a mis en évidence que des valeurs de n identiques pouvaient être observées dans des contextes géologiques différents (troisième chapitre de la thèse, Ferroud et al. 2018). Par exemple, les régimes linéaire ($n = 1$) et radial ($n = 2$) ont été observés à la fois dans les milieux fracturés et les milieux granulaires. De toute évidence, les écoulements et les propriétés hydrauliques sont différents selon que le milieu est composé d'un socle rocheux fracturé ou de sédiments. De plus, la revue de littérature sur les séquences de dimensions d'écoulement (deuxième chapitre de la thèse) a également montré qu'un même régime d'écoulement (ou une série de régimes d'écoulement) peut être associé à plusieurs modèles analytiques différents. Par exemple, le régime linéaire ($n = 1$) peut être à la fois associé à 1) une faille de conductivité hydraulique infinie (Gringarten et al. 1974, Gringarten et Ramey 1975), 2) une faille de conductivité hydraulique finie (Cinco-Ley et al. 1978, Cinco-Ley et Samaniego-V. 1981b, Abbaszadeh et Cinco-Ley 1995), 3) un aquifère étroit et allongé (Escobar et al. 2004b) et 4) un aquifère sédimentaire tels que les systèmes fluviaux (Corbett et al. 2012). Un autre exemple de non-unicité peut également être mentionné avec le régime

sphérique ($n = 3$) qui peut être associé à la fois aux aquifères partiellement captés (Moncada et al. 2005, Escobar et al. 2012a), aux aquifères à substratum incliné (article 3 de la thèse soumis) et aux aquifères ayant une limite en coin (*pinchout boundaries*) (Horne et Temeng 1982). Ce problème de non-unicité des signatures de $ds/dlogt$ et des modèles conceptuels avait précédemment été énoncé par Doe (1991) et Mattar (1999), mais ces auteurs n'avaient pas présenté d'exemple spécifique.

- ✓ Comme le signal de la dérivée-log du rabattement est très sensible aux changements de débit de la pompe, l'analyse du signal en remontée apparaît comme un moyen de s'affranchir du bruit associé aux variations de débit de pompage. Quelques mises en garde doivent cependant être considérées lors de l'analyse de la remontée. En effet, dans certains cas, le signal de la descente et de la remontée sont différents. Mattar (1999) met en garde sur le fait que la plupart des solutions analytiques sont développées pour un essai de pompage. Sans donner d'explications, il avance que lorsque le signal est influencé par des limites hydrauliques ou des hétérogénéités, les courbes théoriques issues de modèles analytiques (*type curves*) ne peuvent être utilisées pour interpréter le signal de remontée. Sans préciser l'origine des données, il montre que l'atteinte des limites imperméables (*pseudo-steady state, depleted aquifer*) s'exprime par une droite de pente unitaire ascendante avec les données de $ds/dlogt$ lors du rabattement (Figure 1 de Mattar (1999)) alors qu'elle s'exprime par une pente unitaire décroissante avec les données de remontée (Figure 3 de Mattar (1999)). Il recommande donc d'utiliser le signal de remontée afin d'aider au diagnostic des régimes d'écoulement plutôt que pour effectuer une analyse quantitative. On pourrait supposer que dans un aquifère fermé, l'atteinte de la pression moyenne peut masquer la fin de la remontée et donc l'identification des limites.

5.3 MÉTHODOLOGIE ET RECOMMANDATIONS POUR L'AMÉLIORATION DE L'INTERPRÉTATION DES ESSAIS DE POMPAGE

Cette section vise à donner quelques recommandations et à proposer une méthodologie d'interprétation des essais de pompage basée sur l'utilisation de la dérivée-log du rabattement et la dimension d'écoulement. Comme énoncé tout au long de cette thèse, ces outils diagnostiques permettent d'améliorer grandement l'analyse qualitative et quantitative des essais de pompage. Par exemple, le troisième chapitre (Ferroud et al. 2018) a quantifié l'erreur commise dans l'estimation de la conductivité hydraulique lorsque le modèle de Theis est appliqué, à tort, à des modèles conceptuels dont le régime d'écoulement est non-radial. En effet, l'estimation de K est sous-estimée de 89% dans un modèle de type « conduit » induisant une séquence de n radiale –linéaire. L'estimation de K est sous-estimée de 100% lorsque le modèle de Theis est employé pour analyser le signal d'un puits pénétrant partiellement l'aquifère, induisant un régime sphérique. De plus, le quatrième chapitre a montré que le ralentissement du taux de rabattement observé dans un modèle à substratum incliné pouvait être confondu avec l'atteinte d'une frontière de recharge, en utilisant l'analyse conventionnelle de Cooper-Jacob, alors qu'en réalité c'est l'expression de l'augmentation de la transmissivité avec la distance radiale qui se traduit par un régime sphérique. L'analyse du signal de la dérivée-log du rabattement permet donc une analyse qualitative plus juste et plus précise des conditions d'écoulement ainsi qu'une meilleure détection des frontières de recharge.

La section suivante propose un enchaînement d'étapes qu'il est pertinent d'appliquer lors d'une interprétation d'essai de pompage basée sur le signal de $ds/dlogt$.

1. Le signal de $ds/dlogt$ étant très sensible aux petites variations de débit, il est souvent très bruité. Il est donc judicieux, dans ce cas, d'effectuer un traitement du signal de la dérivée-log de s avant d'interpréter l'essai de pompage. Dans un premier temps, il est conseillé de supprimer les données aberrantes ou extrêmes (*outliers*) parce qu'elles génèrent un bruit inutile et qu'elles peuvent induire des confusions dans l'interprétation des données (Nobakht et Mattar 2009). Ensuite, des algorithmes de convolution (Duhamel 1833, Kuchuk et Avestaran 1985, Roumboutsos et Stewart 1988, Kuchuk 1990, Onur et al. 2002, Kuchuk et al. 2010) et de déconvolution (Stewart et al. 1983, Kuchuk et Avestaran 1985, von Schroeter et al. 2001, Gringarten 2010, Pimonov et al. 2010, Onur et Kuchuk 2012, Cumming et al. 2013, Obeahon et al. 2014) peuvent être appliqués afin de corriger les variations de $ds/dlogt$ induites par les changements de débit. De nombreux algorithmes de convolution et de déconvolution sont disponibles dans la littérature, le livre présenté par Kuchuk et al. (2010) en propose une synthèse. Corriger les fluctuations du rabattement induites par les variations de débit permet grandement d'améliorer le signal mais nécessite que les données de rabattement s et de débit Q soient mesurées précisément et à chaque pas de temps pendant toute la durée de l'essai de pompage. Aujourd'hui, les sondes de pression à acquisition automatique (*dataloggers*) permettent d'améliorer la justesse et la précision des levés en réduisant l'incertitude de mesure due à la lecture du rabattement et à la mesure du temps. De plus, comme les données sont généralement analysées sur des diagrammes log-log, nous recommandons de mesurer s et Q avec un pas de temps

logarithmique lors des essais de pompage de longue durée (ou de sélectionner les données de façon logarithmiques dans une base de données existantes) afin d'éviter une densification des données aux temps longs. Enfin, que le signal de $ds/d\log t$ ait été corrigé des variations de débit ou non, un algorithme de lissage peut être appliqué sur les séries temporelles de la dérivée-log de s . Tel qu'énoncé dans le premier article, plusieurs algorithmes de différentiation sont proposés. (Escobar et al. 2004a) ont d'ailleurs évalué la performance de sept algorithmes de lissage : Bourdet, Clarck, Horne, Simons, Spline, Van Golf-Racht et l'application de fonctions polynomiales de premier et de deuxième degré. En ajoutant un bruit aléatoire sur les données, ils concluent que les fonctions de Spline, Bourdet et Horne offrent la meilleure différentiation des données, c'est à dire que les données lissées reproduisent le mieux les données initiales. Dans le cadre de cette thèse, les données ont été différenciées à partir de l'algorithme de Bourdet et al. (1989), qui a été implémenté dans le code IDL (Interactive Data Language). Ce code est un langage vectoriel qui est un outil très répandu dans la recherche et l'industrie, notamment en télédétection et en astronomie pour le traitement et la visualisation des données ainsi que pour le développement d'analyses interactives. Enfin, Ramos et al. (2017) ont proposé une méthode simplifiée afin de calculer la dérivée-log de s à partir de l'approche de régularisation variationnelle (*variational regularization approach*). Cette méthode offre également un lissage des données de $ds/d\log t$ satisfaisant en filtrant les faibles et les hautes fréquences de fluctuations. Ramos et al. (2017) ont d'ailleurs implémenté l'algorithme dans une feuille de calcul Excel ainsi qu'un code Fortran qu'ils ont mis à disposition gratuitement à l'adresse suivante : (<http://h2ogeo.upc.edu/en/investigation-hydrogeology/software>).

2. Une fois que le signal de la dérivée-log du rabattement est convenable et que des caractéristiques spécifiques peuvent être observées, la phase qualitative de l'interprétation peut commencer. Dans la plupart des revues pétrolières les analyses graphiques diagnostiques sont utilisées afin de faciliter la sélection du modèle analytique. En effet, étant plus sensible aux petites variations de rabattement, le signal de la dérivée-log réduit grandement la non-unicité du signal du rabattement. En outre, en plus d'aider à sélectionner le modèle conceptuel le plus représentatif de l'aquifère pompé, l'analyse des séquences de la dimension d'écoulement offre la possibilité d'interpréter le comportement hydrodynamique de l'aquifère pour n'importe quelle valeur de n observée lors d'un essai de pompage puisque le modèle GRF permet d'interpréter l'évolution géométrique du front de pression. Nous recommandons donc vivement d'intégrer l'analyse séquentielle de n dans les interprétations d'essai de pompage. Certains auteurs ont recours à un calage automatique des droites du signal $ds/dlogt$ (sur un diagramme log-log) (*best-fitting codes*) afin d'estimer n (Leveinen et al. 1998, Kuusela-Lahtinen et al. 2003, Verbovšek 2009). Dans le cadre, de cette thèse nous avons préféré estimer n à partir d'un calage manuel des droites du signal car notre base de données d'essais de pompage (issus d'études pour l'alimentation en eau potable de municipalités) ne contenait pas suffisamment de mesures du débit (et donc d'informations sur les possibles fluctuations de débit au cours du pompage) pour pouvoir corriger les variations de s associées aux variations de Q à partir d'algorithmes de déconvolution. L'analyse graphique nous a donc permis d'identifier de façon qualitative les périodes où les variations du débit influencent le signal de $ds/dlogt$ pour ainsi les écarter de l'analyse des dimensions d'écoulement. De plus, le code SIREN a été spécialement développé afin d'améliorer la détermination graphique de n en ajustant simultanément le

signal de s sur un diagramme semi-log et le signal de $ds/dlogt$ sur un diagramme log-log. Cette approche combine les avantages des deux graphiques : le premier est peu sensible aux variations de débit de la pompe mais ne permet pas de déterminer les régimes d'écoulement, le second est très sensible aux variations de débit mais reflète clairement les séquences de régimes d'écoulement

3. Tel que mentionné dans le deuxième chapitre, l'analyse des séquences de n aide grandement à sélectionner un modèle conceptuel pour interpréter un essai de pompage. Cependant, le problème de non-unicité du signal de $ds/dlogt$ qui, même s'il est beaucoup plus faible que le celui du signal de s , requiert de combiner l'analyse hydraulique avec des informations géologiques (Massonnat et Bandiziol 1991, Liang et al. 2012). Lorsqu'un modèle analytique approprié est sélectionné, les propriétés hydrauliques peuvent être estimées.

4. L'approche proposée par Tiab (1993a, 1993b, 1993c, 1993d, 1995, 2005) est particulièrement appropriée pour estimer les propriétés hydrauliques et les dimensions de l'aquifère (par exemple, sa profondeur, le diamètre d'un aquifère de type « conduit », etc.) à partir du signal de la dérivée log de s (en axes log-log). Cette méthode consiste à dériver les modèles analytiques afin que les propriétés hydrauliques et les dimensions de l'aquifère s'estiment à partir de lectures graphiques de droites, de points d'intersections et d'ordonnées à l'origine du signal de $ds/dlogt$. Dans la même perspective, le quatrième chapitre a développé empiriquement, à partir d'une analyse de sensibilité, des équations afin d'estimer les propriétés hydrauliques d'un aquifère à substratum incliné.

5. La revue pétrolière propose également l'analyse du signal de la *Primary Pressure Derivative* (PPD) et du signal de la *Beta-pressure derivative* (ou β -*derivative*), en

complément de l'analyse du signal de la dérivée-log de s (*pressure derivative*) afin de faciliter son interprétation. Le signal de la PPD est défini par les séries temporelles de ds/dt et permet, selon Mattar et Zaoral (1992), de différencier les effets du puits avec le signal de l'aquifère. Les signaux de s , $ds/dlogt$ et ds/dt sont donc affichés en fonction de t sur un même graphique diagnostique dont les axes sont log-log. Mattar et Zaoral (1992) ont observé que le signal de la PPD est toujours constant ou décroissant lorsque l'évolution du rabattement reflète le comportement hydraulique de l'aquifère. Ils en concluent que toute augmentation du signal de la PPD reflète des effets associés au puits. Le signal de la *Beta-pressure derivative* est défini par les séries temporelles de $dlogs/dlogt$ et fourni une caractérisation unique des régimes d'écoulement avec une loi de puissance tel que l'emmagasinement du puits, un aquifère avec des limites imperméables, un aquifère avec 2 failles parallèles ou 3 failles perpendiculaires, un puits interceptant une faille verticale de conductivité hydraulique finie ou infinie (Hosseinpour-Zonoozi 2006, Ilk et al. 2007, Idorenyin et al. 2011, Shahamat et al. 2015).

6. Le logiciel HydroGesoSphere, initialement développé par Therrien et al. (2010) puis commercialisé par Aquanty, est un logiciel qui s'est montré particulièrement adapté au cours de cette thèse afin d'investiguer numériquement le signal hydraulique d'un essai de pompage dans des modèles conceptuels spécifiques. En effet, ce logiciel, qui a prouvé sa robustesse dans de nombreuses études hydrogéologiques (Therrien et al. 2010) permet de modéliser des écoulements en 3-D et de créer des configurations géologiques particulières (par exemple le substratum incliné présenté dans le quatrième chapitre, le modèle à faille verticale de conductivité hydraulique finie et alimentée par la matrice présenté par Rafini et Larocque (2009, 2012). Le développement d'un code à partir d'IDL a permis de suivre la

diffusion du front de pression dans l'aquifère et ainsi de connaître la forme de l'onde de pression à chaque pas de temps. L'utilisation combinée de HGS et d'IDL est donc tout à fait appropriée afin de tester des hypothèses de terrain ainsi que pour approfondir les connaissances sur l'interprétation conceptuelle et physique de la dimension d'écoulement, notamment lorsque n est fractionnaire.

Dans l'objectif d'estimer K et S_s , il convient de considérer le fait que certains phénomènes, tels que les effets du puits, des phénomènes de drainance et l'influence d'injection ou de pompage dans des puits voisins, peuvent masquer le signal de la dérivée-log de s et/ou fausser l'estimation des propriétés hydrauliques.

L'utilisation de la dérivée log du rabattement pour aider à investiguer le comportement hydrodynamique de l'aquifère et les conditions géologiques autour du puits est une philosophie nouvelle dans l'interprétation des essais de pompage en hydrogéologie. Il est cependant important de garder à l'esprit qu'étant donné le problème de non-unicité du signal de $ds/d\log t$, le choix d'un modèle analytique nécessite tout de même d'avoir des informations sur la géologie (Massonnat et Bandiziol 1991, Liang et al. 2012). Comme le rappellent justement Ramos et al. (2017), tout l'art de l'interprétation des essais de pompage consiste à réaliser de façon la plus juste et précise possible, le portrait de l'aquifère, d'un point de vue qualitatif et quantitatif, en associant toutes les informations disponibles (notamment les coupes stratigraphiques en forage, les profils géophysiques, les observations géologiques de terrain et les signatures hydrauliques induites par le pompage). La validation de l'interprétation par un modèle mathématique, qu'il soit analytique ou numérique est une étape importante afin d'effectuer un contrôle de la qualité de la

modélisation de l'aquifère. Les étapes de la méthodologie proposée sont synthétisées dans l'organigramme suivant (Figure 5.1).

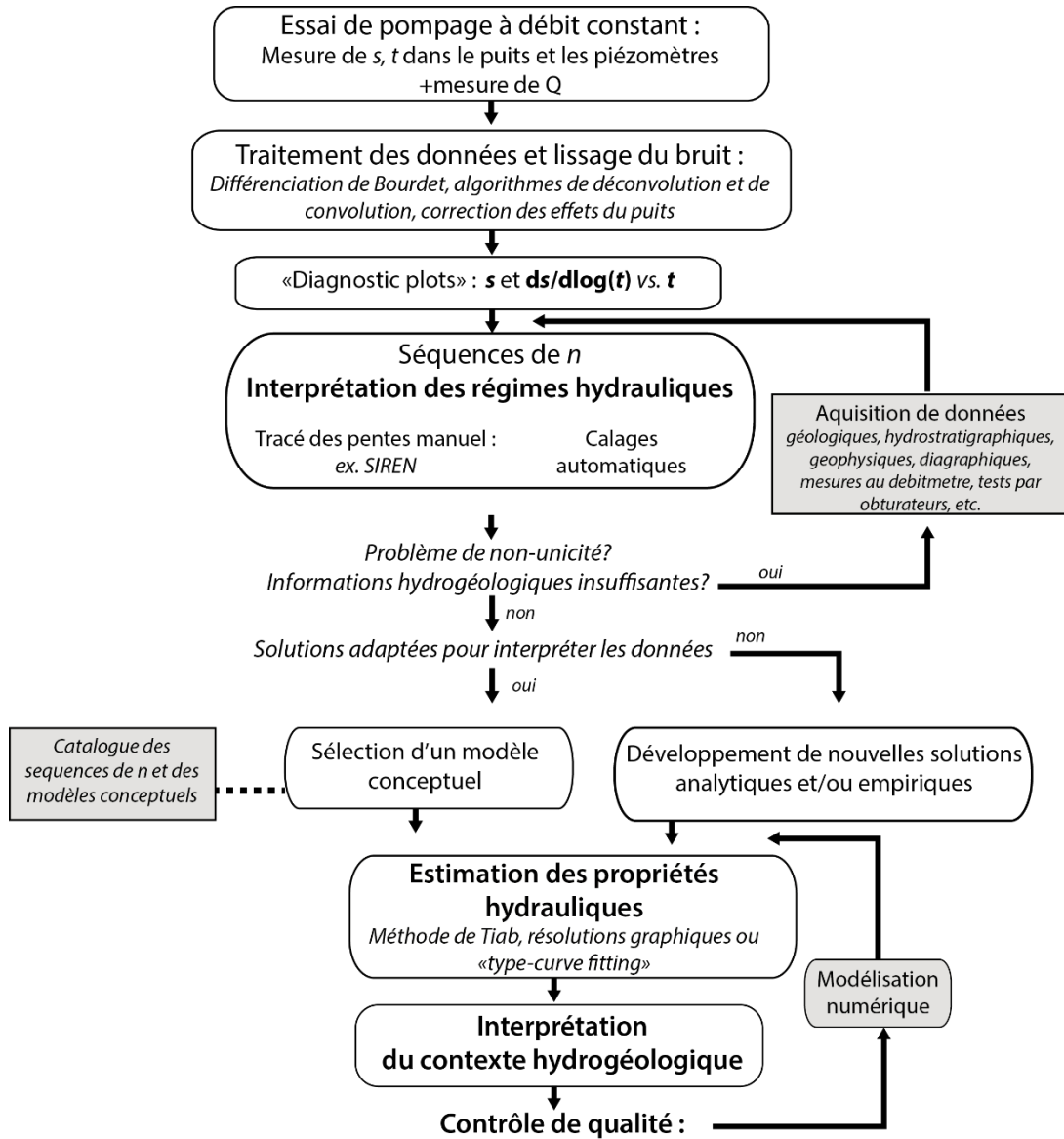


Figure 5.1 : Méthodologie proposée pour l'interprétation des essais de pompage à débit constant à partir du signal de la dérivée-logarithmique du rabattement et de la dimension d'écoulement.

5.4 CONCLUSION

Un des objectifs de la présente thèse est d'aider à propager auprès des hydrogéologues les outils basés sur l'interprétation du signal de $ds/dlogt$ et l'analyse séquentielle de n afin : 1- que ces outils soient couramment utilisés dans les études hydrogéologiques; 2- d'améliorer l'estimation des propriétés hydrauliques des aquifères; 3- de caractériser avec plus de justesse les écoulements autour des puits et 4- de conceptualiser la réalité géologique environnant le puits en représentant plus fidèlement sa complexité et ainsi obtenir de meilleurs modèles d'aquifère. L'utilisation d'un essai de pompage pour investiguer les conditions hydrauliques et géologiques tel que nous l'avons présenté dans cette thèse est une approche encore nouvelle en hydrogéologie, du moins dans le monde de la consultation et elle pourrait adéquatement compléter les études des coupes stratigraphiques en forage et les investigations géophysiques. Le potentiel de diagnostic des méthodes présentées est donc très fort et devrait contribuer de façon significative à améliorer la justesse de nos investigations hydrogéologiques. Cette thèse ainsi que d'autres travaux actuels dans le monde prêchent en ce moment dans ce sens et comme nous le recommandons plus loin, de nombreux progrès sont encore attendus car beaucoup de comportements hydrauliques restent à caractériser et qu'un même signal peut être induit par des milieux très différents (problème de la non-unicité du signal de $ds/dlogt$).

Afin de prendre part à l'émancipation de ces outils diagnostiques, ce travail de recherche a d'abord élaboré une revue de littérature récente et orientée sur les travaux publiés, à la fois, en hydrogéologie et par l'industrie pétrolière, dans le cadre du deuxième chapitre. Ce travail de synthèse a permis de compiler une base de données de signatures de la dérivée

logarithmique du rabattement et de présenter les modèles conceptuels qui leur sont associés. Dans un deuxième temps, l'objectif était d'observer l'occurrence des différentes dimensions d'écoulement ainsi que leurs séquences telles qu'elles s'observent dans la nature à partir d'un jeu de données observées dans des contextes hydrogéologiques variés. L'objectif était : i) de vérifier la nécessité d'améliorer les outils d'interprétation des essais de pompage et ii) d'analyser statistiquement les relations entre les valeurs de n et différents contextes géologiques tels que les aquifères de socle rocheux cristallins, de milieux rocheux carbonatés, les arènes granitiques et les aquifères fluvio-glaciaires. L'interprétation physique de la dimension d'écoulement a été plus souvent abordée par des analyses numériques et a encore été peu étudiée avec des données de terrain. Quelques études ont proposé un portrait de n dans la nature (Kuusela-Lahtinen et al. 2003, Audouin et Bodin 2008, Verbovšek 2009, 2011), mais elles se concentraient principalement sur un contexte géologique particulier : soit le roc carbonaté, soit le roc cristallin. Encore aucune étude n'avait comparé les valeurs de n dans des milieux géologiques autres que ces deux contextes de milieux rocheux fracturés. En effet, l'étude de l'occurrence de n dans les milieux granulaires n'avait encore jamais été abordée. Ce troisième chapitre a également permis de présenter le logiciel SIREN qui a été conçu dans le but d'améliorer le calage manuel des pentes de la dérivée-log du rabattement en se basant sur la combinaison d'un calage couplé avec un diagramme semi-logarithmique de s versus t et un graphique log-log de $ds/d\log t$ versus t . Ces deux axes de recherche présentés dans les chapitres 2 et 3 ont permis de cibler un contexte géologique encore non caractérisé à ce jour : i) qui soit observé dans la nature (en l'occurrence, ici dans cette thèse, un aquifère à substratum incliné) ii) nécessitant une mise à jour des techniques d'interprétation d'essai de pompage et iii) qui

n'ai pas déjà été analysé ni dans l'industrie pétrolière ni en hydrogéologie. Le quatrième chapitre porte donc sur l'analyse numérique d'un essai de pompage à débit constant réalisé dans un aquifère à substratum incliné. Il s'agit d'une amélioration du modèle d'Hantush (1962) dont l'épaisseur de l'aquifère augmente exponentiellement. Le logiciel HydroGeoSphere a été sélectionné pour ses capacités à discrétiser l'équation de diffusivité en 3-D ainsi que pour sa flexibilité à définir des géométries de maillage fidèles à la réalité et parce que de nombreuses études ont attesté sa robustesse de calcul et sa stabilité numérique dans la résolution de problèmes complexes (Therrien et al. 2010). Dans le cadre de cet article, l'étude numérique aura permis d'une part d'identifier l'expression hydraulique (comprenant une dimension sphérique) d'un aquifère à substratum incliné et d'autre part de développer des équations empiriques (suite à des analyses de sensibilité à partir de simulations) permettant l'estimation des propriétés hydrauliques et de la pente du substratum de ce type d'aquifère. Auparavant, ce diagnostic ne pouvait pas se réaliser par des approches conventionnelles d'interprétation des essais de pompage. En effet, appliquer la méthode de Theis pour estimer la conductivité hydraulique de l'aquifère à substratum incliné aurait induit une erreur de 731% alors que l'erreur n'est que de 1% en utilisant les nouvelles équations empiriques développées pour ce modèle conceptuel.

Les trois articles de cette thèse, soit : 1-la revue de littérature sur les séquences de n et les modèles conceptuels associés; 2-l'observation de l'occurrence des valeurs de n et des séquences de n dans la nature ainsi que 3-le développement d'équations empiriques pour améliorer le calcul des propriétés hydrauliques dans les aquifères à substratum incliné ont été rédigés entre autres, dans l'optique de diffuser l'approche séquentielle de n afin qu'elle

soit couramment intégrée au sein des pratiques des hydrogéologues-chercheurs et des hydrogéologues-praticiens. Ces travaux ont été accompagnés de 3 présentations orales aux congrès internationaux de l'AIH (Association Internationale des Hydrogéologues) tenus respectivement au Maroc, en Italie et en France (Ferroud et al. 2014, 2015a, 2016), la présentation d'une affiche au colloque de l'Acfas (2014), une présentation orale au colloque de l'Acfas (2018), une présentation orale au congrès de *Joint Assembly AGU-GAG-MAC-CGU* (Ferroud et al. 2015b) ainsi qu'une présentation de poster au carrefour des sciences de la Terre de l'UQAC (2015) afin de promouvoir ces outils diagnostiques basés sur l'analyse de $ds/dlogt$ et n .

L'amélioration de la compréhension des écoulements souterrains et de la conceptualisation de la géologie autour des puits a des retombées importantes pour les praticiens dans divers domaines tels que l'hydrogéologie, la géotechnique, l'exploration pétrolière ou le stockage de déchets nucléaires et gazeux, en permettant :

- de mieux déterminer les aires d'alimentation des captages,
- de mieux gérer et prévoir le transfert des polluants,
- d'avoir une meilleure connaissance de la quantité et de la disponibilité de la ressource souterraine (eau, pétrole, gaz)
- d'avoir une meilleure connaissance des contaminations croisées entre réservoirs (gaz schiste/eau, aquifères superficiel/souterrain...),
- d'implanter des sites d'enfouissement ou de stockage de déchets nucléaires et de gaz (CO₂, méthane, etc.) de façon plus sécuritaire,

- d'étudier la stabilité des terrains, en vue de la construction d'ouvrages géotechniques tels que la construction de tunnels, et d'étudier la stabilité des talus et des barrages,
- d'avoir une meilleure prise en compte des écoulements souterrains dans la gestion environnementale (ex. : alimentation des cours d'eau par les nappes, évolution des zones humides).

5.5 PISTES DE RECHERCHE

Cette section énumère quelques pistes de recherche qui ont vu le jour tout au long de cette thèse ou que nous jugeons importantes d'approfondir dans l'optique de continuer à développer et à améliorer le diagnostic des essais de pompage. L'approche séquentielle des dimensions d'écoulement n'en est qu'à ses débuts et de nombreuses pistes restent encore à explorer afin d'améliorer l'interprétation des essais de pompage!

✓ L'analyse statistique de l'occurrence de n dans la nature a mis en évidence une éventuelle relation entre la dimension d'écoulement et les effets de drainance. Tel que précisé dans le deuxième chapitre, depuis que Barker (1988) a proposé le modèle GRF, l'interprétation de la dimension d'écoulement a évolué. Initialement, les dimensions fractionnaires (n non-entier) étaient uniquement associées à des modèles fracturés ayant une organisation fractale du réseau de fractures. Doe (1991) a élargi cette interprétation à des modèles non-fractals ayant une hétérogénéité des propriétés hydrauliques et/ou des variations de géométrie de la source ou de l'aquifère. En se basant sur ce principe, Rafini

et Larocque (2009, 2012) ont montré qu'une faille verticale, qui devrait induire un régime linéaire ($n = 1$), produit en fait un régime bilinéaire ($n = 1.5$) car elle est alimentée par la matrice. Dans cette même idée, nous avons observé une corrélation entre la dimension sub-sphérique ($n = 2.5$) et les aquifères de socle rocheux fracturés alimentés par un horizon granulaire sus-jacent. De plus, dans un rapport, Doe (2002) avait d'ailleurs avancé, sans donner d'explication, que les milieux associés à un régime radial ($n = 2$) peuvent induire une dimension d'écoulement supérieure à 2 lorsque le système subit des phénomènes de drainance. La base de données a également mis évidence une signature sub-radiale uniphasee ($n = 1.3$) récurrente aux contextes d'eskers : 7 des 8 essais de pompage situés dans des eskers ont montré une dimension d'écoulement $n = 1.3$. Tous ces essais de pompage proviennent d'eskers situés en Abitibi-Temiscamingue (ABTE). Ces systèmes fluvio-glaciaires sont généralement constitués de sable et de graviers qui ont été déposés par des rivières issues d'eau de fonte et s'écoulant au sein du glacier (Clark et Walder 1994, Levasseur 1995). Ces dépôts peuvent être stratifiés selon l'historique des débits de la rivière. Étant donné que les sédiments ont été déposés au sein de tunnels intra-glaciaires, les eskers ont généralement des formes étroites et allongées (de type « conduit »). On s'attendrait donc à observer un régime linéaire ($n = 1$) qui refléterait la forme longiligne des eskers. Lorsque le glacier s'est retiré, les eskers de l'ABTE ont été recouverts par des dépôts sédimentaires, notamment des horizons d'argile (Allard 1974). Le fait que la dimension d'écoulement soit sub-radiale et fractionnaire ($n = 1.3$) reste encore énigmatique mais pourrait exprimer une alimentation en eau des eskers par les sédiments fluvio-lacustres et/ou les sables littoraux déposés latéralement. Il serait intéressant d'obtenir une coupe précise des eskers induisant une dimension sub-radiale ($n = 1.3$) et d'effectuer des

simulations numériques afin de vérifier cette hypothèse. De plus, dans le cadre de sa maîtrise, Marie-Noëlle Riverin (2006) a proposé une caractérisation approfondie des écoulements du système aquifère de l'esker Saint-Mathieu/Berry (Abitibi, Québec) à partir de nombreuses données de terrain (analyses géochimiques, bilans hydrologiques, datations, coupes stratigraphiques, hydrogrammes, jaugeages de ruisseaux, mesures piézométriques, MNT, profils géophysiques, essais de perméabilité) et de modélisation numérique (Feflow). Toutes les données de terrain qui sont synthétisées dans son mémoire de maîtrise sont mises à disposition en ligne. Une étude de ces données pourrait éventuellement amener d'autres pistes de recherche ou conforter l'hypothèse d'une alimentation latérale par les sédiments déposés en discordance avec les eskers. Aussi, il existe des solutions analytiques prenant en compte des compartiments qu'il serait intéressant de tester pour analyser le comportement hydrodynamique des eskers (Butler Jr. 1988, Dewandel et al. 2018).

✓ La conceptualisation physique de la dimension d'écoulement a beaucoup été abordée par l'approche numérique et est encore très peu investiguée à partir d'observations de terrain. La géophysique ainsi que les diagraphies en forage permettraient d'affiner les connaissances sur le système aquifère (par exemple, la présence et l'orientation de failles, les épaisseurs de dépôts, etc.) et ainsi aiderait à comprendre le sens physique de la dimension d'écoulement. En effet, l'association entre la géophysique de surface avec le cumul des informations diagraphiques au puits de pompage et aux piézomètres d'observation permettrait de construire un modèle géologique fiable. Par exemple, si la densité de forages est suffisante, la diagraphie permettrait de localiser des zones de failles

et de déterminer leur orientation. Elle permettrait aussi de définir précisément la nature, l'épaisseur et éventuellement l'anisotropie des dépôts. Au début de ce projet de doctorat, des investigations au TDEM (*Time Domain Electromagnetic Method*) ont été réalisées sur des sites localisés dans le Charlevoix-Haute-Côte-Nord et le Saguenay-Lac-Saint-Jean (Québec) dans le cadre des projets PACES (Programme d'acquisition de connaissances sur les eaux souterraines). Cette méthode TDEM, qui est basée sur la diffusion d'un champ électromagnétique pour déterminer la résistivité électrique des terrains, s'est avérée très efficace, au Québec, pour déterminer l'épaisseur des dépôts car le contraste de résistivité électrique entre le socle rocheux et les sédiments est important (Simard et al. 2015). En revanche, elle s'est montrée inefficace pour localiser des failles dans le socle rocheux car la différence de résistivité entre les formations géologiques du socle rocheux n'était pas assez importante. La combinaison de plusieurs méthodes géophysiques complémentaires permettrait de conceptualiser le système aquifère en localisant les structures d'écoulement tels que des failles, des conduits plus perméables au sein de sédiments, des zones intensément fracturées. Les méthodes sismiques sont également des outils très utiles pour l'investigation souterraine. Elles sont basées sur une étude des vitesses de propagation des ondes S (cisaillement) et P (pression) dans le milieu suite à une perturbation (explosion de dynamites). Les vitesses sismiques sont liées à la dureté, au degré de consolidation et à la porosité des roches. Elles permettent ainsi d'avoir une connaissance de la lithologie des roches encaissantes (fort contraste des vitesses de propagation selon la densité du milieu) et de l'état d'altération de la roche (vitesse de propagation des ondes sismiques plus faible si la roche est intensément fracturée). La diagraphie serait intéressante pour la compréhension conceptuelle de la dimension d'écoulement car elle permet de détecter

précisément les zones d'écoulement le long du trou de forage et de différencier les venues d'eau par leur débit, leur température et leur conductivité électrique.

✓ Les modèles expérimentaux n'ont encore jamais été utilisés pour améliorer la compréhension de la dimension d'écoulement. Ils permettraient de tester physiquement l'influence de la géométrie de l'aquifère ou de conditions d'hétérogénéité simples sur la dimension d'écoulement. Les maquettes hydrogéologiques permettraient de savoir jusqu'à quel degré de précision le modèle GRF permet d'identifier ces modifications de géométrie et de les interpréter. L'avantage de cette approche est qu'elle permet d'avoir un contrôle sur la géométrie, tout en considérant des conditions « réelles ». Cette approche expérimentale permettrait ainsi d'intégrer la dispersion du rabattement liée à l'hétérogénéité diffuse et au bruit instrumental. Il est cependant important de considérer l'influence des limites physiques de la maquette qui peuvent avoir une influence étant donné que l'échelle d'observation est très petite. L'approche numérique quant à elle permet de tester très rapidement une grande variété de contextes différents, d'avoir un contrôle sur une plus large gamme de paramètres (conductivité hydraulique, emmagasinement, connectivité du réseau de fracture...) et de simuler des écoulements sur des surfaces à l'échelle du kilomètre. Les deux approches sont donc complémentaires car l'une permet d'intégrer la dispersion des mesures de la dérivée logarithmique du rabattement associée à un pompage réel alors que l'autre permet de modéliser aisément la géométrie, l'échelle et la variabilité spatiale des paramètres. Cette optique a d'ailleurs été envisagée au début du doctorat. Nous avons construit un montage hydrogéologique se présentant sous la forme d'une cuve en plexiglas remplie de sable, dans laquelle un écoulement régional (longitudinal, unidirectionnel) est créé en imposant

une différence de charge hydraulique à deux extrémités du montage. Des sondes piézométriques ont été construites afin de mesurer le niveau d'eau dans les piézomètres. Elles permettaient de mesurer manuellement la baisse du niveau d'eau pendant un pompage à débit constant (environ 1 L/min). L'interprétation de ces « minis » essais de pompage n'a pas été possible car les données étaient trop bruitées. Cela peut être dû à une trop forte incertitude de mesure sur le niveau d'eau et sur le temps pendant le pompage (lié à la précision de l'instrument de mesure, au fait que des personnes différentes mesurent les rabattements et le temps, et que l'incertitude de lecture est importante,) et/ou à un bruit trop important du milieu. Ce bruit pourrait être lié à i) l'effet d'emménagement et aux effets pariétaux des piézomètres, ii) à l'écoulement de l'eau dans un sable qui n'est pas complètement saturé (présence d'air dans les pores), etc. Faute de temps dans le doctorat, ce projet n'a pas abouti à des résultats probants, mais il serait intéressant de reprendre ce travail en améliorant la précision de mesure de la variation temporelle du rabattement.

Encore très peu d'études ont combiné le suivi de l'évolution temporelle de la pression (comportement hydrodynamique) avec le suivi de l'évolution temporelle de l'hydrogéochimie au cours d'un essai de pompage (mesures en continu de la conductivité électrique, la température et le pH avec également des échantillonnages fréquents d'eau pour analyser les éléments majeurs, mineurs, traces et des isotopes). À notre connaissance, seulement les travaux de Roques (2013) et de Roques et al. (2014) ont abordé cette problématique. L'approche proposée est basée sur l'hypothèse que, selon ses temps de résidence et les lithologies traversées, l'eau acquiert une signature chimique (faciès particulier) qui retranscrit son origine lorsqu'on la pompe. L'approche proposée nécessite cependant de

réaliser une étude géochimique afin de déterminer les différents faciès hydro-lithologiques. Certes, les écoulements d'eau et la diffusion de la pression à travers l'aquifère ont des comportements différents, mais cette approche pourrait éventuellement faire des liens entre des changements géochimiques et la contribution de nouvelles structures hydrauliques au fur et à mesure que le front de pression se propage à travers le système. Cela permettrait i) de détecter de possibles connexions hydrauliques entre les aquifères, notamment entre les aquifères granulaires et fracturés (de telles connexions ont d'ailleurs été mises en évidence dans la région de Sauguenay/Lac-Saint-Jean (SLSJ, Québec) par Chesnaux et al. (2012)), ii) de mieux cibler un modèle conceptuel de fonctionnement de l'aquifère et iii) d'étudier le rôle des failles dans la circulation des écoulements souterrains. Permettent-elles un écoulement préférentiel ? Permettent-elles la mobilisation d'une masse d'eau plus profonde dont le faciès est différent ?). Par exemple, on peut se demander si dans un modèle bilinéaire avec une faille verticale alimentée par la matrice, i) il est possible d'observer des changements géochimiques reflétant la contribution de la matrice ou de la faille et ii) s'il est possible d'établir des liens entre ces changements géochimiques et la séquence $n = 2 - 4 - 1.5 - 2$. Tel que présenté par Rafini et Larocque (2009) cette séquence indique que le front de pression se diffuse d'abord radialement ($n = 2$) dans la matrice puis à travers la faille alimentée par la matrice ($n = 1.5$) (ce régime d'écoulement est précédé par une courte période de transition associée à une pente unitaire décroissante du signal de $ds/d\log t$). Enfin, le régime d'écoulement redevient radial ($n = 2$) lorsque la diffusion de l'onde de pression à travers la matrice masque la diffusion à travers la faille.

✓ La base de données d'essais de pompage ainsi que les observations de terrain fournies par Audouin et Bodin (2008), Verbovšek (2009), Liang et al. (2012) et Odling et al. (2013) ont montré que les dimensions d'écoulement observées dans la nature sont, dans la plupart des cas, plus complexes que ce que le suppose le modèle de Theis. En effet, les valeurs de n fractionnaires et non-radiales ainsi que les séquences de n associées à un même essai de pompage attestent de la complexité des écoulements dans la nature. Tel que le montre le deuxième chapitre, certaines valeurs de n et certaines séquences de n disposent de modèles conceptuels pour être interprétées. En revanche, il existe encore beaucoup de valeurs et de séquences de n qui n'ont pas encore d'interprétation physique. Il est donc important de continuer à développer de nouveaux modèles conceptuels, qui intègrent plus de complexité, ainsi que de nouvelles solutions analytiques et empiriques.

✓ Tel que présenté dans le quatrième chapitre, les logiciels numériques, par exemple HGS, sont des outils intéressants pour développer de nouveaux modèles conceptuels. En effet, ils permettent i) de suivre l'évolution du front de pression et ainsi de mieux comprendre le comportement des écoulements lors du pompage et ii) de développer empiriquement des équations pour estimer les propriétés hydrauliques, de façon plus adéquate. Les modèles numériques sont des outils intéressants pour développer de nouvelles solutions empiriques ainsi que pour vérifier la validité d'une interprétation hydrodynamique. En parallèle, il est également très pertinent de développer des solutions analytiques et de comparer les résultats aux solutions empiriques.

✓ La théorie de Barker (1988) ne s'applique qu'aux aquifères à nappe captive. En revanche, comme pour la solution de Theis, la solution de Barker pourrait s'appliquer à un aquifère libre, à condition que la baisse de la hauteur saturée de l'aquifère au droit du puits soit minime (Dewandel, communication personnelle). Il serait donc important de tester la validité du concept de Barker ($A(r) \sim r^{n-1}$) dans des aquifères à nappe libre. La base de données d'essais de pompage présentée dans le premier article était composée de signaux d'aquifères à nappe captive ainsi que d'aquifères à nappe libre. Celle-ci n'a pas montré de corrélation entre les aquifères à nappe libre et la dimension d'écoulement.

✓ Une autre piste de recherche essentielle pour l'interprétation des essais de pompage est d'analyser le signal hydraulique dans les piézomètres d'observation. En effet, il serait important de savoir comment s'exprime un essai de pompage aux piézomètres. Est-ce que l'évolution du rabattement ressentie aux piézomètres pourrait aider à conceptualiser l'hétérogénéité des propriétés hydrauliques ainsi que la configuration des écoulements au sein de l'aquifère pompé? L'intégration des observations aux piézomètres permettrait-elle de caractériser les propriétés de l'aquifère avec une meilleure définition et sur une plus large extension ? Pour cela une comparaison des données de terrain à des modélisations numériques et/ou analytiques est recommandée.

✓ Dans le même ordre d'idée, il serait intéressant d'établir, en appliquant le principe de superposition, des solutions basées sur le signal de la dérivée-log de s afin d'interpréter des essais de pompage simultanés.

✓ Il serait également intéressant de vérifier que les solutions basées sur les essais de pompage sont également valides pour les essais d'injection.

✓ Il serait aussi pertinent i) d'investiguer plus précisément les différences de signatures entre la descente et la remontée qui est souvent moins bruitée car non soumise aux variations de débit de pompage. Il est cependant important de connaître ces variations du débit de pompage. En effet, comme précisé précédemment, Mattar (1999) avait observé une différence entre le signal de descente (*drawdown*) et celui de remontée (*buildup*) pour un même modèle conceptuel. Daungkaew et al. (2000) mentionnent qu'effectivement le signal de remontée a l'avantage de ne pas être affecté par les fluctuations du débit de pompage. En revanche, l'inconvénient du signal de remontée est que la pression tend à se stabiliser au fur et à mesure que l'aquifère retourne à son équilibre induisant une diminution de la variation de la pression (Daungkaew et al. 2000). Par conséquent, plus le signal de remontée est long, plus il devient difficile à interpréter car le ratio signal/bruit diminue.

✓ Étant données la forte sensibilité du signal hydraulique de $ds/d\log t$ aux petites variations de débit du pompage, il est conseillé d'avoir recours à des sondes à enregistrement automatique afin de mesurer précisément et fréquemment la pression et le débit de pompage. En effet, si le débit est mesuré à chaque pas de temps, il sera possible de corriger les variations involontaires de débit de la pompe. Les simulations numériques présentées dans le premier article ont d'ailleurs montré qu'une variation continue du débit de la pompe pouvait induire une dimension d'écoulement apparente qui est différente de la dimension d'écoulement réellement représentative du comportement de l'aquifère. Ne pas

corriger les variations de s associées aux variations de Q peut ainsi induire des difficultés, voir même induire en erreur le diagnostic hydrodynamique. Le développement d'algorithmes pour améliorer la correction des bruits associés notamment aux variations de débit de la pompe, aux effets de marées ainsi qu'aux variations barométriques est donc une piste de recherche déterminante dans l'amélioration de la qualité du diagnostic basé sur l'interprétation des signatures de la dérivée-log de s . La littérature pétrolière bourgeoise actuellement de recherches sur le développement d'algorithmes de déconvolution et de convolution. Gringarten (2008) présente les algorithmes de déconvolution comme étant l'avenir de l'analyse de la dérivée-log de s . Il est temps, que ces outils soient intégrés au sein des analyses hydrogéologiques. L'analyse de la dérivée-log de s tend à s'émanciper en hydrogéologie : telle que l'atteste l'augmentation des publications sur le domaine dans les revues spécialisées en hydrogéologie ainsi que l'intégration du signal $ds/d\log t$ au sein des logiciels numériques (par exemple AQUANTY, OUAIP, SIREN, nSIGHTS). Il est maintenant temps d'intégrer les algorithmes de déconvolution au sein des logiciels numériques couramment utilisés par les hydrogéologues.

✓ Le code SIREN, qui a été développé au sein de l'équipe de recherche de l'UQAC dans le cadre d'un partenariat avec l'industrie, aide grandement à réduire la subjectivité de l'estimation de n grâce à un calage combiné entre un graphique semi-log de s et un graphique log-log de $ds/d\log t$. Le code SIREN est encore en développement. Il reste notamment à intégrer de façon exhaustive les solutions analytiques afin de pouvoir estimer les propriétés hydrauliques dans un large éventail de modèles conceptuels. L'algorithme de

lissage de Bourdet est intégré dans le code, mais il reste encore à intégrer les algorithmes de déconvolution.

✓ L'approche de Tiab (1993a, 1993b, 1993c, 1993d, 1995) améliore grandement l'interprétation des essais de pompage car elle permet une analyse graphique du signal de $ds/dlogt$ au lieu d'un calage de courbes théoriques issues de modèles analytiques. Celle-ci consiste à développer analytiquement des solutions basées sur les pentes, les ordonnées à l'origine et des points d'intersection du signal de $ds/dlogt$ afin de déterminer les dimensions physiques du domaine (par exemple, le positionnement des frontières imperméables et à charge constante de l'aquifère, l'épaisseur de l'aquifère, etc.) ainsi que les propriétés hydrauliques de l'aquifère. Il serait avantageux d'intégrer cette approche dans les pratiques en hydrogéologie et de continuer à développer les analyses graphiques de $ds/dlogt$ dans de nouveaux modèles conceptuels. Le développement des solutions peut se résoudre analytiquement ou se déterminer par une approche numérique, tel que présenté dans le quatrième chapitre de cette thèse.

✓ Étant donné que l'approche séquentielle de la dimension d'écoulement permet de suivre l'évolution hydrodynamique de l'aquifère, elle permet donc indirectement d'investiguer la géologie autour du puits. De ce fait, elle permettrait en théorie d'améliorer la délimitation des périmètres de protection. Par exemple, si le puits capte une faille verticale, le périmètre de protection le plus adapté serait un ellipsoïde centré autour de la faille. Comment l'analyse de $ds/dlogt$ et des séquences de n vont permettre d'améliorer le tracé des périmètres de protection ? Dans le cas d'aquifères complexes (non-theissiens),

comment intégrer une connaissance plus précise et plus complexifiée de l'aquifère dans les méthodes de délimitation des périmètres de protection?

✓ D'un point de vue plus fondamental, la question de l'estimation du rayon d'influence r_{inf} est encore ambiguë et reste ouverte. Ce rayon d'influence représente le rayon transitoire qui est atteint par le front d'onde. En d'autres termes, il représente le rayon maximum où la pression de l'aquifère est affectée par l'essai de pompage en régime transitoire. Ce rayon dépend des propriétés intrinsèques du milieu (la conductivité hydraulique et l'emmagasinement). Il n'existe pas de consensus sur une définition standard pour estimer le rayon d'influence. Plusieurs équations sont proposées dans la littérature et peuvent mener parfois à des valeurs de r très différentes. En hydrogéologie, deux équations sont souvent utilisées (Équation (5.2) (Cooper et Jacob 1946) et (5.3) (Shapiro et al. 1997)).

$$r = 1.5 \sqrt{\frac{Kt}{S_s}} \quad (5.2)$$

$$r = \sqrt{4\pi \frac{Kt}{S_s}} \quad (5.3)$$

La littérature pétrolière a également proposé plusieurs autres formules, entre autres, Van Poolen (1964), Earlougher (1977), Stewart (2007) et Kuchuk (2009). Une synthèse a été proposée par Kuchuk (2009). Il est également important de constater que l'onde de pression se déforme selon les propriétés hydrauliques du milieu et la géométrie des écoulements, ce

qui porte à penser que la détermination du rayon d'influence dépend de la dimension d'écoulement. Hsieh et al. (2007) soulèvent un point très important à considérer lorsqu'on étudie la problématique de la détermination du rayon d'influence : la constante de l'équation qui permet d'estimer r_{inf} varie avec le critère de définition du rayon d'influence. Ce critère représente la précision pour laquelle on détecte le front de pression. Actuellement, la littérature n'a pas encore défini une valeur critique représentant la différence entre la pression initiale de l'aquifère et celle influencée par l'essai de pompage qu'il faut considérer pour estimer r_{inf} . Hsieh et al. (2007) montrent d'ailleurs que si cette différence de pression permettant de détecter le front de pression varie de 0.1095 à 10^{-9} , le coefficient de l'équation varie alors de 4 à 71.15 . Nous avons également entrepris des simulations numériques afin d'analyser la vitesse de diffusion et la forme du rayon d'influence dans des modèles conceptuels de type Theis (régime d'écoulement radial) et à aquifère à substratum incliné (régime d'écoulement sphérique). Nous avons d'abord calculé l'évolution transitoire de la charge hydraulique en tout point de l'espace discrétisé à partir des logiciels GeoSlope et HydroGeoSphere. Puis, à partir d'un code écrit sous IDL (Interactive Data Language), nous avons suivi la diffusion du front de pression. À l'heure actuelle, ces travaux sont encore préliminaires, mais nos premiers résultats semblent indiquer que les équations (5.2) et (5.3) ne sont pas adaptées pour calculer le rayon d'influence, ni pour le modèle conceptuel de type Theis, ni pour la modèle à SI. Maintenant que le signal de $ds/dlogt$ permet de détecter différents régimes d'écoulement (notamment les régimes non-radiaux), il est important d'adapter les solutions permettant d'estimer r_{inf} à la complexité et à la variété des formes du front de pression. Par exemple, dans le cas d'un modèle induisant un front de pression ellipsoïdal ou non centré sur le puits de pompage, plusieurs rayons d'influence devraient

être définis. Ce travail commence à être considéré dans la littérature pétrolière : Aguilera (2006) a proposé une équation pour calculer le rayon d'influence dans un modèle associé à un régime d'écoulement linéaire, tel que des paléo chenaux ou lorsque le puits est situé entre deux failles imperméables.

LISTE DE RÉFÉRENCES

- Abbaszadeh, M., et Cinco-Ley, H. 1995. Pressure-transient behavior in a reservoir with a finite-conductivity fault [en ligne]. *SPE Formation Evaluation*, **10**(01) : 26–32. doi: 10.2118/24704-PA.
- Abdassah, D., et Ershaghi, I. 1986. Triple-Porosity Systems for Representing Naturally Fractured Reservoirs [en ligne]. *SPE Formation Evaluation*, **1**(02) : 113–127. doi: 10.2118/13409-PA.
- Acuna, J.A., et Yortsos, Y.C. 1995. Application of fractal geometry to the study of networks of fractures and their pressure transient [en ligne]. *Water Resources Research*, **31**(3) : 527–540. doi: 10.1029/94WR02260.
- Aguilera, R. 2006. Radius and Linear Distance of Investigation and Interconnected Pore Volume in Naturally Fractured Reservoirs [en ligne]. *Journal of Canadian Petroleum Technology*, **45**(12). doi: 10.2118/06-12-04.
- Allard, M. 1974. Géomorphologie des eskers abitibiens [en ligne]. *Cahiers de géographie du Québec*, **18**(44) : 271. doi: 10.7202/021195ar.
- Anderson, D., Scotts, G.W., Mattar, L., Ilk, D., et Blasingame, T. 2006. Production Data Analysis--Challenges, Pitfalls, Diagnostics [en ligne]. Society of Petroleum Engineers. doi: 10.2118/102048-MS.
- Anisur Rahman, N.M., et Mattar, L. 2007. New analytical solution to pressure transient problems in commingled, layered zones with unequal initial pressures subject to step changes in production rates [en ligne]. *Journal of Petroleum Science and Engineering*, **56**(4) : 283–295. doi: 10.1016/j.petrol.2006.10.002.
- Atangana, A., et Botha, J.F. 2013. A generalized groundwater flow equation using the concept of variable-order derivative [en ligne]. *Boundary Value Problems*, **2013**(1) : 1–11. doi: 10.1186/1687-2770-2013-53.
- Audouin, O., et Bodin, J. 2008. Cross-borehole slug test analysis in a fractured limestone aquifer [en ligne]. *Journal of Hydrology*, **348**(3–4) : 510–523. doi: 10.1016/j.jhydrol.2007.10.021.
- Azari, M., Wooden, W.O., et Coble, L.E. 1990. A Complete Set of Laplace Transforms for Finite-Conductivity Vertical Fractures Under Bilinear and Trilinear Flows [en ligne]. Society of Petroleum Engineers. doi: 10.2118/20556-MS.
- Azi, A.C., Gbo, A., Whittle, T., et Gringarten, A. 2008. Evaluation of confidence intervals in well test interpretation results [en ligne]. *Dans* Society of Petroleum Engineers paper No. 113888, Europec/EAGE Conference and Exhibition, 9-12 June 2008, Rome, Italy. doi: 10.2118/113888-MS.
- Bangoy, L.M., Bidaux, P., Drogue, C., Plégat, R., et Pistre, S. 1992. A new method of characterizing fissured media by pumping tests with observation wells [en ligne]. *Journal of Hydrology*, **138**(1–2) : 77–88. doi: 10.1016/0022-1694(92)90156-P.

- Barker, J. 2007. Diffusion in Hydrogeology. *Diffusion Fundamentals*, **6** : 50.1-50.18.
- Barker, J.A. 1988. A generalized radial flow model for hydraulic tests in fractured rock [en ligne]. *Water Resources Research*, **24**(10) : 1796–1804. doi: 10.1029/WR024i010p01796.
- Barlow, J.R.B., et Coupe, R.H. 2012. Groundwater and surface-water exchange and resulting nitrate dynamics in the Bogue Phalia basin in northwestern Mississippi [en ligne]. *Journal of Environment Quality*, **41**(1) : 155–169. doi: 10.2134/jeq2011.0087.
- Barry, F., Ophori, D., Hoffman, J., et Canace, R. 2009. Groundwater flow and capture zone analysis of the Central Passaic River Basin, New Jersey [en ligne]. *Environmental Geology*, **56**(8) : 1593–1603. doi: 10.1007/s00254-008-1257-5.
- Bear, J., et Jacobs, M. 1965. On the movement of water bodies injected into aquifers [en ligne]. *Journal of Hydrology*, **3**(1) : 37–57. doi: 10.1016/0022-1694(65)90065-X.
- Beauheim, R.L., et Roberts, R.M. 1998. Flow-dimension analysis of hydraulic tests to characterize water-conducting features [en ligne]. *Dans Water-conducting Features in Radionuclide Migration, GEOTRAP Project Workshop Proceedings, Barcelona, Spain, June 10-12, 1998. Paris, France: OECD NEA. 287-294. ISBN 92-64-17124-X. Disponible à <http://www.osti.gov/scitech/biblio/1904> [cité le 2 novembre 2013].*
- Beauheim, R.L., et Roberts, R.M. 2002. Hydrology and hydraulic properties of a bedded evaporite formation [en ligne]. *Journal of Hydrology*, **259**(1–4) : 66–88. doi: 10.1016/S0022-1694(01)00586-8.
- Beauheim, R.L., Roberts, R.M., et Avis, J.D. 2004. Well testing in fractured media: flow dimensions and diagnostic plots [en ligne]. *Journal of Hydraulic Research*, **42**(sup1) : 69–76. doi: 10.1080/00221680409500049.
- Bense, V.F., et Person, M.A. 2006. Faults as conduit-barrier systems to fluid flow in siliciclastic sedimentary aquifers [en ligne]. *Water Resources Research*, **42**(5) : n/a–n/a. doi: 10.1029/2005WR004480.
- Bhatt, K. 1993. Uncertainty in wellhead protection area delineation due to uncertainty in aquifer parameter values [en ligne]. *Journal of Hydrology*, **149**(1–4) : 1–8. doi: 10.1016/0022-1694(93)90095-Q.
- Billaux, D., et Gentier, S. 1990. *Numerical and Laboratory Studies of Flow in a Fracture. A* a Balkema, Rotterdam.
- Birsoy, Y.K., et Summers, W.K. 1980. Determination of Aquifer Parameters from Step Tests and Intermittent Pumping Data [en ligne]. *Ground Water*, **18**(2) : 137–146. doi: 10.1111/j.1745-6584.1980.tb03382.x.
- Biryukov, D., et Kuchuk, F.J. 2012. Transient pressure behavior of reservoirs with discrete conductive faults and fractures [en ligne]. *Transport in Porous Media*, **95**(1) : 239–268. doi: 10.1007/s11242-012-0041-x.

- Black, J.H. 1994. Hydrogeology Of Fractured Rocks – A Question Of Uncertainty About Geometry [en ligne]. *Applied Hydrogeology*, **2**(3) : 56–70. doi: 10.1007/s100400050049.
- Bourdet, D., Ayoub, J.A., et Pirard, Y.M. 1989. Use of pressure derivative in well test interpretation [en ligne]. *SPE Formation Evaluation*, **4**(2) : 293–302. doi: 10.2118/12777-PA.
- Bourdet, D., Whittle, T., Douglas, A., et Picard, Y. 1983. A new set of types curves simplifies well test analysis. *World Oil*, **196** : 95–106.
- Bowman, D.O., Roberts, R.M., et Holt, R.M. 2012. Generalized radial flow in synthetic flow systems [en ligne]. *Groundwater*, **51**(5) : 768–774. doi: 10.1111/j.1745-6584.2012.01014.x.
- Caine, J.S., Evans, J.P., et Forster, C.B. 1996. Fault zone architecture and permeability structure [en ligne]. *Geology*, **24**(11). doi: 10.1130/0091-7613(1996)024<1025:FZAAPS>2.3.CO;2.
- Carrera, J. 1993. An overview of uncertainties in modelling groundwater solute transport [en ligne]. *Journal of Contaminant Hydrology*, **13**(1–4) : 23–48. doi: 10.1016/0169-7722(93)90049-X.
- Cello, P.A., Walker, D.D., Valocchi, A.J., et Loftis, B. 2009. Flow Dimension and Anomalous Diffusion of Aquifer Tests in Fracture Networks [en ligne]. *Vadose Zone Journal*, **8**(1) : 258–268. doi: 10.2136/vzj2008.0040.
- Chang, J., et Yortsos, Y.C. 1990. Pressure-transient analysis of fractal reservoirs [en ligne]. *SPE Formation Evaluation*, **5**(01) : 31–38. doi: 10.2118/18170-PA.
- Chang, Y.-C., Yeh, H.-D., Liang, K.-F., et Kuo, M.-C.T. 2011. Scale dependency of fractional flow dimension in a fractured formation [en ligne]. *Hydrology and Earth System Sciences*, **15**(7) : 2165–2178. doi: 10.5194/hess-15-2165-2011.
- Chapuis, R.P. 2007. Guide des essais de pompage et leurs interprétations [en ligne]. Bibliothèque et archives nationales du Québec, Québec (Canada). Disponible à http://www.mddelcc.gouv.qc.ca/eau/souterraines/guide_pompage/guide_pompage_1-4.pdf.
- Chesnaux, R., Dal Soglio, L., et Rafini, S. communication personnelle. A numerical analysis to illustrate the usefulness of diagnostic plots in characterizing the hydraulic properties of heterogeneous granular aquifers.
- Chesnaux, R., Lambert, M., Walter, J., Fillastre, U., Hay, M., Rouleau, A., Daigneault, R., Moisan, A., et Germaneau, D. 2011. Building a geodatabase for mapping hydrogeological features and 3D modeling of groundwater systems: Application to the Saguenay–Lac-St.-Jean region, Canada [en ligne]. *Computers & Geosciences*, **37**(11) : 1870–1882. doi: 10.1016/j.cageo.2011.04.013.
- Chesnaux, R., Rafini, S., et Elliott, A.-P. 2012. A numerical investigation to illustrate the consequences of hydraulic connections between granular and fractured-rock

- aquifers [en ligne]. *Hydrogeology Journal*, **20**(8) : 1669–1680. doi: 10.1007/s10040-012-0912-9.
- Chow, V.T. 1952. On the determination of transmissibility and storage coefficients from pumping test data [en ligne]. *Eos, Transactions American Geophysical Union*, **33**(3) : 397–404. doi: 10.1029/TR033i003p00397.
- Cinco-Ley, H., Samaniego V., F., et Dominguez A., N. 1978. Transient Pressure Behavior for a Well With a Finite-Conductivity Vertical Fracture [en ligne]. *Society of Petroleum Engineers Journal*, **18**(04) : 253–264. doi: 10.2118/6014-PA.
- Cinco-Ley, H., et Samaniego-V., F. 1981a. Transient Pressure Analysis for Fractured Wells [en ligne]. *Journal of Petroleum Technology*, **33**(09) : 1749–1766. doi: 10.2118/7490-PA.
- Cinco-Ley, H., et Samaniego-V., F. 1981b. Transient pressure analysis: finite conductivity fracture case versus damaged fracture case [en ligne]. *Dans SPE Annual Technical Conference and Exhibition*, 4-7 October, 1981, San Antonio, Texas, USA, SPE-10179-MS. SPE Annual Technical Conference and Exhibition. doi: 10.2118/10179-MS.
- Clark, P., et Walder, J. 1994. Subglacial Drainage, Eskers, and Deforming Beds Beneath the Laurentide and Eurasian Ice Sheets [en ligne]. *Geological Society of America Bulletin*, **106**(2) : 304–314. doi: 10.1130/0016-7606(1994)106<0304:SDEADB>2.3.CO;2.
- Cooper, H.H., Jr., et Jacob, C.E. 1946. A generalized graphical method for evaluating formation constants and summarizing well-field history [en ligne]. *Transactions, American Geophysical Union*, **27** : 526–534. doi: 10.1029/TR027i004p00526.
- Corbett, P.W.M., Hamdi, H., et Gurav, H. 2012. Layered fluvial reservoirs with internal fluid cross flow: a well-connected family of well test pressure transient responses [en ligne]. *Petroleum Geoscience*, **18**(2) : 219–229. doi: 10.1144/1354-079311-008.
- Culham, W.E. 1974. Pressure Buildup Equations for Spherical Flow Regime Problems [en ligne]. *Society of Petroleum Engineers Journal*, **14**(06) : 545–555. doi: 10.2118/4053-PA.
- Cumming, J.A., Wooff, D.A., Whittle, T., Crossman, R.J., et Gringarten, A. 2013. Assessing the non-uniqueness of the well test interpretation model using deconvolution [en ligne]. *Dans Society of Petroleum Engineers paper No. 164870, EAGE Annual Conference & Exhibition incorporating SPE Europec*, 10-13 June, London, UK. doi: 10.2118/164870-MS.
- Dal Soglio, L. 2012. Simulation numérique d'essai de pompage pour le diagnostic des discontinuités structurales et des hétérogénéités des aquifères de dépôts.
- Daungkaew, S., Hollaender, F., et Gringarten, A. 2000. Frequently Asked Questions in Well Test Analysis [en ligne]. *Society of Petroleum Engineers*. doi: 10.2118/63077-MS.

- De Dreuzy, J.-R. 1999. Analyse des propriétés hydrauliques des réseaux de fractures. Discussion des modèles d'écoulement compatibles avec les principales géométries. Thèse Doctorat, France.
- Dershowitz, W.S., Foxford, T., et Doe, T.W. 1998. FRDFNT: Research Report, Fracture Data Analysis Technology [en ligne]. Disponible à <http://www.fracturedreservoirs.com/niper/database/REPORTS/FracSys98/FracSys98.htm#TopOfPage> [cité le 3 novembre 2013].
- Dewandel, B., Lachassagne, P., Zaidi, F.K., et Chandra, S. 2011. A conceptual hydrodynamic model of a geological discontinuity in hard rock aquifers: Example of a quartz reef in granitic terrain in South India [en ligne]. *Journal of Hydrology*, **405**(3–4) : 474–487. doi: 10.1016/j.jhydrol.2011.05.050.
- Doe, T.W. 1991. Fractional dimension analysis of constant-pressure well tests [en ligne]. *Dans* Society of Petroleum Engineers paper No. 22702, SPE Annual Technical Conference and Exhibition, 6-9 October, 1991, Dallas, Texas, USA. p. 461–467. doi: 10.2118/22702-MS.
- Doe, T.W. 2002. Generalized dimension analysis of build-up and pressure interference tests. Stockholm Suède. IPR-02-70.
- Döll, P. 2009. Vulnerability to the impact of climate change on renewable groundwater resources: a global-scale assessment [en ligne]. *Environmental Research Letters*, **4**(3) : 035006. doi: 10.1088/1748-9326/4/3/035006.
- Doughty, C., et Karasaki, K. 2002. Flow and transport in hierarchically fractured rock [en ligne]. *Journal of Hydrology*, **263**(1–4) : 1–22. doi: 10.1016/S0022-1694(02)00032-X.
- de Dreuzy, J.-R., Davy, P., et Bour, O. 2000. Percolation parameter and percolation-threshold estimates for three-dimensional random ellipses with widely scattered distributions of eccentricity and size [en ligne]. *Physical Review E*, **62**(5) : 5948–5952. doi: 10.1103/PhysRevE.62.5948.
- Duhamel, J. 1833. Memoire sur la methode generale relative au mouvement de la chaleur dans les corps solides polonge dans les milieux dont la temprature varie avec le temps. *Journal de L'École Polytechnique*, **14** : 20–77.
- Earlougher, R.C. 1977. Advances in well test analysis. Henry L. Doherty Memorial Fund of AIME, New York.
- Eckhardt, K., et Ulbrich, U. 2003. Potential impacts of climate change on groundwater recharge and streamflow in a central European low mountain range [en ligne]. *Journal of Hydrology*, **284**(1–4) : 244–252. doi: 10.1016/j.jhydrol.2003.08.005.
- Eggleston, J., et Rojstaczer, S. 1998. Identification of large-scale hydraulic conductivity trends and the influence of trends on contaminant transport [en ligne]. *Water Resources Research*, **34**(9) : 2155–2168. doi: 10.1029/98WR01475.

- Ehlig-Economides, C. 1988. Use of the pressure derivative for diagnosing pressure-transient behavior [en ligne]. *Journal of Petroleum Technology*, **40**(10) : 1280–1282. doi: 10.2118/18594-PA.
- Ehlig-Economides, C.A., et Vera, F.E. 2013. Diagnosing Pressure-Dependent-Permeability in Long-Term Shale Gas Pressure and Production Transient Analysis [en ligne]. *Dans Society of Petroleum Engineers paper No. 168698, Unconventional Resources Technology Conference, 12-14 August, Denver, Colorado, USA. Society of Exploration Geophysicists, American Association of Petroleum Geologists, Society of Petroleum Engineers.* p. 569–578. doi: 10.1190/urtec2013-059.
- Escobar, F.H., Corredor, C.M., Gomez, B.E., Cantillo, J.H., et Prent, L.A. 2012a. Pressure and pressure derivative analysis for slanted and partially penetrating wells. *Asian Research Publishing Network (ARPN)*, **7**(8) : 932–938.
- Escobar, F.H., Hernández, D.P., et Saavedra, J.A. 2010. Pressure and pressure derivative analysis for long naturally fractured reservoirs using the TDS technique. *DYNA*, **77**(163) : 102–114.
- Escobar, F.H., Hernández, Y.A., et Hernández, C.M. 2007. Pressure transient analysis for long homogeneous reservoirs using TDS technique [en ligne]. *Journal of Petroleum Science and Engineering*, **58**(1–2) : 68–82. doi: 10.1016/j.petrol.2006.11.010.
- Escobar, F.H., et Montealegre-M, M. 2007. A complementary conventional analysis for channelized reservoirs. *CT&F - Ciencia, Tecnología y Futuro*, **3**(3) : 137–146.
- Escobar, F.H., Muñoz, O., Sepúlveda, J., et Montealegre, M. 2005. New finding on pressure response in long, narrow reservoirs. *CT&F - Ciencia, Tecnología y Futuro*, **3**(1) : 151–160.
- Escobar, F.H., Navarrete, J.M., et Losada, H.D. 2004a. Evaluation of Pressure Derivative Algorithms for Well-Test Analysis [en ligne]. *Society of Petroleum Engineers.* doi: 10.2118/86936-MS.
- Escobar, F.H., Rojas, M.M., et Bonilla, L.F. 2012b. Transient-rate analysis for long homogeneous and naturally fractured reservoir by the TDS technique. *Journal of Engineering and Applied Sciences*, **7**(3) : 353–370.
- Escobar, F.H., Saavedra, N., Hernandez, C., Hernandez, Y., Pilataxi, J., et Pinto, D. 2004b. Pressure and Pressure Derivative Analysis for Linear Homogeneous Reservoirs Without Using Type-Curve Matching [en ligne]. *Society of Petroleum Engineers.* doi: 10.2118/88874-MS.
- Fadlelmawla, A.A., et Dawoud, M.A. 2006. An approach for delineating drinking water wellhead protection areas at the Nile Delta, Egypt [en ligne]. *Journal of Environmental Management*, **79**(2) : 140–149. doi: 10.1016/j.jenvman.2005.06.001.
- Ferris, J. 1949. Ground Water [en ligne]. *Dans Hydrology.* John Wiley & Sons Inc, New York, United-States. p. 198–272. Disponible à <http://babel.hathitrust.org/cgi/pt?id=mdp.39015004516681;view=1up;seq=11>.

- Ferroud, A., Chesnaux, R., et Rafini, S. 2014. Development and application of diagnostic tools for the determination of hydraulic properties in complex aquifers. *Dans* 41st IAH International Congress « Groundwater : Challenges and Strategies », September 15-19, 2014, Marrakech, Morocco. Marrakech (Morocco).
- Ferroud, A., Chesnaux, R., et Rafini, S. 2015a. Pumping test diagnostic plots for the investigation of flow patterns in complex aquifers: numerical results. *Dans* 42nd IAH International Congress « Hydrogeology: Back to the future », September 13-18, 2015, Rome, Italy.
- Ferroud, A., Chesnaux, R., et Rafini, S. 2015b. Statistical analysis of flow dimension occurrences in natural aquifers from various geological environments: input on their conceptual interpretation. *Dans* Joint Assembly AGU-GAC-MAC-CGU, May 3-7, 2015, Montreal, Canada. Montreal (Canada).
- Ferroud, A., Chesnaux, R., et Rafini, S. 2016. Numerical investigations of the spherical flow regimes induced by constant-rate pumping tests. *Dans* 43rd IAH congress, September 25-29, 2016 Montpellier, France.
- Ferroud, A., Chesnaux, R., et Rafini, S. 2018. Insights on pumping well interpretation from flow dimension analysis: The learnings of a multi-context field database [en ligne]. *Journal of Hydrology*, **556** : 449–474. doi: 10.1016/j.jhydrol.2017.10.008.
- Figueiredo, B., Tsang, C.-F., Niemi, A., et Lindgren, G. 2016. Review: The state-of-art of sparse channel models and their applicability to performance assessment of radioactive waste repositories in fractured crystalline formations [en ligne]. *Hydrogeology Journal* : 1–16. doi: 10.1007/s10040-016-1415-x.
- Forster, C.B., Lachmar, T.E., et Oliver, D.S. 1997. Comparison of models for delineating wellhead Protection areas in confined to semiconfined aquifers in alluvial basins [en ligne]. *Ground Water*, **35**(4) : 689–697. doi: 10.1111/j.1745-6584.1997.tb00135.x.
- Geier, J.E., Doe, T.W., Benabderrahman, A., et Hassler, L. 1996. Generalized radial flow interpretation of well tests for the site-94 project [en ligne]. Disponible à <http://dspace.library.dc-uoit.ca/uoit/handle/dcuoit/902> [cité le 25 octobre 2013].
- Giese, M., Reimann, T., Liedl, R., Maréchal, J.-C., et Sauter, M. 2017. Application of the flow dimension concept for numerical drawdown data analyses in mixed-flow karst systems [en ligne]. *Hydrogeology Journal*, **25**(3) : 799–811. doi: 10.1007/s10040-016-1523-7.
- Gringarten, A. 2008. From Straight Lines to Deconvolution: The Evolution of the State of the Art in Well Test Analysis [en ligne]. *SPE Reservoir Evaluation & Engineering*, **11**(1). doi: 10.2118/102079-PA.
- Gringarten, A. 2010. Practical use of well-test deconvolution [en ligne]. *Dans* Society of Petroleum Engineers paper No. 134534, SPE Annual Technical Conference and Exhibition, 19-22 September, Florence, Italy. doi: 10.2118/134534-MS.

- Gringarten, A., et Ramey, H.J. 1975. An Approximate Infinite Conductivity Solution for a Partially Penetrating Line-Source Well [en ligne]. Society of Petroleum Engineers Journal, **15**(02) : 140–148. doi: 10.2118/4733-PA.
- Gringarten, A., Ramey, H.J., et Raghavan, R. 1974. Unsteady-State Pressure Distributions Created by a Well With a Single Infinite-Conductivity Vertical Fracture [en ligne]. Society of Petroleum Engineers Journal, **14**(04) : 347–360. doi: 10.2118/4051-PA.
- Gringarten, A., Ramey, H.J., et Raghavan, R. 1975. Applied Pressure Analysis for Fractured Wells [en ligne]. Journal of Petroleum Technology, **27**(07) : 887–892. doi: 10.2118/5496-PA.
- Gringarten, A., et Witherspoon, P. 1972. A method of analyzing pump test data from fractured aquifers. *Dans* Int. Soc. Rock Mechanics and Int. Ass. Eng. Geol. Proc. Symp. Rock Mechanics. Stuttgart. p. 1–9.
- Grubb, S. 1993. Analytical model for estimation of steady-state capture zones of pumping wells in confined and unconfined aquifers [en ligne]. Ground Water, **31**(1) : 27–32. doi: 10.1111/j.1745-6584.1993.tb00824.x.
- Hammond, P.A., et Field, M.S. 2014. A reinterpretation of historic aquifer tests of two hydraulically fractured wells by application of inverse analysis, derivative analysis, and diagnostic plots [en ligne]. Journal of Water Resource and Protection, **06**(05) : 481–506. doi: 10.4236/jwarp.2014.65048.
- Hantush, M.S. 1956. Analysis of data from pumping tests in leaky aquifers [en ligne]. Transactions, American Geophysical Union, **37**(6) : 702. doi: 10.1029/TR037i006p00702.
- Hantush, M.S. 1960. Modification of the theory of leaky aquifers [en ligne]. Journal of Geophysical Research, **65**(11) : 3713–3725. doi: 10.1029/JZ065i011p03713.
- Hantush, M.S. 1966. Wells in homogeneous anisotropic aquifers. Water Resources Research. Water Resources Research, **2**(2) : 273–279.
- Hantush, M.S., et Jacob, C.E. 1955. Non-steady radial flow in an infinite leaky aquifer [en ligne]. Eos, Transactions American Geophysical Union, **36**(1) : 95–100. doi: 10.1029/TR036i001p00095.
- Horne, R.N. 1990. Modern well test analysis: a computer-aided approach. Petroway, Palo Alto, Calif.
- Horne, R.N. 1995. Modern well test analysis: a computer-aided approach. Petroway.
- Horne, R.N., et Temeng, K.O. 1982. Recognition and Location of Pinchout Boundaries by Pressure Transient Analysis [en ligne]. Journal of Petroleum Technology, **34**(03) : 517–519. doi: 10.2118/9905-PA.
- Hosseinpour-Zonoozi, N. 2006, décembre. Development of the β -pressure derivative. MSc., Texas A&M University, Texas, USA.

- Hsieh, B.Z., Chilingar, G.V., et Lin, Z.S. 2007. Propagation of Radius of Investigation from Producing Well [en ligne]. *Energy Sources, Part A: Recovery, Utilization, and Environmental Effects*, **29**(5) : 403–417. doi: 10.1080/15567030601003759.
- Huet, M. 2015, janvier. Comparaison de méthodes d'estimation de la recharge des aquifères : exemple de la région Charlevoix-Haute-Côte-Nord [en ligne]. masters, Université du Québec à Chicoutimi, Chicoutimi. Disponible à <http://constellation.uqac.ca/3828/> [cité le 16 janvier 2018].
- Idorenyin, E., Okouma Mangha, V., et Mattar, L. 2011. Analysis of Production Data Using the Beta-Derivative [en ligne]. Society of Petroleum Engineers. doi: 10.2118/149361-MS.
- Ilk, D., Hosseinpor-Zonoozi, N., Amini, S., et Blasingame, T.A. 2007. Application of the Beta-Integral Derivative Function to Production Analysis. *Dans* SPE 107967, 2007 SPE Rocky Mountain Oil and Gas Technology Symposium, Denver, Colorado, USA.
- Ji, S.-H., Lee, D.H., Yeo, I.W., Park, K.-W., et Koh, Y.-K. 2013. Derivative-Assisted Classification of Fractured Zones Crossing a Deep Borehole [en ligne]. *Groundwater*. doi: 10.1111/gwat.12035.
- Jourde, H., Bidaux, P., et Pistre, S. 1998. Fluid flow modelling in orthogonal fracture networks: influence of pumping well location on the hydrodynamic response of the modelled aquifer. *Bulletin De La Societe Geologique De France*, **169**(5) : 635–644.
- Jourde, H., Cornaton, F., Pistre, S., et Bidaux, P. 2002a. Flow behavior in a dual fracture network [en ligne]. *Journal of Hydrology*, **266**(1–2) : 99–119. doi: 10.1016/S0022-1694(02)00120-8.
- Jourde, H., Pistre, S., Perrochet, P., et Drogue, C. 2002b. Origin of fractional flow dimension to a partially penetrating well in stratified fractured reservoirs. New results based on the study of synthetic fracture networks [en ligne]. *Advances in Water Resources*, **25**(4) : 371–387. doi: 10.1016/S0309-1708(02)00010-6.
- Karanta, G. 2002, octobre. Étude comparative de méthodes de détermination de périmètres de protection autour des ouvrages de captage dans les aquifères captifs fracturés du sud-ouest du Québec. [en ligne]. masters, Université du Québec, Institut national de la recherche scientifique, Québec. Disponible à <http://espace.inrs.ca/349/> [cité le 7 décembre 2015].
- Kruseman, G., De Rider, N., et Meilhac, A. 1973. Interprétation et discussion des pompages d'essai [en ligne]. International Institute for landreclamation and improvement, Wageningen, **Bulletin 11, 2nd edition**. Disponible à <http://library.wur.nl/WebQuery/wurpubs/fulltext/72326>.
- Kruseman, G.P., et de Ridder, N.A. 1994. Analysis and evaluation of pumping test data. 2. ed. (compl. rev.), repr. International Institute for Land Reclamation and Improvement, Wageningen.
- Kuchuk, F.J. 1990. Applications of Convolution and Deconvolution to Transient Well Tests [en ligne]. *SPE Formation Evaluation*, **5**(04) : 375–384. doi: 10.2118/16394-PA.

- Kuchuk, F.J. 2009. Radius of Investigation for Reserve Estimation From Pressure Transient Well Tests [en ligne]. Society of Petroleum Engineers. doi: 10.2118/120515-MS.
- Kuchuk, F.J., et Ayestaran, L. 1985. Analysis of Simultaneously Measured Pressure and Sandface Flow Rate in Transient Well Testing (includes associated papers 13937 and 14693) [en ligne]. *Journal of Petroleum Technology*, **37**(02) : 323–334. doi: 10.2118/12177-PA.
- Kuchuk, F.J., et Biryukov, D. 2013. Pressure transient tests and flow regimes in fractured reservoirs [en ligne]. SPE Annual Technical Conference and Exhibition. Society of Petroleum Engineers, New Orleans, Louisiana, USA. doi: 10.2118/166296-MS.
- Kuchuk, F.J., Onur, M., et Hollaender, F. 2010. Pressure Transient Formation and Well Testing: Convolution, Deconvolution and Nonlinear Estimation. Elsevier.
- Kuusela-Lahtinen, A., Niemi, A., et Luukkonen, A. 2003. Flow dimension as an indicator of hydraulic behavior in site characterization of fractured rock [en ligne]. *Ground Water*, **41**(3) : 333–341. doi: 10.1111/j.1745-6584.2003.tb02602.x.
- Lachassagne, P. 2008. Overview of the Hydrogeology of Hard Rock Aquifers: Applications for their Survey, Management, Modelling and Protection [en ligne]. *Dans Groundwater Dynamics in Hard Rock Aquifers. Sous la direction de S. Ahmed, R. Jayakumar, et A. Salih.* Springer Netherlands. p. 40–63. Disponible à http://link.springer.com/chapter/10.1007/978-1-4020-6540-8_3 [cité le 13 juin 2013].
- Lachassagne, P., Wyns, R., et Dewandel, B. 2011. The fracture permeability of Hard Rock Aquifers is due neither to tectonics, nor to unloading, but to weathering processes [en ligne]. *Terra Nova*, **23**(3) : 145–161. doi: 10.1111/j.1365-3121.2011.00998.x.
- Le Borgne, T., Bour, O., de Dreuzy, J.R., Davy, P., et Touchard, F. 2004. Equivalent mean flow models for fractured aquifers: Insights from a pumping tests scaling interpretation [en ligne]. *Water Resources Research*, **40**(3) : W03512. doi: 10.1029/2003WR002436.
- Lee, S.-T., et Brockenbrough, J.R. 1986. A New Approximate Analytic Solution for Finite-Conductivity Vertical Fractures [en ligne]. *SPE Formation Evaluation*, **1**(01) : 75–88. doi: 10.2118/12013-PA.
- Lemieux, J.-M., Therrien, R., et Kirkwood, D. 2006. Small scale study of groundwater flow in a fractured carbonate-rock aquifer at the St-Eustache quarry, Québec, Canada [en ligne]. *Hydrogeology Journal*, **14**(4) : 603–612. doi: 10.1007/s10040-005-0457-2.
- Lemieux, Y., Tremblay, A., et Lavoie, D. 2003. Structural analysis of supracrustal faults in the Charlevoix area, Quebec: relation to impact cratering and the St-Laurent fault system. *Canadian Journal of Earth Sciences*, **40**(2) : 221–235.
- Levasseur, D. 1995. Les eskers : essai de synthèse bibliographique [en ligne]. Disponible à <http://id.erudit.org/iderudit/033066ar> [cité le 16 décembre 2014].

- Leveinen, J. 2000. Composite model with fractional flow dimensions for well test analysis in fractured rocks [en ligne]. *Journal of Hydrology*, **234**(3–4) : 116–141. doi: 10.1016/S0022-1694(00)00254-7.
- Leveinen, J. 2001. Conceptual and analytical modeling of fracture zone aquifers in hard rock - Implications of pumping tests in the Pohjukansalo well field, east-central Finland [en ligne]. Geological Survey of Finland, Nuclear Waste Disposal Research. YST-105. Disponible à <http://arkisto.gtk.fi/yyst/yyst-105.pdf> [cité le 11 novembre 2013].
- Leveinen, J., Rönkä, E., Tikkanen, J., et Karro, E. 1998. Fractional flow dimensions and hydraulic properties of a fracture-zone aquifer, Leppavirta, Finland [en ligne]. *Hydrogeology Journal*, **6**(3) : 327–340. doi: 10.1007/s100400050156.
- Liang, H., Lin, S., Huang, T., Chen, D., et Tom Kuo, M. 2012. Identifying the flow dimension in fractured rock using an interference test. *Journal of Petroleum and Gas Engineering*, **3**(6) : 114–123.
- Lods, G., et Gouze, P. 2004. WTFM, Software for Well Test Analysis in Fractured Media Combining Fractional Flow with Double Porosity and Leakance Approaches [en ligne]. *Comput. Geosci.*, **30**(9–10) : 937–947. doi: 10.1016/j.cageo.2004.06.003.
- Long, J.C.S., Remer, J.S., Wilson, C.R., et Witherspoon, P.A. 1982. Porous Media Equivalents for Networks of Discontinuous Fractures [en ligne]. *Water Resources Research*, **18** : 645–658. doi: 10.1029/WR018i003p00645.
- Maréchal, J.C., Dewandel, B., et Subrahmanyam, K. 2004. Use of hydraulic tests at different scales to characterize fracture network properties in the weathered-fractured layer of a hard rock aquifer [en ligne]. *Water Resources Research*, **40**(11) : W11508. doi: 10.1029/2004WR003137.
- Maréchal, J.-C., Ladouche, B., Dörfliker, N., et Lachassagne, P. 2008. Interpretation of pumping tests in a mixed flow karst system [en ligne]. *Water Resources Research*, **44**(5) : W05401. doi: 10.1029/2007WR006288.
- Massonnat, G.J., et Bandiziol, D. 1991. Interdependence Between Geology and Well Test Interpretation [en ligne]. Society of Petroleum Engineers. doi: 10.2118/22740-MS.
- Mattar, L. 1994. Practical Well Test Interpretation [en ligne]. Society of Petroleum Engineers. doi: 10.2118/27975-MS.
- Mattar, L. 1997. Derivative Analysis Without Type Curves [en ligne]. Society of Petroleum Engineers. doi: 10.2118/97-51.
- Mattar, L. 1999. Derivative analysis without type curves [en ligne]. *Journal of Canadian Petroleum Technology*, **38**(13). doi: 10.2118/99-13-63.
- Mattar, L. 2004. Well test interpretation [en ligne]. Calgary, Alberta, Canada. Disponible à <http://www.spe.org/training/courses/WTI.php>.
- Mattar, L., et Zaoral, K. 1992. The primary pressure derivative (PPD) a new diagnostic tool in well test interpretation [en ligne]. *Journal of Canadian Petroleum Technology*, **31**(4). doi: 10.2118/92-04-06.

- Meier, P.M., Carrera, J., et Sánchez-Vila, X. 1998. An evaluation of Jacob's Method for the interpretation of pumping tests in heterogeneous formations [en ligne]. *Water Resources Research*, **34**(5) : 1011–1025. doi: 10.1029/98WR00008.
- Mejias, M., Renard, P., et Glenz, D. 2009. Hydraulic testing of low-permeability formations: A case study in the granite of Cadalso de los Vidrios, Spain [en ligne]. *Engineering Geology*, **107**(3–4) : 88–97. doi: 10.1016/j.enggeo.2009.05.010.
- Moench, A.F. 1985. Transient Flow to a Large-Diameter Well in an Aquifer With Storative Semiconfining Layers [en ligne]. *Water Resources Research*, **21**(8) : 1121–1131. doi: 10.1029/WR021i008p01121.
- Moncada, K., Tiab, D., Escobar, F.H., Montealegre, M., Chacon, A., Zamora, R., et Nese, S.-L. 2005. Determination of vertical and horizontal permeabilities for vertical oil and gas wells with partial completion and partial penetration using pressure and pressure derivative plots without type-curve matching. *CT&F - Ciencia, Tecnología y Futuro*, **3**(1) : 77–94.
- Nadeau, S., Rosa, E., Cloutier, V., Daigneault, R.-A., et Veillette, J. 2015. A GIS-based approach for supporting groundwater protection in eskers: Application to sand and gravel extraction activities in Abitibi-Témiscamingue, Quebec, Canada [en ligne]. *Journal of Hydrology: Regional Studies*, **4**, **Part B** : 535–549. doi: 10.1016/j.ejrh.2015.05.015.
- Nastev, M., Savard, M.M., Lapcevic, P., Lefebvre, R., et Martel, R. 2004. Hydraulic properties and scale effects investigation in regional rock aquifers, south-western Quebec, Canada [en ligne]. *Hydrogeology Journal*, **12**(3) : 257–269. doi: 10.1007/s10040-004-0340-6.
- Neuman, S.P. 1972. Theory of flow in unconfined aquifers considering delayed response of the water table [en ligne]. *Water Resources Research*, **8**(4) : 1031–1045. doi: 10.1029/WR008i004p01031.
- Neuman, S.P., et Witherspoon, P.A. 1969. Theory of flow in a confined two aquifer system [en ligne]. *Water Resources Research*, **5**(4) : 803–816. doi: 10.1029/WR005i004p00803.
- Nobakht, M., et Mattar, L. 2009. Diagnostics of data quality for analysis of production data [en ligne]. *Dans Society of Petroleum Engineers papier No. 2009-137, Canadian International Petroleum Conference, 16-18 June, Calgary, Alberta, USA.* doi: 10.2118/2009-137.
- Novakowski, K.S., et Lapcevic, P.A. 1988. Regional hydrogeology of the Silurian and Ordovician sedimentary rock underlying Niagara Falls, Ontario, Canada [en ligne]. *Journal of Hydrology*, **104** : 211–236. doi: 10.1016/0022-1694(88)90166-7.
- Obeahon, P.P., Sedgwick, A., et Okereke, O. 2014. Practical application of multi rate deconvolution [en ligne]. *Dans Society of Petroleum Engineers paper No. 172446, SPE Nigeria Annual International Conference and Exhibition, 5-7 August, Lagos, Nigeria.* doi: 10.2118/172446-MS.

- Odling, N.E., West, L.J., Hartmann, S., et Kilpatrick, A. 2013. Fractional flow in fractured chalk; a flow and tracer test revisited [en ligne]. *Journal of Contaminant Hydrology*, **147** : 96–111. doi: 10.1016/j.jconhyd.2013.02.003.
- Onur, M., Hegeman, P.S., et Kuchuk, F.J. 2002. Pressure-Pressure Convolution Analysis of Multiprobe and Packer-Probe Wireline Formation Tester Data [en ligne]. *Society of Petroleum Engineers*. doi: 10.2118/77343-MS.
- Onur, M., et Kuchuk, F.J. 2012. A New Deconvolution Technique Based on Pressure-Derivative Data for Pressure-Transient-Test Interpretation [en ligne]. *SPE Journal*, **17**(1). doi: 10.2118/134315-PA.
- Papadopoulos, I.S., et Hilton H. 1967. Drawdown in a well of large diameter [en ligne]. *Water Resources Research*, **3**(1) : 241–244. doi: 10.1029/WR003i001p00241.
- Paradis, D., Martel, R., Karanta, G., Lefebvre, R., Michaud, Y., Therrien, R., et Nastev, M. 2007. Comparative study of methods for WHPA delineation [en ligne]. *Ground Water*, **45**(2) : 158–167. doi: 10.1111/j.1745-6584.2006.00271.x.
- Pechstein, A., Attinger, S., Krieg, R., et Coptly, N.K. 2016. Estimating transmissivity from single-well pumping tests in heterogeneous aquifers [en ligne]. *Water Resources Research*, **52**(1) : 495–510. doi: 10.1002/2015WR017845.
- Pimonov, E., Ayan, C., Onur, M., et Kuchuk, F.J. 2010. A New Pressure/Rate-Deconvolution Algorithm To Analyze Wireline Formation-Tester and Well-Test Data [en ligne]. *SPE Reservoir Evaluation & Engineering*, **13**(04) : 603–613. doi: 10.2118/123982-PA.
- Polek, J., Karasaki, K., Long, J.C.S., et Barker, J. 1989. Flow to wells in fractured rock with fractal structure. *Dans Fractal Aspects of Materials*. Materials Research Society.
- van Poolen, H.K. 1964. Radius-of-drainage and stabilization-time equations. *The Oil and Gas Journal* : 138–146.
- Pulido, H., Samaniego, F., River, J., et Camacho, R. 2003. Decline Curve Analysis in a Naturally Fractured Reservoir with a Finite-Conductivity Fault [en ligne]. *Stanford Geothermal Workshop*. Stanford, USA. Disponible à https://pangea.stanford.edu/ERE/db/IGAstandard/record_detail.php?id=96.
- Rafini, S. 2004. Contrôle structural des écoulements en milieux fractures contribution de l'approche combinée simulation de flux – analyse de la déformation. Université du Québec à Montréal.
- Rafini, S. 2008. Comportement hydraulique des milieux faillés [The hydraulic behaviour of faulted environments]. [en ligne]. PhD, Université du Québec à Montréal, Montréal. Disponible à <http://www.archipel.uqam.ca/1684/> [cité le 1 juillet 2013].
- Rafini, S., Chesnaux, R., et Dal Soglio, L. 2014. A numerical analysis to illustrate the usefulness of drawdown log-derivative diagnostic plots in characterizing the heterogeneity of non-Theis aquifers. *Dans 2014 GSA Annual Meeting*, October 19-22, 2014 Vancouver, British Columbia, Canada.

- Rafini, S., Chesnaux, R., et Ferroud, A. 2017. A numerical investigation of pumping-test responses from contiguous aquifers [en ligne]. *Hydrogeology Journal*, **3**(25) : 877–894. doi: 10.1007/s10040-017-1560-x.
- Rafini, S., et Larocque, M. 2009. Insights from numerical modeling on the hydrodynamics of non-radial flow in faulted media [en ligne]. *Advances in Water Resources*, **32**(8) : 1170–1179. doi: 10.1016/j.advwatres.2009.03.009.
- Rafini, S., et Larocque, M. 2012. Numerical modeling of the hydraulic signatures of horizontal and inclined faults [en ligne]. *Hydrogeology Journal*, **20**(2) : 337–350. doi: 10.1007/s10040-011-0812-4.
- Raghavan, R. 2004. A review of applications to constrain pumping test responses to improve on geological description and uncertainty [en ligne]. *Reviews of Geophysics*, **42**(4) : RG4001. doi: 10.1029/2003RG000142.
- Ramos, G., Carrera, J., Gómez, S., Minutti, C., et Camacho, R. 2017. A stable computation of log-derivatives from noisy drawdown data: COMPUTATION OF NOISY LOG-DERIVATIVES [en ligne]. *Water Resources Research*, **53**(9) : 7904–7916. doi: 10.1002/2017WR020811.
- Renard, P. 2005. The future of hydraulic tests [en ligne]. *Hydrogeology Journal*, **13**(1) : 259–262. doi: 10.1007/s10040-004-0406-5.
- Renard, P. 2017. Hytool: an open source matlab toolbox for the interpretation of hydraulic tests using analytical solutions [en ligne]. *The Journal of Open Source Software*, **2**(19) : 441. doi: 10.21105/joss.00441.
- Renard, P., Glenz, D., et Mejias, M. 2009. Understanding diagnostic plots for well-test interpretation [en ligne]. *Hydrogeology Journal*, **17**(3) : 589–600. doi: 10.1007/s10040-008-0392-0.
- Riverin, M.-N. 2006. Caractérisation et modélisation de la dynamique d'écoulement dans le système aquifère de l'esker Saint-Mathieu / Berry, Abitibi, Québec. [en ligne]. MSc., Université du Québec, Institut national de la recherche scientifique, Québec. Disponible à <http://espace.inrs.ca/434/> [cité le 4 mai 2016].
- Robinson, P.C. 1983. Connectivity of fracture systems-a percolation theory approach [en ligne]. *Journal of Physics A: Mathematical and General*, **16**(3) : 605–614. doi: 10.1088/0305-4470/16/3/020.
- Rondot, J. 1989. Géologie de Charlevoix. Série de manuscits bruts. Rapport MB 89-21, Ministère de l'Énergie et des Ressources du Québec.
- Roques, C. 2013. Hydrogéologie des zones de faille du socle cristallin : implications en terme de ressources en eau pour le Massif Armoricaïn [en ligne]. Rennes 1. Disponible à <http://www.theses.fr/2013REN1S138> [cité le 12 novembre 2014].
- Roques, C., Bour, O., Aquilina, L., Dewandel, B., Leray, S., Schroetter, J., Longuevergne, L., LE Borgne, T., Hochreutener, R., Labasque, T., Lavenant, N., Vergnaud-Ayraud, V., et Mougin, B. 2014. Hydrological behavior of a deep sub-vertical fault in

- crystalline basement and relationships with surrounding reservoirs [en ligne]. *Journal of Hydrology*, 509 : 42–54. doi: 10.1016/j.jhydrol.2013.11.023.
- Rouleau, A. 1988. A numerical Simulator for Flow and Transport in Stochastic Discrete Fracture Networks. Inland Waters Directorate, **Technical Bull.**(155) : 204.
- Rouleau, A., et Gale, J.E. 1987. Stochastic discrete fracture simulation of groundwater flow into an underground excavation in granite [en ligne]. *International Journal of Rock Mechanics and Mining Sciences & Geomechanics*, **24**(2) : 99–112. doi: 10.1016/0148-9062(87)91929-2.
- Rouboutsos, A., et Stewart, G. 1988. A Direct Deconvolution or Convolution Algorithm for Well Test Analysis [en ligne]. Society of Petroleum Engineers. doi: 10.2118/18157-MS.
- Rozemeijer, J.C., van der Velde, Y., McLaren, R.G., van Geer, F.C., Broers, H.P., et Bierkens, M.F.P. 2010. Integrated modeling of groundwater–surface water interactions in a tile-drained agricultural field: The importance of directly measured flow route contributions [en ligne]. *Water Resources Research*, **46**(11) : W11537. doi: 10.1029/2010WR009155.
- Sánchez-Vila, X., Meier, P.M., et Carrera, J. 1999. Pumping tests in heterogeneous aquifers: An analytical study of what can be obtained from their interpretation using Jacob's Method [en ligne]. *Water Resources Research*, **35**(4) : 943–952. doi: 10.1029/1999WR900007.
- Scanlon, B.R., Healy, R.W., et Cook, P.G. 2002. Choosing appropriate techniques for quantifying groundwater recharge [en ligne]. *Hydrogeology Journal*, **10**(1) : 18–39. doi: 10.1007/s10040-001-0176-2.
- von Schroeter, T., Hollaender, F., et Gringarten, A. 2001. Deconvolution of well test data as a nonlinear total least squares problem [en ligne]. *Dans* Society of Petroleum Engineers paper No. 71574, SPE Annual Technical Conference and Exhibition, 30 September-3 October, 2001, New Orleans, Louisiana, USA. doi: 10.2118/71574-MS.
- Shahamat, M.S., Mattar, L., et Aguilera, R. 2015. Analysis of Decline Curves on the Basis of Beta-Derivative [en ligne]. *SPE Reservoir Evaluation & Engineering*, **18**(02) : 214–227. doi: 10.2118/169570-PA.
- Shapiro, S.A., Huenges, E., et Borm, G. 1997. Estimating the crust permeability from fluid-injection-induced seismic emission at the KTB site [en ligne]. *Geophysical Journal International*, **131**(2) : F15–F18. doi: 10.1111/j.1365-246X.1997.tb01215.x.
- Shapiro, S.A., Patzig, R., Rothert, E., et Rindschwentner, J. 2003. Triggering of Seismicity by Pore-pressure Perturbations: Permeability-related Signatures of the Phenomenon [en ligne]. *pure and applied geophysics*, **160**(5–6) : 1051–1066. doi: 10.1007/PL00012560.
- Simard, P.T., Chesnaux, R., Rouleau, A., Daigneault, R., Cousineau, P.A., Roy, D.W., Lambert, M., Poirier, B., et Poignant-Molina, L. 2015. Imaging Quaternary glacial deposits and basement topography using the transient electromagnetic method for

- modeling aquifer environments [en ligne]. *Journal of Applied Geophysics*, **119** : 36–50. doi: 10.1016/j.jappgeo.2015.05.006.
- Smith, E.D., et Vaughan, N.D. 1985. Aquifer Test Analysis in Nonradial Flow Regimes: A Case Study [en ligne]. *Ground Water*, **23**(2) : 167–175. doi: 10.1111/j.1745-6584.1985.tb02789.x.
- Stewart, G. 2007. Depth of investigation and relation to gauge resolution. *Dans A presentation at SPE ATW on Reservoir Testing in a World of High Production Values*, Bali, Indonesia.
- Stewart, G., Wittmann, M.J., et Meunier, D. 1983. Afterflow Measurement and Deconvolution in Well Test Analysis [en ligne]. SPE Annual Technical Conference and Exhibition, San Francisco, CA. October 5-8, 1983. Society of Petroleum Engineers. doi: 10.2118/12174-MS.
- Taylor, R.G., Scanlon, B., Döll, P., Rodell, M., van Beek, R., Wada, Y., Longuevergne, L., Leblanc, M., Famiglietti, J.S., Edmunds, M., Konikow, L., Green, T.R., Chen, J., Taniguchi, M., Bierkens, M.F.P., MacDonald, A., Fan, Y., Maxwell, R.M., Yechieli, Y., Gurdak, J.J., Allen, D.M., Shamsudduha, M., Hiscock, K., Yeh, P.J.-F., Holman, I., et Treidel, H. 2013. Ground water and climate change [en ligne]. *Nature Climate Change*, **3**(4) : 322–329. doi: 10.1038/nclimate1744.
- Theis, C.V. 1935. The relation between the lowering of the piezometric surface and the rate and duration of discharge of a well using ground-water storage [en ligne]. *Transactions, American Geophysical Union*, **16** : 519–524. doi: 10.1029/TR016i002p00519.
- Therrien, R., McLaren, R., Sudicky, E., et Panday, S. 2010. HydroGeoSphere, A three-dimensional numerical model describing fully integrated subsurface and surface flow and solute transport [en ligne]. DRAFT, Univ. of Waterloo, Waterloo, Ont., Canada. Disponible à (Available at <http://www.science.uwaterloo.ca/~mclaren/public/hydrosphere.pdf>).
- Tiab, D. 1993a. Analysis of pressure and pressure derivatives without type curve matching - IV. Flow and no-flow boundaries. to be submitted for presentation at the SPE Eastern Regional Meeting, Pittsburgh.
- Tiab, D. 1993b. Analysis of pressure and pressure derivatives without type-curve matching - V. Naturally Fractured Reservoirs. to be submitted for presentation at the SPE Eastern Regional Meeting, Pittsburgh.
- Tiab, D. 1993c. Analysis of pressure and pressure derivatives without type-curve matching - I. Skin and Wellbore Storage [en ligne]. Society of Petroleum Engineers. doi: 10.2118/25426-MS.
- Tiab, D. 1993d. Analysis of pressure and pressure derivative without type-curve matching - III. Vertically fractured wells in closed systems [en ligne]. SPE Western Regional Meeting. Society of Petroleum Engineers, Anchorage, Alaska, USA. doi: 10.2118/26138-MS.

- Tiab, D. 1994. Analysis of pressure and pressure derivative without type-curve matching: Vertically fractured wells in closed systems [en ligne]. *Journal of Petroleum Science and Engineering*, **11**(4) : 323–333. doi: 10.1016/0920-4105(94)90050-7.
- Tiab, D. 1995. Analysis of pressure and pressure derivative without type-curve matching — Skin and wellbore storage [en ligne]. *Journal of Petroleum Science and Engineering*, **12**(3) : 171–181. doi: 10.1016/0920-4105(94)00040-B.
- Tiab, D. 2005. Analysis of pressure derivative data of hydraulically fractured wells by the Tiab's Direct Synthesis technique [en ligne]. *Journal of Petroleum Science and Engineering*, **49**(1–2) : 1–21. doi: 10.1016/j.petrol.2005.07.001.
- Todd, D.K. 1980. *Groundwater hydrology*. 2nd ed. JWiley, New York ; Toronto.
- van Tonder, G.J., Botha, J.F., Chiang, W.-H., Kunstmann, H., et Xu, Y. 2001. Estimation of the sustainable yields of boreholes in fractured rock formations [en ligne]. *Journal of Hydrology*, **241**(1–2) : 70–90. doi: 10.1016/S0022-1694(00)00369-3.
- Tsang, C.-F., et Neretnieks, I. 1998. Flow channeling in heterogeneous fractured rocks [en ligne]. *Reviews of Geophysics*, **36**(2) : 275–298. doi: 10.1029/97RG03319.
- Valdes-Perez, A.R., Pulido, H., Cinco-Ley, H., et Galicia-Muñoz, G. 2011. A new bilinear flow model for naturally fractured reservoirs with transient interporosity transfer. *Dans PROCEEDINGS, Thirty-Sixth Workshop on Geothermal Reservoir Engineering Stanford University, Stanford, California, January 31 - February 2, 2011, SGP-TR-191*.
- Verbovšek, T. 2009. Influences of Aquifer Properties on Flow Dimensions in Dolomites [en ligne]. *Ground Water*, **47**(5) : 660–668. doi: 10.1111/j.1745-6584.2009.00577.x.
- Verbovšek, T. 2011. Hydrogeology and Geochemistry of Fractured Dolomites—A case study of Slovenia [en ligne]. *Dans Aquifers: formation, transport, and pollution*. Nova Science Publishers, Hauppauge, N.Y. p. 87–147. Disponible à http://www.geo.ntf.uni-lj.si/tverbovsek/papers/Aquifers%20-%20Formation%20Transport%20and%20Pollution_pageproof.pdf [cité le 4 novembre 2013].
- Vorosmarty, C.J., Green, P., Salisbury, J., et Lammers, R.B. 2000. Global Water Resources: Vulnerability from Climate Change and Population Growth [en ligne]. *Science*, **289**(5477) : 284–288. doi: 10.1126/science.289.5477.284.
- Wada, Y., van Beek, L.P.H., Wanders, N., et Bierkens, M.F.P. 2013. Human water consumption intensifies hydrological drought worldwide [en ligne]. *Environmental Research Letters*, **8**(3) : 034036. doi: 10.1088/1748-9326/8/3/034036.
- Walker, D.D., Cello, P.A., Valocchi, A.J., et Loftis, B. 2006. Flow dimensions corresponding to stochastic models of heterogeneous transmissivity [en ligne]. *Geophysical Research Letters*, **33**(7) : L07407. doi: 10.1029/2006GL025695.
- Walker, D.D., et Roberts, R.M. 2003. Flow dimensions corresponding to hydrogeologic conditions. *Water resources research*, **39**(12) : 1349.

- Warren, J.E., et Root, P.J. 1963. The behavior of naturally fractured reservoirs [en ligne]. Society of Petroleum Engineers Journal, **3**(03) : 245–255. doi: 10.2118/426-PA.
- Winberg, A. 2000. Äspö Hard Rock Laboratory: final report of the first stage of the tracer retention understanding experiments [en ligne]. Svensk kärnbränslehantering AB/Swedish Nuclear Fuel and Waste Management, Stockholm. Disponible à <http://catalog.hathitrust.org/Record/003556044>.
- Worthington, S.R.H., Davies, G.J., et Alexander Jr., E.C. 2016. Enhancement of bedrock permeability by weathering [en ligne]. Earth-Science Reviews, **160** : 188–202. doi: 10.1016/j.earscirev.2016.07.002.
- Wyssling, L. 1979. Eine neue formel zur Berechnung der Zuströmungsdauer (Laufzeit) des grundwassers zu einem grundwasser pumpwerk. Eclogae Geologicae Helvetiae, **72**(2) : 401–406.
- Zanini, L., Novakowski, K. s., Lapcevie, P., Bickerton, G. s., Voralek, J., et Talbot, C. 2000. Ground Water Flow in a Fractured Carbonate Aquifer Inferred from Combined Hydrogeological and Geochemical Measurements [en ligne]. Ground Water, **38**(3) : 350–360. doi: 10.1111/j.1745-6584.2000.tb00220.x.

ANNEXES

ANNEXE 1 (Tableau 7 ; chapitre 3) : Table 3.7: Principal data (locations, well names, confinement conditions, simplified lithologies and pumping test durations) and n-sequences of the pumping tests in the database. In the fifth column, the letters in brackets refer to an evaluation of the quality of the signal: VG = very good, G = good, MG = mediocre-good, M = mediocre and U = either an undefinable slope of the $ds/d\log t$ signal or a slope that has not been considered as a flow dimension, but rather as a transition or a boundary effect.

Location	Well name	Confinement conditions	Simplified lithology	Sequence of n	Pumping test duration (min)
Mirabel (Quebec)	Lésage	-	Alluvial deposits	6.2 (MG); 1.3 (G); 4 (M);	4100
Longue-Rive (Quebec)	P-1	Confined	Alluvial deposits	1.3 (M); 3 (VG); 2.7 (M);	4320
Longue-Rive (Quebec)	P-2	Confined	Alluvial deposits	3 (MG); 2.7 (G);	4320
Saint-Thomas-Didyme (Quebec)	PU-1	Confined	Alluvial deposits	2 (M); 1.5 (MG); 2 (MG);	4320
Saint Siméon (Quebec)	P-1	Confined	Alluvial deposits	2 (M); 4.7 (VG); 2.5 (MG); 0.8(G);	5490
La Malbaie ; Rivière Malbaie (Quebec)	PE-R1	Confined	Alluvial deposits	1.3 (G); 2 (G);	5955
Abtibi-Temiscamingue (Quebec)	PP-2	Confined	Alluvial deposits	1.3 (G);	13105
Baie-Saint-Paul (Quebec)	P-1	Confined (artesian)	Alluvial deposits	1 (G); 3 (VG);	5810
Abtibi-Temiscamingue (Quebec)	PP-4	Unconfined	Alluvial deposits	1.3 (G);	1440
Abtibi-Temiscamingue (Quebec)	PP-6	Unconfined	Alluvial deposits	2 (MG); 0 (G); 1.3 (MG);	1440
La Malbaie ; Joyeuse (Quebec)	PP-5D	Unconfined	Alluvial deposits	3 (G); 1.7 (G); 0 (VG);	4320
Desbiens (Quebec)	P-1	Unconfined	Alluvial deposits	2 (G); 0.8 (G);	4320
Desbiens (Quebec)	P-2	Unconfined	Alluvial deposits	2 (M); 1 (G);	4320
La Baie (Quebec)	PW-2004	Unconfined	Alluvial deposits	1 (VG);	4320
Shishaw (Quebec)	PW-1	Unconfined	Alluvial deposits	1 (VG);	4320
Abtibi-Temiscamingue (Quebec)	PP-1	Unconfined	Alluvial deposits	1.4 (G);	4320
Abtibi-Temiscamingue (Quebec)	PP-3	Unconfined	Alluvial deposits	1.3 (G);	4440
Abtibi-Temiscamingue (Quebec)	1/78	Unconfined	Alluvial deposits	1.3 (G);	5280
Saint-Honoré (Quebec)	PW-1	Unconfined	Alluvial deposits	4 (G); 1 (G);	10142
Saint-Honoré (Quebec)	PW-2	Unconfined	Alluvial deposits	4 (M); 1 (G);	10142
Abtibi-Temiscamingue (Quebec)	PS-1	Unconfined	Alluvial deposits	1.3 (MG); 3 (MG); 0.6 (MG);	11520
Mirabel (Quebec)	MT2	-	Carbonates	2 (MG); 2.9 (G);	2880
Nord Pas-de-Calais (France)	Monceau_SD2	-	Carbonates	1 (VG);	2880
Mirabel (Quebec)	StJanvHamel	-	Carbonates	1 (G); 2.8 (G); 1 (G);	4320
Mirabel (Quebec)	CK42	-	Carbonates	0.8 (M); 2.5 (G); 2 (G);	4441
Mirabel (Quebec)	StAnne_G_P-8	-	Carbonates	4 (G); 1.5 (VG); 2 (VG); 0(G);	9372
The Alpes (France)	Fich_23	Confined	Carbonates	1.6 (G); 0.8 (G); 4 (M);	1080
Mirabel (Quebec)	R17	Confined	Carbonates	2 (MG); 0 (MG); 2 (MG);	2880
Mirabel (Quebec)	Bell	Confined	Carbonates	2 (VG);	4080
Mirabel (Quebec)	Demix2	Confined	Carbonates	2 (G); 3.8 (MG); 2 (MG);	4295
La Malbaie ; Joyeuse (Quebec)	PP-6R	Confined	Carbonates	1.8 (G); 1 (M);	4320
Mirabel (Quebec)	Chatam	Confined	Carbonates	2.4 (G); 3.5 (G);	4320
Mirabel (Quebec)	Greenalko	Confined	Carbonates	2.3 (G); 2 (G);	4320
Mirabel (Quebec)	Leclerc	Confined	Carbonates	2 (M); 0 (M); 1.6 (G);	4320
Mirabel (Quebec)	StJanv_G_Stja2	Confined	Carbonates	0.6 (G); 4 (MG);	10245

Table 3.7: End of Table 3.7

Mirabel (Quebec)	Hamel	Confined	Carbonates	0.5 (G); U (U);	10259
Nord Pas-de-Calais (France)	StHil_F3	Semi Confined	Carbonates	1.2 (G); 2 (VG);	720
Nord Pas-de-Calais (France)	Lim_PZ6	Semi Confined	Carbonates	3 (VG); 0.8 (VG); 4 (M);	1444
Nord Pas-de-Calais (France)	Maubeuge_FE2	Semi Confined	Carbonates	0 (MG); 4 (MG); 0 (MG);	2520
Midi-Pyrenees (France)	Combes	Semi Confined	Carbonates	2 (MG); 0 (MG);	2620
Midi-Pyrenees (France)	Faha	Semi Confined	Carbonates	0.8 (G); 3 (MG); 2 (MG);	2955
Nord Pas-de-Calais (France)	Bachan	Semi Confined	Carbonates	2.5 (G);	4320
Kef (Tunisie)	Ain_Chaam	Unconfined	Carbonates	2 (G); 5 (M); 2 (G);	240
Mirabel; St Eustache (Quebec)	SE5	Unconfined	Carbonates	0.6 (MG); 3.5 (MG);	333
Nord Pas-de-Calais (France)	Monceau_FE1	Unconfined	Carbonates	1.6 (M); 2.8 (G);	2880
Kef (Tunisie)	Ain_Mizeb	Unconfined	Carbonates	0.8 (M); 4 (G); 2 (G);	4317
Isle-aux-Coudres (Quebec)	PE-1	Unconfined	Carbonates	1.5 (GM);	4320
Mirabel (Quebec)	Mbarett	-	Carbonates+Alluvial deposits	1.5 (MG); 2.5 (G); 1.2 (G);	4320
Mirabel (Quebec)	1_87	Confined	Carbonates+Alluvial deposits	2.5 (G); 0 (MG); 2 (G);	4080
Saint-Félicien (Quebec)	PE-3	Confined	Carbonates+Alluvial deposits	1.7 (G); 2.5 (G);	4345
Pays de la Loire (France)	Mout_3	-	Crystalline rocks	3.2 (VG);	900
Pays de la Loire (France)	Mout_2	-	Crystalline rocks	3 (M); 4 (MG); 1.5 (G);	900
Lozère (France)	LaNarce	-	Crystalline rocks	3.4 (G); 4 (M);	2970
Mirabel (Quebec)	PA-2	-	Crystalline rocks	0.8 (G); 2.5 (G); 1 (G);	4320
Mirabel (Quebec)	Oka1	-	Crystalline rocks	2.5 (MG); 0 (G);	4320
Pays de la Loire (France)	Mout	Confined	Crystalline rocks	2.5 (G); 0.5 (G); 2 (G);	900
La Malbaie ; Kane (Quebec)	PK-2R	Confined	Crystalline rocks	0.6 (M); 2.5 (G); 2 (M);	4320
La Malbaie ; Kane (Quebec)	PK-3R	Confined	Crystalline rocks	1 (VG); 2 (M); 4.6(VG);	4320
La Malbaie ; Kane (Quebec)	PK-8R	Confined	Crystalline rocks	1.2 (G); 4 (G); 1 (MG);	4320
La Malbaie ; Saint-Fidèle (Quebec)	PP-3	Confined	Crystalline rocks	2 (G); 1.5 (G);	4320
Les Escoumins (Quebec)	F-5	Confined	Crystalline rocks	1.5 (MG); 2 (VG); 2.7 (G); 4(M);	4320
Saint-Aimé-des-Lacs (Quebec)	F-1R	Confined	Crystalline rocks	1.7 (G); 2.5 (G);	4320
Petit-Saguenay (Quebec)	P-1	Confined	Crystalline rocks	1 (G); 1.7 (G); 2.5 (G);	4320
Ferland-et-Boileau (Quebec)	PP	Confined	Crystalline rocks	1 (G); 1.7 (M);	4435
Saint-Irénée (Quebec)	SI/FE-607	Confined	Crystalline rocks	0 (G); 1.5 (VG); 0 (G);	8601
Pays de la Loire (France)	Beaufou	Confined (artesian)	Crystalline rocks	1.7 (MG); 2.7 (MG); 1 (MG);	21153
La Malbaie ; Saint-Fidèle (Quebec)	P-3	Confined	Crystalline rocks	1 (G);	2280
Pays de la Loire (France)	Frapp	Semi-confined	Crystalline rocks	1.4 (G); 2.8 (G);	900
La Malbaie ; Joyeuse (Quebec)	PJ-7R + PJ-6R	Unconfined	Crystalline rocks	3 (MG); 1.2 (VG); 2(G);	4320